ISSN 2413-5577

№ 3 Июль – Сентябрь 2025

Экологическая безопасность прибрежной и шельфовой зон моря

Ecological Safety of Coastal and Shelf Zones of Sea

No. 3 July – September 2025

ecological-safety.ru

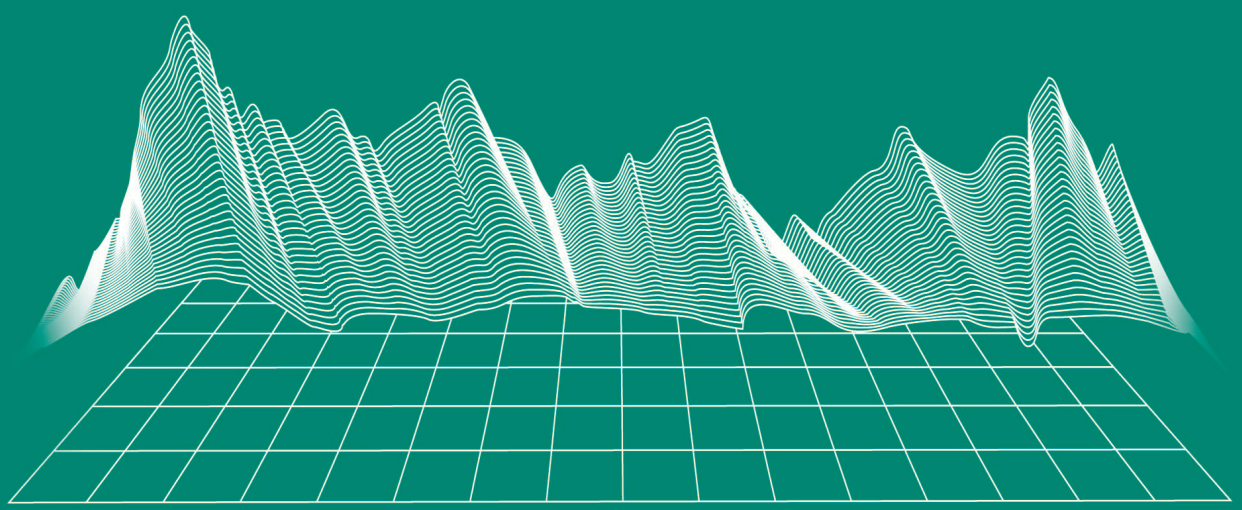

ISSN 2413-5577

No. 3, 2025

July – September

Publication frequency:
Quarterly

16+

ECOLOGICAL SAFETY OF COASTAL AND SHELF ZONES OF SEA

Scientific and theoretical peer reviewed journal

FOUNDER AND PUBLISHER:
Federal State Budget Scientific Institution
Federal Research Centre
"Marine Hydrophysical Institute of RAS"

The Journal publishes original research results, review articles (at the editorial board's request) and brief reports.

The Journal aims at publication of results of original scientific research concerning the state and interaction of geospheres (atmosphere, lithosphere, hydrosphere, and biosphere) within coastal and shelf areas of seas and oceans, methods and means of study thereof, ecological state of these areas under anthropogenic load as well as environmental protection issues.

The Journal's editorial board sees its mission as scientific, educational and regulatory work to preserve the ecological balance and restore the resource potential of coastal and shelf areas believing that despite the geographical limitations of the areas under study, the processes taking place within them have a significant impact on the waters of the seas and oceans and economic activity.

The Journal publishes original research materials, results of research performed by national and foreign scientific institutions in the coastal and shelf zones of seas and oceans, review articles (at the editorial board's request) and brief reports on the following major topics:
- Scientific basis for complex use of shelf natural resources
- Marine environment state and variability
- Coastal area state and variability; coast protection structures
- Monitoring and estimates of possible effects of anthropogenic activities
- Development and implementation of new marine environment control and monitoring technologies

The outcome of the research is information on the status, variability and possible effects of anthropogenic activities in the coastal and shelf marine areas, as well as the means to perform calculations and to provide information for making decisions on the implementation of activities in the coastal zone.

e-mail: ecology-safety@mhi-ras.ru

website: http://ecological-safety.ru

Founder, Publisher and Editorial Office address:
2, Kapitanskaya St.,
Sevastopol, 299011, Russia

Phone, fax: + 7 (8692) 54-57-16

EDITORIAL BOARD

Yuri N. Goryachkin – **Editor-in-Chief**, Chief Research Associate of FSBSI FRC MHI, Dr.Sci. (Geogr.), Scopus ID: 6507545681, ResearcherID: I-3062-2015, ORCID 0000-0002-2807-201X (Sevastopol, Russia)
Vitaly I. Ryabushko – **Deputy Editor-in-Chief**, Head of Department of FSBSI FRC A. O. Kovalevsky Institute of Biology of the Southern Seas of RAS, Chief Research Associate, Dr.Sci. (Biol.), ResearcherID: H-4163-2014, ORCID ID: 0000-0001-5052-2024 (Sevastopol, Russia)
Elena E. Sovga – **Deputy Editor-in-Chief**, Leading Research Associate of FSBSI FRC MHI, Dr.Sci. (Geogr.), Scopus ID: 7801406819, ResearcherID: A-9774-2018 (Sevastopol, Russia)
Vladimir V. Fomin – **Deputy Editor-in-Chief**, Head of Department of FSBSI FRC MHI, Dr.Sci. (Phys.-Math.), ResearcherID: H-8185-2015, ORCID ID: 0000-0002-9070-4460 (Sevastopol, Russia)
Tatyana V. Khmara – **Executive Editor**, Junior Research Associate of FSBSI FRC MHI, Scopus ID: 6506060413, ResearcherID: C-2358-2016 (Sevastopol, Russia)
Vladimir N. Belokopytov – Leading Research Associate, Head of Department of FSBSI FRC MHI, Dr.Sci. (Geogr.), Scopus ID: 6602381894, ORCID ID: 0000-0003-4699-9588 (Sevastopol, Russia)
Sergey V. Berdnikov – Chairman of FSBSI FRC Southern Scientific Centre of RAS, Dr.Sci. (Geogr.), ORCID ID: 0000-0002-3095-5532 (Rostov-on-Don, Russia)
Valery G. Bondur – Director of FSBSI Institute for Scientific Research of Aerospace Monitoring "AEROCOSMOS", vice-president of RAS, academician of RAS, Dr.Sci. (Tech.), ORCID ID: 0000-0002-2049-6176 (Moscow, Russia)
Temir A. Britayev – Chief Research Associate, IEE RAS, Dr.Sci. (Biol.), ORCID ID: 0000-0003-4707-3496, ResearcherID: D-6202-2014, Scopus Author ID: 6603206198 (Moscow, Russia)
Elena F. Vasechkina – Deputy Director of FSBSI FRC MHI, Dr.Sci. (Geogr.), ResearcherID: P-2178-2017 (Sevastopol, Russia)
Isaac Gertman – Head of Department of Israel Oceanographic and Limnological Research Institute, Head of Israel Marine Data Center, Ph.D. (Geogr.), ORCID ID: 0000-0002-6953-6722 (Haifa, Israel)
Sergey G. Demyshev – Head of Department of FSBSI FRC MHI, Chief Research Associate, Dr.Sci. (Phys.-Math.), ResearcherID C-1729-2016, ORCID ID: 0000-0002-5405-2282 (Sevastopol, Russia)
Nikolay A. Diansky – Chief Research Associate of Lomonosov Moscow State University, associate professor, Dr.Sci. (Phys.-Math.), ResearcherID: R-8307-2018, ORCID ID: 0000-0002-6785-1956 (Moscow, Russia)
Vladimir A. Dulov – Head of Laboratory of FSBSI FRC MHI, professor, Dr.Sci. (Phys.-Math.), ResearcherID: F-8868-2014, ORCID ID: 0000-0002-0038-7255 (Sevastopol, Russia)
Victor N. Egorov – Scientific Supervisor of FSBSI FRC A. O. Kovalevsky Institute of Biology of the Southern Seas of RAS, academician of RAS, professor, Dr.Sci. (Biol.), ORCID ID: 0000-0002-4233-3212 (Sevastopol, Russia)
Vladimir V. Efimov – Head of Department of FSBSI FRC MHI, Dr.Sci. (Phys.-Math.), ResearcherID: P-2063-2017 (Sevastopol, Russia)
Vladimir B. Zalesny – Leading Research Associate of FSBSI Institute of Numerical Mathematics of RAS, professor, Dr.Sci. (Phys.-Math.), ORCID ID: 0000-0003-3829-3374 (Moscow, Russia)
Andrey G. Zatsepin – Head of Laboratory of P.P. Shirshov Institute of Oceanology of RAS, Chief Research Associate, Dr.Sci. (Phys.-Math.), ORCID ID: 0000-0002-5527-5234 (Moscow, Russia)
Sergey K. Konovalov – Director of FSBSI FRC MHI, corresponding member of RAS, Dr.Sci. (Geogr.), ORCID ID: 0000-0002-5200-8448 (Sevastopol, Russia)
Gennady K. Korotaev – Scientific Supervisor of FSBSI FRC MHI, corresponding member of RAS, professor, Dr.Sci. (Phys.-Math.), ResearcherID: K-3408-2017 (Sevastopol, Russia)
Arseniy A. Kubryakov – Deputy Director of FSBSI FRC MHI, Head of the Laboratory of innovative methods and means of oceanological research, Dr.Sci. (Phys.-Math.), ORCID ID: 0000-0003-3561-5913 (Sevastopol, Russia)
Alexander S. Kuznetsov – Leading Research Associate, Head of Department of FSBSI FRC MHI, Ph.D. (Tech.), ORCID ID: 0000-0002-5690-5349 (Sevastopol, Russia)
Michael E. Lee – Head of Department of FSBSI FRC MHI, Dr.Sci. (Phys.-Math.), professor, ORCID ID: 0000-0002-2292-1877 (Sevastopol, Russia)
Pavel R. Makarevich – Chief Research Associate, MMBI KSC RAS, Dr.Sci. (Biol.), ORCID ID: 0000-0002-7581- 862X, ResearcherID: F-8521-2016, Scopus Author ID: 6603137602 (Murmansk, Russia)
Ludmila V. Malakhova – Leading Research Associate of A. O. Kovalevsky Institute of Biology of the Southern Seas of RAS, Ph.D. (Biol.), ResearcherID: E-9401-2016, ORCID ID: 0000-0001-8810-7264 (Sevastopol, Russia)
Gennady G. Matishov – Deputy Academician – Secretary of Earth Sciences Department of RAS, Head of Section of Oceanology, Physics of Atmosphere and Geography, Scientific Supervisor of FSBSI FRC Southern Scientific Centre of RAS, Scientific Supervisor of FSBSI Murmansk Marine Biological Institute KSC of RAS, academician of RAS, Dr.Sci. (Geogr.), professor, ORCID ID: 0000-0003-4430-5220 (Rostov-on-Don, Russia)
Alexander V. Prazukin – Leading Research Associate of FSBSI FRC A. O. Kovalevsky Institute of Biology of the Southern Seas of RAS, Dr.Sci. (Biol.), ResearcherID: H-2051-2016, ORCID ID: 0000-0001-9766-6041 (Sevastopol, Russia)
Anatoly S. Samodurov – Head of Department of FSBSI FRC MHI, Dr.Sci. (Phys.-Math.), ResearcherID: V-8642-2017 (Sevastopol, Russia)
Dimitar I. Trukhchev – Institute of Metal Science, equipment, and technologies "Academician A. Balevski" with Center for Hydro- and Aerodynamics at the Bulgarian Academy of Sciences, Dr.Sci. (Phys.-Math.), professor (Varna, Bulgaria)
Naum B. Shapiro – Leading Research Associate of FSBSI FRC MHI, Dr.Sci. (Phys.-Math.), ResearcherID: A-8585-2017 (Sevastopol, Russia)

РЕДАКЦИОННАЯ КОЛЛЕГИЯ

Горячкин Юрий Николаевич – **главный редактор**, главный научный сотрудник ФГБУН ФИЦ МГИ, д. г. н., Scopus Author ID: 6507545681, ResearcherID: I-3062-2015, ORCID ID: 0000-0002-2807-201X (Севастополь, Россия)

Рябушко Виталий Иванович – **заместитель главного редактора**, заведующий отделом ФГБУН ФИЦ «ИнБЮМ им. А.О. Ковалевского РАН», главный научный сотрудник, д. б. н., ResearcherID: H-4163-2014, ORCID ID: 0000-0001-5052-2024 (Севастополь, Россия)

Совга Елена Евгеньевна – **заместитель главного редактора**, ведущий научный сотрудник ФГБУН ФИЦ МГИ, д. г. н., Scopus Author ID: 7801406819, ResearcherID: A-9774-2018 (Севастополь, Россия)

Фомин Владимир Владимирович – **заместитель главного редактора**, заведующий отделом ФГБУН ФИЦ МГИ, д. ф.-м. н., ResearcherID: H-8185-2015, ORCID ID: 0000-0002-9070-4460 (Севастополь, Россия)

Хмара Татьяна Викторовна – **ответственный секретарь**, научный сотрудник ФГБУН ФИЦ МГИ, Scopus Author ID: 6506060413, ResearcherID: C-2358-2016 (Севастополь, Россия)

Белокопытов Владимир Николаевич – ведущий научный сотрудник, заведующий отделом ФГБУН ФИЦ МГИ, д. г. н., Scopus Author ID: 6602809060, ORCID ID: 0000-0003-4699-9588 (Севастополь, Россия)

Бердников Сергей Владимирович – председатель ФГБУН ФИЦ ЮНЦ РАН, д. г. н., ORCID ID: 0000-0002-3095-5532 (Ростов-на-Дону, Россия)

Бондур Валерий Григорьевич – директор ФГБНУ НИИ «АЭРОКОСМОС», вице-президент РАН, академик РАН, д. т. н., ORCID ID: 0000-0002-2049-6176 (Москва, Россия)

Британев Темир Аланович – главный научный сотрудник ФГБУН ИПЭЭ, д. б. н., ORCID ID: 0000-0003-4707-3496, ResearcherID: D-6202-2014, Scopus Author ID: 6603206198 (Москва, Россия)

Васечкина Елена Федоровна – заместитель директора ФГБУН ФИЦ МГИ, д. г. н., ResearcherID: P-2178-2017 (Севастополь, Россия)

Гертман Исаак – глава департамента Израильского океанографического и лимнологического исследовательского центра, руководитель Израильского морского центра данных, к. г. н., ORCID ID: 0000-0002-6953-6722 (Хайфа, Израиль)

Демышев Сергей Германович – заведующий отделом ФГБУН ФИЦ МГИ, главный научный сотрудник, д. ф.-м. н., ResearcherID: C-1729-2016, ORCID ID: 0000-0002-5405-2282 (Севастополь, Россия)

Дианский Николай Ардальянович – главный научный сотрудник МГУ им. М. В. Ломоносова, доцент, д. ф.-м. н., ResearcherID: R-8307-2018, ORCID ID: 0000-0002-6785-1956 (Москва, Россия)

Дулов Владимир Александрович – заведующий лабораторией ФГБУН ФИЦ МГИ, профессор, д. ф.-м. н., ResearcherID: F-8868-2014, ORCID ID: 0000-0002-0038-7255 (Севастополь, Россия)

Егоров Виктор Николаевич – научный руководитель ФГБУН ФИЦ ИнБЮМ им. А.О. Ковалевского РАН, академик РАН, профессор, д. б. н., ORCID ID: 0000-0002-4233-3212 (Севастополь, Россия)

Ефимов Владимир Васильевич – заведующий отделом ФГБУН ФИЦ МГИ, д. ф.-м. н., ResearcherID: P-2063-2017 (Севастополь, Россия)

Залесный Владимир Борисович – ведущий научный сотрудник ФГБУН ИВМ РАН, профессор, д. ф.-м. н., ORCID ID: 0000-0003-3829-3374 (Москва, Россия)

Зацепин Андрей Георгиевич – руководитель лаборатории ФГБУН ИО им. П.П. Ширшова РАН, главный научный сотрудник, д. ф.-м. н., ORCID ID: 0000-0002-5527-5234 (Москва, Россия)

Коновалов Сергей Карпович – директор ФГБУН ФИЦ МГИ, член-корреспондент РАН, д. г. н., ORCID ID: 0000-0002-5200-8448 (Севастополь, Россия)

Коротаев Геннадий Константинович – научный руководитель ФГБУН ФИЦ МГИ, член-корреспондент РАН, профессор, д. ф.-м. н., ResearcherID: K-3408-2017 (Севастополь, Россия)

Кубряков Арсений Александрович – заместитель директора ФГБУН ФИЦ МГИ, зав. лабораторией инновационных методов и средств океанологических исследований, д. ф.-м. н., ORCID ID: 0000-0003-3561-5913 (Севастополь, Россия)

Кузнецов Александр Сергеевич – ведущий научный сотрудник, заведующий отделом ФГБУН ФИЦ МГИ, к. т. н., ORCID ID: 0000-0002-5690-5349 (Севастополь, Россия)

Ли Михаил Ен Гон – заведующий отделом ФГБУН ФИЦ МГИ, профессор, д. ф.-м. н., ORCID ID: 0000-0002-2292-1877 (Севастополь, Россия)

Макаревич Павел Робертович – главный научный сотрудник ММБИ КНЦ РАН, д. б. н., ORCID ID: 0000-0002-7581-862X, ResearcherID: F-8521-2016, Scopus Author ID: 6603137602 (Мурманск, Россия)

Малахова Людмила Васильевна – ведущий научный сотрудник ФГБУН ФИЦ ИнБЮМ им. А.О. Ковалевского РАН, к. б. н., ResearcherID: E-9401-2016, ORCID ID: 0000-0001-8810-7264 (Севастополь, Россия)

Матишов Геннадий Григорьевич – заместитель академика-секретаря Отделения наук о Земле РАН – руководитель Секции океанологии, физики атмосферы и географии, научный руководитель ФГБУН ФИЦ ЮНЦ РАН, научный руководитель ФГБУН ММБИ КНЦ РАН, академик РАН, д. г. н., профессор, ORCID ID: 0000-0003-4430-5220 (Ростов-на-Дону, Россия)

Празукин Александр Васильевич – ведущий научный сотрудник ФГБУН ФИЦ ИнБЮМ им. А.О. Ковалевского РАН, д. б. н., Researcher ID: H-2051-2016, ORCID ID: 0000-0001-9766-6041 (Севастополь, Россия)

Самодуров Анатолий Сергеевич – заведующий отделом ФГБУН ФИЦ МГИ, д. ф.-м. н., ResearcherID: V-8642-2017 (Севастополь, Россия)

Трухчев Димитър Иванов – старший научный сотрудник Института океанологии БАН, профессор, д. ф.-м. н. (Варна, Болгария)

Шапиро Наум Борисович – ведущий научный сотрудник ФГБУН ФИЦ МГИ, д. ф.-м. н., ResearcherID: A-8585-2017 (Севастополь, Россия)

CONTENTS

№ 3. 2025 July – September, 2025

СОДЕРЖАНИЕ

№ 3. 2025 Июль – Сентябрь, 2025

Original paper

Synoptic Variability of Bio-Optical and Hydrological Parameters off the Crimea Coast According to Data from *in situ* Measurements in Summer 2023

Yu. V. Artamonov, E. A. Skripaleva *, A. A. Latushkin, A. V. Fedirko

Marine Hydrophysical Institute of RAS, Sevastopol, Russia
* *e-mail: sea-ant@yandex.ru*

Abstract
The paper studies the synoptic variability of the light beam attenuation coefficient and intensity of chlorophyll a fluorescence on the sea surface and its relationship with the distributions of hydrological parameters based on the hydrological and bio-optical measurements carried out off the coast of Crimea during the 127th cruise of R/V *Professor Vodyanitsky* in summer 2023. The measurements were carried out on a finer station grid with the vessel moving from west to east twice with a weekly interval (14–20 June and 22–28 June). It is shown that due to Rim Current penetration into the polygon during the 2nd stage of measurements, the Azov-Kerch waters flew into the polygon water area more intensely. This was accompanied by a decrease in waters transparency and salinity, and an increase in temperature, which was also influenced by the ongoing seasonal heating. In most of the study area, data from both measurement stages revealed a significant tendency of increasing chlorophyll a fluorescence intensity in water areas with a higher beam attenuation coefficient. Changes of the vertical thermohaline and bio-optical waters structure on a scale of about a week were observed in the entire measurement layer and were manifested in changes in the number and values of the maxima of the chlorophyll a fluorescence intensity, the light beam attenuation coefficient, temperature and salinity vertical gradients, as well as their depths. The main maximum of the light beam attenuation coefficient was observed either in the surface layer or in the layer of seasonal thermocline and halocline, while the maximum of the chlorophyll a fluorescence intensity was located under the layer of seasonal thermocline and halocline. The study found a significant linear correlation between the distributions of the depth of the seasonal thermocline and the depths of the maximum of the light beam attenuation coefficient and chlorophyll a fluorescence intensity, as well as between the depths of the seasonal halocline and the maximum intensity of chlorophyll a fluorescence.

Keywords: Black Sea, hydrological stations, light beam attenuation coefficient, chlorophyll a fluorescence, temperature, salinity, water circulation, synoptic variability

Acknowledgements: The work was carried out under FSBSI FRC MHI state assignment FNNN-2024-0014 “Ocean and atmosphere interaction” and FNNN-2024-0012 “Operational Oceanology”. The data were obtained at the Center for Collective Use R/V *Professor Vodyanitsky* of FSBSI FRC A.O. Kovalevsky Institute of Biology of the Southern Seas of RAS.

© Artamonov Yu. V., Skripaleva E. A., Latushkin A. A., Fedirko A. V., 2025

This work is licensed under a Creative Commons Attribution-Non Commercial 4.0 International (CC BY-NC 4.0) License

For citation: Artamonov, Yu.V., Skripaleva, E.A., Latushkin, A.A. and Fedirko, A.V., 2025. Synoptic Variability of Bio-Optical and Hydrological Parameters off the Crimea Coast According to Data from *in situ* Measurements in Summer 2023. *Ecological Safety of Coastal and Shelf Zones of Sea*, (3), pp. 6–24.

Синоптическая изменчивость биооптических и гидрологических параметров у берегов Крыма по данным экспедиционных измерений летом 2023 года

Ю. В. Артамонов, Е. А. Скрипалева *, А. А. Латушкин, А. В. Федирко

Морской гидрофизический институт РАН, Севастополь, Россия
** e-mail: sea-ant@yandex.ru*

Аннотация

По данным гидрологических и биооптических измерений, выполненных у берегов Крыма в ходе 127-го рейса НИС «Профессор Водяницкий» летом 2023 г., исследована синоптическая изменчивость показателя ослабления направленного света и интенсивности флуоресценции хлорофилла *a* на поверхности моря и ее связь с распределениями гидрологических параметров. Измерения проводили по учащенной сетке станций с продвижением судна с запада на восток дважды с недельным интервалом (14–20 июня и 22–28 июня). Показано, что проникновение потока Основного Черноморского течения на полигон во время 2-го этапа измерений привело к более интенсивному поступлению на акваторию полигона азово-керченских вод. Это сопровождалось понижением прозрачности и солености вод и повышением температуры, на которую также оказывал влияние продолжающийся сезонный прогрев. На большей части полигона, по данным обоих этапов измерений, выявлена значимая тенденция к увеличению интенсивности флуоресценции хлорофилла *a* в областях вод с повышенными значениями показателя ослабления направленного света. Показано, что изменения вертикальной термохалинной и биооптической структуры вод на масштабе около недели наблюдались во всем слое измерений и проявлялись в изменении количества и значений максимумов интенсивности флуоресценции хлорофилла *a*, показателя ослабления направленного света, вертикальных градиентов температуры и солености, а также глубин залегания этих параметров. Основной максимум значений показателя ослабления направленного света прослеживался или в поверхностном слое, или в слое сезонных термоклина и галоклина, а максимум интенсивности флуоресценции хлорофилла *a* располагался под слоем сезонных термоклина и галоклина. Выявлена значимая линейная корреляция между распределениями глубины залегания сезонного термоклина и глубин залегания максимумов показателя ослабления направленного света и интенсивности флуоресценции хлорофилла *a*, а также между глубинами залегания сезонного галоклина и максимума интенсивности флуоресценции хлорофилла *a*.

Ключевые слова: Черное море, гидрологические станции, показатель ослабления направленного света, флуоресценция хлорофилла *a*, температура, соленость, циркуляция вод, синоптическая изменчивость

Благодарности: работа выполнена в рамках тем государственного задания ФГБУН ФИЦ МГИ FNNN-2024-0014 «Взаимодействие океана и атмосферы» и FNNN-2024-0012 «Оперативная океанология». Данные получены в Центре коллективного пользования «НИС Профессор Водяницкий» ФГБУН ФИЦ «Институт биологии южных морей имени А.О. Ковалевского РАН».

Для цитирования: Синоптическая изменчивость биооптических и гидрологических параметров у берегов Крыма по данным экспедиционных измерений летом 2023 года / Ю. В. Артамонов [и др.] // Экологическая безопасность прибрежной и шельфовой зон моря. 2025. № 3. С. 6–24. EDN QEZZHL.

Introduction

In recent years, there has been a noticeable increase in anthropogenic pressure on the coastal part of the Black Sea, making assessments of the ecological state of seawater, which is largely reflected in its hydro-optical structure, increasingly relevant [1, 2]. To assess changes in the ecological state of the waters under the influence of various natural and anthropogenic factors, the light beam attenuation coefficient (LAC) is widely used, which reflects the total suspended solids (TSS) content and characterizes water transparency [1)] [3–7]. An important characteristic for assessing primary bioproductivity in water is the content of the photosynthetically active pigment chlorophyll a (*Chl-a*) in marine phytoplankton, determined from measurements of *Chl-a* fluorescence (*F*) or direct measurements [8–13]. In this regard, an important element of environmental monitoring is the study of the variability of LAC and *Chl-a* content at different time scales and the relationship between this variability and the characteristics of the hydrological structure of waters.

Effective monitoring of the hydrological and bio-optical structure of surface waters is conducted using remote sensing methods [2, 14–18]. The use of satellite data has enabled the identification of variability in bio-optical characteristics at different time scales on the surface of the Black Sea [19–22], as well as investigation of the relationship between bio-optical parameters and the thermohaline structure and dynamics of water [23, 24]. According to data from the SeaWiFS and MODIS-Aqua ocean color scanners from the atlas *Bio-optical Characteristics of Russian Seas from Satellite Ocean Color Data*, *Chl-a* concentration exhibits two main peaks in the seasonal cycle: spring (March–May) and autumn (October–November). At the same time, the backscattering coefficient of suspended particles exhibits a pronounced maximum in June [20]. Analysis of the climatic seasonal cycle of *Chl-a* concentration, the diffuse light attenuation coefficient K_d (490), and the remote sensing reflectance R_{rs} (555) based on data from the MODIS-Aqua and NPP-VIIRS satellite scanners from the Copernicus array showed that the main maxima of *Chl-a* concentration and K_d (490) on the northwestern shelf are observed during the period of the highest water warming rate in May. In the southern part of the western shelf and in the deep-water part of the sea, these maxima occur in November, coinciding with the maximum cooling rate of the water. The maximum R_{rs} (555) values in most of the Black Sea are recorded in June, when the water warms most rapidly [21]. According to data from the MODIS-Aqua

---

[1)] Mankovsky, V.I., Solov'iev, M.V. and Mankovskaya, E.V., 2009. [*Hydrooptical Properties of the Black Sea*]. A Reference Book. Sevastopol: MGI NAN Ukrainy, 41 p. (in Russian).

ocean color scanner, the influence of the Rim Current (RC) on the distribution of the remote sensing reflectance is observed in April as a band of elevated R_{rs} values above the continental slope [23]. According to Copernicus data, south of the Crimean coast, the influence of the RC on the spatial distribution of average monthly climatic fields of *Chl-a* and R_{rs} (555) is manifested as "tongues" of water with elevated *Chl-a* concentration, R_{rs} (555), temperature, and reduced salinity. The maximum westward spread of waters carried by the RC (almost to 32° E) in the climatic fields of bio-optical and thermohaline parameters is observed in February, during the period of increased zonal geostrophic velocity of the RC [24]. In [22], based on SeaWiFS and MODIS satellite measurements, trends in interannual variability of chlorophyll concentration on the shelf of the northern Black Sea off the Caucasian and Crimean coasts for the period from 1997 to 2015 were analyzed. It was shown that, despite high variability in average annual chlorophyll concentrations across different years, no long-term trend in the distribution of these values was observed, and no pronounced interannual trends were identified [22].

Information about the bio-optical structure of deep-sea waters can only be obtained using contact methods, while conducting hydrological and bio-optical observations quasi-synchronously with instrumental measurements of currents significantly enhances the interpretation of bio-optical field distribution characteristics. Regular expeditionary studies in the northern Black Sea have enabled the assessment of bio-optical and hydrological fields and their variability across various spatial and temporal scales [11, 13, 24–34]. A summary of detailed hydro-optical surveys conducted as part of the expeditionary research program of Marine Hydrophysical Institute of the Russian Academy of Sciences from 2016 to 2020 on R/V *Professor Vodyanitsky* showed that the main sources of increased TSS concentration in the surface layer off the Crimean coast are low-salinity, turbid waters from the Kerch Strait, riverine inputs from the Caucasian coast, and desalinated waters from the northwestern shelf. In the deep-water part of the sea, localized areas of turbid water were identified, formed under the influence of vertical circulation in regions of cyclonic circulation and meanders of the RC. The vertical structure of TSS concentration was characterized by an upper quasi-homogeneous layer, typically coinciding in thickness with the upper quasi-homogeneous layer of thermohaline parameters. Within this layer, a significant negative linear correlation was observed between TSS concentration and temperature and salinity, while a positive correlation was found with density. In the seasonal thermocline and pycnocline layer, a subsurface maximum of TSS concentration was observed. Below the core of the cold intermediate layer, in the main thermocline, halocline, and pycnocline, an intermediate minimum of TSS concentration was noted. Below this minimum, another layer of increased turbidity was observed, coinciding with the upper boundary of the hydrogen sulfide zone [28].

In June 2023, during the 127th cruise of R/V *Professor Vodyanitsky* in the coastal waters of the Black Sea off the Crimean coast, a comprehensive hydrological and bio-optical survey was conducted, yielding results of particular interest.

Hydrological and bio-optical measurements were performed at a dense network of stations, repeated twice at approximately one-week intervals. The coordinates of the stations surveyed during the two measurement stages were nearly identical, enabling comparison of the measured parameter distributions and assessment of their differences due to synoptic variability. The aim of this study is to analyze the synoptic-scale variability of the light beam attenuation coefficient and *Chl-a* fluorescence distributions off the Crimean coast in the summer of 2023 and to evaluate their relationship with changes in the hydrological structure of the waters.

Materials and methods

Hydrological measurements during the 127th cruise of R/V *Professor Vodyanitsky* in June 2023 were conducted within Russian territorial waters off the Crimean coast, from Cape Sarych to Cape Chauda (Fig. 1). While maintaining the total expedition time (25 days), the measurement area was reduced compared to previous cruises due to administrative restrictions. This allowed for the increased number of hydrological stations, enabling detailed spatial distributions of hydro-optical parameters that reflect the current state of the water structure in the coastal zone of Crimea. The first measurement stage was carried out from June 14 to 20 (64 stations) (Fig. 1, *a*), the second stage from June 22 to 28 (62 stations) (Fig. 1, *b*), with the station coordinates during the two stages almost coinciding.

Seawater temperature (°C) and salinity (PSU) were measured using the IDRONAUT OCEAN SEVEN 320 PlusM CTD probe [2]. The speed and direction of currents (cm/s) were measured using a Workhorse Monitor 300 kHz ADCP acoustic Doppler current profiler [3].

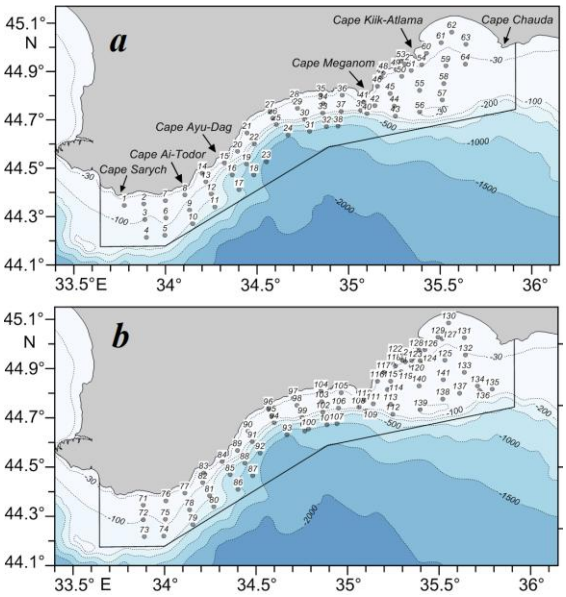

Fig. 1. Map of hydrological stations surveyed near Crimean coasts during the 1st (14–20 June 2023) (*a*) and 2nd (22–28 June 2023) (*b*) cruises of R/V *Professor Vodyanitsky*

[2] URL: http://www.technopolecom.ru/dounloads/doc_212.pdf

[3] URL: https://www.bodc.ac.uk/data/documents/nodb/pdf/workhorse_monitor.pdf

The intensity of chlorophyll a fluorescence (*F Chl-a*, relative units) and the light beam attenuation coefficient at a wavelength of 660 nm (ε_{660}, m^{-1}) were measured using the KONDOR hydrobiophysical multiparametric submersible autonomous complex [4], primarily during daylight hours. Additionally, surface wind speed W (m/s) was continuously recorded at each station using the AIRMAR-220WX shipboard weather station.

In quantitative assessments of the consistency of distributions of bio-optical parameters and the depths of their maxima, as well as seasonal thermoclines and haloclines, the statistical reliability of linear correlation coefficients *R* was evaluated with a statistical significance level of α=0.01 (99% confidence level) according to the methodology [5].

Results

During the first measurement stage, the light beam attenuation coefficient varied within the survey area between 0.6 and 0.83 m^{-1} (Fig. 2, *a*). The most turbid waters (values ε_{660} > 0.77 m^{-1}) were observed in the coastal part of Feodosia Gulf, southeast of Ayu-Dag and at the western boundary of the polygon.

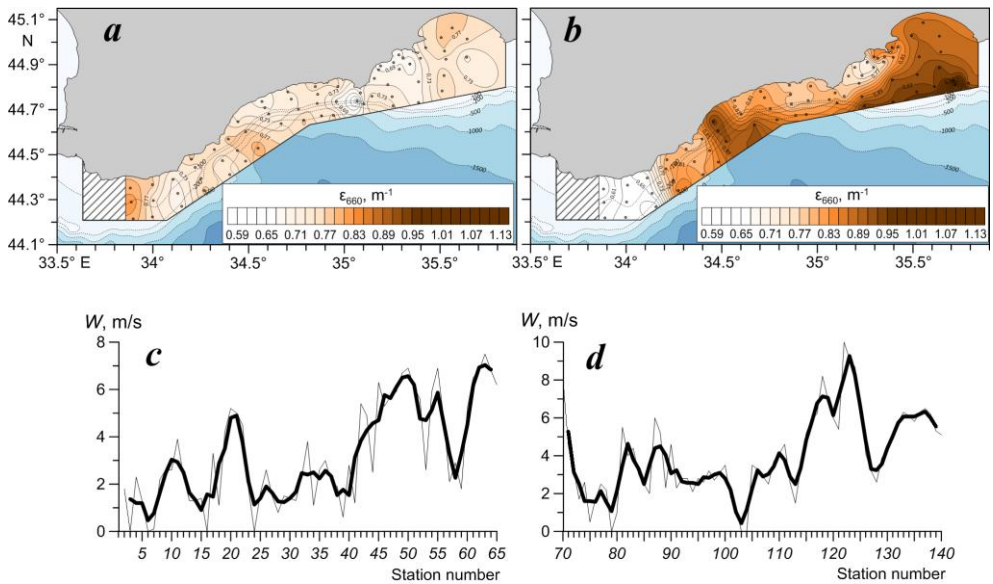

Fig. 2. Distributions of ε_{660} values on the surface (*a*, *b*) and wind speed *W* (*c*, *d*) at stations according to data from the 1st (*a*, *c*) and 2nd (*b*, *d*) stages of the 127th cruise of R/V *Professor Vodyanitsky*. Bold curves in fragments *c*, *d* – smoothing by a moving average over three stations

[4] Available at: http://ecodevice.com.ru/ecodevice-catalogue/multiturbidimeter-kondor [Accessed: 27 August 2025].

[5] Malinin, V.N., 2008. [*Statistical Methods of Analysis of Hydrometeorological Information*]. Saint Petersburg, Izd-vo RGGMU, 408 p. (in Russian).

The increased turbidity in the shallow part of Feodosia Gulf, at depths less than 30 m, was associated with a significant increase in wind speed at stations *61–63* (Fig. 2, *c*), which caused resuspension of bottom and coastal sediments. The clearest waters (values $\varepsilon_{660} < 0.67$ m^{-1}) were observed along the Meganom transect.

During the second stage, one week later, water turbidity at the surface increased significantly across most of the polygon. The ε_{660} values for most of the polygon's water area ranged from 0.65 to 1.15 m^{-1} (Fig. 2, *b*). The highest ε_{660} values (> 0.91 m^{-1}) were recorded east of Cape Ayu-Dag and at the southern border in the eastern part of the polygon. A noticeable increase in ε_{660} values (0.83–0.89 m^{-1}) was observed near the coast in the area of Cape Kiik-Atlam, where, during the first stage of measurements, ε_{660} values did not exceed 0.73 m^{-1}. As in the coastal part of Feodosia Gulf at stations *61–63*, this increase in turbidity was associated with increased wind speed at stations *120–128* (Fig. 2, *d*). The waters with the highest transparency (ε_{660} values < 0.63 m^{-1}) were located at the western border of the polygon, where the highest turbidity was observed during the first stage.

The distribution of *F Chl-a* intensity on the sea surface during the two measurement stages was highly heterogeneous. For technical reasons, *F Chl-a* measurements in the first stage began at station *24* (Fig. 3). Consequently, the comparison of *F Chl-a* distribution was limited to the central and eastern parts of the polygon. During the first measurement stage, *F Chl-a* values ranged from 0.32 to 0.53 relative units, with a patchy spatial distribution. The highest *F Chl-a* values (0.47–0.53 relative units) were observed at the southern border of the polygon, approximately between 34.6° and 34.8° E. The lowest *F Chl-a* values (< 0.35 relative units) were recorded near the coast in the Cape Meganom area and in the eastern part of Feodosia Gulf (Fig. 3, *a*).

During the second stage of measurements, a general increase in *F Chl-a* values was observed across almost the entire water area of the polygon (Fig. 3, *b*). The highest *F Chl-a* values ranged from 0.59 to 0.61 relative units. The lowest *F Chl-a* values (< 0.33 relative units), as in the first stage, were observed at the eastern border of the polygon. In the coastal zone near Cape Meganom, where the lowest *F Chl-a* values were observed during the first stage, a noticeable increase in *F Chl-a* intensity (0.45–0.50 relative units) was recorded during the second stage (Fig. 3, *b*).

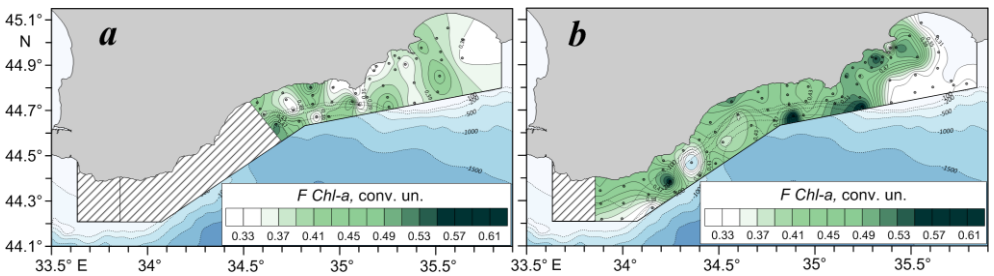

Fig. 3. Distributions of chlorophyll a fluorescence intensity during the 1st (*a*) and 2nd (*b*) stages of the 127th cruise of R/V *Professor Vodyanitsky*

Notably, during the second stage, waters at the eastern border of the polygon with reduced *F Chl-a* intensity were characterized by increased turbidity (Fig. 2, *b*; 3, *b*).

Overall, despite the observed differences in the distribution of the light beam attenuation coefficient and *F Chl-a* intensity between the first and second stages, a significant trend of increasing *F Chl-a* intensity was identified in areas of elevated water turbidity across most of the polygon (Fig. 4). The exception is the water area at the eastern border of the polygon, characterized by increased turbidity during the second stage. In this area, a decrease in *F Chl-a* intensity was observed (Fig. 2, *b*; 3, *b*; 4, *c*).

Analysis of the distribution of flow vectors based on instrumental measurements showed that differences between the distribution of ε_{660} values during the two measurement stages were associated with noticeable changes in water circulation (Fig. 5). Thus, the main westward flow characterizing the RC was most clearly traced only in the western part of the polygon during the first stage, while east of Cape Ai-Todor, a flow in the opposite eastern direction was observed (Fig. 5, *a*). In the eastern part of the polygon, well-defined synoptic vortices were observed – cyclonic south of Feodosia Gulf (Feodosia cyclone) and anticyclonic slightly west of the Karadag traverse (Karadag anticyclone). This water circulation pattern shows that over most of the water area east of Cape Ai-Todor, the main RC flow was located further south, outside the polygon.

During the second stage, the circulation pattern changed significantly (Fig. 5, *b*). Across most of the water area, except for Feodosia Gulf, westward currents corresponding to the RC flow were observed. In the central part of the polygon, one branch of the RC flow turned north, then northeast, forming the Crimean anticyclone, while the other branch continued westward.

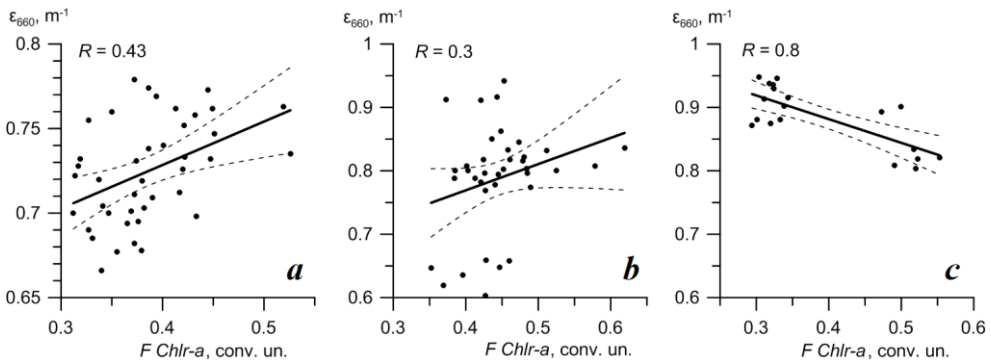

Fig. 4. Graphs of the linear correlation between the values of *F Chl-a* and ε_{660} according to the data of the 1st stage at stations *24–65* (*a*), the 2nd stage at stations *71–119* (*b*) and *120–141* (*c*). Dashed lines are the boundaries of the 99% confidence interval

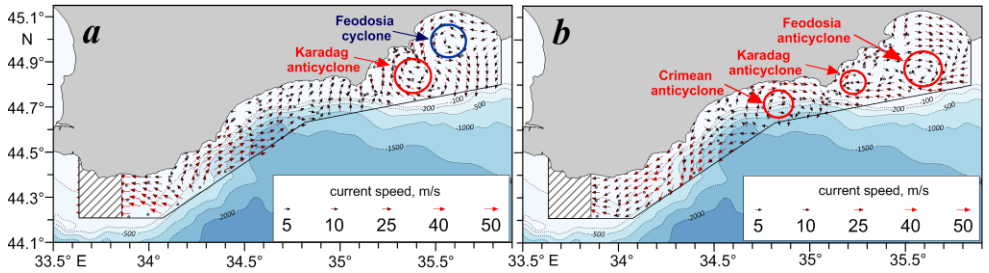

Fig. 5. Distributions of vectors of instrumentally measured currents (cm/s) in the surface layer according to data from the 1st (*a*) and 2nd (*b*) stages of the 127th cruise of R/V *Professor Vodyanitsky*. Anticyclonic eddies are shown in red, cyclonic eddies are shown in blue

The Karadag anticyclone persisted in the eastern part of the polygon. Instead of the Feodosia cyclone, an anticyclonic vortex formed closer to the southern border of the polygon, provisionally named the Feodosia anticyclone (Fig. 5, *b*).

The distributions of temperature (TPM) and salinity (SPM) at the sea surface during the two measurement stages differed significantly (Fig. 6). Weekly temporal changes were evident in a noticeable increase in TPM values (22.6–25.3°C) during the second stage compared to the first stage, when TPM values ranged from 20.6 to 23.4°C (Fig. 6, *a*, *b*). This increase in TPM was associated with both ongoing seasonal warming of surface waters, as the second stage occurred one week later, and the inflow of water into the polygon's water area, carried by the RC flow from the southeast to the shores of Crimea. These waters were characterized by elevated temperatures and reduced salinity [24], which was associated with the influence of the Azov-Kerch desalination, in which Azov Sea waters penetrate through the Kerch Strait and move westward along the northern periphery of the RC [24, 35]. The influence of Azov-Kerch desalination on the salinity field at the sea surface (Fig. 6, *c*, *d*) was most clearly evident during the second stage of measurements in the central part of the polygon. Desalinated waters with SPM values below 17.9 PSU, carried by the RC flow, spread along the periphery of the Crimean anticyclone to the northeast, then followed the coast in an easterly direction and further to the southeast (Fig. 6, *d*).

In addition to reduced salinity, the Azov-Kerch waters are also characterized by increased turbidity [24, 35], which led to an increase in ε_{660} values during the second stage of measurements, most evident in the southeastern and central parts of

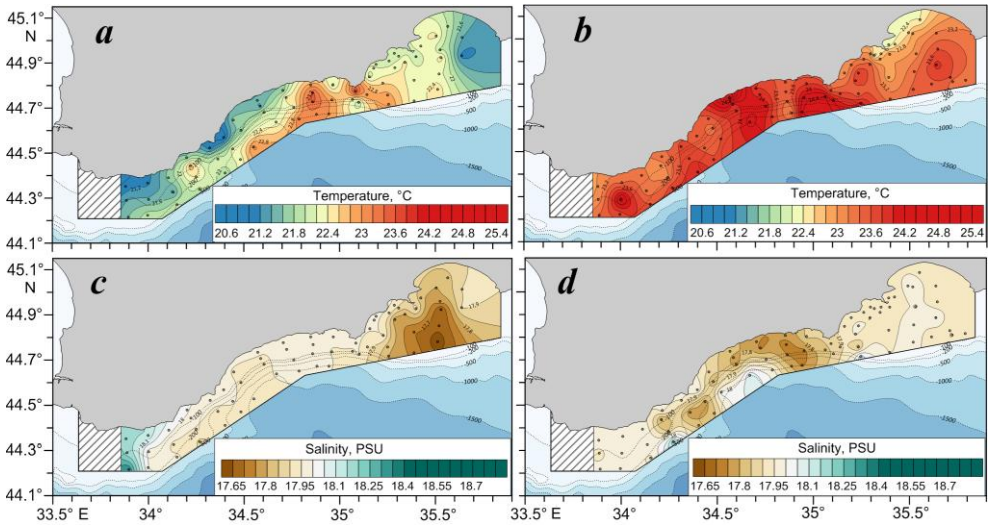

Fig. 6. Distributions of temperature (*a*, *b*) and salinity (*c*, *d*) at the 2 m horizon according to data from the 1st (*a*, *c*) and 2nd (*b*, *d*) stages of the 127th cruise of R/V *Professor Vodyanitsky*

the polygon (Fig. 2, *b*). Notably, in the eastern part of the polygon, where increased turbidity was observed during the second stage, a noticeable decrease in *Chl-a* fluorescence intensity was recorded. This may be associated with the penetration of Azov-Kerch waters into the southeastern part of the polygon, which then spread along the periphery of the Feodosia anticyclone to the entire eastern part of the water area. According to [36], during the measurement period (June), the concentration of *Chl-a* in the Sea of Azov reaches its lowest values.

Thus, changes in the distribution of the light beam attenuation coefficient, temperature, and salinity at the sea surface on a synoptic time scale (approximately one week) were primarily due to variability in water circulation. The penetration of the RC flow into the polygon during the second stage of measurements led to a more intensive inflow of Azov-Kerch waters into the polygon's water area, which was accompanied by a decrease in transparency and salinity and an increase in temperature, further influenced by ongoing seasonal warming.

The vertical distribution of the light beam attenuation coefficient, *F Chl-a* intensity, temperature, and salinity showed that the thermohaline and bio-optical fields were characterized by well-defined summer vertical stratification. Examples of vertical profiles of ε_{660}, *F Chl-a*, and vertical gradients of temperature (VTG) and salinity (VSG) at stations measured at the same point at weekly intervals in different parts of the polygon are shown in Fig. 7. Synoptic changes in the vertical bio-optical and thermohaline structure of the water column on a scale of approximately one week were observed throughout the measurement layer and were evident in changes in the number and magnitude of the ε_{660}, *F Chl-a*, VTG (in absolute terms) and VSG maxima, as well as their depths.

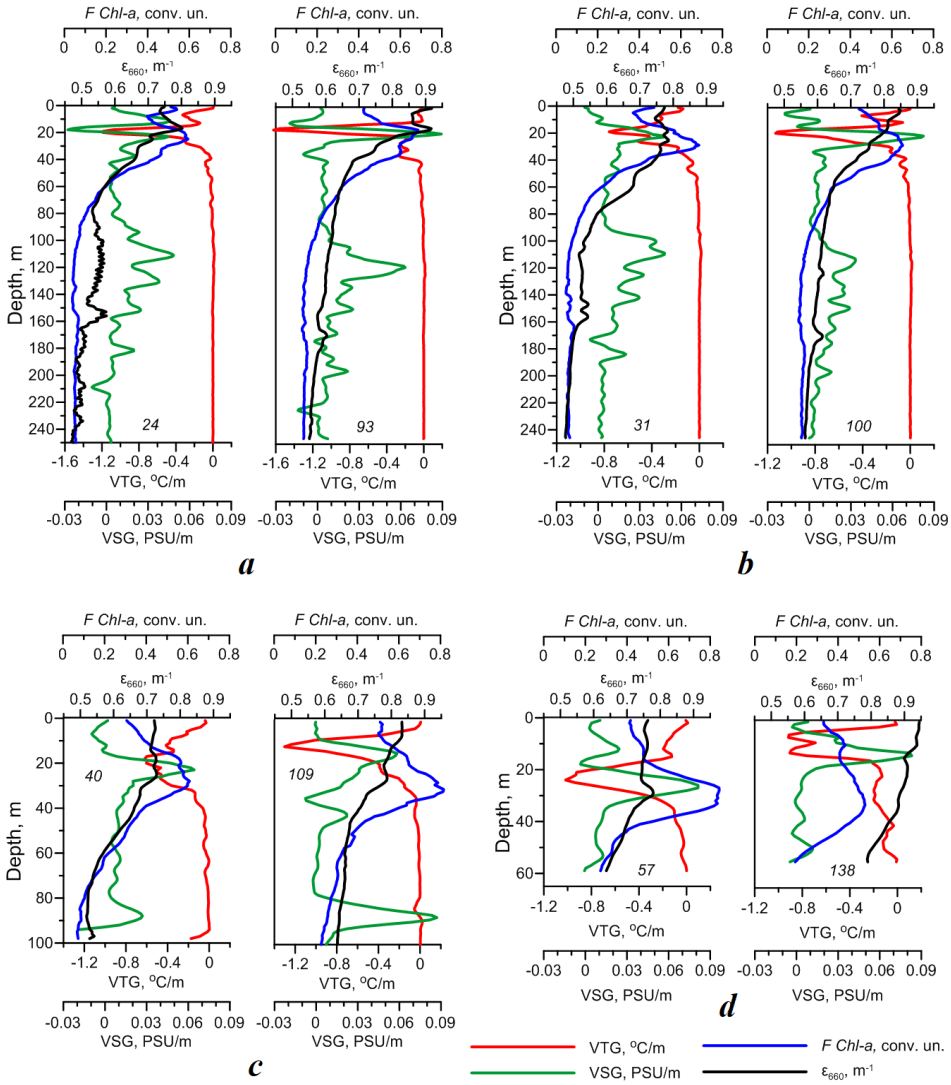

Fig. 7. Vertical distributions of *F Chl-a*, ε_{660}, VTG and VSG values at stations carried out at the same point with a weekly interval in different parts of the polygon. The station numbers are indicated on the graphs

For example, at station *24* (stage 1), one main ε_{660} maximum (0.8 m^{-1}) was observed at a depth of 18 m. One week later (station *93*, stage 2), two ε_{660} maxima (0.92 m^{-1}) were observed – at the surface and at a depth of 16 m. The main *F Chl-a* intensity maximum at station *24* was located at a depth of 25 m, while at station *93*, it was at a depth of 18 m, with its value increasing from 0.6 to 0.7 relative units (Fig. 7, *a*).

The thermohaline structure at station *24* was characterized by one main maximum VTG (1.2°C/m) at a depth of 20 m and two maximum VSG (0.045 PSU/m) at depths of 11 m and 22 m. One week later (station *93*), one maximum VTG and VSG were observed at depths of 18–20 m, with values increasing to 1.6°C/m and 0.09 PSU/m, respectively (Fig. 7, *a*).

Further east, at station *31* (stage 1), two maxima of ε_{660} (0.78 m^{-1}) were detected at depths of 18 m and 23 m. One week later (station 100), ε_{660} maxima (0.85 m^{-1}) were observed in the surface layer. The maximum *F Chl-a* intensity, based on data from both stages, was located at a depth of 30 m, with its value decreasing from 0.7 relative units (station *31*) to 0.65 relative units (station *100*) (Fig. 7, *b*). The seasonal thermocline (VTG ~ 0.78°C/m) and halocline (VSG ~ 0.05 PSU/m) at station *31* were located at depths of 20–21 m. One week later (station *100*), their depth remained unchanged, but their values increased to 1.17°C/m and 0.08 PSU/m, respectively (Fig. 7, *b*).

In the Cape Meganom area at station *40* (stage 1), maxima of ε_{660} (0.74 m^{-1}) were observed at depths of 18 m and 25 m. One week later (station *109*), these maxima increased to 0.84 m^{-1} and were observed in the surface layer at depths of 2–7 m. The maximum *F Chl-a* intensity at stations *40* and *109* was detected at depths of 28 m and 32 m, respectively, with its value increasing from 0.6 to 0.8 relative units (Fig. 7, *c*). The maximum VTG value increased from 0.6°C/m (station *40*) to 1.3°C/m (station *109*). The maximum VSG values at both stations ranged from 0.06 to 0.063 PSU/m. The depths of the seasonal thermocline and halocline decreased from 18 m and 22 m at station *40* to 12 m and 15 m at station *109* (Fig. 7, *c*).

In the eastern part of the polygon, at shallow station *57*, the main maxima ε_{660} (0.77 m^{-1}) were observed at a depth of 30 m. One week later (station *138*), the ε_{660} maxima (0.95 m^{-1}) were observed in the surface layer at depths of 2–10 m. The maximum *F Chl-a* intensity, in contrast, decreased from 0.95 relative units (station *57*) to 0.77 relative units (station *138*). It was observed in the layer 27–32 m at station *57* and at a depth of 32 m at station *138* (Fig. 7, *d*). The depths of the VTG and VSG maxima at station *57* were 24 m and 27 m, respectively. At station *138*, two well-defined VTG maxima were observed at depths of 5 m and 12 m, while the depth of the VSG maximum decreased to 12 m. The maximum VTG values decreased from 1°C/m (station *57*) to 0.9°C/m (station *138*), and the maximum VSG values at both stations ranged from 0.080 to 0.082 PSU/m (Fig. 7, *d*).

Notably, at deep-water stations, another maximum of ε_{660} was observed below the main halocline, located approximately in the 150–170 m layer (Fig. 7, *a*, *b*), which, according to [37], corresponds to the lower boundary of the suboxic redox zone and the upper layer of the hydrogen sulfide zone. According to previous expedition measurements, a maximum concentration of TSS was also detected at these depths [29, 30]. This increase in ε_{660} values (up to 0.6 m^{-1}) was observed in both measurement stages, but the depth of these maxima varied by 10–15 m over the week (Fig. 7, *a*, *b*).

Overall, during the second stage of measurements, an increase in the maximum VTG (Fig. 8, *a*) and VSG (Fig. 8, *b*) values was observed across most of the polygon, indicating more pronounced vertical thermohaline stratification. In the subsurface layer, there was also an increase in ε_{660} values, particularly in the eastern part of the polygon (Fig. 8, *c*), an increase in *F Chl-a* intensity across most of the polygon, and a decrease in these values in the eastern part of the polygon (Fig. 8, *d*).

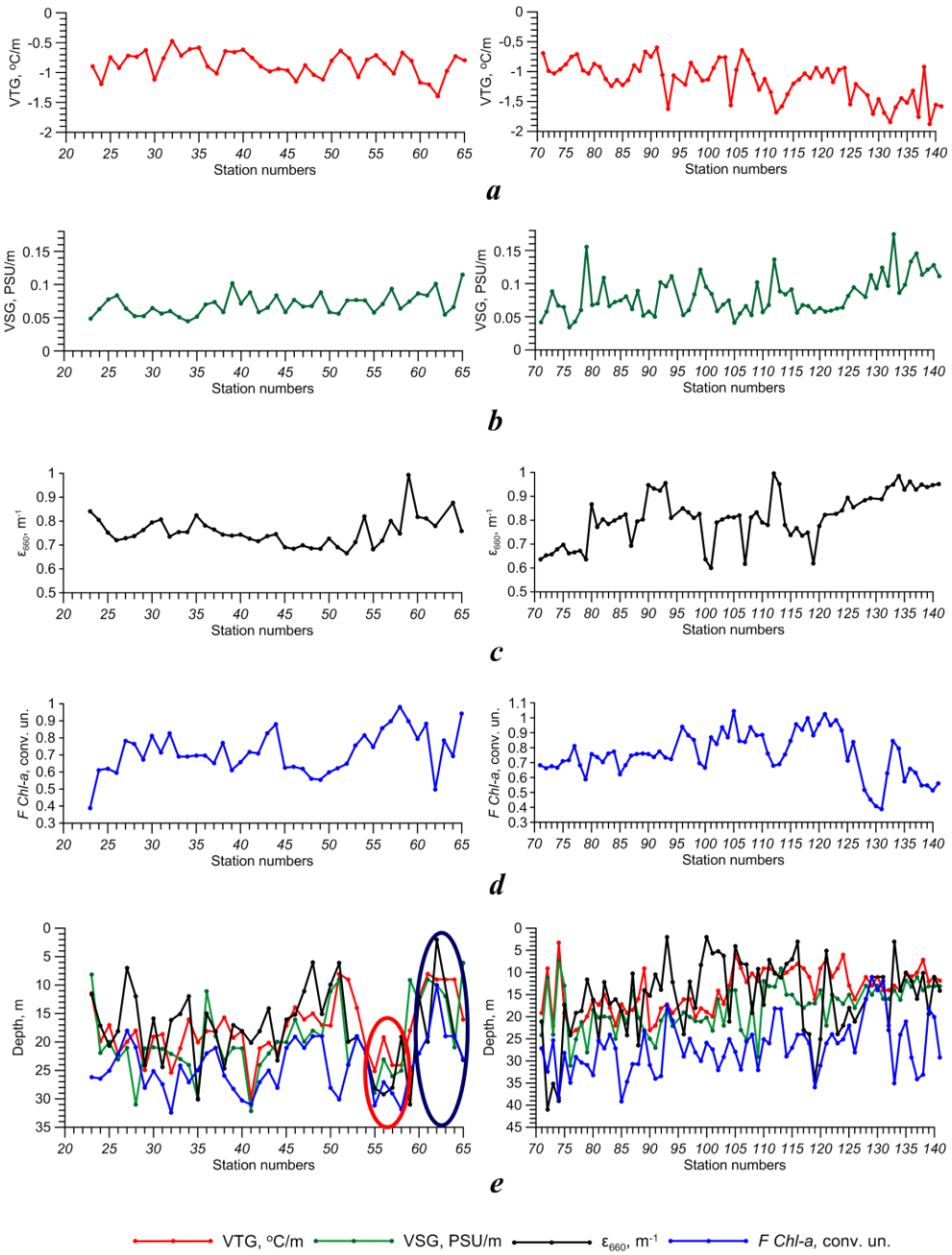

Fig. 8. Distributions of the main maxima of VTG (*a*), VSG (*b*), ε_{660} (*c*), *F Chl-a* (*d*) values, their depths (*e*) at stations according to data from the 1st (left) and 2nd (right) stages of the 127th cruise of R/V *Professor Vodyanitsky*. The red ellipse highlights the depths of the parameters at stations located in the area of the Karadag anticyclone, and the blue ellipse highlights the depths of the parameters at stations located in the area of the Feodosia cyclone.

The distribution of the depths of the main maxima of VTG, VSG, ε_{660} and *F Chl-a* intensity at all stations showed that the depths of the seasonal thermocline during the first stage ranged from 7 to 30 m, while during the second stage, the thermocline rose closer to the surface and was located at depths of 4–24 m (Fig. 8, *e*). The seasonal halocline was observed at depths of 6 to 32 m during both stages (Fig. 8, *e*). Analysis of vertical profiles of ε_{660} values during both stages showed that the maximum ε_{660} values were observed either in the surface layer or within the seasonal thermocline and halocline layers, consistent with the depth of the maximum concentration of TSS according to long-term expedition measurements [28]. According to data from all stations, the maximum *F Chl-a* intensity was located below the seasonal thermocline and halocline layers (Fig. 8, *e*). The distribution of depths of the maximum thermohaline and bio-optical parameters during the first stage of measurements clearly showed the dynamics of water masses. There was a noticeable increase in these depths at stations located in the Karadag anticyclone area (stations *54–59*, highlighted with a red ellipse) and a decrease at stations in the Feodosia cyclone area (stations *60–65*, highlighted with a blue ellipse) (Fig. 8, *e*). Analysis of the vertical structure of water circulation showed that these synoptic vortices were clearly visible throughout the entire upper 50 m layer.

During the second stage of measurements, synoptic anticyclonic vortices were evident only in the upper 10 m layer, so the circulation features were minimally reflected in the distribution of the depths of the thermohaline and bio-optical parameters (Fig. 8, *e*).

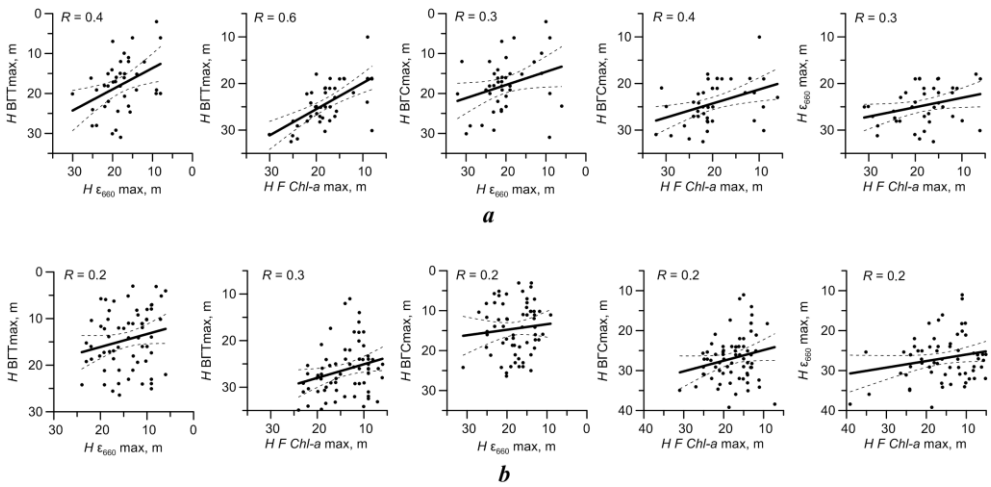

Fig. 9. Graphs of the linear correlation between the depths of occurrence of the maxima of *F Chl-a*, ε_{660}, VTG and VSG according to the data of the 1st (*a*) and 2nd (*b*) stages of the 127th cruise of R/V *Professor Vodyanitsky*. Dashed lines are the boundaries of the confidence interval of the 99% level of statistical significance

Quantitative assessments of the consistency of the distributions of the depths of the maximum bio-optical parameters and the seasonal thermocline and halocline (Fig. 9) showed that the strongest relationship between these parameters was observed during the first stage of measurements (Fig. 9, *a*). A significant direct linear correlation, with a statistical significance level of $\alpha = 0.01$ (99% confidence level), was found between the depth of the seasonal thermocline and the depths of the maximum ε_{660} and *F Chl-a* intensity, as well as between the depths of the seasonal halocline and the maximum *F Chl-a* intensity. The correlation coefficients *R* for these relationships were 0.4, 0.6, and 0.4, respectively. The linear correlation between the depth of the seasonal halocline and the maximum ε_{660}, as well as between the maxima of ε_{660} and *F Chl-a*, was weaker, with *R* values of 0.3 (Fig. 9, *a*).

During the second stage of measurements, the relationship between the distributions of the depths of the maximum bio-optical parameters and the seasonal thermocline and halocline remained significant at $\alpha = 0.01$, but weakened noticeably, with *R* values not exceeding 0.3 (Fig. 9, *b*).

Conclusions

According to hydrological and bio-optical measurements conducted in June 2023 during the 127th cruise of R/V *Professor Vodyanitsky* off the coast of Crimea, the variability of the distribution of the light beam attenuation coefficient and *F Chl-a* intensity on a synoptic scale was analyzed, and the relationship between this variability and changes in the hydrological structure of the waters was assessed. Across most of the polygon, data from both measurement stages revealed a significant trend of increasing *F Chl-a* intensity in areas with elevated light beam attenuation coefficient values. It was shown that changes in the distribution of temperature, salinity, and LAC values at the sea surface on a weekly time scale were associated with changes in water circulation. During the second stage of measurements, warmer, less saline, and more turbid Azov-Kerch waters penetrated the polygon with the RC flow, leading to a decrease in salinity in the central part of the polygon, an increase in turbidity in the southeastern and central parts of the polygon, and an increase in temperature, further influenced by ongoing seasonal warming. The Azov-Kerch waters entering the southeastern part of the polygon and then spreading to the entire eastern part of the water area along the periphery of the Feodosia anticyclone contributed to a decrease in *F Chl-a* intensity in the area of increased turbidity at the eastern border of the polygon, as the concentration of *Chl-a* in the Sea of Azov during the measurement period was reduced.

It has been shown that synoptic changes in the vertical thermohaline and bio-optical structure of waters on a scale of approximately one week were observed throughout the measurement layer and were evident in changes in the number and magnitude of the maxima of LAC, *F Chl-a*, VTG and VSG, as well as their depths. During the second stage of measurements, thermohaline fields were characterized by more pronounced vertical stratification across most of the polygon.

In the subsurface layer, as at the surface, there was an increase in LAC values, particularly in the eastern part of the polygon, an increase in *F Chl-a* intensity across most of the polygon, and a decrease in these values in the eastern part of the polygon. The main LAC maxima were observed either in the surface layer or within the seasonal thermocline and halocline layers, while the maximum *F Chl-a* intensity was located below the seasonal thermocline and halocline layers. At deep-water stations, another LAC maximum was observed below the main halocline layer, located in the 150–170 m layer, corresponding to the lower boundary of the suboxic redox zone and the upper layer of the hydrogen sulfide zone.

A significant linear correlation was found between the depth of the seasonal thermocline and the depths of the maximum LAC values and *F Chl-a* intensity, as well as between the depth of the seasonal halocline and the maximum *F Chl-a* intensity, based on data from the first stage of measurements, with *R* coefficients of 0.4, 0.6, and 0.4, respectively.

REFERENCES

1. Ivanov, V.A., Katunina, E.V. and Sovga, E.E., 2016. Assessment of Anthropogenic Impacts on the Ecosystem of the Waters of the Herakleian Peninsula in the Vicinity of Deep Drains, *Processes in GeoMedia*, (5), pp. 62–68 (in Russian).
2. Bondur, V.G., Ivanov, V.A., Vorobiev, V.E., Dulov, V.A., Dolotov, V.V., Zamshin, V.V., Kondratiev, S.I., Lee, M.E. and Malinovsky, V.V., 2020. Ground-to-Space Monitoring of Anthropogenic Impacts on the Coastal Zone of the Crimean Peninsula. *Physical Oceanography*, 27(1), pp. 95-107. https://doi.org/10.22449/1573-160X-2020-1-95-107
3. Eisma, D., 1993. *Suspended Matter in the Aquatic Environment*. Berlin, Heidelberg: Springer-Verlag, 315 p. https://doi.org/10.1007/978-3-642-77722-6
4. Man'kovskii, V.I. and Solov'ev, M.V., 2003 Relationship between the Beam Attenuation Coefficient and the Concentration of Suspended Matter in Black-Sea Waters. *Physical Oceanography*, 13(2), 123–128. https://doi.org/10.1023/A:1023752514790
5. Izrael, Yu.A. and Tsyban, A.V., 2009. [*Anthropogenic Ecology of the Ocean*]. Moscow: Flinta, 520 p. (in Russian).
6. Kukushkin, A.S., Agafonov, E.A. and Prokhorenko, Yu.A., 2006. Distribution of the Beam Attenuation Coefficient in the Black Sea Surface Coastal Waters. *Morskoy Gidrofizicheskiy Zhurnal*, (5), pp. 30–43 (in Russian).
7. Kukushkin, A.S., 2017. Spatial and Temporal Variability of the Water Transparency Distribution in the North-Western Black Sea. *Atmospheric and Oceanic Optics*, 30(9), pp. 750–762. https://doi.org/10.15372/AOO20170904 (in Russian).
8. Hoepffner, N. and Sathyendranath, S., 1992 Bio-Optical Characteristics of Coastal Waters: Absorption Spectra of Phytoplankton and Pigment Distribution in the Western North Atlantic. *Limnology and Oceanography*, 37(8), pp. 1660–1679. https://doi.org/10.4319/lo.1992.37.8.1660
9. McManus, G.B. and Dawson, R., 1994. Phytoplankton Pigments in the Deep Chlorophyll Maximum of the Caribbean Sea and the Western Tropical Atlantic Ocean. *Marine Ecology Progress Series*, 113, pp. 199–206. https://doi.org/10.3354/meps113199
10. Mordasova, N.V., 2014. Indirect Estimation of Water Productivity by the Chlorophyll Content. *Trudy VNIRO*, 152, pp. 41–56 (in Russian).

11. Moiseeva, N.A., Churilova, T.Ya., Efimova, T.V., Krivenko, O.V. and Matorin, D.N., 2019. Fluorescence of Chlorophyll a During Seasonal Water Stratification in the Black Sea. *Physical Oceanography*, 26(5), pp. 425–437. https://doi.org/10.22449/1573-160X-2019-5-425-437

12. Temerdashev, Z.A., Pavlenko, L.F., Ermakova, Ya.S., Korpakova, I.G. and Eletskii, B.D., 2019. Extraction-Fluorimetric Determination of Chlorophyll "A" in the Natural Waters. *Analytics and Control*, 23(3), pp. 323–333 (in Russian).

13. Mansurova, I.M., Stelmakh, L.V. and Farber, A.A., 2023. Vertical Distribution of Chlorophyll "A" Concentration in the Black Sea in the Summer and Autumn Periods according to the Data of the Probe CTD Complex and Direct Measurements. *Monitoring systems of environment*, (2), pp. 84–91 (in Russian).

14. Volpe, V., Silvestri, S. and Marani, M., 2011. Remote sensing retrieval of suspended sediment concentration in shallow waters. *Remote Sensing of Environment*, 115(1), pp. 44–54. https://doi.org/10.1016/j.rse.2010.07.013

15. Kremenchutskiy, D.A., Kubryakov, A.A., Zav'yalov, P.O., Konovalov, B.V., Stanichniy, S.V. and Aleskerova, A.A., 2014. Determination of the Suspended Matter Concentration in the Black Sea Using to the Satellite MODIS Data. In: MHI, 2014. *Ekologicheskaya Bezopasnost' Pribrezhnoy i Shel'fovoy Zon i Kompleksnoe Ispol'zovanie Resursov Shel'fa* [Ecological Safety of Coastal and Shelf Zones and Comprehensive Use of Shelf Resources]. Sevastopol: ECOSI-Gidrofizika. Iss. 29, pp. 5–9 (in Russian).

16. Suslin, V.V., Churilova, T.Ya., Lee, M., Moncheva, S. and Finenko, Z.Z., 2018. Comparison of the Black Sea Chlorophyll-A Algorithms for SeaWIFS and Modis Instruments. *Fundamental and Applied Hydrophysics*, 11(3), pp. 64–72. https://doi.org/10.7868/S2073667318030085 (in Russian).

17. Xiaolong, Y., Zhongping, L., Fang, S., Menghua, W., Jianwei, W., Lide, J. and Zhehai, S., 2019. An Empirical Algorithm to Seamlessly Retrieve the Concentration of Suspended Particulate Matter from Water Color across Ocean to Turbid River Mouths. *Remote Sensing of Environment*, 235, 111491. https://doi.org/10.1016/j.rse.2019.111491

18. Zamshin, V.V., Matrosova, E.R., Khodaeva, V.N. and Chvertkova, O.I., 2021. Quantitative Approach to Studying Film Pollution of the Sea Surface Using Satellite Imagery. *Physical Oceanography*, 28(5), pp. 567–578. https://doi.org/10.22449/1573-160X-2021-5-567-578

19. Suetin, V.S., Suslin, V.V., Korolev, S.N. and Kucheryavyi, A.A., 2002. Analysis of the Variability of the Optical Properties of Water in the Black Sea in Summer 1998 according to the Data of a SeaWiFS Satellite Instrument. *Physical Oceanography*, 12(6), pp. 331–340. https://doi.org/10.1023/A:1021729229168

20. Kopelevich, O.V., Sheberstov, S.V., Saling, I.V., Vazyulya, S.V. and Burenkov, V.I., 2015. Seasonal and Inter-Annual Changeability of Bio-Optical Characteristics in the Surface Layer of the Barents, White, Black and Caspian Seas from Satellite Data. *Fundamental and Applied Hydrophysics*, 8(1), pp. 7–16 (in Russian).

21. Artamonov, Yu.V., Skripaleva, E.A., Latushkin, A.A. and Fedirko, A.V., 2019. Multi-Year Average Intra-Annual Cycle of Hydrooptical Characteristics, Chlorophyll A and Surface Temperature of the Black Sea from Satellite Data. *Sovremennye Problemy Distantsionnogo Zondirovaniya Zemli iz Kosmosa*, 16(1), pp. 171–180 (in Russian).

22. Kovalyova, I.V., Finenko, Z.Z. and Suslin, V.V., 2021. Trends of Long-Term Changes in Chlorophyll Concentration, Primary Production of Phytoplankton and Water Temperature in the Shelf Regions of the Black Sea. *Sovremennye Problemy Distantsionnogo Zondirovaniya Zemli iz Kosmosa*, 18(4), pp. 228–235 (in Russian).

23. Karabashev, G.S. and Evdoshenko, M.A., 2015. Manifestations of the Rim Current, Coccolithophore Blooms, And Continental Runoff in the Long-Term Monthly Mean Distributions of Satellite Reflectance Coefficients of the Black Sea. *Oceanology*, 55(1), pp. 36–46. https://doi.org/10.1134/S0001437015010087
24. Artamonov, Yu.V., Latushkin, A.A., Skripaleva, E.A. and Fedirko, A.V., 2019. Rim Current Manifestation in the Climatic Fields of Hydro-Optical and Hydrological Characteristics at the Coast of Crimea. In: SPIE, 2019. *Proceedings of SPIE*. Bellingham: SPIE. Vol. 11208: 25th International Symposium on Atmospheric and Ocean Optics: Atmospheric Physics, 112084X. https://doi.org/10.1117/12.2540803
25. Lomakin, P.D., Chepyzhenko, A.I. and Chepyzhenko, A.A., 2007. Estimation to concentrations of total suspension and dissolved organic matter of the artificial origin in the bays of the Crimea according to optical measurements. In: MHI, 2007. *Ekologicheskaya Bezopasnost' Pribrezhnoy i Shel'fovoy Zon i Kompleksnoe Ispol'zovanie Resursov Shel'fa* [Ecological Safety of Coastal and Shelf Zones and Comprehensive Use of Shelf Resources]. Sevastopol: MHI. Iss. 15, pp. 168–176 (in Russian).
26. Lee, M.E., Latushkin, A.A. and Martynov, O.V., 2018. Long-Term Transparency Variability of the Black Sea Surface Waters. *Fundamental and Applied Hydrophysics*, 11(3), pp. 40–46. https://doi.org/10.7868/S207366731803005X (in Russian).
27. Efimova, T.V., Churilova, T.Ya., Skorokhod, E.Yu., Moiseeva, N.A. and Zemlianskaia, E.A., 2020. Vertical Distribution of Bio-Optical Properties of the Azov – Black Sea Basin Waters in April – May, 2019. *Physical Oceanography*, 27(5), pp. 525–534. https://doi.org/10.22449/1573-160X-2020-5-525-534
28. Latushkin, A.A., Artamonov, Yu.V., Skripaleva, E.A. and Fedirko, A.V., 2022. The Relationship of the Spatial Structure of the Total Suspended Matter Concentration and Hydrological Parameters in the Northern Black Sea according to Contact Measurements. *Fundamental and Applied Hydrophysics*, 15(2), pp. 124–137. https://doi.org/10.48612/fpg/4heu-kxbn-gg7t (in Russian).
29. Artamonov, Yu.V., Skripaleva, E.A., Latushkin, A.A., Fedirko, A.V. and Ryabokon, D.A., 2022. Hydrological Water Structure and Distribution of Total Suspended Matter off the Coast of Crimea in Spring 2021. *Ecological Safety of Coastal and Shelf Zones of Sea*, (4), pp. 6–24.
30. Stelmakh, L., Kovrigina, N. and Gorbunova, T., 2023. Phytoplankton Seasonal Dynamics under Conditions of Climate Change and Anthropogenic Pollution in the Western Coastal Waters of the Black Sea (Sevastopol Region). *Journal of Marine Science and Engineering*, 11(3), 569. https://doi.org/10.3390/jmse11030569
31. Latushkin, A.A., Artamonov, Yu.V., Skripaleva, E.A. and Fedirko, A.V., 2023. Spatial Structure of Turbidity and Chlorophyl-A Fields near the Crimean Coasts according to Natural Measurement In July 2022. In: IO RAS, 2023. *Proceedings of the XII All-Russian Conference with International Participation "Current Problems in Optics of Natural Waters". 25–27 October 2023, Saint Petersburg. Vol. 13*. Moscow: Shirshov Institute Publishing House, pp. 92–96 (in Russian).
32. Krasheninnikova, S.B. and Babich, S.A., 2022. Spatial Distribution of Chlorophyll-A Concentration in Hydrological, Hydrochemical and Hydroptical Conditions of the Black Sea in Spring 2021. *Proceedings of the T.I.Vyazemsky Karadag Scientific Station – Nature Reserve of the Russian Academy of Sciences*. (3), pp. 13–22 (in Russian).
33. Korchemkina, E.N. and Mankovskaya, E.V., 2024. Spectral Reflectance Coefficient, Color Characteristics and Relative Transparency of the Black Sea Waters in Spring, 2019 and 2021: Comparative Variability and Empirical Relationships. *Physical Oceanography*, 31(1), pp. 3–17.

34. Piontkovski, S.A., Zagorodnyaya, Yu.A., Serikova, I.M., Minski, I.A., Kovaleva, I.V. and Georgieva, E.Yu., 2024. Interannual Variability of Physical and Biological Characteristics of Crimean Shelf Waters in Summer Season (2010–2020). *Ecological Safety of Coastal and Shelf Zones of Sea*, (2), pp. 39–59.

35. Aleskerova, A.A., Kubryakov, A.A., Goryachkin, Yu.N. and Stanichny, S.V., 2017. Propagation of Waters from the Kerch Strait in the Black Sea. *Physical Oceanography*, (6), pp. 47–57. https://doi.org/10.22449/1573-160X-2017-6-47-57

36. Saprygin, V.V., Berdnikov, S.V., Kulygin, V.V., Dashkevich, L.V. and Mestetskiy, L.M., 2018. Spatial Distribution and Seasonal Dynamics of the Chlorophyll A Concentration in the Sea of Azov Based on MERIS Images. *Oceanology*, 58(5), pp. 689–699. https://doi.org/10.1134/S0001437018050132

37. Yakushev, E.V., Chasovnikov, V.K., Podymov, O.I., Pakhomova, S.V., Stunzhas, P.A. and Murray, J.W., 2008. Vertical Hydro-Chemical Structure of the Black Sea. In: A.G. Kostianoy, A.N. Kosarev, eds., 2008. *The Black Sea Environment. The Handbook of Environmental Chemistry*. Berlin, Heidelberg: Springer, Vol. 5Q, pp. 277–307. https://doi.org/10.1007/698_5_088

Submitted 25.09.2024; accepted after review 08.11.2024;
revised 24.06.2025; published 30.09.2025

About the authors:

Yuri V. Artamonov, Leading Research Associate, Marine Hydrophysical Institute of RAS (2 Kapitanskaya St., Sevastopol, 299011, Russian Federation), DSc (Geogr.), **ResearcherID: AAC-6651-2020**, **ORCID ID: 0000-0003-2669-7304**, *artam-ant@yandex.ru*

Elena A. Skripaleva, Senior Research Associate, Marine Hydrophysical Institute of RAS (2 Kapitanskaya St., Sevastopol, 299011, Russian Federation), PhD (Geogr.), **ResearcherID: AAC-6648-2020**, **ORCID ID: 0000-0003-1012-515X**, *sea-ant@yandex.ru*

Aleksandr A. Latushkin, Senior Research Associate, Marine Hydrophysical Institute of RAS (2 Kapitanskaya St., Sevastopol, 299011, Russian Federation), PhD (Geogr.), **Researcher ID: U-8871-2019, ORCID ID: 0000-0002-3412-7339**, *sevsalat@gmail.com*

Aleksandr V. Fedirko, Junior Research Associate, Marine Hydrophysical Institute of RAS (2 Kapitanskaya St., Sevastopol, 299011, Russian Federation), **ResearcherID: AAC-6629-2020, ORCID ID: 0000-0002-8399-3743**, *vault102@gmail.com*

Contribution of the authors:

Yuri V. Artamonov – general scientific supervision of the research, statement of study aims and objectives, development of methods, qualitative analysis of the results and interpretation thereof, discussion of the study results, drawing conclusions

Elena A. Skripaleva – review of literature on the study topic, qualitative analysis of the results and interpretation thereof, processing and description of the study results, discussion of the study results, drawing conclusions, article text preparation and refinement

Aleksandr A. Latushkin – preparation and maintenance of hydro-optical equipment, obtaining *in situ* data, participation in discussion of the article materials

Aleksandr V. Fedirko – development and debugging of software for data processing, computer implementation of algorithms, chart and diagram construction, participation in discussion of the article materials

All the authors have read and approved the final manuscript.

Original paper

Variability of Parameters of the Carbonate System of the Northern Black Sea Surface Waters During Coccolithophorid Blooms

N. A. Orekhova *, E. N. Korchemkina, E. V. Medvedev, I. N. Mukoseev

Marine Hydrophysical Institute of RAS, Sevastopol, Russia
** e-mail: natalia.orekhova@mhi-ras.ru*

Abstract
The paper studies dynamics of carbonate system parameters during the spring-summer coccolithophores bloom using data on temperature, salinity, carbonate system parameters (CO_2, pH and alkalinity) and backscattering index ($b_{bp}(550)$, m^{-1}) for the northern Black Sea surface waters during the 127th and 131st cruises of R/V *Professor Vodyanitsky*. Within the studied periods (June 2023, May–June 2024) coccolithophores concentrations exceeded 1.00 million cells/L, while high pCO_2 (mean 486 ± 18 μatm) was also observed. The surface water layer was oversaturated with CO_2 compared to the atmosphere, with a mean water CO_2 supersaturation of 14% (58 μatm). However, no pronounced relationship was found between coccolith concentrations and pCO_2, pH and alkalinity values, which may indicate a non-core contribution of the bloom to CO_2 concentrations in the surface waters. It was found that even during the coccolithophores blooming period, temperature is the key factor determining the surface waters pCO_2. The spatial distribution of suspended matter concentration represented by coccoliths was determined by water dynamics and current structure in the Black Sea.

Keywords: carbonate system, carbon dioxide partial pressure, coccolithophores, Black Sea

Acknowledgments: The work was carried out under state assignment of MHI RAS FNNN-2025-0001 “Monitoring of CO_2 concentrations in the surface water layer and atmosphere in Russian inland seas” and FNNN-2024-0012 “Analysis, diagnosis and real-time forecast of the state of hydrophysical and hydrochemical fields of marine water areas based on mathematical modelling using data from remote and in situ methods of measurements”.

For citation: Orekhova, N.A., Korchemkina, E.N., Medvedev, E.V. and Mukoseev, I.N., 2025. Variability of Parameters of the Carbonate System of the Northern Black Sea Surface Waters During Coccolithophorid Blooms. *Ecological Safety of Coastal and Shelf Zones of Sea*, (3), pp. 25–40.

© Orekhova N. A., Korchemkina E. N., Medvedev E. V., Mukoseev I. N., 2025

This work is licensed under a Creative Commons Attribution-Non Commercial 4.0 International (CC BY-NC 4.0) License

Изменчивость параметров карбонатной системы поверхностного слоя вод северной части Черного моря в период «цветения» кокколитофорид

Н. А. Орехова *, Е. Н. Корчёмкина, Е. В. Медведев, И. Н. Мукосеев

Морской гидрофизический институт РАН, Севастополь, Россия
* *e-mail: natalia.orekhova@mhi-ras.ru*

Аннотация
Рассмотрена динамика параметров карбонатной системы в период весенне-летнего «цветения» кокколитофорид с использованием данных о температуре и солености, параметров карбонатной системы (CO_2, pH и щелочности) и показателя рассеяния назад взвесью (b_{bp}(550), м$^{-1}$) для поверхностного слоя вод в северной части Черного моря в 127-м и 131-м рейсах НИС «Профессор Водяницкий». В исследуемые периоды (июнь 2023 г., май – июнь 2024 г.) концентрации кокколитофорид превышали 1.00 млн кл/л, также отмечено высокое значение pCO_2 (среднее 486 ± 18 мкатм). Поверхностный слой вод был пересыщен CO_2 по сравнению с атмосферой, среднее пересыщение вод CO_2 составило 14 % (58 мкатм). Однако выявлено отсутствие выраженной связи между концентрациями кокколитов и величинами pCO_2, pH и щелочности, что может указывать на неосновной вклад «цветения» в концентрации CO_2 в поверхностном слое вод. Установлено, что даже в период «цветения» кокколитофорид ключевым фактором, определяющим величину pCO_2 поверхностного слоя вод, является температура воды. При этом пространственное распределение концентрации взвеси, представленной кокколитами, определялось динамикой вод и структурой течений в Черном море.

Ключевые слова: карбонатная система, парциальное давление углекислого газа, кокколитофориды, Черное море

Благодарности: работа выполнена в рамках государственного задания ФИЦ МГИ РАН FNNN-2025-0001 «Мониторинг концентрации CO_2 в поверхностном слое вод и атмосфере во внутренних морях России» и FNNN-2024–0012 «Оперативная океанология». Данные получены в 127-м и 131-м рейсах НИС «Профессор Водяницкий» (Центр коллективного пользования «НИС Профессор Водяницкий» Федерального государственного бюджетного учреждения науки Федерального исследовательского центра «Институт биологии южных морей имени А. О. Ковалевского Российской академии наук»).

Для цитирования: Изменчивость параметров карбонатной системы поверхностного слоя вод северной части Черного моря в период «цветения» кокколитофорид / Н. А. Орехова [и др.] // Экологическая безопасность прибрежной и шельфовой зон моря. 2025. № 3. С. 25–40. EDN VCOCEY.

Introduction

The continuous increase in atmospheric CO_2 concentrations and its further absorption by ocean waters, which are one of the main natural CO_2 sinks, has led to a decrease in the buffer capacity of those waters and a change in the hydrochemical characteristics of the World Ocean. In particular, there has been an increase in the concentration of hydrogen ions in seawater [1]. According to [2–4], over the past 250 years, the pH of surface ocean waters has decreased by approximately 0.11,

which corresponds to a 30–40% increase in the concentration of hydrogen ions. In addition, there has been a decrease in oxygen concentrations and the spread of oxygen-deficient zones in the waters of the World Ocean [5, 6]. At the same time, the increase in CO_2 concentrations in water and the atmosphere, as well as changes in the hydrochemical characteristics of the ocean, have a negative impact on biological organisms, including those with carbonate skeletons [2–4, 7].

In the waters of the World Ocean, the main reserve of dissolved carbon is in inorganic form and amounts to about 38 Gt C (1 Gt = 10^9 t) [1]. The atmosphere contains significantly less carbon, and significant carbon fluxes are formed at the boundary between the surface waters and the sea-surface atmosphere [1, 7, 8]. As a result, at the boundary with the atmosphere, as well as between the surface and deeper waters, various forms of carbon, including CO_2, are redistributed [2, 3], leading to changes in its concentrations.

The exchange of CO_2 between water and the atmosphere occurs due to the diffusion of gaseous CO_2 across the phase boundary, with the total exchange being proportional to the difference in partial pressures of gaseous CO_2 in the air and seawater. Thus, it is closely related to the solubility of CO_2 in seawater (K_0), which determines the ratio of CO_2 in seawater to the partial pressure of CO_2 in the gas phase [5] at chemical equilibrium:

$$K_0 = [CO_2]_{sw}/pCO_{2,\,sw}.$$

In addition to physical transport and temperature contributions, the dynamics of CO_2 concentration in the surface waters is determined by biological processes as well as bya complex set of abiotic chemical reactions [2–4].

The combination of CO_2 dissolution and carbonic acid dissociation products forms a carbonate system, which can be described by a system of equilibria [1, 2, 4]:

$$CO_2\,(g) \leftrightarrow CO_2\,(aq) \leftrightarrow CO_2\,(aq) + H_2O \leftrightarrow H^+ + HCO_3^- \leftrightarrow 2H^+ + CO_3^{2-}, \quad (1)$$

$$Ca^{2+} + CO_3^{2-} \leftrightarrow CaCO_3\,(s). \quad (2)$$

Hydrogen ions (H^+) (or pH) are one of the main components describing the state of the carbonate system; their concentration is closely related to the concentration of CO_2. An increase in CO_2 concentration is accompanied by an increase in the concentration of hydrogen ions and a decrease in pH:

$$pH = -\lg a_{H+}, \text{ or, conventionally, } pH \approx -\lg [H^+]. \quad (3)$$

Another important parameter of the carbonate system – one not directly dependent on CO_2 concentration – is total alkalinity (Alk), which is typically defined as the excess of proton acceptors (bases formed from weak acids) over proton donors measured relative to a reference point; formally, the acid dissociation constant pK_a = 4.5 corresponds approximately to the equivalence point of H_2CO_3 in seawater. In aerobic ocean waters, carbonate alkalinity constitutes up to 96–99% of the total alkaline reserve [9], which is expressed as:

$$Alk = [HCO_3^-] + 2[CO_3^{2-}]. \quad (4)$$

Carbonate alkalinity determines the buffering capacity of the system, and the dissolution of CO_2 primarily causes a shift in chemical equilibrium, altering the ratio of inorganic forms of carbon, while the concentration of total dissolved inorganic carbon remains nearly constant.

The primary chemical and biological processes governing the dynamics of the carbonate system in the water column are those involving organic matter – namely, its production and destruction:

$$6\,CO_2 + 6\,H_2O \leftrightarrow 6\,H^+ + 6\,HCO_3^- \leftrightarrow C_6H_{12}O_6 + 6\,O_2. \quad (5)$$

as well as the processes of carbonate formation/dissolution:

$$CaCO_3 + CO_2 + H_2O \leftrightarrow Ca^{2+} + 2HCO_3^-. \quad (6)$$

One group of marine phytoplankton involved in carbonate processes are coccolithophores. Their cells are covered with layers of plates –coccoliths – formed from calcium carbonate. The most abundant species in the Black Sea is *Emiliania huxley*, which can account for up to 99% of the total coccolithophore population. Cells of this species can shed coccoliths, a process in which the ratio of detached coccoliths to cells can reach 400:1 [11, 12]. Obviously, by possessing carbonate skeletons, coccolithophores during intense blooms (when their population exceeds 1 million cells/L [13]), significantly affect the optical and thermal characteristics of the surface waters of the World Ocean. The coccoliths cause strong light scattering, which reduces water transparency, and increase the ocean surface albedo, thereby reducing the insolation of the surface water layer [14]. An increase in backward scattering leads to higher values of upwelling sea radiance and the radiance coefficient [12]. This property enables the estimation of coccolithophore cell abundance, detached coccolith concentration, and overall carbonate concentration through the remote sensing of upwelling radiance [15]. The rate of carbonate formation, and consequently the rate of CO_2 drawdown, can increase or decrease based on limiting factors such as light intensity, temperature, nutrient concentrations, and carbon dioxide availability [16, 17].

Thus, by participating in the carbon cycle, these algae influence the oceanic CO_2 budget. However, accounting for all relevant factors and establishing a direct link between coccolithophore abundance/biomass and their carbon fixation rate remains highly challenging [18].

The study aims to evaluate the relationship between carbonate system parameters and coccolithophore blooms in the late spring. To this end, we investigate the spatiotemporal dynamics of temperature, salinity, carbonate system parameters (CO_2, pH, and alkalinity), and backscattering coefficient ($b_{bp}(550)$, m^{-1}) in the surface layer of the northern Black Sea.

Materials and methods

The data were obtained during the 127th (June 14, 2023–July 7, 2023) and 131st (May 27, 2023–June 21, 2024) cruises of R/V *Professor Vodyanitsky* off the southeastern coast of Crimea (Fig. 1).

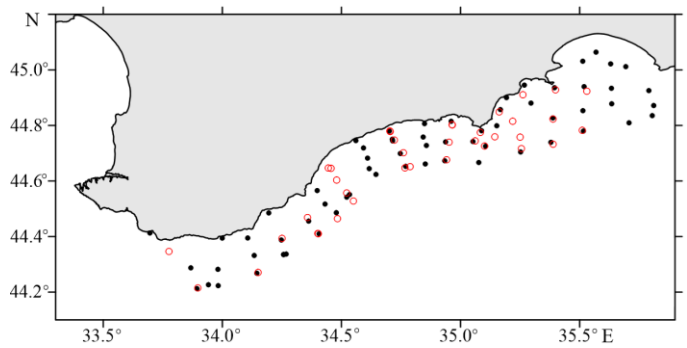

Fig. 1. The scheme of stations of points where the carbonate system parameters and optical characteristics were determined. The red circles stand for stations surveyed in the 127th cruise of R/V *Professor Vodyanitsky*, the black ones stand for those surveyed in the 131st cruise

The temperature and salinity of the surface water layer were measured using Sea-Bird 911plus CTD or IDRONAUT OCEAN SEVEN 320 PlusM sounding complexes; at shallow stations (depth less than 50 m), a SeaSun CTD48M hydrological CTD probe was used.

Water samples were collected from a depth of 1.5–3.0 m using a submersible pump. Atmospheric air was collected at a height of 10 m above sea level, ensuring the absence of local CO_2 sources.

CO_2 concentration was determined using a LI-7000 infrared analyzer with a CO_2 concentration range of 0–3000 μmol/mol. A special module (equilibrator) was used to determine the CO_2 concentration in water, ensuring contact between the analyzed water and air to achieve equilibrium pCO_2 in the gas phase.

The device was calibrated using argon (volume fraction of CO_2 = 0 μmol/mol) and a calibration mixture with a CO_2 concentration of 440 μmol/mol. The measurement uncertainty of this method is 1% [19]. Argon was used as the carrier gas.

The pH value was measured using I-160 and I-160MP ionometers calibrated on the NBS scale with buffer solutions [20]. Total alkalinity was determined by direct titration with potentiometric termination, titrating 50 ml of seawater with a 0.02M [1)] solution of hydrochloric acid. The titration was performed using a high-precision Metrohm Dosimat 765 piston burette, and the endpoint was determined with a Hanna HI-2215 pH meter. All measurements were made according to the established methodology [2)].

[1)] Bordovsky, O.K., ed., 1978. [*Methods of Hydrochemical Research of the Ocean*]. Moscow: Nauka, 267 p. (in Russian).

[2)] Dickson, A.G. and Goyet, C., eds., 1994. *Handbook of Methods for the Analysis of the Various Parameters of the Carbon Dioxide System in Sea Water. Version 2.* Oak Ridge, Tennessee: DOE, 187 p. (ORNL/CDIAC-74).

Optical characteristics

The backscattering coefficient at a wavelength of 550 nm ($b_{bp}(550)$, m^{-1}) was calculated based on data from measurements of the spectral reflectance coefficient of the water column in the visible range using a semi-analytical algorithm [21]. A spectrophotometer developed in the laboratory of the Department of Marine Optics and Biophysics of the FRC MHI was used to determine the reflectance coefficient [22]. The measurement methodology is consistent with NASA protocols for sub-satellite measurements [3)]. To convert backscattering to the number of separated coccoliths N_c (pcs/m^3), an empirical relationship from [23] was used:

$$b_{b_{\text{cocc}}}(546) = 1.1 \cdot 10^{-13} N_c, \quad (7)$$

where $b_{b_{\text{cocc}}}(546)$ is the backscattering coefficient of a coccolith suspension at a wavelength of 546 nm.

Changes in scattering within 5 nm range are neglected in this work.

It should be noted that eq. (7) was derived from the Black Sea data in the 1990s; consequently, the coefficients may not be directly applicable today. As shown in [24], these coefficients can vary significantly over a few days in a single area, although the linear relationship itself remains consistent. Therefore, the concentrations of suspended coccoliths and coccolithophore cells reported here should be regarded as estimates accurate only to a coefficient. This coefficient is introduced for convenience, particularly as the water also contains terrigenous suspended matter, which is difficult to estimate precisely.

To calculate the number of cells N_{cocc} (million cells/liter), we used the formula from [25], which was also obtained based on data from 1996–1998:

$$N_{\text{cocc}} = 160\, b_{bp}(555) - 0.32 \qquad R^2 = 0.82, \quad (8)$$

where $b_{b_{\text{cocc}}}(555)$ is the backscattering at a wavelength of 555 nm.

Results

According to the calculations, the backscattering coefficient $b_{bp}(550)$, during the late spring hydrological season ranged from 0.008 to 0.020 m^{-1} (in 2023) and from 0.004 to 0.021 m^{-1} (in 2024). In other seasons, values of 0.003–0.009 m^{-1} are typical for the Black Sea [26]. This indicates that suspended matter of coccolithophore origin contributed at least half of the total backscattering.

The calculated number of coccoliths and coccolithophore cells, derived using this parameter (following formulas (8) and (9) [23, 25]), is presented in Table 1. The ratio of cells to coccoliths at the measured scattering levels averaged approximately 88 and 94 in the 127th and 131st cruises, respectively. This result implies that the formulas assume a relationship between elevated backscattering and an increase in the number of detached coccoliths per cell.

[3)] Zibordi, G., Voss, K.J., Johnson, B.C. and Mueller, J.L., 2019. *Ocean Optics and Biogeochemistry Protocols for Satellite Ocean Colour Sensor Validation. Vol. 3: Protocols for Satellite Ocean Colour Data Validation: in situ Optical Radiometry*. Dartmouth, NS, Canada: IOCCG, 67 p. http://dx.doi.org/10.25607/OBP-691

Table 1. Data of hydrological-hydrochemical and bio-optical characteristics of the Black Sea surface waters in late spring period

Parameter	127th cruise (14 June 2023–7 July 2023)*		131st cruise (27 May 2023–21 June 2024)	
	Average	Value range	Average	Value range
T, °C	23.0 ± 0.8	20.7–24.6	20.2 ± 1.5	16.8–25.7
S, ‰	17.88 ± 0.11	17.63–18.35	18.38 ± 0.14	17.99–18.62
$pCO_{2\ sea}$, µatm	480 ± 7	460–501	498 ± 23	449–546
$pCO_{2\ air}$, µatm	421 ± 5	411–441	435 ± 3	423–448
ΔpCO_2, µatm	59 ± 9	36–79	70 ± 31	15–117
N_{cocc}, million cells/L	1.39 ± 0.28	0.87–2.95	1.16 ± 0.55	0.32–2.97
$N_c \cdot 10^9$, pcs./m^3	112 ± 19	82–225	102 ± 37	44–226
Alk, mmol/L	3.224 ± 0.019	3.170–3.279	3.250 ± 0.033	3.137–3.296
pH	8.30 ± 0.02	8.25–8.37	8.27 ± 0.02	8.23–8.32

* The bio-optic and pCO_2 measurements were synchronized using the period of 14–26 June.

Table 1 presents the main hydrological characteristics and parameters of the carbonate system in the surface waters of the Black Sea, as measured during the 127th and 131st cruises of R/V *Professor Vodyanitsky*.

As shown in Table 1, coccolithophore blooms of varying intensity occurred during the study period, with an average coccolith concentration exceeding $100 \cdot 10^9$ pcs/m^3. In this study, we focus on the coccolith concentration (N_c) as the most reliable metric. This is because optical methods allow for its direct calculation, unlike the ratio of cells to coccoliths, which varies with the bloom stage. On average, this ratio was approximately 90 coccoliths per cell, as noted previously. Furthermore, we posit that coccoliths likely contribute more significantly to the CO_2 concentration than coccolithophore cells, in accordance with equation (6).

In all cases, the surface waters were oversaturated with CO_2 relative to the atmosphere (Table 1), indicating that it acted as a source of carbon dioxide to the atmosphere.

In June 2023, coccolithophore cell density reached 2.95 million cells/L, with a mean value of 1.39 million cells/L. The concentration of coccoliths averaged $112 \cdot 10^9$ pcs/m^3 (Table 1). The predominance of carbonate-based cells drove high pCO_2 levels – a result of CO_2 formation according to equation (6)) – leading to oversaturation of the surface waters with CO_2 relative to the atmosphere. The mean pCO_2 in the surface layer was 480 ± 7 µatm, ranging from 460 to 501 µatm. Elevated surface water temperatures (reaching 24.6°C with a mean of 23.0 ± 0.8°C) also contributed to the high pCO_2 values, as indicated by the average nature of the relationship between these parameters – the correlation coefficient of pCO_2 with temperature in the surface waters is 0.52.

Fig. 2 presents the dynamics of the studied parameters during the 127th cruise. The principal trends observed include an increase in temperature and pCO_2 alongside a decrease in coccolith concentration.

Fig. 3 illustrates parameter changes at the end of the spring hydrological season of 2024 (late May–June). During this period, coccolithophore blooms occurred again, with cell densities averaging 1.16 million cells/L with a range of 0.32–2.96 million cells/L. The concentration of coccoliths averaged $102 \cdot 10^9$ pcs/m^3 (Table 1).

As expected, the surface waters were also significantly oversaturated with CO_2 compared to the atmosphere (the pCO_2 gradient could reach more than 100 µatm), and deep evasive conditions were observed in the surface waters of the Black Sea (CO_2 flux directed from water to the atmosphere). The average pCO_2 value in the surface layer of water was 498 µatm, with a pCO_2 range of 449 to 546 µatm (10%). The surface water temperature reached 20°C, with an increase in pCO_2 observed along this temperature rise, with maximum pCO_2 values corresponding

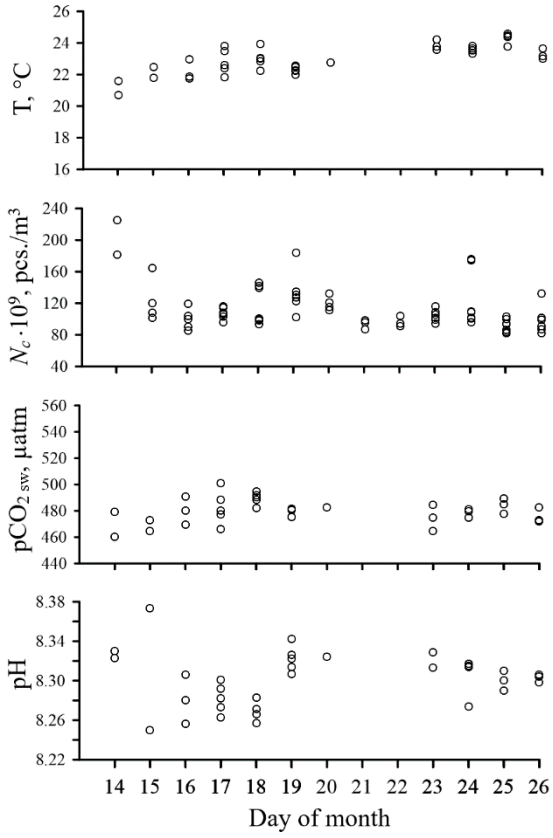

Fig. 2. Changes in pH, pCO_2, coccoliths and temperature of the surface waters in June 2023 (127th cruise of R/V *Professor Vodyanitsky*)

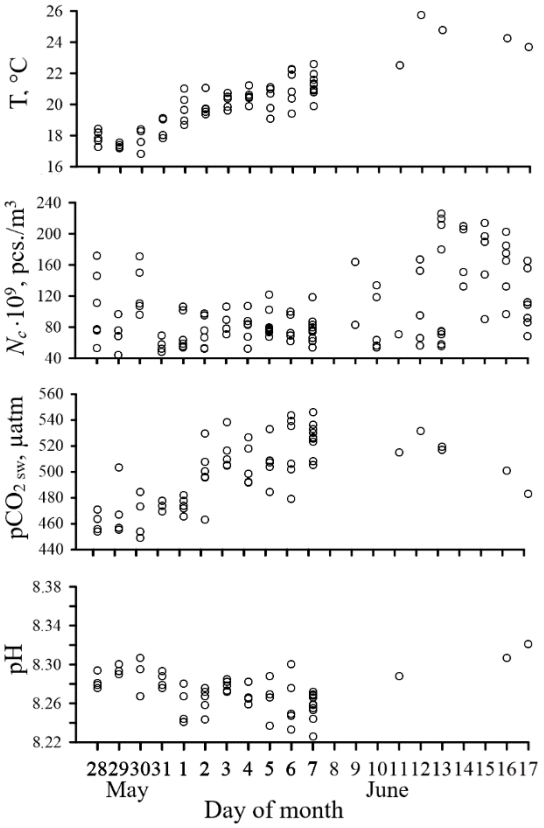

Fig. 3. Dynamics of pH, pCO_2, coccoliths and temperature of the surface water layer in May–June 2024 (131st cruise of R/V *Professor Vodyanitsky*)

to the highest recorded temperatures (Fig. 3). The correlation coefficient between pCO_2 and surface water temperature was 0.68, indicating that temperature played a significant role in controlling the CO_2 concentration.

The maximum pCO_2 values in the water corresponded to the maximum temperatures of the surface layer of water (Fig. 3).

The pH values (Figs. 2, 3) and total alkalinity varied within narrow limits during the study periods. The average pH was 8.30 ± 0.02 in 2023 and 8.27 ± 0.02 in 2024 (Table 1), consistent with long-term observational data for this period.

Alkalinity exhibited minimal interannual variability, with values of 3.224 ± 0.019 in 2023 and 3.250 ± 0.033 in 2024. However, significant spatial heterogeneity was observed. This heterogeneity was primarily attributed to the influence of salinity (correlation coefficient 0.73), rather than to physicochemical processes associated with organic matter transformation or blooms.

Discussion

During the spring-summer phytoplankton bloom (late May–June), coccolithophores comprise the majority of the biomass (50–60%) [11, 13, 27]. Their development in this period is determined by a combination of abiotic factors – including light, temperature, and nutrient concentration – as well as biotic factors such as grazing by microzooplankton [11].

During the study perio ds, coccolithophore concentrations exceeded 1.0 million cells/L (Table 1), indicating a bloom state. High pCO_2 (average 486 ± 18 µatm) was also observed in the surface waters , with an average value of 442 ± 44 µatm (according to our data for 2015–2024, covering the period from March to December).

The average CO_2 oversaturation of the water relative to the atmosphere was 14% (58 μatm). It can be assumed that the high pCO_2 values were contributed to by coccolithophore bloom, which is accompanied by CO_2 production (equation (6), right to left). In addition, the increase in the sea surface temperature (Table 1) contributes to the shift of the carbonate equilibrium system towards CO_2 accumulation (equation (1)), as well as the intensification of organic matter destruction (equation (5), right to left) formed during the spring phytoplankton bloom.

In June 2023 (127^{th} cruise of R/V *Professor Vodyanitsky*), the average coccolithophore content was 1.39 million cells/L, corresponding to $112 \cdot 10^9$ coccoliths/m^3 (Table 1). However, a decrease in the number of coccoliths was observed during the month (see Fig. 2). This may indicate the attenuation of the bloom and the gradual dissolution of carbonates, occurring according to the scheme of equation (6) (direction from left to right). This process should be accompanied by a decrease in CO_2 concentration and an increase in bicarbonate concentration, which in turn leads to an increase in pH; according to equations (4) and (6), alkalinity should also increase. However, no such trend was observed either spatially or seasonally: according to long-term observations for this region in the absence of coccolithophore blooms (March), the average alkalinity values are 3.281 ± 0.062 mmol/dm^3, and pH is 8.26 ± 0.09, which are statistically indistinguishable from their late spring values (Table 1). At the same time, the waters were significantly undersaturated with CO_2 compared to the atmosphere (average pCO_2 gradient = -46 ± 21 μatm). Thus, it can be assumed that this biological process is not decisive for the dynamics of CO_2 or for the dynamics of other hydrochemical characteristics (pH and alkalinity). This is also confirmed by correlation analysis data: the correlation coefficient between pCO_2 and the number of coccoliths is −0.22, indicating a weak relationship. The closest relationships were between pCO_2 and temperature (correlation coefficient 0.52) and pH (correlation coefficient −0.53).

At the end of May–June 2024, coccolithophore blooms were also observed (1.16 million cells/L; Table 1), corresponding to $102 \cdot 10^9$ coccoliths/m^3. Based on the dynamics of the studied hydrochemical and bio-optical parameters, two periods can be distinguished: May 28–June 7 and June 11–17 (Fig. 3). Thus, the change in the number of coccoliths indicates the development of the bloom during the voyage from May to June. In the first period, the average number of coccoliths was $(83 \pm 20) \times 10^9$ pcs/m^3, and in the second, $(131 \pm 49) \times 10^9$ pcs/m^3, with maximum values reaching 226×10^9 pcs/m^3.

In the first period, against the backdrop of rising sea surface temperatures and no visible trend toward an increase in the number of coccolith particles, there was an increase in pCO_2 and a decrease in the pH of the surface waters (Fig. 3). This may indicate the beginning of coccolith formation and gradual accumulation, accompanied by an increase in pCO_2 (equation (6) from right to left) and a decrease in pH (Fig. 3). The following period (June 11–17) is characterized by an increase in the number of coccoliths, a decrease in pCO_2, and an increase in pH (Fig. 3). The increase in the number of coccoliths and the concentration of coccolithophores (the average concentration during this period was 1.66 million cells/L) indicates blooming.

However, the gradual decrease in pCO_2 and increase in pH observed at this time most likely indicate the presence of an additional factor contributing to CO_2 binding. In this case, coccolith formation is not the main process determining the concentration of CO_2 and hydrogen ions.

Thus, based on the dynamics of coccolith numbers in late spring, three periods can be distinguished: the beginning of the bloom and gradual accumulation of coccolithophores (late May – early June; average number of coccoliths $83 \cdot 10^9$ pcs/m^3), their accumulation and bloom outbreak during June (average number of coccoliths $131 \cdot 10^9$ pcs/m^3), and then the attenuation of the bloom by the end of June (average number of coccoliths $112 \cdot 10^9$ pcs/m^3) followed by carbonate decomposition (Fig. 2, 3).

We attempted to describe the dynamics of pCO_2 in terms of processes involving inorganic carbon and its transformation, as well as changes in the parameters of the carbonate system (equations (1), (2), (5), (6)). However, the lack of a statistically significant correlation between the number of coccolithophore cells (and the number of coccoliths) and either pCO_2 (correlation coefficients of −0.22 and −0.06 for cruises 127 and 131, respectively) or alkalinity (correlation coefficients of 0.05 and 0.09 for cruises 127 and 131, respectively), along with their moderate correlation with pH (correlation coefficients of 0.30 and 0.40 for 127th and 131st cruises, respectively), indicates that coccolithophores do not play a key role in the state of the carbonate system and its parameters.

The lack of correlation between coccolithophore concentration and alkalinity suggests that changes in alkalinity are not related to biological processes but are primarily determined by an abiotic factor – changes in salinity (correlation coefficients of 0.86 and 0.88 for 127th and 131st cruises, respectively). It should be noted that the ranges of alkalinity variation during the voyages were small – approximately 4% (statistically significant changes are greater than 2%) of the average value.

As expected, in accordance with equations (1)–(5), the change in pH was opposite to the change in pCO_2: an increase in pCO_2 was accompanied by a decrease in pH. This relationship was most clearly expressed in the 131st cruise. In the first period (May 28, 2024–June 7, 2024), the increase in pCO_2 was 10%, and the decrease in pH was less pronounced in percentage terms, but the concentration of hydrogen ions (equation (3)) increased by ~7%. After that (June 11–17, 2024), there was an 8% decrease in pCO_2 and a 7% decrease in hydrogen ion concentration. The correlation coefficient between pH and pCO_2 was −0.53 and −0.57 for 127th and 131st cruises, respectively, indicating a moderate relationship and the contribution of the abiotic component to CO_2 dynamics (equation (1), carbonate equilibrium system).

Nevertheless, the contribution of the temperature to the dynamics of pCO_2 was most pronounced, with correlation coefficients of 0.52 and 0.71 for 127th and 131st cruises, respectively. At the same time, an increase in temperature contributes to both the intensification of biological processes and a shift in the equilibrium in the carbonate system towards CO_2 accumulation.

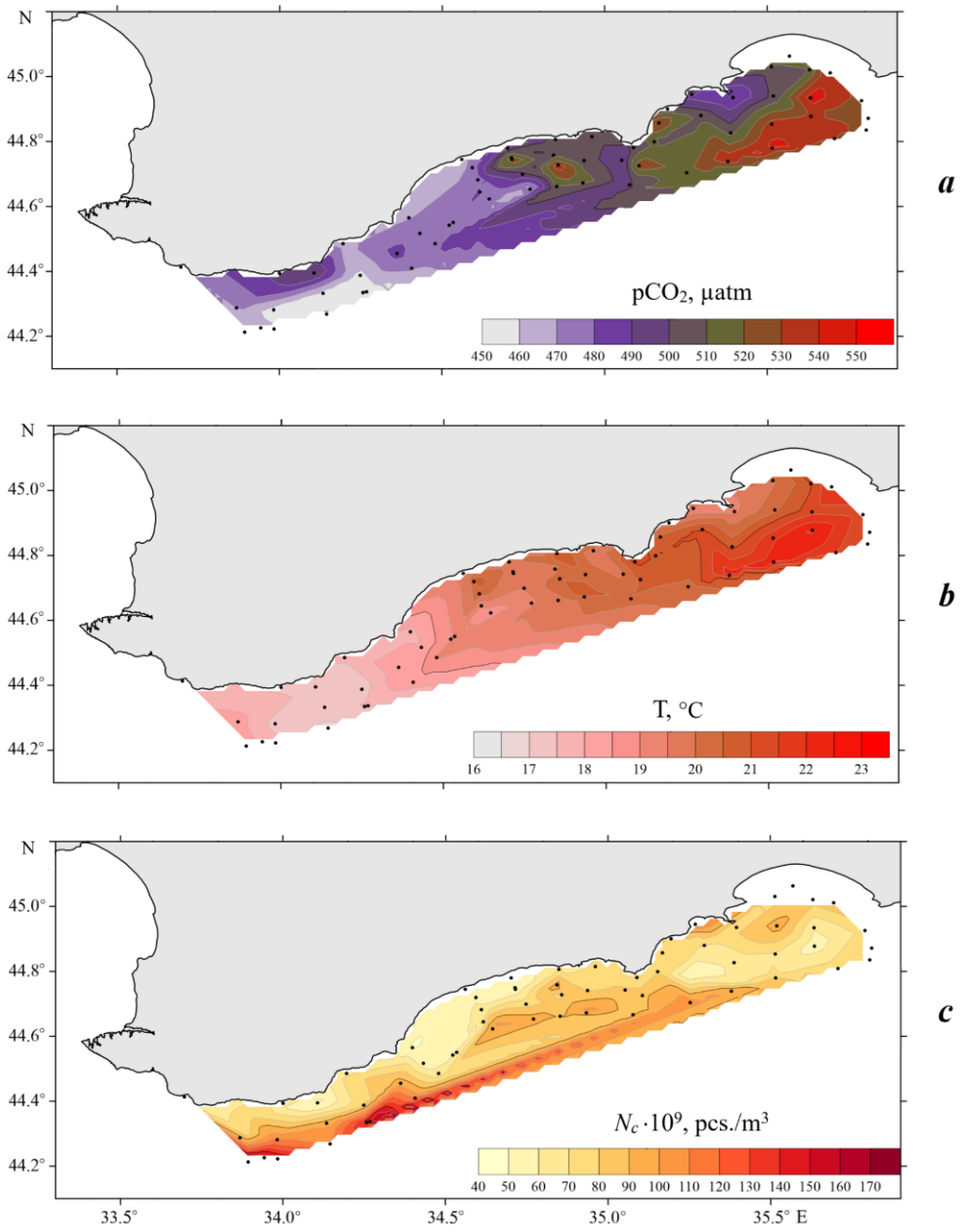

Fig. 4. Spatial distribution of pCO_2 (*a*), temperature (*b*) and coccoliths (*c*) in the surface water layer based on data from the 131st cruise (1st stage, 28.05–07.06.2024)

The influence of sea surface temperature on pCO_2 is also evident in the spatial distribution of these parameters. This is exemplified by data from the 131st cruise (Figure 4), which shows that areas of maximum pCO_2 coincide with regions of elevated surface water temperature.

Furthermore, the spatial distribution of coccoliths did not correspond with the pCO_2 pattern (Fig. 4, *a*, *c*), which also confirms the assumption about the minor contribution of the biotic factor to the pCO_2 value of the surface water layer.

Based on the calculated data (Fig. 4, *c*) and satellite imagery data (for example, URL: http://dvs.net.ru/mp/data/modis/2406/24062955.gif), it is assumed that fields of suspended matter, consisting mainly of coccoliths, are formed under the influence of a hydrodynamic factor: water, enriched with coccolithophore cells and the suspended matter they produce, is carried along with the Main Black Sea Current from the southern regions of the sea. As a result, a field of suspended matter concentrations is formed, where clearer water is pressed against the shore and more turbid water is observed in the open sea part of the polygon.

Conclusions

During the study periods (May–July), coccolithophore blooms (more than 100 million cells/L) were observed in the surface waters, and the proportion of suspended matter of coccolithic origin was 50% or more. The spatial distribution of the concentration of suspended matter represented by coccolithophores was determined by the dynamics of the water and the structure of currents in the Black Sea.

The waters were oversaturated with CO_2 compared to the atmosphere, with an average pCO_2 of 486 ± 18 μatm, which is ~ 20% higher than the average annual pCO_2 value for this region.

Analysis of coccolith dynamics in late spring allowed us to identify three periods: the beginning of blooming and gradual accumulation of coccolithophores (late May – early June; average number of coccoliths $83 \cdot 10^9$ pcs/m^3), their accumulation and bloom outbreak during June (average number of coccoliths $131 \cdot 10^9$ pcs/m^3), and then the attenuation of the bloom by the end of June (average number of coccoliths $112 \cdot 10^9$ pcs/m^3) followed by carbonate decomposition.

No statistically significant correlation was found between the number of coccolithophore cells (and the number of coccoliths) and either pCO_2 (correlation coefficient −0.22 and −0.06 for 127th and 131st cruises, respectively) or alkalinity (correlation coefficients of 0.05 and 0.09 for the 127th and 131st cruises, respectively), as well as a moderate correlation with pH (correlation coefficients of 0.30 and 0.40 for the 127th and 131st cruises, respectively). The absence of a pronounced relationship between coccolith concentrations and pCO_2, pH, and alkalinity values suggests that, despite the contribution of coccolithophore blooms to maintaining high CO_2 concentrations in the sea surface, this factor is not the main one.

The temperature factor contributes most significantly to the dynamics of pCO_2, with correlation coefficients of 0.52 and 0.71 for 127th and 131st cruises, respectively. This is primarily due to the fact that an increase in temperature contributes to both the intensification of biological processes and a shift in the equilibrium in the carbonate system towards CO_2 accumulation. Thus, even during the coccolithophore bloom period, temperature is the key factor determining the pCO_2 value of the surface water layer.

REFERENCES

1. Zeebe, R.E., 2012. History of Seawater Carbonate Chemistry, Atmospheric CO_2, and Ocean Acidification. *Annual Review of Earth and Planetary Sciences*, 40(1), pp. 141–165. https://doi.org/10.1146/annurev-earth-042711-105521
2. Takahashi, T., Sutherland, S.C., Sweeney, C., Poisson, A., Metzl, N., Tilbrook, B., Bates, N., Wanninkhof, R., Feely, R.A. [et al.], 2002. Global Sea–Air CO_2 Flux Based on Climatological Surface Ocean pCO_2, and Seasonal Biological and Temperature Effects. *Deep Sea Research Part II: Topical Studies in Oceanography*, 49(9–10), pp. 1601–1622. https://doi.org/10.1016/s0967-0645(02)00003-6
3. Wanninkhof, R., 2014. Relationship Between Wind Speed And Gas Exchange Over The Ocean Revisited. *Limnology and Oceanography: Methods*, 12(6), pp. 351–362. https://doi.org/10.4319/lom.2014.12.351
4. Schulz, K.G. and Maher, D.T., 2023. Atmospheric Carbon Dioxide and Changing Ocean Chemistry. In: A. Reichelt-Brushett, ed., 2023. *Marine Pollution – Monitoring, Management and Mitigation.* Springer Textbooks in Earth Sciences, Geography and Environment. Cham: Springer, pp. 247–259. https://doi.org/10.1007/978-3-031-10127-4_11
5. DeVries, T., 2022. The Ocean Carbon Cycle. *Annual Review of Environment and Resources*, 47, pp. 317–341. https://doi.org/10.1146/annurev-environ-120920-111307
6. Feely, R.A., Jiang, L.-Q., Wanninkhof, R., Carter, B.R., Alin, S.R., Bednaršek, N. and Cosca, C.E., 2023. Acidification of the Global Surface Ocean: What We Have Learned from Observations. *Oceanography*, 36(2–3), pp. 120–129. https://doi.org/10.5670/oceanog.2023.222
7. Zeebe, R.E. and Wolf-Gladrow, D., 2001. *CO_2 in Seawater: Equilibrium, Kinetics, Isotopes*. Elsevier Oceanography Series, vol. 65. Amsterdam, The Netherlands: Elsevier Science, 360 p.
8. Jessen, G.L., Lichtschlag, A., Ramette, A., Pantoja, S., Rossel, P.E., Schubert, C.J., Struck, U. and Boetius, A., 2007. Hypoxia Causes Preservation of Labile Organic Matter and Changes Seafloor Microbial Community Composition (Black Sea). *Science Advances*, 3(2), e1601897. https://doi.org/10.1126/sciadv.1601897
9. Capet, A., Stanev, E.V., Beckers, J.-M., Murray, J.W. and Grégoire, M., 2016. Decline of the Black Sea Oxygen Inventory. *Biogeosciences*, 13(4), pp. 1287–1297. https://doi.org/10.5194/bg-13-1287-2016
10. Diaz, R.J. and Rosenberg, R., 2008. Spreading Dead Zones and Consequences for Marine Ecosystems. *Science*, 321(5891), pp. 926–929. https://doi.org/10.1126/science.1156401
11. Stelmakh, L.V., 2018. Environmental and Physiological Bases of Coccolithophorid *Emiliania Huxleyi* Spring Bloom Development in the Black Sea. *Monitoring Systems of Environment*, 13, pp. 85–92 (in Russian).
12. Korchemkina, E.N. and Mankovskaya, E.V., 2020. Optical Properties of the Black Seawaters near Oceanographic Platform during Coccolithophore Blooms in 2012 and 2017. *Fundamental and Applied Hydrophysics*, 13(2), pp. 25–34. https://doi.org/10.7868/S2073667320020033 (in Russian).
13. Mikaelyan, A.S., Silkin, V.A. and Pautova, L.A., 2011. Coccolithophorids in the Black Sea: Their Interannual and Long-Term Changes. *Oceanology*, 51(1), pp. 39–48. https://doi.org/10.1134/S0001437011010127
14. Kopelevich, Ol., Sheberstov, S. and Vazyulya, Sv., 2020. Effect of a Coccolithophore Bloom on the Underwater Light Field and the Albedo of the Water Column. *Journal of Marine Science and Engineering*, 8, 456. https://doi.org/10.3390/jmse8060456

15. Hopkins, J. and Balch, W.M., 2018. A New Approach to Estimating Coccolithophore Calcification Rates from Space. *Journal of Geophysical Research: Biogeosciences*, 123(5), pp. 1447–1459. https://doi.org/10.1002/2017JG004235

16. Barcelos e Ramos, J., Müller, M.N. and Riebesell, U., 2010. Short-Term Response of the Coccolithophore *Emiliania huxleyi* to an Abrupt Change in Seawater Carbon Dioxide Concentrations. *Biogeosciences*, 7(1), pp. 177–186. https://doi.org/10.5194/bg-7-177-2010

17. Zhang, Y. and Gao, K., 2021. Photosynthesis and Calcification of the Coccolithophore Emiliania Huxleyi Are More Sensitive to Changed Levels of Light and CO2 under Nutrient Limitation. *Journal of Photochemistry and Photobiology B: Biology*, 217, 112145. https://doi.org/10.1016/j.jphotobiol.2021.112145

18. Feng, Y., Roleda, M.Y., Armstrong, Ev., Boyd, Ph.W. and Hurd, C.L., 2016. Environmental Controls on the Growth, Photosynthetic and Calcification Rates of a Southern Hemisphere Strain of the Coccolithophore Emiliania huxleyi: Environmental Controls on E. huxleyi Physiology. *Limnology and Oceanography*, 62(2), pp. 519–540. https://doi.org/10.1002/lno.10442

19. Khoruzhiy, D.S., 2010. Usage of Device Complex AS-C3 for Detection of Carbon Dioxide Partial Pressure and Inorganic Carbon Concentration in Sea Environment. In: MHI, 2010. *Ekologicheskaya Bezopasnost' Pribrezhnoy i Shel'fovoy Zon i Kompleksnoe Ispol'zovanie Resursov Shel'fa* [Ecological Safety of Coastal and Shelf Zones and Comprehensive Use of Shelf Resources]. Sevastopol: MHI. Iss. 23, pp. 260–272 (in Russian).

20. Bordovskiy, O.K and Chernyakova, A.M., eds., 1992. *Modern Methods of Ocean Hydrochemical Investigations*. Moscow: P.P.Shirshov Institute of Oceanology, 201 p. (in Russian).

21. Lee, M.E., Shybanov, E.B., Korchemkina, E.N. and Martynov, O.V., 2015. Determination of the Concentration of Seawater Components based on Upwelling Radiation Spectrum. *Physical Oceanography*, (6), pp. 15–30. https://doi.org/10.22449/1573-160X-2015-6-15-30

22. Lee, M.E. and Martynov, O.V., 2000. [Radiance Coefficient Meter for Sub-Satellite Measurements of Bio-Optical Parameters of Water]. In: MHI, 2000. *Ekologicheskaya Bezopasnost' Pribrezhnoy i Shel'fovoy Zon i Kompleksnoe Ispol'zovanie Resursov Shel'fa* [Ecological Safety of Coastal and Shelf Zones and Comprehensive Use of Shelf Resources]. Sevastopol: MHI. Iss. 1, pp. 163–173 (in Russian).

23. Mankovsky, V.I., Vladimirov, V.L., Afonin, E.I., Mishonov, A.V., Solov'ev, M.V., Anninskiy, B.E., Georgieva, L.V. and Yunev, O.A., 1996. *Long-Term Variability of the Black Sea Water Transparency and Factors Determined its Strong Decrease in the Late 1980s Early 1990s*. Sevastopol: MGI, 32 p. (in Russian).

24. Balch, W.M., Kilpatrick, K.A., Holligan, P., Harbour, D. and Fernandez, E., 1996. The 1991 Coccolithophore Bloom in the Central North Atlantic. 2. Relating Optics to Coccolith Concentration. *Limnology and Oceanography*, 41(8), pp. 1684–1696. https://doi.org/10.4319/lo.1996.41.8.1684

25. Churilova, T.Ya. and Suslin, V.V., 2012. On Causes of Emiliania Huxleyi Domination in Phytoplankton of Deep Waters Part of the Black Sea in Early Summer. In: MHI, 2012. *Ekologicheskaya Bezopasnost' Pribrezhnoy i Shel'fovoy Zon i Kompleksnoe Ispol'zovanie Resursov Shel'fa* [Ecological Safety of Coastal and Shelf Zones and Comprehensive Use of Shelf Resources]. Sevastopol: MHI. Iss. 26, vol. 2, pp. 195-203 (in Russian).

26. Chami, M., Shybanov, E.B., Churilova, T.Y., Khomenko, G.A., Lee, M.E.-G., Martynov, O.V., Berseneva, G.A. and Korotaev, G.K., 2005. Optical Properties of the Particles in the Crimea Coastal Waters (Black Sea). *Journal of Geophysical Research: Oceans*, 110(C11), C11020. https://doi.org/10.1029/2005JC003008

27. Lifanchuk, A.V. and Fedorov, A.V., 2018. Change of Ecological Strategies in the Phytoplankton Community of the North-Eastern Part of the Black Sea during the Annual Cycle. *Hydrosphere Ecology*, (1) (in Russian).

Submitted 05.03.2025; accepted after review 05.05.2025;
revised 24.06.2025; published 30.09.2025

About the authors:

Natalia A. Orekhova, Head of Laboratory for Monitoring and Research of Greenhouse Gas and Oxygen Fluxes in the Marine Environment, Marine Hydrophysical Institute of RAS (2 Kapitanskaya St., Sevastopol, 299011, Russian Federation), PhD (Geogr.), **ORCID ID: 0000-0002-1387-970X, ResearcherID: I-1755-2017, Scopus Author ID: 35784884700**, *natalia.orekhova@mhi-ras.ru*

Elena N. Korchemkina, Senior Research Associate, Marine Hydrophysical Institute of RAS (2 Kapitanskaya Str., Sevastopol, 299011, Russian Federation), PhD (Phys.-Math.), **ORCID ID: 0000-0003-0526-4083, ResearcherID: I-1595–2015, Scopus Author ID: 23004799100**, *korchemkina@mhi-ras.ru*

Eugene V. Medvedev, Junior Research Associate, Marine Hydrophysical Institute of RAS (2 Kapitanskaya St., Sevastopol, 299011, Russian Federation), **ORCID ID: 0000-0003-0624-5319, ResearcherID: C-7016-2016,** *eugenemedvedev@mhi-ras.ru*

Igor N. Mukoseev, Senior Research Associate, Marine Hydrophysical Institute of RAS (2 Kapitanskaya St., Sevastopol, 299011, Russian Federation), **ORCID ID: 0009-0000-3485-1004,** *igor.mukos@gmail.com*

Contribution of the authors:

Natalia A. Orekhova – concept statement, study tasks statement, analysis and summary of the study results

Elena N. Korchemkina – concept statement, analysis and summary of the study results, preparation of the article text

Eugene V. Medvedev – participation in discussion of the results, analysis and summary of the study results, preparation of the article text

Igor N. Mukoseev – preparation of the article materials

All the authors have read and approved the final manuscript.

Original paper

Self-Purification Capacity of the Yalta Port Ecosystem in Relation to Inorganic Forms of Nitrogen for 2012–2022

I. V. Mezentseva [1], **E. E. Sovga** [2] *, **T. V. Khmara** [2]

[1] *Sevastopol Branch of the N. N. Zubov State Oceanographic Institute, Sevastopol, Russia*
[2] *Marine Hydrophysical Institute of RAS, Sevastopol, Russia*
* *e-mail: science-mhi@mail.ru*

Abstract
A database of nutrients and dissolved oxygen for 2012–2022 was formed from long-term monitoring results of the hydrochemical indicators of the Yalta Port water area. The paper shows dynamics of nutrients for the studied water area and determines inorganic forms of nitrogen (nitrites, nitrates, ammonium) as priority pollutants in the port ecosystem. The self-purification capacity of the Yalta Port water ecosystem was assessed by calculating the specific assimilation capacity (AC_{sp}) in relation to nitrates, nitrites and ammonium using the balance method. The rates and times of removal of these inorganic nitrogen forms from the mentioned ecosystem were calculated. The paper analyses the obtained AC_{sp} values for the Yalta Port water ecosystem for two periods (2012–2017 and 2018–2022). The study shows that for nitrates, there is an increase in AC_{sp} from 31.49 to 36.07 μg/(L·day) for these periods, respectively. The same dependence was established for nitrites. For this nitrogen form, the change in AC_{sp} ranged from 0.08 to 0.1 μg/(L·day). As for ammonium, an inverse relationship was observed for these periods: a decrease in the AC_{sp} value from 8.67 to 7.56 μg/(L·day). The paper compares the obtained AC_{sp} values in relation to inorganic forms of nitrogen for the Yalta Port water ecosystem with similar values for the Sevastopol Bay ecosystem, which is under high anthropogenic load, affected by river runoff and has limited water exchange with the open sea. The more intensive hydrodynamic regime is suggested to account for the higher self-purification capacity in relation to inorganic forms of nitrogen in the Yalta Port ecosystem (as part of Yalta Bay) if compared with Sevastopol Bay.

Keywords: nutrients, biogenic nitrogen, ecosystem, self-purification capacity, assimilation capacity, Yalta Port

Acknowledgements: The study was performed under state assignment of MHI RAS on topic FNNN-2024-0016 “Coastal research”.

For citation: Mezentseva, I.V., Sovga, E.E. and Khmara, T.V., 2025. Self-Purification Capacity of the Yalta Port Ecosystem in Relation to Inorganic Forms of Nitrogen for 2012–2022. *Ecological Safety of Coastal and Shelf Zones of Sea*, (3), pp. 41–53.

© Mezentseva I. V., Sovga E. E., Khmara T. V., 2025

This work is licensed under a Creative Commons Attribution-Non Commercial 4.0 International (CC BY-NC 4.0) License

Самоочистительная способность экосистемы Ялтинского порта в отношении неорганических форм азота за 2012–2022 годы

И. В. Мезенцева [1], Е. Е. Совга [2] *, Т. В. Хмара [2]

[1] *Севастопольское отделение Государственного океанографического института им. Н. Н. Зубова, Севастополь, Россия*

[2] *Морской гидрофизический институт РАН, Севастополь, Россия*

* *e-mail: science-mhi@mail.ru*

Аннотация

По результатам многолетнего мониторинга гидрохимических показателей акватории Ялтинского порта за 2012–2022 гг. сформирована база данных о концентрации биогенных элементов и растворенного кислорода за указанный период. Для исследуемой акватории показана динамика содержания биогенных элементов и выделены неорганические формы азота (нитриты, нитраты, аммоний) как приоритетные загрязняющие вещества в экосистеме порта. Оценка самоочистительной способности экосистемы акватории Ялтинского порта выполнена путем расчета балансовым методом величины удельной ассимиляционной емкости ($АЕ_{уд}$) в отношении нитратов, нитритов и аммония. Рассчитаны также скорости и время удаления этих неорганических форм азота из указанной экосистемы. Проанализированы полученные значения $АЕ_{уд}$ для экосистемы акватории Ялтинского порта за два периода: 2012–2017 и 2018–2022 гг. Показано, что в отношении нитратов наблюдается увеличение $АЕ_{уд}$ от 31.49 до 36.07 мкг/(л·сут) за указанные периоды соответственно. Такая же зависимость установлена для нитритов: изменение $АЕ_{уд}$ составило от 0.08 до 0.1 мкг/(л·сут). В отношении аммония за указанные периоды наблюдается обратная зависимость – уменьшение $АЕ_{уд}$ от 8.67 до 7.56 мкг/(л·сут). Приведены результаты сравнения полученных значений $АЕ_{уд}$ в отношении неорганических форм азота для экосистемы акватории Ялтинского порта с соответствующими показателями для экосистемы б. Севастопольской, которая характеризуется высокой антропогенной нагрузкой, подвержена влиянию стока рек и имеет затрудненный водообмен с открытым морем. Высказывается предположение, что причиной более высокой, чем у экосистемы б. Севастопольской, способности к самоочищению в отношении неорганических форм азота экосистемы Ялтинского порта (как части Ялтинского залива) является более интенсивный гидродинамический режим.

Ключевые слова: биогенные элементы, биогенный азот, экосистема, самоочистительная способность, ассимиляционная емкость, Ялтинский порт

Благодарности: работа выполнена в рамках государственного задания ФГБУН МГИ по теме FNNN-2024-0016 «Прибрежные исследования».

Для цитирования: *Мезенцева И. В., Совга Е. Е., Хмара Т. В.* Самоочистительная способность экосистемы Ялтинского порта в отношении неорганических форм азота за 2012–2022 годы // Экологическая безопасность прибрежной и шельфовой зон моря. 2025. № 3. С. 41–53. EDN ZFXLJK.

Introduction

The coastal waters of the Southern Coast of Crimea, in particular Yalta Bay, being recreational and resort areas, experience significant anthropogenic pressure with pronounced seasonality.

The Yalta Port water area, with depths of up to 8.5 m, is part of Yalta Bay and is bounded by a harbour with a protective breakwater. The water area is under additional anthropogenic pressure due to year-round navigation in the port and runoff from mountain rivers. As a result, higher concentrations of pollutants, including nutrients (phosphates, nitrates, nitrites, ammonium and silicon), are observed in the Yalta Port waters compared to similar indicators in the entire Yalta Bay.

The eutrophication level for the aquatic environment is determined by the distribution of biogenic nitrogen and phosphorus compounds, their seasonal and annual variations and recirculation degree. The sources of inorganic nitrogen (nitrites, nitrates and ammonium) entering the sea are river waters, domestic and industrial effluents and atmospheric precipitation. The nitrogen cycle in the surface layer of water is associated with nitrification $NH_4^+ \rightarrow NO_2^- \rightarrow NO_3^-$ and ammonification $NO_3^- \rightarrow NO_2^- \rightarrow NH_4^+$.

To date, numerous studies have been devoted to the hydrological and hydrochemical characteristics of the coastal waters of the Southern Coast of Crimea, including Yalta Bay. Work [1] summarises information on the hydrometeorological conditions of the Yalta coastal zone based on all observation data from 1870 to 2003 and on the hydrochemical regime in 1986–2004. Work [2] compares the hydrochemical characteristics of two water areas (the Yalta Port area and Yalta Bay) analysing the annual dynamics of concentrations of biogenic substances (nitrogen NO_2^-, NO_3^-, NH_4^+, N_{tot}, phosphorus PO_4^{3-}, P_{tot} and silicon SiO_2) as well as dissolved oxygen (O_2) and water temperature in the surface layer for 1987–2004 and 2005–2010. The presented results show changes in the ecological state of the surface water layer of Yalta Port during the study periods.

The inflow of significant amounts of nutrients and pollutants into Yalta Bay is caused by the runoff from the mountain rivers: Derikoyka (Bystraya) and Uchan-Su (Vodopadnaya) with their tributaries, Lyuka (which supplies water to Yalta), and others [1)]. Of note, according to work [3, p. 61], "the Vodopadnaya River mouth and the adjacent waters of Yalta City Beach are in an area of ecological risk due to elevated levels of nitrates and nitrites in the river water and severe bacterial contamination by *Escherichia coli* in the seawater (several hundred-fold above sanitary standards values during the high season)". According to the data [1)], the channel, floodplain and mouth of the Bystraya River and the adjacent water area of the Yalta

[1)] Borisova, Yu., 2014. The Uchan-Su River. In: Yu. Borisova, 2014. *Plantarium. Plants and Lichens of Russian and Adjusted Countries: The Open Online Plant Atlas and Field Guide.* Available at: https://www.plantarium.ru/page/landscapes/point/2563.html [Accessed: 29 August 2025] (in Russian).

passenger seaport are in an ecological risk zone. Elevated levels of nitrates and nitrites were recorded in the river water. The seasonal dynamics of inorganic nitrogen and phosphorus in the mouth zone of the Vodopadnaya River was studied in work [4]. The studies revealed that nutrient concentrations in the freshwater of the estuary significantly exceeded those in the seawater: nitrites (7.2-fold), ammonium (3.0-fold), nitrates (62.9-fold), and mineral phosphorus (13.2-fold). The total mineral nitrogen concentration in the river water was 27.9 times higher than in the seawater.

Currently, comprehensive monitoring of the background environmental condition in the coastal waters of Crimea, especially in the areas adjacent to the infrastructure of cargo, passenger, fishing and military fleets. Therefore, a proper assessment of the baseline condition is difficult.

The effectiveness of natural self-purification of marine ecosystems is determined by interdependent processes, such as input of pollutants, their deposition in bottom sediments and interaction with marine aerosols, the redistribution of pollutants and their transformation by biota, and the dynamic removal of pollutants beyond the water area. Under intense anthropogenic pressure, the first step towards normalising the ecological status of shallow marine waters is to assess their self-purification capacity by calculating the assimilation capacity (AC) of the ecosystem in relation to a priority pollutant or complex.

The AC concept developed by Yu. A. Izrael and A. V. Tsiban [5], based on the results of comprehensive oceanographic studies, was tested on the Baltic Sea ecosystem for benz(a)pyrene, polychlorinated biphenyls and a number of toxic metals (Cu, Zn, Pb, Cd, Hg). According to [5], the AC indicator characterises the ability of a marine ecosystem to withstand the addition of a certain amount of pollutants without developing irreversible biological consequences. AC has the dimension of a substance flux (mass of substance per unit of volume per unit of time). As shown in [6, 7], when using the balance method for calculating AC, the most difficult task is calculating the integral residence time of pollutants in the ecosystem under study. This quantity depends largely on the physical and chemical properties of a particular pollutant, the hydrodynamic parameters of the water area, and the set of processes (physical, chemical, microbiological) responsible for destruction of the pollutant or its removal beyond the boundaries of the water area under study.

The work is aimed to determine the priority pollutant based on the results of long-term monitoring of nutrients in the Yalta Port water area and to assess the self-purification capacity of the ecosystem by calculating the specific AC (AC_{sp}) in relation to inorganic forms of nitrogen (NO_3^-, NO_2^-, NH_4^+).

Notably, a literature data analysis reveals that this study provides the first calculation of this kind for the ecosystem of the Yalta Port water area.

Materials and methods of the study

To achieve our objective, a database on the Yalta Port water area was created. It was based on materials from the annual reports Sea Water Quality by Hydrochemical Indicators for 2018–2022 by the Federal State Budgetary Institution State Oceanographic Institute [2)] and materials from the database of Marine Hydrophysical Institute. According to work [2)], hydrochemical studies of the biogenic complex were carried out by the Yalta Environmental Pollution Monitoring Laboratory using methods approved by the Roshydromet hydrochemical monitoring system [3)].

Samples were collected in the Yalta Port water area at a single point with a depth of 6 m at the base of the breakwater annually from January to December, with standard hydrological monitoring conducted every ten days. Trends in the seasonal and long-term dynamics of nutrients and dissolved oxygen against the background of changes in temperature and salinity of the surface and bottom water layers of the Yalta Port water area for 2018–2022 were considered. Changes in the ecological situation in the water area were assessed compared to the previous period of 2013–2017 [8].

The analysed database consisted of 1,920 measurements of total nitrogen and phosphorus content, mineral nitrogen complexes (nitrites, nitrates, ammonium), phosphates, silicon and dissolved oxygen, as well as sea water temperature and salinity. The number of analysed samples and concentration limits are presented in Table 1.

The characteristics of the database for 2013–2017 are presented in work [2)]. In this study, AC was calculated using the balance method proposed by Yu. A. Izrael and A. V. Tsiban [5]. The authors of this paper have adapted the method for marine ecosystems where state hydrochemical monitoring is carried out [8], for example, in Sevastopol Bay with regard to inorganic nitrogen and phosphorus [9, 10]. According to [7], the final formulas for estimating the mean value $\overline{A}_{mi}$ and standard deviation $\sqrt{D[A_{mi}]}$ for AC of a marine ecosystem (m) in relation to the i-th pollutant are as follows:

$$AE_{mi} = \overline{A}_{mi} \pm \sqrt{D[A_{mi}]}, \tag{1}$$

$$\overline{A}_{mi} = \frac{Q_m \cdot C_{thr\,i}}{C_{\max i}} \cdot \overline{v}_i, \quad D[A_{mi}] = \left(\frac{Q_m \cdot C_{thr\,i}}{C_{\max i}} \right)^2 \cdot D[v_i], \tag{2}$$

where Q_m is the volume of water in the calculation area; $C_{thr\,i}$ is the threshold concentration of a pollutant; $C_{\max\,i}$ is the maximum concentration of a pollutant in the ecosystem; v_i is the rate of removal of a pollutant from the ecosystem, the average value $\overline{v}_i$ and dispersion $D[v_i]$ of which are determined according to

---

[2)] Korshenko, A.N., ed., 2024. *Marine Water Pollution*. Annual Report 2022. Ivanovo: PresSto, 302 p. (in Russian).

[3)] Oradovsky, S.G., ed., 1993. *Guide on the Chemical Analysis of Sea Waters.* RD 52.10.243-92. Saint Petersburg: Gidrometeoizdat, 264 p. (in Russian).

Table 1. Characteristics of the used data for 2018–2022

Parameter	MPC	Average	Maximum (% of MPC)	Standard deviation
PO_4^{3-}, µg/L	50	12	48 (96)	8.48
P_{tot}, µg/L	–	54.9	172	34.76
NO_2^-, µg/L	24	3.7	15.4 (64)	2.80
NO_3^-, µg/L	9032	140	953 (11)	201.77
NH_4^+, µg/L	389	18.6	104 (27)	14.27
N_{tot}, µg/L	–	1157	4301	831.60
Si_2O_2, µg/L	368	265	1698 (461)	303.91
O_2, %	–	91	109	6.49
Salinity, ‰	–	16.98	19.41	2.52
Temperature, °C	–	17.1	26.7	5.87

Note. The number of samples taken to determine the nutrient concentrations is 120 for each parameter, and 360 for each of oxygen content, temperature and salinity.

the original algorithm [6, 7]. In the equation above, the most difficult part of calculating AC is the quantitative assessment of the integral residence time of a pollutant in the ecosystem under study.

For areas under state monitoring, including the waters of Yalta Bay and Yalta Port, work [7] suggests a method to estimate the residence time of pollutants in the ecosystem. This indicator is calculated as the ratio of the change in pollutant concentration per unit of time to its average concentration, as well as the average rate of pollutant removal, determined from the complete data set for a specific water area (in our case, Yalta Port). The specific rate of pollutant removal is estimated using the equation

$$\tau = C / \nu,$$

where τ is the residence time of a pollutant in the ecosystem; C is the concentration of a pollutant in seawater; ν is the specific elimination rate of a pollutant from the ecosystem.

The specific rate of pollutant removal from the ecosystem of the studied water area was determined by the change in pollutant concentration in seawater per unit of time using the formula

$$v_n = (C_n - C_{n+1}) / (t_n - t_{n+1}),$$

where v_n is the specific rate of pollutant removal from the ecosystem during the selected period of concentration decrease $t_n - t_{n+1}$; C_n is the concentration during the period t_n; C_{n+1} is the concentration during the period t_{n+1} ; for $n = 1, ..., N$, where N is the sample size. Using the ratio of the average concentration of the i-th substance under study and the average rate of its removal (for all selected periods), the integral time of the pollutant residence in the ecosystem is calculated:

$$\tau_i = C_{\text{av}.i} / v_{\text{av}.i}.$$

The calculation results from the above equations are shown in Table 2.

The reliability of the calculated AC values is ensured by the analysis of a large dataset from long-term monitoring observations (1,920 measurements) over 10 years. It should be noted that for the Yalta Port water area, some boundaries with adjacent water areas are not strictly defined (i. e., they are permeable), therefore, AC_{sp} per unit volume (1 dm^3) was calculated as a relative value characteristic of the central part of the port water area [7].

To calculate AC parameters, only data from the water area under consideration was used, which allowed for a better assessment of its response to pollutant inputs and its self-purification capacity compared to using MPCs, which are accepted for all marine ecosystems disregarding regional peculiarities.

The average values of all forms of inorganic nitrogen during the observation period did not exceed the corresponding MPCs. This allowed us to use these average values as a threshold level in calculating the self-purification capacity of the ecosystem under study, which is one of the prerequisites for using Izrael's balance method [5] for calculation, the second prerequisite being the availability of long-term monitoring data.

Results and discussion

During the study period, the salinity in the Yalta Port water area varied between 4.59 and 19.41 ‰, with strong desalination (less than 10 ‰) observed in the surface water layer in 2018, 2019, 2021 and 2022. Oxygen saturation remained consistently low (averaging 89–92%), resulting in a dissolved oxygen deficit of 25–37%. The actual concentration of dissolved oxygen varied significantly, ranging from 5.29 to 10.99 mg/L.

The average values for 2018–2022 for all mineral forms of nutrients did not exceed the MPC. As can be seen from Table 1, only the MPC for silicon was exceeded during the study period, which is quite understandable given the significant volume of fresh river water entering Yalta Bay [1)]. The maximum phosphate content in 2021 was close to the threshold value (96% of the MPC).

A single sample of surface water taken on 15 July 2022 in the port area contained high concentrations of nitrates and ammonium: 953 μg/L (0.11 MPC) and 190 μg/L (0.49 MPC), respectively. The maximum total nitrogen content in the surface waters of the port area during this period reached 20,779 μg/L, which is five times higher than that for other samples that year (4,301 μg/L) (Table 1) and previous years (1559–3266 μg/L) and is obviously associated with heavy rainfall and the transport of nutrients with river water from the catchment area [3, 4]. The nitrite content reached its maximum (15.4 μg/L) in 2019, when the second maximum of ammonium content (104 μg/L) was recorded, which in other years did not exceed 69 μg/L. The dynamics of average and extreme values of the studied nutrients for 2018–2022 are presented in Fig. 1.

With relatively little change in the aeration of the waters (O_{2av}) of the Yalta Port water area during the described period, an increase in the average annual concentration of phosphorus and nitrogen was observed [8]. Thus, the total phosphorus content (P_{tot}) increased from 16 μg/L in 2018 to 77 μg/L in 2021, and that of nitrogen (N_{tot}) increased from 650 μg/L in 2019 to 1440 μg/L in 2022. Among mineral complexes, the maximum increase in the average annual concentration is characteristic of nitrates (from 51 μg/L in 2018 to 228 μg/L in 2022), while less noticeable for phosphates (from 6.5–11.7 μg/L in 2018–2020 to 15.7–16.3 μg/L in 2021–2022)

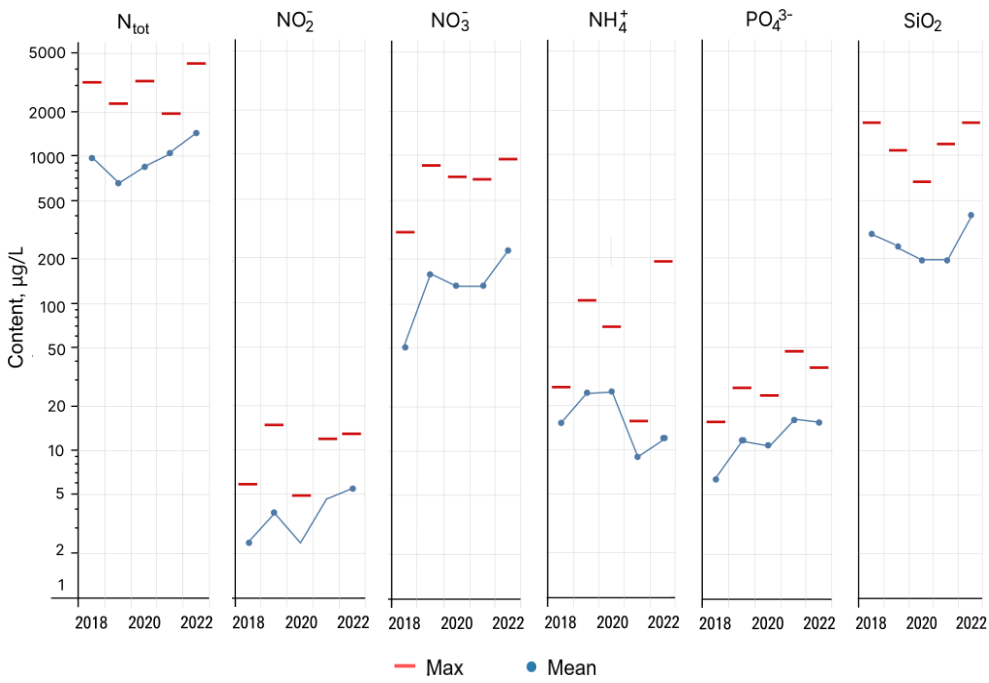

Fig. 1. Long-term dynamics of average and extreme values of nutrients content in the water area of the port of Yalta in 2018–2022

and nitrites (from 2.4–3.8 to 4.7–5.5 μg/L in the specified years). The dynamics of ammonium nitrogen concentration showed a decrease from 24–25 μg/L in 2019–2020 to 9 μg/L in 2021.

An analysis of the database for 2018–2022 showed that inorganic forms of nitrogen (NO_3^-, NO_2^-, NH_4^+) were the priority nutrients in Yalta Port: their concentrations increased by 50–120% over five years (the dynamics of phosphates and silicon were not as pronounced), and their contribution to total nitrogen reached 70%. At the same time, comparative estimates of inorganic and total nitrogen content based on data for two periods (2013–2017 [8] and 2018–2022) showed a twofold increase in the total content of mineral forms of nitrogen (on average from 84 μg/L in 2013–2017 to 161 μg/L in 2018–2022) in the waters of Port of Yalta against a significant decrease in the total content of this pollutant (on average from 1212 to 996 μg/L for the specified periods) (Fig. 2). Due to the reduction in the organic component contribution, the total share of mineral nitrogen increased from 7 to 16%.

The created database allowed us to assess the self-purification capacity of the port's water ecosystem by calculating its AC for inorganic forms of nitrogen (nitrates and nitrites) that showed steady growth, as well as for ammonium, whose content changed insignificantly. The characteristics of the self-purification capacity of the marine waters of the Yalta Port ecosystem with regard to nitrates, nitrites and ammonium for 2013–2017 and 2018–2022 are presented in Table 2.

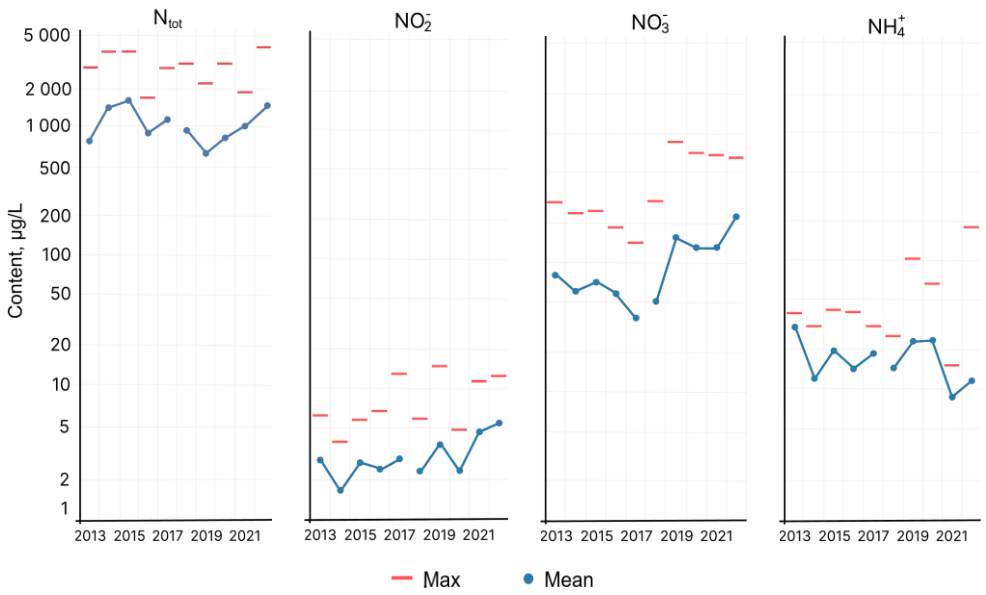

Fig. 2. Content of inorganic and total nitrogen in the Port of Yalta water area in 2013–2017 and 2018–2022

Table 2. Calculation results for the specific value of AC_{sp} in the ecosystem of the Port of Yalta water area in relation to inorganic forms of nitrogen for 2013–2017 and 2018–2022

Forms of nitrogen	Content, μg/L		v_n, μg/(L·day)	τ_i, day	AC_{sp}, μg/(L·day)
	mean	max			
2013–2017					
Nitrites (NO_2^-)	2.5	13.5	0.049	52–55	0.081
Nitrates (NO_3^-)	61.6	300.0	1.120	55–59	31.490
Ammonium (NH_4^+)	19.8	43.0	0.180	113–120	8.660
2018–2022					
Nitrites (NO_2^-)	3.7	15.4	0.065	58–60	0.097
Nitrates (NO_3^-)	140.0	953.0	4.210	33–37	36.070
Ammonium (NH_4^+)	16.5	104.0	0.220	81–83	7.560

As shown in Table 2, the average elimination time for nitrites from the Yalta Port water area in 2018–2022 was 58–60 days, while in 2013–2017 it was 52–55 days. In 2018–2022, the time required to remove nitrates and ammonium from the ecosystem decreased by approximately 20 and 30 days, respectively.

Nitrate removal occurs much faster. The removal rate varies widely: its maximum values for nitrites reach 0.302 μg/(L·day), nitrates – 9.86 μg/(L·day) and ammonium nitrogen – 2.95 μg/(L·day), which exceeds the average values for the period by 2.3–9.2 times.

An analysis of AC_{sp} dynamics showed that the ecological situation in the Yalta Port water area in terms of nitrite and nitrate concentrations in 2018–2022 improved compared to 2013–2017, but deteriorated in terms of ammonium content. The decrease in AC_{sp} for ammonium as a reduced inorganic form of nitrogen indicates an increase in the inflow of untreated municipal wastewater into the Yalta Port water area in the recent period.

To verify the obtained parameters of the self-purification capacity of the Yalta Port water area ecosystem, they were compared with the corresponding AC_{sp} values for the Sevastopol Bay ecosystem published in [10, 11]. For Sevastopol Bay as a whole, the AC_{sp} for nitrites was 0.047 μg/(L·day) and for nitrates it was 25.92 μg/(L·day). An analysis of the results showed that these values are lower than those obtained for the ecosystem of the Yalta Port water area (Table 2).

This indicates a more favourable state of the water area, apparently due to increased water dynamics.

The AC_{sp} value for ammonium in the Yalta Port water area was 7.56 μg/(L·day), which exceeded the average value for the Sevastopol basin (5.67 μg/(L·day)) and the value in the bay's most problematic eastern part (1.99 μg/(L·day)), which is affected by the Chernaya River runoff [11, 13].

The self-purification capacity for inorganic nitrogen was compared for Port of Yalta and Sevastopol Bay. Although they share common pollution sources (technogenic and recreational press, inflow with river waters), the Yalta Port ecosystem revealed a significantly greater self-purification potential. We attribute this difference to the distinct hydrodynamic conditions of these water areas.

Unlike Sevastopol Bay, which has limited water exchange with the open sea, Port of Yalta is characterized by complex hydrodynamic processes [13]. These are driven by the western and south-western currents of the Rim Current, which flow along the southern coast of Crimea. Furthermore, the interaction of the Rim Current's northern boundary with the shelf topography, such as capes and bays, significantly shapes the local circulation. Future research will focus on how this interaction affects the self-purification capacity of the Southern Coast of Crimea's coastal ecosystems.

Thus, the calculated AC_{sp} values for each form of inorganic nitrogen allow us to assess the self-purification capacity limit specifically for the ecosystem of the Yalta Port water area, in contrast to the uniform MPC adopted for all marine ecosystems disregarding local peculiarities.

When assessing the self-purification capacity of the Yalta Port water area ecosystem in cases of emergency discharge, the AC_{sp} should be used as a reference, which is 0.097 μg/(L·day) for nitrites, 36.1 μg/(L·day) for nitrates and 7.56 μg/(L·day) for ammonium nitrogen. Regulating discharges, given the established quantitative limits covering the entire range of disposal processes, will improve the environmental condition of the port's water area and, as a result, reduce the negative impact on Yalta Bay as a whole.

Conclusions

Based on long-term monitoring results (2012–2022), a database has been created on the content of nutrients and dissolved oxygen in the waters of Port of Yalta. We used this database to assess the dynamics of nutrients and identify inorganic forms of nitrogen (nitrites, nitrates, ammonium) as priority pollutants of the port ecosystem.

For the first time for this ecosystem, over two periods (2012–2017 and 2018–2022), the AC_{sp} for inorganic forms of nitrogen (nitrates, nitrites and ammonium) was estimated using the balance method, and the rate and time of their removal from the studied ecosystem were calculated.

The decrease in AC_{sp} for ammonium as a reduced inorganic form of nitrogen, obtained for 2018–2022, indicates that the amount of untreated municipal wastewater entered the Yalta Port water area during this period was greater than during the first period.

The AC_{sp} values, obtained for the ecosystem of the Yalta Port water area for 2018–2022 for all inorganic forms of nitrogen, were compared with similar indicators for the ecosystem of Sevastopol Bay, an area with high anthropogenic pressure and limited water exchange with the open sea.

The calculated AC_{sp} values for each form of inorganic nitrogen (nitrates, nitrites, ammonium) can be used by local authorities for quantitative and qualitative assessment of municipal and storm water discharge as main sources of these forms of nitrogen.

References

1. Ivanov, V.A., Repetin, L.N. and Malchenko, Yu.A., 2005. [*Climate Changes of Hydrometeorologocal and Hydrochemical Conditions of the Yalta Coastal Area*]. Sevastopol: MHI, 163 p. (in Russian).
2. Sovga, E.E., Godin, E.A., Plastun, T.V. and Mezentseva, I.V., 2014. Assessment of Hydrochemical Regime of the Yalta Bay Coastal Waters. *Morskoy Gidrofizicheskiy Zhurnal*, (3), pp. 48–59 (in Russian).
3. Vetrova, N.M., Ivanenko, T.A., Gaisarova, A.A. and Mennanov, E.E., 2019. The Problem of Ecological Risk Zones in the Coastal Areas of the Crimea. *Biospheric Compatibility: Human, Region, Technologies*, (2), pp. 59–73. https://doi.org/10.21869/23-11-1518-2019-26-2-59-73 (in Russian).
4. Egorov, V.N., Bobko, N.I., Marchenko, Yu.G. and Sadogurskiy, S.Ye., 2021. Nutrient Content and Limitation of the Phytoplankton Primary Production in the Estuary Area of the Vodopadnaya River (South Coast of Crimea). *Ecological Safety of Coastal and Shelf Zones of Sea*, (3), pp. 37–51. https://doi.org/10.22449/2413-5577-2021-3-37-51 (in Russian).
5. Izrael, Yu.A. and Tsyban, A.V., 1989. [*Anthropogenic Ecology of the Ocean*]. Moscow: Gidrometeoizdat, 529 p. (in Russian).
6. Sovga, E., Mezentseva, I. and Verzhevskaia, L., 2015. Assimilation Capacity of the Ecosystem of Sevastopol Bay. In: E. Ozhan, ed., 2015. *Proceedings of the Twelfth International Conference on the Mediterranean Coastal Environment MEDCOAST' 2015, 6–10 October 2015. Varna, Bulgaria*. Varna. Vol. 1. P. 317–326.
7. Sovga, E.E. and Mezentseva, I.V., 2017. Methodological Aspects of Estimates of Self-Purifying Ability of Marine Shallow Water Ecosystems (Gulfs, Bays, Ports). *Ecological Safety of Coastal and Shelf Zones of Sea*, (3), pp. 57–68 (in Russian).
8. Ivanov, V.A., Sovga, E.E. and Mezentseva, I.V., 2019. Long-Term Dynamics of Biogenic Elements and Oxygen in the Yalta Port Water Area in 2013–2017. *Ecological Safety of Coastal and Shelf Zones of Sea*, (2), pp. 86–93. https://doi.org/10.22449/2413-5577-2019-2-86-93 (in Russian).
9. Sovga, E.E., Mezentseva, I.V. and Kotelyanets, E.A., 2017. Assimilation Capacity of the Marine Shallow Water Ecosystems with Various Anthropogenic Impacts as the Estimation Method of Its Self-Purification Ability. *Problems of Ecological Monitoring and Ecosystem Modelling*, 28(4), pp. 39–52. https://doi.org/10.21513/0207-2564-2017-4-38-51 (in Russian).

10. Sovga, E.E., Mezentseva, I.V. and Khmara, T.V., 2022. Simulation of Seasonal Hydrodynamic Regime in the Sevastopol Bay and of Assessment of the Self-Purification Capacity of Its Ecosystem. *Fundamental and Applied Hydrophysics*, 15(2), pp. 110–123. https://doi.org/10.48612/fpg/92ge-ahz6-n2pt (in Russian).
11. Mezentseva, I.V. and Sovga, E.E., 2019. Self-Purification Ability of the Ecosystem of the East Part of the Sevastopol Bay with Respect to Inorganic Nitrogen. *Ecological Safety of Coastal and Shelf Zones of Sea,* (1), pp. 71–77. https://doi.org/10.22449/2413-5577-2019-1-71-77 (in Russian).
12. Sovga, E.E., Mezentseva, I.V. and Slepchuk, K.A., 2020. Comparison of Assimilative Capacity and Trophic Index for Various Parts of the Sevastopol Bay Water Area. *Ecological Safety of Coastal and Shelf Zones of Sea*, (3), pp. 63–76. https://doi.org/10.22449/2413-5577-2020-3-63-76 (in Russian).
13. Repetin, L.N., Romanov, A.S. and Churilova, T.Ya., 2010. Upwelling in the Area of Anticyclone Vorticity on the South Crimea Shelf. *Ecological Safety of Coastal and Shelf Zones of Sea*, 22, pp. 205–227 (in Russian).

Submitted 28.11.2024; accepted after review 11.01.2025;
revised 24.06.2025; published 30.09.2025

About the authors:

Irina V. Mezentseva, Senior Research Associate, Sevastopol Branch of the N. N. Zubov State Oceanographic Institute (61 Sovetskaya St., Sevastopol, 299011, Russian Federation), PhD (Geogr.), **ORCID ID: 0000-0001-9771-0380**, *mez-irina@mail.ru*

Elena E. Sovga, Leading Research Associate, Marine Hydrophysical Institute of RAS (2 Kapitanskaya St., Sevastopol, 299011, Russian Federation), DSc (Geogr.), **ORCID ID: 0000-0002-0670-4573, ResearcherID: A-9774-2018**, *science-mhi@mail.ru*

Tatiyana V. Khmara, Research Associate, Marine Hydrophysical Institute of RAS (2 Kapitanskaya St., Sevastopol, 299011, Russian Federation), **Scopus Author ID: 6506060413, ResearcherID: C-2358-2016**, *xmara@mhi-ras.ru*

Contribution of the authors:

Irina V. Mezentseva – calculations of the assimilation capacity of the Yalta Port ecosystem, analysis of the calculation results

Elena E. Sovga – study task statement, analysis of the method of assimilation capacity calculation, comparison of the assimilation capacity values of the ecosystems of Yalta Port and Sevastopol Bay, preparation of the manuscript

Tatiyana V. Khmara – calculations, discussion of the study results, data analysis and visualisation, article editing

All the authors have read and approved the final manuscript

ISSN 2413-5577, Ecological Safety of Coastal and Shelf Zones of Sea, 2025, No. 3, pp. 54–66.

Original paper

The Tier Structure of the *Ericaria–Gongolaria* Phytocenosis in the Coastal Zone of Protected Areas of Sevastopol

D. A. Kandaurova *, N. A.Milchakova

A. O. Kovalevsky Institute of Biology of the Southern Seas of RAS, Sevastopol, Russia
* *e-mail: dkandaurova@ibss-ras.ru*

Abstract
The paper describes the taxonomic diversity of the *Ericaria–Gongolaria* phytocenosis (*Ericaria crinita* + *Gongolaria barbata* – *Cladostephus spongiosus* – *Ellisolandia elongata*), which is the key part of the coastal ecosystems of specially protected natural areas of Sevastopol. The material was collected according to a standard procedure in the waters of six protected sites at depths of 1–5 m in summers from 2016 to 2021 during the peak of the macrophyte growing season. When analyzing the samples, we considered the species composition of the phytocenosis, the duration of life cycle of macroalgae, and their distribution by tiers and depths. The phytocenosis structure was found to be characterized by a high phytodiversity. Totally, 34 species of macroalgae were recorded. Two of them were found in the first tier, seven species were included in the second tier, and 25 taxa were represented in the third tier. The greatest diversity was found in red (Rhodophyta) algae: their share accounted for 52% of the total number of species. The contribution of brown (Ochrophyta) and green (Chlorophyta) macroalgae was 2.2 times less (24% each). In terms of life cycle, perennial and annual algae predominated: their share was 44 and 38%, respectively. The largest contribution of perennial species (70%) was registered near Cape Aya and Cape Sarych. In general, *Ericaria–Gongolaria* phytocenosis of different specially protected natural areas was characterized by low floral similarity: the values of the Jacquard coefficient (*Kj*) ranged from 7.1 to 66.7% and the average value was 21%. The taxonomic diversity, full tier structure and the predominance of perennial species indicate the stability of the key phytocenosis in specially protected natural areas of Sevastopol and effectiveness of their environmental regime.

Keywords: macrophytobenthos, *Ericaria crinita*, *Gongolaria barbata*, phytocenosis, phytocenosis vertical structure, species composition, marine protected areas, southwestern Crimea, Black Sea

Acknowledgements: This work was carried out within the framework of IBSS state research assignment “Biodiversity as the basis for the sustainable functioning of marine ecosystems, criteria and scientific principles for its conservation” (no. 124022400148-4). The authors sincerely thank the staff of the Laboratory of Phytoresources of the Department of Biotechnology and Phytoresources of A.O. Kovalevsky Institute of Biology of the Southern Seas of RAS for their assistance in processing samples of macrophytobenthos.

© Kandaurova D. A., Milchakova N. A., 2025

This work is licensed under a Creative Commons Attribution-Non Commercial 4.0 International (CC BY-NC 4.0) License

For citation: Kandaurova, D.A. and Milchakova, N.A., 2025. The Tier Structure of the *Ericaria–Gongolaria* Phytocenosis in the Coastal Zone of Protected Areas of Sevastopol. *Ecological Safety of Coastal and Shelf Zones of Sea*, (3), pp. 54–66.

Ярусная структура эрикариево-гонголяриевого фитоценоза в прибрежной зоне особо охраняемых природных территорий Севастополя

Д. А. Кандаурова *, Н. А. Мильчакова

ФГБУН ФИЦ «Институт биологии южных морей им. А. О. Ковалевского РАН», Севастополь, Россия

* *e-mail: dkandaurova@ibss-ras.ru*

Аннотация

Дана характеристика таксономического разнообразия эрикариево-гонголяриевого фитоценоза (*Ericaria crinita + Gongolaria barbata – Cladostephus spongiosus – Ellisolandia elongata*), ключевого в составе макрофитобентоса особо охраняемых природных территорий г. Севастополя. Материал отбирали по стандартной методике в акваториях шести заповедных объектов на глубинах от 1 до 5 м в летний сезон с 2016 по 2021 г. в пик вегетационного периода макрофитов. При анализе проб учитывали видовой состав фитоценоза, продолжительность жизненного цикла макроводорослей, их распределение по ярусам и глубинам. Установлено, что ярусная структура фитоценоза характеризуется высоким разнообразием таксонов видового ранга. Из 34 выявленных видов макроводорослей в первом ярусе встречались два, во втором – семь и в третьем – 25 видов. Наибольшим разнообразием характеризовались красные (Rhodophyta) водоросли, на долю которых приходилось 52 % общего количества таксонов, вклад бурых (Ochrophyta) и зеленых (Chlorophyta) был меньше почти в 2.2 раза (по 24 %). По продолжительности жизненного цикла преобладали многолетние и однолетние водоросли, доля которых составляла 44 и 38 % соответственно, максимальный вклад многолетних видов (70 %) зарегистрирован у м. Айя и м. Сарыч. Показано, что на разных участках особо охраняемых природных территорий эрикариево-гонголяриевый фитоценоз характеризовался низким флористическим сходством, значения коэффициента Жаккара (*Kj*) варьировали от 7.1 до 66.7 % при среднем значении 21 %. Таксономическое разнообразие, полночленная ярусная структура и преобладание многолетних видов отражают устойчивость ключевого фитоценоза и могут свидетельствовать об эффективности действующего природоохранного режима на особо охраняемых природных территориях г. Севастополя.

Ключевые слова: макрофитобентос, *Ericaria crinita, Gongolaria barbata,* фитоценоз, вертикальная структура фитоценоза, видовой состав, охраняемые акватории, Юго-Западный Крым, Черное море

Благодарности: работа выполнена в рамках государственного задания ФИЦ ИнБЮМ по теме «Биоразнообразие как основа устойчивого функционирования морских экосистем, критерии и научные принципы его сохранения» (№ гос. регистрации 124022400148-4). Авторы приносят искреннюю благодарность коллективу лаборатории фиторесурсов отдела биотехнологий и фиторесурсов ФИЦ ИнБЮМ за помощь в проведении экспедиционных исследований и обработке проб макрофитобентоса.

Для цитирования: *Кандаурова Д. А., Мильчакова Н. А.* Ярусная структура эрикариево-гонголяриевого фитоценоза в прибрежной зоне особо охраняемых природных территорий Севастополя // Экологическая безопасность прибрежной и шельфовой зон моря. 2025. № 3. С. 54–66.

Introduction

The nature conservation network of Specially Protected Natural Areas (SPNAs) in the city of Sevastopol comprises 19 sites, covering a total area of 23,768 km^2 (30% of the city's territory). This represents one of the highest figures among the subjects of the Russian Federation [1)]. Although Marine Protected Areas (MPAs) account for only 3% of the total area of these protected sites, they play a significant role in conserving the biodiversity of coastal ecosystems. According to various estimates [2)], the proportion of protected macrophyte species within the waters of SPNAs ranges from 18.2 to 45.5% of the species listed in the Red Book of Sevastopol [3)].

The benthic vegetation of the MPA is dominated by the *Ericaria–Gongolaria* phytocenosis, comprising *Ericaria crinita* + *Gongolaria barbata* – *Cladostephus spongiosus* – *Ellisolandia elongata*, which is one of the key ecosystems for the Black Sea coastal ecosystems and is protected at the international level [4), 5)]. The coenosis-forming species, *Ericaria crinita* (Duby) Molinari & Guiry and *Gongolaria barbata* (Stackhouse) Kuntze, also hold protected status [6), 7)]. Along the open shores of southwestern Crimea, the *Ericaria–Gongolaria* phytocenosis forms a belt type [8)] vegetation structure [1], with maximum productivity and the ecological-phytocenotic optimum of *E. crinita* and *G. barbata* recorded at depths from 1 to 5 m [8)], where the influence of factors driving the transformation of benthic communities is most pronounced. The primary factor is anthropogenic impact, which leads to biotope degradation, pollution from inadequately treated or untreated domestic wastewater, etc. [2, 3].

---

1) Sevastopol City Administration, 2023. [*Annual Report on State and Protection of Environment of the City of Sevastopol in 2023*]. Sevastopol: Main Department of Natural Resources and Ecology of the City of Sevastopol. Part 1, 194 p. (in Russian).

2) Milchakova, N.A., ed., 2015. [*Marine Protected Areas of Crimea. Scientific Reference Book*]. Sevastopol, Simferopol: N. Orianda, 300 p. (in Russian).

3) Dovgal, I.V. and Korzhenevskiy, V.V., eds., 2018. *The Red Data Book of Sevastopol.* Sevastopol: ROST-DOAFK, 432 p. (in Russian).

4) EEC Council, 1992. *Habitats Directive 92/43/EEC*. Available at: https://eur-lex.europa.eu/legal-content/EN/TXT/PDF/?uri= CELEX:31992L0043 [Accessed: 22 August 2025].

5) Gubbay, S., Rodwell, J.R., Garcia Criado, M., Borg. J., Otero, M., Janssen, J.A.M., Haynes, T., Beal, S., Nieto, A. [et al.], 2016. *European Red List of Habitats. Part 1. Marine habitats*. Luxembourg: Publications Office of the European Union, 2016. 52 p. https://doi.org/10.2779/032638

6) Ena, A.V. and Fateryga, A.V., eds., 2015. *Red Book of the Republic of Crimea. Plants, algae and fungi*. Simferopol: ARIAL, 480 p. (in Russian).

7) Dumont, H.J., ed., 1999. *Black Sea Red Data Book.* New York: United Nations Office for Project Services, 413 p.

8) Kalugina-Gutnik, A.A., 1975. [*Phytobenthos of the Black Sea*]. Kiev: Naukova Dumka, 246 p. (in Russian).

Over the past two decades, negative anthropogenic factors have impacted the coastal waters of Crimea and Black Sea regions, including protected areas, leading to a decline in macrophyte diversity, a shift in their lower growth boundary toward the shore, reduced productivity of macrophytobenthos, and alterations in the spatial distribution and vertical structure of phytocenoses [2, 4–6]. Under conditions of high anthropogenic pressure and coastal water pollution, macrophytobenthos transformation has been marked by outbreaks of short-cycle and epiphytic algae, changes in the tiered structure of benthic phytocenoses, reduced ecosystem stability, and a consequent decline in the self-purification capacity of coastal ecosystems [4, 5, 7–12]. As a result of anthropogenic succession, *E. crinita* and *G. barbata* have lost their dominant positions in many areas of the coastal zone along the Caucasian shelf, as well as off the coasts of Romania, Bulgaria and Turkey, including MPAs [11, 13, 14]. Similarly, in the Mediterranean Sea, their phytocenoses, particularly in the lower tiers, have experienced a replacement of perennial species with short-cycle or ephemeral species, predominantly green and calciphilic red algae [6, 15–20]. Concurrently, in many Mediterranean MPAs, the area occupied by phytocenoses of perennial brown algae, including species of the genera *Ericaria* and *Gongolaria*, has significantly decreased, largely due to biotope degradation resulting from inadequate regulation of fishing in protected areas [19–22].

Considering the role of key brown algae phytocenoses – the primary producers in the coastal ecosystems of southwestern Crimea – and the limited research on their structure, the objective of this study was to characterize the species composition and tiered structure of the *Ericaria–Gongolaria* phytocenosis and to evaluate its stability in the waters of SPNAs of Sevastopol.

Materials and methods of research

The vertical tiered structure of the *Ericaria–Gongolaria* phytocenosis was investigated in six SPNAs in Sevastopol, including two State Natural Preserves (SNPs) – *Cape Aya* and *Karansky* – and four Natural Monuments (NMs): the *Coastal Aquatic Complex* (CAC) *at Cape Sarych*, *CAC at Cape Fiolent*, *CAC at Tauric Chersonese*, and *CAC at Cape Lukull* (Fig. 1). In the coastal zones of these protected areas, this phytocenosis occurs on rocky-block substrates at depths ranging from 0.5 to 10 m.

The study focuses on lithophytic macroalgae of the *Ericaria–Gongolaria* phytocenosis, a key component of the Black Sea macrophytobenthos [8].

Material was collected at depths of 1, 3 and 5 m, corresponding to the ecological-phytocenotic optimum for *E. crinita* and *G. barbata*, during the summer periods of 2016–2021. Quantitative samples of macrophytes were collected using a standard method [8], employing a 25 × 25 cm sampling frame at each depth horizon in four replicates. To assess the species diversity across tiers, qualitative samples were gathered at various horizons within the phytocenosis distribution zone.

When processing the samples, the species composition, biomass of macrophytes by vertical tiers, the number of cenosis-forming lithophytic macroalgae, and

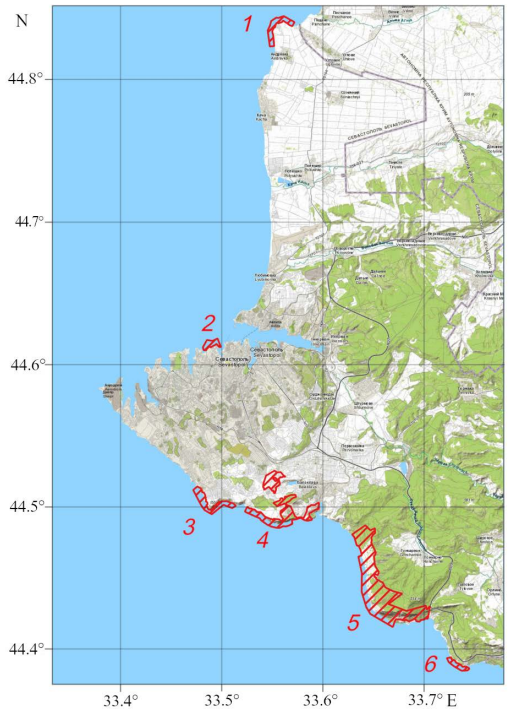

Fig. 1. The map of specially protected natural areas of Sevastopol: *1* – Natural Monument at Cape Lukull, *2* – Natural Monument at Tauric Chersonese, *3* – Natural Monument at Cape Fiolent, *4* – State Nature Preserve Karansky, *5* – State Nature Preserve Cape Aya, *6* – Natural Monument at Cape Sarych (the borders of objects are highlighted in red colour)

total projective cover of the phytocenosis were evaluated. A total of 93 quantitative and 20 qualitative samples of macrophytobenthos were collected and analyzed along six vertical transects located in the central part of SPNAs.

To characterize the vertical tiered structure of the *Ericaria–Gongolaria* phytocenosis, we analyzed the species composition of lithophytes in the 1st–3rd tiers. For the 4th tier, comprising crustose lithophytes, only the presence or absence of species was recorded using the underwater photofixation method [6].

A comparative analysis of the diversity of lithophytic synusiae was conducted across three vertical tiers, evaluating the proportion of species by division (Chlorophyta, Ochrophyta, Rhodophyta) and life cycle duration. For each species, the coefficient of occurrence Po (%) was calculated using the formula:

$$P_o = P\frac{a}{n}100,$$

where a represents the number of sites where the species was recorded; and n is the total number of surveyed sites [9].

The similarity of the species composition of the phytocenosis across the water areas of the SPNAs was assessed using the Jaccard coefficient Kj (%) [9]

$$Kj = 100\frac{c}{a+b-c},$$

where a is the number of species in one site; b is the number of species in another site; and c is the number of species common to both sites.

[9] Pesenko, Yu.A., 1982. [*Principles and Methods of Quantitative Analysis in Fauna Studies*]. Moscow: Nauka, 287 p. (in Russian).

To evaluate the similarity of the vertical tier structure of the *Ericaria–Gongolaria* phytocenosis in SPNAs, a cluster analysis was performed using data on species occurrence and presence or absence [10]. Macroalgal names were updated to reflect recent taxonomic revisions and nomenclature changes [11].

Results and discussion

The phytodiversity of the tiered structure of the *Ericaria–Gongolaria* phytocenosis in the coastal zone of Sevastopol's SPNAs exhibited high species richness, comprising 34 species. These were distributed as follows: 2 species in the 1st tier, 7 in the 2nd tier, and 25 in the 3rd tier. The 1st tier was dominated by the coenosis-forming species *Ericaria crinita* and *Gongolaria barbata*, the second was dominated by *Phyllophora crispa* (Hudson) P. S. Dixon, *Cladostephus spongiosus* (Hudson) C. Agardh and *Ulva rigida* C. Agardh, the third by *Apoglossum ruscifolium* (Turner) J. Agardh, *Chondria da-syphylla* (Woodward) C. Agardh, *Dictyota fasciola* (Roth) J. V. Lamouroux, *Ellisolandia elongata* (J. Ellis & Solander) K. R. Hind & G. W. Saunders, *Gelidium crinale* (Hare ex Turner) Gaillon, *G. spinosum* (S. G. Gmelin) P. C. Silva, *Jania rubens* (Linnaeus) J. V. Lamouroux, *J. virgata* (Zanardini) Montagne, *Laurencia coronopus* J. Agardh and *Vertebrata subulifera* (C. Agardh) Kuntze.

Analysis of the species composition by taxonomic division revealed that red algae (Rhodophyta) contributed the largest proportion, accounting for 52% of the total species, while brown algae (Ochrophyta) and green algae (Chlorophyta) each represented 24%. Notably, species proportions varied significantly across vertical tiers. In the 2nd tier, brown algae comprised 57% of the species, seven times higher than in the 3rd tier (8%). Conversely, green and red algae were 2–2.2 times less (29% and 64%, and 14% and 28%, respectively).

The number of species in SPNAs varied significantly across vertical tiers, ranging from one to five species in the 2nd tier and from one to eight in the 3rd tier. In the 2nd tier, the highest frequency of occurrence (*P*o = 75–100%) was recorded for *C. spongiosus*, *Ph. crispa*, and *U. rigida*. In the 3rd tier, high occurrence frequencies (from 50 to 75%) were noted for *A. ruscifolium*, *D. fasciola*, *E. elongata*, *G. crinale*, *G. spinosum*, *J. rubens*, *J. virgata*, *C. dasyphylla*, *L. coronopus*, and *V. subulifera*.

The highest species richness of lithophytes in the 2nd and 3rd tiers was observed in the waters of the NM *CAC at Cape Fiolent*, while the lowest was recorded in the *Karansky SNP* (Fig. 2). The greatest proportion of red algae was found in the coastal zones of the *Cape Aya SNP* and the NM *CAC at Cape Sarych*, accounting for 67% and 80% of the total species, respectively [8]. Brown algae contributed 23% in the NM *CAC at Cape Lukull*, indicating relatively clean water conditions in these areas [2]. A high proportion of green algae (38%) was recorded in the *CAC at Cape Fiolent*, likely due to elevated recreational pressure in the coastal zone during spring and summer.

---

10) Zaytsev, G.N., 1990. [*Mathematics in Experimental Botany*]. Moscow: Nauka, 296 p. (in Russian).

11) Algaebase Team. Algaebase. 2025. [online] Available at: http://www:algaebase.org [Accessed: 22 August 2025].

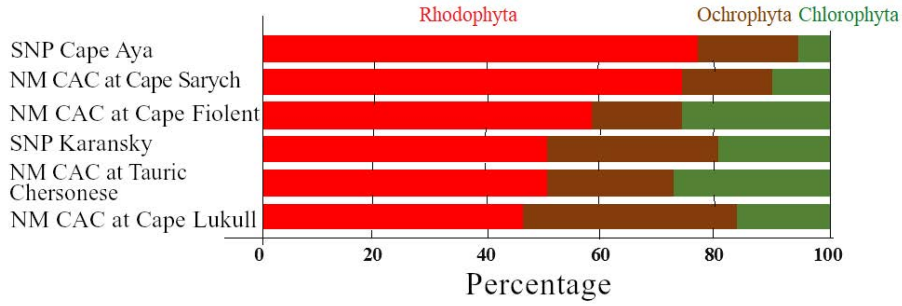

Fig. 2. Ratio of green, brown and red algae of the *Ericaria–Gongolaria* phytocenosis in the marine area of specially protected natural areas of Sevastopol

Analysis of species richness across the tiers in SPNAs of Sevastopol revealed slight variations with depth. The 1st tier, dominated by *E. crinita* and *G. barbata*, occurs at depths of 1 to 5 m and 3 to 5 m, respectively. In the 2nd and 3rd tiers, the highest number of species was recorded at depths of 1 and 5 m (22 species each), while diversity was lower at 3 m (15 species). The proportion of species by taxonomic division also varied slightly with depth; across all sites, red algae contributed twice as much to species richness as green and brown algae. In the 3rd tier, the proportion of Rhodophyta was three times higher than that of Ochrophyta and Chlorophyta, whereas no such pattern was observed in the 2nd tier.

Across SPNAs, the number of macroalgal species in the tiers also varied slightly with depth (Fig. 3). The highest phytodiversity was observed in the NM *CAC at Cape Fiolent* at a depth of 1 m. In the 2nd tier, the greatest species richness (five species) was recorded in the phytocenosis of the NM *CAC at Cape Fiolent* at 1 m, while the lowest (one species) was recorded in the *Karansky SNP* and the NM *CAC at Cape Sarych* at 3 m. Near Cape Lukull, species richness in the 2nd tier increased slightly with depth, reaching a maximum at 5 m.

In the 3rd tier, the highest species richness was observed in the waters of the NM *CAC at Tauric Chersonese* and the NM *CAC at Cape Sarych* at a depth of 5 m (7 and 8 species, respectively). The lowest species richness was recorded at depths of 3 and 5 m in the *Karansky SNP* and at 1 m in the NM *CAC at Tauric Chersonese* (one species each). Notably, in certain areas of the *Cape Aya* and *Karansky SNPs*, as well as the NM *CAC at Cape Fiolent*, at depths from 3 to 5 m within the ecological-phytocenotic optimum of the phytocenosis [8], no algae were found in the 2nd and 3rd tiers, which is probably due to the high density of coenosis-forming species in the 1st tier [1].

Comparative analysis of the phytodiversity across the three tiers of the *Ericaria – Gongolaria* phytocenosis revealed that the total species richness in SPNAs of Sevastopol was 1.3 times higher (34 species) than in other areas of the Crimean and Caucasian coasts (27 species) [1, 2, 5, 8, 10, 11, 13, 14, 23]. However, within protected waters, the number of taxa in the tiers ranged from 8 to 17 species, compared to 6 to 27 species in other areas of the Russian Black Sea shelf.

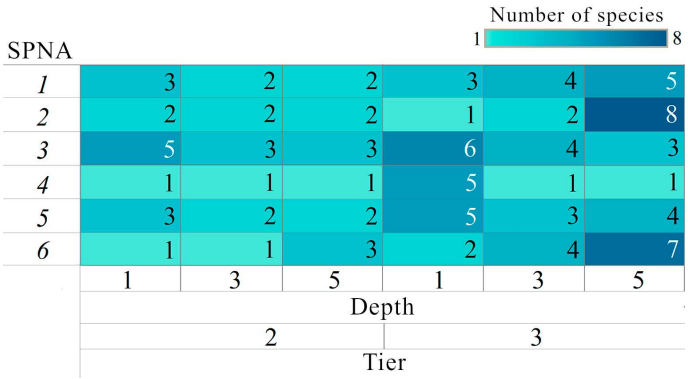

Fig. 3. The change in the number of species in the 2nd and 3rd tiers of the *Ericaria–Gongolaria* phytocenosis at depths of 1, 3 and 5 m in the marine area of specially protected natural areas of Sevastopol (see Fig. 1)

In the phytocenoses of protected areas, the 2nd tier contained 7 species, 1.6 times fewer than the 11 species reported elsewhere, while the 3rd tier exhibited 1.5 times greater species richness (21 species) compared to other studies (14 species). The increased diversity in the 3rd tier may be attributed to the presence of certain macroalgae, specifically *A. ruscifolium*, *C. dasyphylla*, *L. coronopus*, *L. obtusa* and *V. subulifera*, which were identified as lithophytic in this study but are typically epiphytic in other regions [8].

Analysis of the proportion of macroalgal species with varying life cycle durations in the tiers of the *Ericaria–Gongolaria* phytocenosis in SPNTs of Sevastopol revealed that perennial algae accounted for 44%, annual algae for 38%, and ephemeroids for 18% of the total species identified. Among brown algae, perennial and short-cycle species predominated; among red algae, perennial and annual species were prevalent; and among green algae, annual species dominated. The 1st tier consisted exclusively of perennial species, while in the 2nd and 3rd tiers, perennial species contributed 43% and 40%, respectively, and short-cycle species accounted for 57% and 52%, respectively. The highest proportion of perennial species (78%) was recorded in the waters of the NM *CAC at Cape Sarych* (Fig. 4), while the lowest (18%) was found in the *Karansky SNP*. The predominance of annual species (67%) in the *Karansky SNP* is likely associated with the influx of domestic and industrial wastewater from the Balaklava collector under specific synoptic conditions [24, 25].

The greatest proportion of perennial algae, ranging from 50 to 70%, was observed in the waters of the NM *CAC at Tauric Chersonese* (depth 1 m), the NM *CAC at Cape Sarych* and the *Cape Aya SNP* (depth 3 and 5 m). No seasonal or ephemeral species were recorded in the phytocenosis of the latter two sites.

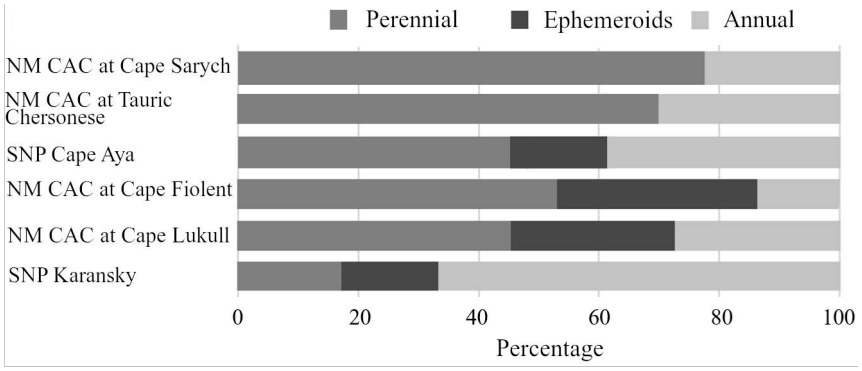

Fig. 4. The ratio of *Ericaria–Gongolaria* phytocenosis species by their life history in the marine area of specially protected natural areas of Sevastopol

The proportion of species with different vegetation periods reflects both the condition of benthic phytocenoses and their resilience to adverse environmental factors [8] [4, 18]. The predominance of perennial species in the *Ericaria–Gongolaria* phytocenosis (Fig. 4) suggests favorable conditions for macrophytobenthos in the coastal zone of Sevastopol's SPNAs, which is confirmed by evidence of improved environmental quality in these protected waters over recent decades [12, 24–26].

Previous studies have demonstrated that increased domestic pollution and eutrophication result in reduced species richness in perennial brown algae phytocenoses of the Black Sea, decreased biomass of coenosis-forming species in the 1st and 2nd tiers, and an increase in coralline calciphilic macroalgae in the 3rd tier [1, 2, 4, 8, 11, 13, 16]. Under the influence of these adverse factors, some key phytocenoses in the Mediterranean Sea have exhibited a replacement of perennial brown algae in the 1st tier with red coralline algae, such as *Corallina officinalis* Linnaeus, *E. elongata*, *J. rubens*, and others. This shift has led to significant structural transformation and a decline in the productivity of macrophytobenthos [17–20].

Analysis of the species diversity across the tiers of the *Ericaria–Gongolaria* phytocenosis in SPNAs revealed low structural similarity. The average value of *Kj* between sites did not exceed 21% (Fig. 5), compared to 56–62% in other areas of the coastal zone of Crimea [8]. The highest number of shared species was observed between the phytocenoses of the *Cape Aya SNP* and the NM *CAC at Cape Sarych* (*Kj* from 33.3 to 46.2%). In other sites, *Kj* values were 3–5 times lower.

Significant variation in *Kj* was observed across depths. The highest species similarity was recorded in the phytocenoses near Cape Aya and Cape Fiolent at a depth of 3 m (*Kj* = 66.7%), while the lowest was found near the *Karansky SNP* and the NM *CAC at Cape Lukull* at depths of 3 and 5 m (*Kj* = 7.1%).

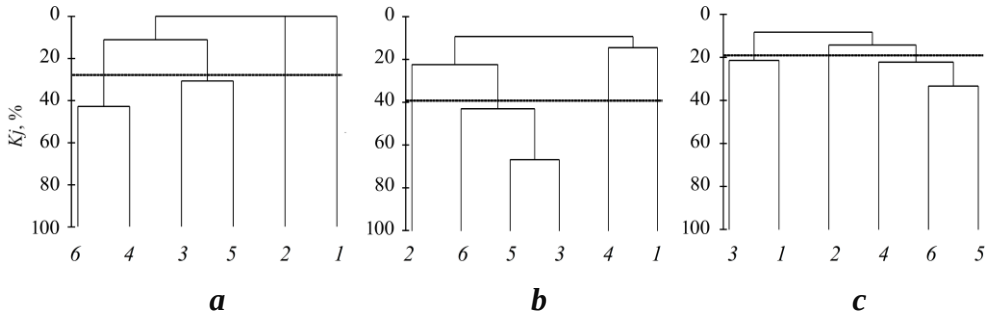

Fig. 5. Dendrogram of similarity in species composition of *Ericaria–Gongolaria* phytocenosis in the specially protected natural areas of Sevastopol (see Fig. 1): *a* – depth of 1 m, *b* – 3 m, *c* – 5 m

Conclusion

The *Ericaria–Gongolaria* phytocenosis (*Ericaria crinita* + *Gongolaria barbata* – *Cladostephus spongiosus* – *Ellisolandia elongata*) is a key component of the Black Sea macrophytobenthos, exhibiting high taxonomic diversity in the coastal SPNAs of Sevastopol. Thirty-four macroalgal species were identified in the lithophytic synusiae across three tiers, of which Chlorophyta and Ochrophyta each contributed 24% to the total species richness, while Rhodophyta accounted for 52%. The 1st tier was dominated by coenosis-forming brown algae (Ochrophyta), in the 2nd and 3rd tiers, their proportions were 57% and 28%, red algae (Rhodophyta) – 29% and 64%, green algae (Chlorophyta) – 14% and 8%, respectively. The proportion of species across taxonomic divisions varied slightly across regions and depths, with brown and red algae consistently 2–3 times more abundant than green algae.

Perennial species predominated in the composition of the tiered synusiae of the phytocenosis, with their highest proportion (53–78%) recorded in the phytocenoses of the NM *CAC at Cape Fiolent*, the NM *CAC at Cape Sarych*, and the *Cape Aya SNP*. In other protected waters of SPNAs of Sevastopol, the proportion ranged from 17 to 46%. The floristic similarity of the species composition across the tiers in these protected areas was low, with the highest number of shared species observed among the phytocenoses of the *Cape Aya SNP*, the NM *CAC at Cape Sarych*, and the NM *CAC at Cape Fiolent*.

Elements of restorative succession, indicative of ecological stability, were identified in the *Ericaria–Gongolaria* phytocoenosis within the coastal zone of SPNAs of Sevastopol. These include a well-developed structure, high floristic diversity across tiers, and the predominance of perennial brown and red algae. The ecological and phytocoenotic characteristics of this phytocoenosis suggest that the protected waters of Sevastopol can be classified as relatively clean. However, due to significant fuel oil inputs into the waters of the *Cape Aya SNP* and the NM *CAC at Cape Fiolent*, regular monitoring of key benthic phytocoenoses, which are critical for the self-purification of coastal waters, remains an essential conservation priority.

REFERENCES

1. Milchakova, N.A., 2003. Macrophytobenthos. In: V. N. Eremeev and A. V. Gaevskaya, eds., 2003. *Modern Condition of Biological Diversity in Near-Shore Zone of Crimea (the Black Sea Sector)*. Sevastopol: ECOSI-Gidrofizika, pp. 152–208 (in Russian).
2. Milchakova, N.A. and Petrov, A.N., 2003 Morphofunctional Analysis of Long-Term Changes of the Structure of *Cystoseira* Phytocenoses (Laspi Bay, the Black Sea). *International Journal of Algae*, 5(3), pp. 47–63. https://doi.org/10.1615/InterJAlgae.v5.i3.40
3. Milchakova, N.A., Alexandrov, V.V. and Ryabogina, V.G., 2019. State of Key Phytocenoses of Marine Protected Areas and Problems Their Conservation (Southwestern Crimea, Black Sea). *Plant Biology and Horticulture: Theory, Innovation*, (149), pp. 113–123 (in Russian).
4. Milchakova, N.A., 2015. Current State of Macrophytobenthos in Karadag Nature Reserve and Adjacent Objects of the Marine Protected Area (Crimea, the Black Sea). In: A. V. Gayevskaya and A. L. Morozova, eds., 2015. *100 Years of the T.I. Vyazemsky's Karadag Scientific Station*. Simferopol: N. Orianda, pp. 506–523 (in Russian).
5. Evstigneeva, I.K. and Tankovskaya, I.N., 2021. Hydro-Botanical Studies of the Protected Water Area of the Western Crimea (Black Sea). *Phytodiversity of Eastern Europe*, 15(4), pp. 16–33 (in Russian).
6. Berov, D., Todorova, V., Dimitrov, L., Rinde, E. and Karamfilov, V., 2018. Distribution and Abundance of Phytobenthic Communities: Implications for Connectivity and Ecosystem Functioning in a Black Sea Marine Protected Area. *Estuarine, Coastal and Shelf Science*, 200, pp. 234–247. https://doi.org/10.1016/j.ecss.2017.11.020
7. Minicheva, G.G., Bolshakov, V.N., Kalashnik, E.S., Zotov, A.B. and Marinets, A.V., 2018. Assessment of the Reactions of the Black Sea Ecosystem's Algaecommunities to Influence of Climatic Factors. *International Journal of Algae*, 28(2), pp. 121–135. https://doi.org/10.15407/alg28.02.121
8. Cernysheva, E.B., 2019. Changes in the Structure of Cystoseira Communities in Various Environmental Conditions (the Black Sea, Sevastopol). *Ecological Safety of Coastal and Shelf Zones of Sea*, (3), pp. 72–81. https://doi.org/10.22449/2413-5577-2019-3-72-81 (in Russian).
9. Kovardakov, S.A. and Prazukin, A.V., 2012. Structural and functional characteristics of the bottom seaweeds community in Kruglaya bay (Sevastopol). In: TNU, 2012. *Optimization and Protection of Ecosystems*. Simferopol: TNU. Iss. 7, pp. 138–148 (in Russian).
10. Kostenko, N.S., Evstigneeva, I.K. and Tankovskaya, I.N., 2018. Phytobenthos. In: N. S. Kostenko, ed., 2018. *The Biology of the Black Sea Offshore Area at the South-Eastern Crimea*. Simferopol: ARIAL, pp. 172–233. https://doi.org/10.21072/978-5-907032-04-0 (in Russian).
11. Lisovskaya, O.A and Nikitina, V.N., 2007. Macrophytobenthos of Caucasus Coast of Black Sea near Tuapse and Big Sochi. *Vestnik of Saint-Petersburg University. Series 3. Biology*, (2), pp. 22–33 (in Russian).
12. Milchakova, N.A., Alexandrov, V.V., Kovardakov, S.A. and Pavshenko, D.A., 2023. Macrophytobenthos of the Natural Monument "Coastal Aquatic Complex at Cape Fiolent" (Sevastopol). In: N. A. Bagrikova, ed., 2023. *Scientific Notes of the «Cape Martyan» Nature Reserve*. Simferopol: ARIAL, Iss. 14, pp. 183–188. https://doi.org/10.25684/2413-3019-2023-14-183-188 (in Russian).

13. Simakova, U.V., Smirnov, I.A., Shabalin, N.V. and Papunov, V.G., 2017. [Macroalgae Community of Utrish Natural Reserve]. In: R. V. Gorbunov, ed., 2017. *All-Russian Scientific Conference «Scientific Researches on the Reserve Territories», devoted to the 160th anniversary of the birth of the Karadag scientific station founder, doctor of medicine, privat-docent of the Moscow University Terenty Ivanovich Vyazemsky, as well as the Year of Specially Protected Natural Territories and the Year of Ecology in Russia, Kurortnoe, October 9–14, 2017*. Simferopol: ARIAL, pp. 47 (in Russian).
14. Afanasyev, D.F., Kamnev, A.N. and Sushkova E.G., 2018. Structure and Seasonal Dynamics of *Cystoseira Crinita* (Fucales, Phaeophyceae) Dominated Communities from the North-Eastern Black Sea. In: A. L. Budantsev, ed., 2018. [*Botany in the Modern World. Proceedings of the XIV Congress of the Russian Botanical Society and the Conference "Botany in the Modern World" (Makhachkala, 18−23 June 2018). Vol. 3: Spore Plants. Mycology. Structural Botany. Plant Physiology and Biochemistry. Plant Embryology*]. Makhachkala: ALEF, pp. 14−16 (in Russian).
15. Sava, D., Doroftei, E. and Arcuş, M., 2011. Ecology and Distribution of Macrophytic Red Algae from the Romanian Black Sea Coast. *Botanica Serbica*, 35(1), pp. 37–41.
16. Birben, Ü., 2020. The Effectiveness of Protected Areas in Biodiversity Conservation: The Case of Turkey. *Cerne*, 25(4), pp. 424–438. https://doi.org/10.1590/01047760201925042644
17. Boudouresque, C.-F., Blanfune, A., Changeux, T., Pergent, G., Perret-Boudouresque, M., Ruitton, S. and Thibaut, T., 2024. Marine Biodiversity in the Mediterranean in the Era of Global Warming. *La Mer*, 61(3–4), pp. 189–231. https://doi.org/10.32211/lamer.61.3-4_189
18. Thibaut, T., Blanfune, A., Boudouresque, C.-F. and Verlaque, M., 2015. Decline and Local Extinction of Fucales in French Riviera: The Harbinger of Future Extinctions? *Mediterranean Marine Science*, 16(1), pp. 206–224. https://doi.org/10.12681/mms.1032
19. Coleman, M.A. and Wernberg, T., 2017. Forgotten Underwater Forests: The Key Role of Fucoids on Australian Temperate Reefs. *Ecology and Evolution*, 7(20), pp. 8406–8418. https://doi.org/10.1002/ece3.3279
20. Rindi, F., Vergés, A., Zuchegna, I., Bianchelli, S., de Caralt, S., Galobart, C., Santamaría, J., Martini, F., Monserrat, M. [et al.], 2023. Standardized Protocol for Reproductive Phenology Monitoring of Fucalean Algae of the Genus *Cystoseira* s.l. with Potential for Restoration. *Frontiers in Marine Science*, 10, 1250642. https://doi.org/10.3389/fmars.2023.1250642
21. Verdura, J., de Caralt, S., Santamaria, J., Vergés, A., Mangialajo, L., Ivesa, L., Farina, S., Cefalí, M.E., Fraschetti, S. [et al.], 2018. Regional Environmental Conditions Determine Tolerance to Future Warming of a Marine Macroalgae Forests. *PeerJ PrePrints*, 2 p. https://doi.org/10.7287/peerj.preprints.26766v1
22. Rendina, F., Falace, A., Alongi, G., Buia, M.C., Neiva, J., Appolloni, L., Marletta, G. and Russo, G.F., 2023. The Lush Fucales Underwater Forests off the Cilento Coast: An Overlooked Mediterranean Biodiversity Hotspot. *Plants*, 12(7), 1497. https://doi.org/10.3390/plants12071497
23. Pavshenko, D.A., 2023. Application of Geobotanical Methods for Studying the Benthic Vegetation of the Black Sea. *Ekosistemy*, (36), pp. 18–29 (in Russian).
24. Kuftarkova, E.A., Rodionova, N.Yu., Gubanov, V.I. and Bobko, N.I., 2008. Hydrochemical Characteristics of Several Bays of Sevastopol Coast. In: YugNIRO, 2008. *Trudy YUGNIRO = YugNIRO Proceedings*. Kerch: YugNIRO Publishers. Vol. 46, pp. 110–111 (in Russian).

25. Gruzinov, V.M., Dyakov, N.N., Mezenceva, I.V., Malchenko, Y.A., Zhohova, N.V. and Korshenko, A.N., 2019. Sources of Coastal Water Pollution near Sevastopol. *Oceanology*, 59(4), pp. 523–532. https://doi.org/10.1134/S0001437019040076

26. Shchurov, S.V., Kovrigina, N.P. and Ladygina, L.V., 2019. Seasonal Variation of Abiotic Factors of Environment and Phytoplankton in the Laspi Bay Mussel Farm Area (2010–2011). *Scientific Notes of V.I. Vernadsky Crimean Federal University. Geography. Geology*, 5(2), pp. 184–201 (in Russian).

Submitted 09.04.2025; accepted after review 01.06.2025;
revised 24.06.2025; published 30.09.2025

About the authors:

Daria A. Kandaurova, Postgraduate Student, Junior Research Associate, A. O. Kovalevsky Institute of Biology of the Southern Seas of RAS (2 Nakhimov Av., Sevastopol, 299011, Russian Federation), **ORCID ID: 0009-0009-2966-6811**, *dkandaurova@ibss-ras.ru*

Nataliya A. Milchakova, Leading Research Associate, Head of Phytoresources Laboratory, A. O. Kovalevsky Institute of Biology of the Southern Seas of RAS (2 Nakhimov Av., Sevastopol, 299011, Russian Federation), PhD (Biol.), **ORCID ID: 0000-0001-5407-7706, ResearcherID: I-1280-2016**, *nmilchakova@ibss-ras.ru*

Contribution of the authors:

Daria A. Kandaurova – processing of macrophytobenthos samples, analysis of the study results, preparation of the article text

Nataliya A. Milchakova – problem statement, determination of the macrophytobenthos species composition, analysis of the study results, preparation of the article text

All the authors have read and approved the final version of the manuscript.

Original paper

Distribution of Bottom Vegetation in the Eastern Part of Sevastopol Bay

N. V. Mironova, T. V. Pankeeva *

A. O. Kovalevsky Institute of the Southern Seas of RAS, Sevastopol, Russia
* *e-mail: tatyanapankeeva@yandex.ru*

Abstract
The paper studies the current state of macrophytobenthos in the eastern part of Sevastopol Bay. The study collected information on the distribution of key macrophyte species and compared changes in their contribution for over 40 years. Hydrobotanical surveys were performed using standard methodology on the same profiles during the summers of 1977, 2017, and 2024. *Gongolaria barbata* and *Ericaria crinita* were found to dominate the bottom vegetation composition at present (2017 and 2024), and green algae (*Cladophora laetevirens, Ulva intestinalis, U. rigida*) were also abundant. In 2024, almost all profiles at 0.5 m depth showed a decrease in total macrophyte biomass and the proportion of *G. barbata* and *E. crinita* due to the damaging effects of the extreme storm. However, at depths of 1 and 3 m, quantitative macrophytobenthos biomass values were about twice as high as those in 2017. A comparative analysis of macrophytobenthos distribution for almost half a century showed that the most significant transformation of the vegetation component was observed in the eastern part of the bay, where higher aquatic vegetation (*Zostera marina, Z. noltei, Stuckenia pectinata, Zannichellia* sp., *Ruppia* sp.) was replaced by thickets of perennial algae (*G. barbata* and *E. crinita*). These changes are probably due to increase in water salinity in the Chyornaya River estuarine zone and changes in the intensity of longshore sediment fluxes in the water area. In the eastern part of the bay, a change in the predominance of *Ulva species* to *G. barbata* and *E. crinita* was recorded during this period, possibly indicating some improvement in environmental quality. The study results can be applied during monitoring of the marine environment state in the bay, as well as for developing coastal protection measures.

Keywords: macrophytobenthos, *Gongolaria barbata*, *Ericaria crinita, Ulva rigida*, *Cladophora laetevirens*, Black Sea, Sevastopol

Acknowledgments: This work was carried out within the framework of IBSS state research assignment “Comprehensive study of the functioning mechanisms of marine biotechnological complexes with the aim of obtaining bioactive substances from hydrobionts” (No. 124022400152-1).

For citation: Mironova, N.V. and Pankeeva, T.V., 2025. Distribution of Bottom Vegetation in the Eastern Part of Sevastopol Bay. *Ecological Safety of Coastal and Shelf Zones of Sea*, (3), pp. 67–80.

© Mironova N. V., Pankeeva T. V., 2025

This work is licensed under a Creative Commons Attribution-Non Commercial 4.0 International (CC BY-NC 4.0) License

Распределение донной растительности в восточной части Севастопольской бухты

Н. В. Миронова, Т. В. Панкеева *

ФГБУН ФИЦ «Институт биологии южных морей имени А.О. Ковалевского РАН», Севастополь, Россия

* *e-mail: tatyanapankeeva@yandex.ru*

Аннотация

Представлены результаты исследования современного состояния макрофитобентоса в восточной части б. Севастопольской. В ходе изучения собраны сведения о распределении ключевых видов макрофитов и проведен сравнительный анализ изменений их вклада в общую биомассу макрофитобентоса за период более 40 лет. Гидроботанические исследования выполняли согласно стандартной методики по одним и тем же разрезам в летний период 1977, 2017 и 2024 гг. Выявлено, что в настоящее время (2017 и 2024 гг.) в составе донной растительности доминируют *Gongolaria barbata* и *Ericaria crinita*, также обильно представлены зеленые водоросли (*Cladophora laetevirens, Ulva intestinalis, U. rigida*). В 2024 г. почти на всех разрезах на глубине 0.5 м отмечено снижение общей биомассы макрофитов, доли *G. barbata* и *E. crinita* вследствие разрушительного воздействия экстремального шторма. При этом на глубине 1 и 3 м количественные показатели биомассы макрофитобентоса были примерно вдвое выше, чем в 2017 г. Сравнительный анализ распределения макрофитобентоса за почти полувековой период показал, что наиболее существенная трансформация растительной компоненты произошла в кутовой части бухты, где произрастающая здесь ранее высшая водная растительность (*Zostera marina, Z. noltei, Stuckenia pectinata, Zannichellia* sp., *Ruppia* sp.) сменилась зарослями многолетних водорослей (*G. barbata* и *E. crinita*). Эти изменения, вероятно, можно объяснить повышением солености воды в приустьевой зоне р. Черной, а также изменением интенсивности вдольбереговых потоков наносов в акватории. В восточной части бухты за этот период зарегистрирована смена доминантных видов водорослей: вместо представителей рода *Ulva* начали преобладать виды *G. barbata* и *E. crinita*, что, возможно, свидетельствует об улучшении качества среды. Результаты работы могут быть применены при мониторинге состояния морской среды в бухте, а также при планировании охранных мероприятий прибрежной зоны моря.

Ключевые слова: макрофитобентос, *Gongolaria barbata, Ericaria crinita, Ulva rigida, Cladophora laetevirens,* Черное море, Севастополь

Благодарности: работа выполнена в рамках государственного задания ФИЦ ИнБЮМ по теме «Комплексное исследование механизмов функционирования морских биотехнологических комплексов с целью получения биологически активных веществ из гидробионтов» № гос. регистрации 124022400152-1.

Для цитирования: *Миронова Н. В., Панкеева Т. В.* Распределение донной растительности в восточной части Севастопольской бухты // Экологическая безопасность прибрежной и шельфовой зон моря. 2025. № 3. С. 67–80. EDN XGKJBD.

Introduction

Macrophytobenthos plays a leading role in the stabilization of coastal geosystems by providing a range of ecosystem functions and services [1–3]. It is well established that benthic vegetation actively responds to environmental changes. Consequently, changes in the species composition and abundance of macrophytes enable phytobenthos to serve as a unique indicator of the ecological condition of coastal waters.

The depth distribution of benthic vegetation is determined by the photic zone's boundary, where algal photosynthesis takes place, primarily influenced by water clarity. Consequently, investigating macrophytobenthos is increasingly critical in waters heavily affected by economic activities.

The eastern part of Sevastopol Bay, subjected to long-term anthropogenic impact, was selected as a model region. Notably, significant volumes of wastewater are discharged into the bay [4–6]. The studied water area experiences active shipping, dredging, and other hydraulic engineering activities, leading to elevated pollutant levels in the water [7, 8]. Numerous contemporary studies have focused on this part of the bay, examining its hydrological and hydrochemical parameters [9, 10], the lithological composition of bottom sediments [11–14], and the quantitative characteristics of meio- and macrozoobenthos communities [15–18]. However, research on benthic vegetation remains limited [19–22].

This study aims to evaluate the current state of macrophytobenthos in the eastern part of Sevastopol Bay and to characterize the interannual dynamics of the distribution of dominant macrophyte species from 1977 to 2024.

Materials and methods of research

The eastern part of Sevastopol Bay has an average depth of 13.1 m, with maximum depths along the fairway reaching 19.5 m. The sea area is characterized by a complex hydrodynamic regime driven by two opposing currents: one flowing westward from the Chyornaya River and another eastwards from the open sea. The ecological condition of the waters in this region is further influenced by water exchange with Yuzhnaya Bay [4, 6, 23].

The apex of the bay is shallow, with an average depth of 4.7 m and a maximum depth of 10.8 m [7]. This semi-enclosed region of the bay is influenced by the Chyornaya River, which causes desalination of surface waters and delivers significant amounts of allochthonous organic and mineral substances, including nutrients and pollutants, through river runoff [23].

In recent decades, the area along the eastern shore of the bay has undergone significant transformation. Coastal fortifications, breakwaters, and piers have been constructed, altering the landscape. The mouth of the Chyornaya River has been modified to accomodate the Sevastopol seaport basin, while the floodplain now hosts a pier and the Chyornaya River shipping canal [24].

Phytobenthos samples were collected in Sevastopol Bay in July 2017 and 2024 and were used as study material. The samples were obtained using vertical profiles by a diver at depths of 0.5, 1, 3 and 5 m, up to the boundary of macrophyte distribution, with quadruplicate sampling conducted within 25 × 25 cm survey plots [1]. A total of 96 quantitative samples were collected and analysed (Table 1). The aim of the work was to study the distribution and biomass of macrophytobenthos in the coastal zone of the eastern part of the bay (profiles *1*–*5*) (Fig. 1). A portable Oregon 650 GPS receiver was used to determine the coordinates of the profiles. The results are presented in Table 1.

The benthic vegetation was characterized using the dominance classification proposed by A. A. Kalugina-Gutnik [2]. To analyze the structure of phytocommunities, the Shannon species diversity index (*H*) was calculated. Algal species identification followed the guide [3], incorporating the latest nomenclature revisions [4]. Data on the composition and distribution of benthic vegetation in the bay for 1977 were obtained by one of the authors, who participated in sample collection during the summer period in the study areas and analyzed them using a similar method.

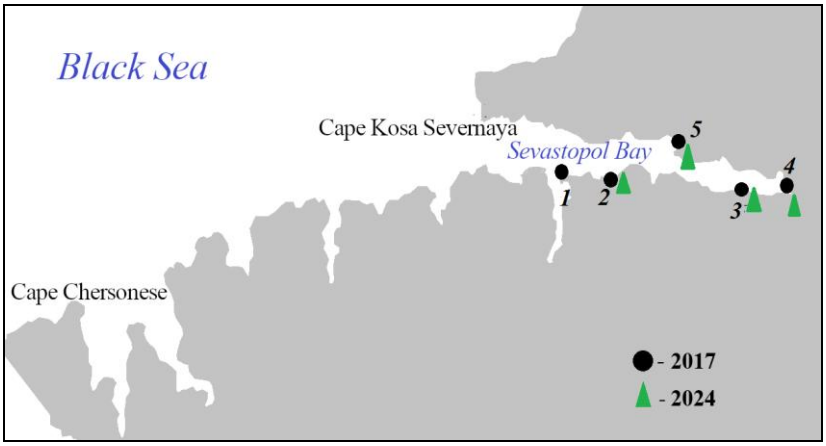

Fig. 1. Schematic map of hydrobotanical profiles in the western part of Sevastopol Bay: *1* – Cape Pavlovsky; *2* – Ushakov Beam; *3* – thermal station; *4* – Inkerman; *5* – Gollandia

[1] Kalugina-Gutnik, A.A., 1969. [Study of the Black Sea Bottom Vegetation Using Lightweight Diving Equipment]. In: Academy of Sciences of the USSR, 1969. [*Marine Underwater Studies*]. Moscow: Nauka, pp. 105–113 (in Russian).

[2] Kalugina-Gutnik, A.A., 1975. [*Phytobenthos of the Black Sea*]. Kiev: Naukova Dumka, 248 p. (in Russian).

[3] Zinova, A.D., 1967. [*Field Guide to Green, Brown and Red Algae of the Southern Seas of the USSR*]. Leningrad: Nauka, 397 p. (in Russian).

[4] Available at: http://www.algaebase.org [Accessed: 22 August 2025].

Table 1. Coordinates and depth range of hydrobotanical profiles, number of sampled macrophytobenthos in Sevastopol Bay

Profile	Coordinates		Depth, m				Number of samples
	°N	°E	0.5	1	3	5	
1	44°36′57″	33°32′4″	+/0	+/0	+/0	+/0	16
2	44°36′57″	33°32′42″	+/+	+/+	+/+	+/–	28
3	44°36′37″	33°34′57″	+/+	+/+	–	–	16
4	44°36′30″	33°36′05″	+/+	+/+	–	–	16
5	44°37′23″	33°33′39″	+/+	+/+	–/+	–	20

Note: Numerator – samples taken in 2017; denominator – samples taken in 2024. Symbol "+" denotes presence of bottom vegetation, and symbol "–" denotes its absence, "0" – no samples were taken.

Results and discussion

Analysis of the collected data revealed that benthic vegetation in the eastern part of Sevastopol Bay is primarily concentrated at depths of 0.5 to 3 m, and in the apex at depths of 0.5 to 1 m. In the early 2000s, O. G. Mironov and colleagues observed dark gray and black silts at depths exceeding 5 m in this region, often characterized by hydrogen sulfide and fuel oil odors [11]. Pollution of water areas with organic matter, oil and its derivatives – originating from river runoff, industrial, agricultural and domestic waste – leads to a degraded oxygen regime, significant siltation of sediments and, consequently, the decline of landscape and biological diversity [6, 13–15, 25].

Distribution of benthic vegetation in the eastern part of the bay in 2017 and 2024

Profile *1*. In 2017, the total macrophyte biomass (TMB) along this profile decreased by 1.5 times as depth increased from 0.5 to 1 m, while the proportion of the dominant species declined by approximately half (Table 2). At these depths, *Gongolaria barbata* (Stackhouse) Kuntze (= *Cystoseira barbata*) was the dominant species (Fig. 2). The macrophytobenthos at these depths included *Dictyota fasciola* (Roth) Howe (9–18% of TMB) and *Cladophora laetevirens* (Dillw.) Kütz. (10–21% of TMB) (Fig. 2). The contribution of epiphytes at depths of 0.5–1 m was minimal (Table 2). Notably, at a depth of 5 m, benthic vegetation was nearly absent, with *C. laetevirens* (60%) and *Ulva rigida L.* (17%) as the primary contributors to TMB. *Zostera marina* L. was occasionally observed within the community at this depth. The species diversity index increased with depth from 1.07 to 2.07, indicating a more complex community structure.

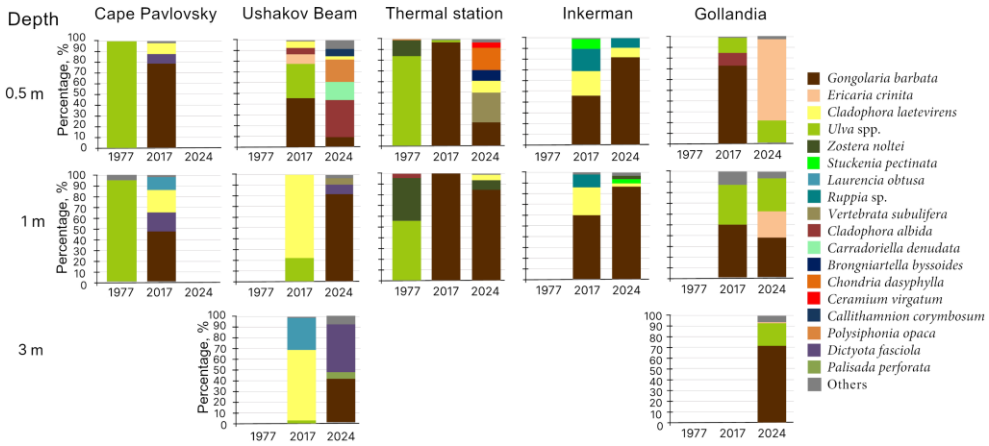

Fig. 2. Interannual and spatial dynamics of species composition of dominant macrophytes

Profile *2.* In 2017, at a depth of 0.5 m in this profile, over 50% of the TMB was contributed by *G. barbata* and *Ericaria crinita* (Duby) Molinari & Guiry (= *Cystoseira crinita*) (Table 2). At this depth, green algae were abundant within the microphytobenthos, including *U. rigida* (32%), *C. laetevirens* (6%), *C. albida* (Nees) Kütz. (6% of TMB) (Fig. 2). At depths of 1–3 m, *C. laetevirens* was dominant (Fig. 2). Within this depth range, TMB decreased by 1.4 times, while the proportion of the dominant species increased to 66–78% (Table 2). *U. rigida* was also present in the community at these depths (3–22% of TMB) (Fig. 2). Notably, at a depth of 3 m, the lithophytic form *Laurencia obtusa* (Huds.) J. V. Lamour was abundant, contributing 30% of TMB (Fig. 2). At a depth of 5 m, TMB was low, with *C. albida* dominating among the algae, accounting for 94% of TMB (Table 2). At this depth, *C. laetevirens* was recorded within the microphytobenthos, contributing 3% of TMB (Fig. 2). The contribution of epiphytic algae to TMB along profile 2 was minimal, ranging from 0 to 5% (Table 2). The species diversity index decreased approximately fivefold with increasing depth, from 2.00 to 0.43 (Table 2).

In 2024, benthic vegetation was recorded at a depth of up to 3 m along profile *2*. At a depth of 0.5 m, the TMB was nearly an order of magnitude lower than in 2017 (Table 2). At this depth, only seedlings of *G. barbata* and *E. crinita* were observed, replacing their previously dominant thickets and contributing just 9% of the TMB (Fig. 2). The microphytobenthos was dominated by *C. albida* (35%), *Polysiphonia opaca* (C. Ag.) Moris et De Notaris (21%), *Carradoriella denudata* (Dillwyn) Savoie et G. W. Saunders (17%), *Callithamnion corymbosum* (Smith) Lyngb. (7% of TMB) (Fig. 2). No epiphytic algae were recorded. At depths of 1–3 m, TMB was two to three times higher than in 2017 (Table 2). *G. barbata* dominated at these depths, although its proportion decreased by half from 1 to 3 m, while the contribution of *D. fasciola* increased from 9 to 45% of TMB (Fig. 2). The contribution of epiphytes ranged from 6 to 7% of TMB. Notably, during the study period,

Table 2. Distribution of dominant macrophyte and epiphyte species and diversity index *H* in Sevastopol Bay in 1977, 2017 and 2024 (by depths)

Profile	Depth, m	Year	Total biomass of macrophytes, $g \cdot m^{-2}$	Proportion, %		*H*
				Gongolaria barbata, *Ericaria crinita*	Epiphytic	
1	0.5	1977	858.3 ± 45.7	0	0	0.67
		2017	1783.8 ± 837.9	79	1	1.07
	1	1977	1171.7 ± 207.8	0	0	1.18
		2017	1192.5 ± 189.9	47	2	1.96
	3	1977	145.2 ± 37.9	0	0	0
	5	2017	16.1 ± 2.5	0	5	2.07
2	0.5	2017	3333.2 ± 603.6	55	5	2.00
		2024	357.2 ± 93.5	9	0	2.91
	1	2017	1332.3 ± 192.3	0	0	0.77
		2024	3782.4 ± 786.9	82	7	1.05
	3	2017	980.0 ± 326.9	0	2	1.13
		2024	1834.6 ± 247.2	41	6	1.77
	5	2017	49.5 ± 5.16	0	0	0.43
3	0.5	1977	231.6 ± 55.8	0	0	1.42
		2017	4042.8 ± 1738.5	97	0	0.24
		2024	1394.8 ± 198.5	22	0	2.60
	1	1977	353.8 ± 96.2	0	0	1.74
		2017	1957.4 ± 665.0	100	0	0.05
		2024	3308.8 ± 976.9	85	5	0.80
4	0.5	2017	1738.0 ± 540.5	46	1	4.27
		2024	4340.7 ± 1067.3	82	0	0.89
	1	2017	1467.4 ± 493.8	60	5	1.03
		2024	2811.4 ± 273.5	87	0	0.88
5	0.5	2017	4532.2 ± 456.7	73	14	1.23
		2024	3888.4 ± 1158.5	76	1	1.09
	1	2017	3146.3 ± 336.9	92	5	0.69
		2024	7307.7 ± 1754.1	94	0	0.68
	3	2024	1647.8 ± 583.2	73	4	1.48

Note: Data for 1977 are taken from the article by A. A. Kalugina-Gutnik [26].

the species diversity index increased across all studied depths, indicating a more complex algal community structure (Table 2).

Profile *3.* In 2017, the TMB decreased twofold as depth increased from 0.5 to 1 m (Table 2). At these depths, *G. barbata* was dominant, with its proportion reaching maximum values (Fig. 2). U. *rigida* and C. *laetevirens* were observed sporadically within the phytocommunity. No epiphytic algae were recorded. Low values of the species diversity index *H* indicated a homogeneous phytocommunity structure, dominated by the primary species (Table 2).

In 2024, along profile *3*, the TMB at a depth of 0.5 m decreased threefold, while at a depth of 1 m, it doubled compared to 2017 values (Table 2). *G. barbata* remained dominant at these depths, although its proportion decreased, particularly at 0.5 m, where lithophytic forms, including *Vertebrata subulifera* (C. Ag.) Kütz. (28%), *Brongniartella byssoides* (Good. et Wood.) F. Schmitz (10%), *Chondria dasyphylla (*Woodw.) C. Ag. (21%), *C. laetevirens* (11%), and *Ceramium virgatum* Roth (5% of TMB), were prominent (Fig. 2). Notably, at a depth of 1 m, where *G. barbata* dominated, *Zostera noltei* Hornem. (9% of TMB) was observed in patches with a silty-sandy substrate. Epiphytic algae were represented by *C. laetevirens.* A simplification of the algal community structure with increasing depth was confirmed by a more than threefold decrease in the species diversity index (Table 2).

Profile *4.* In 2017, along this section, the TMB decreased slightly as depth increased from 0.5 to 1 m, while the proportion of the dominant species (*G. barbata*) increased (Table 2). At these depths, the microphytobenthos included green algae (*C. laetevirens* (23–26%) and *U. rigida* (1–2%)) and higher aquatic vegetation represented by the genera *Ruppia, Stuckenia, and Zannichellia* (12–30% of the TMB) (Fig. 2). The contribution of epiphytes increased with depth from 1 to 5% of TMB. Notably, the species diversity index reached its maximum at a depth of 0.5 m, indicating a polydominant community structure (Table 2).

In 2024, along profile *4*, the depth distribution of macrophytobenthos remained consistent with previous years. The TMB decreased by 1.5 times as depth increased from 0.5 to 1 m, while its values were approximately twice as high as in 2017 (Table 2). *G. barbata* dominated at these depths. The macrophytobenthos included *C. laetevirens* (3–9%) and the seagrasses *Ruppia spiralis L.*, *Stuckenia pectinate* (L.) Börner (formerly *Potamogeton pectinatus)*, and Z. *noltei* (7–9% of TMB) (Fig. 2). No epiphytic algae were recorded. The species diversity index varies within a narrow range (Table 2).

Profile *5.* In 2017, along this profile, the TMB decreased by 1.4 times as depth increased from 0.5 to 1 m (Table 2). *G. barbata* dominated at these depths, contributing 73 to 92% of the TMB. *U. rigida* and *C. albida* were also present, with their contribution decreasing with depth from 14 to 6% and from 12 to 1% of the TMB, respectively (Fig. 2). Notably, as depth increased, the proportion of epiphytes decreased nearly threefold, the phytocommunity structure simplified, and the species diversity index decreased by half (Table 2).

In 2024, along profile *5*, benthic vegetation was recorded at depths up to 3 m. The highest TMB was observed at a depth of 1 m; at 0.5 m, TMB was approximately half as high, and at 3 m, it was four times lower (Table 2). *E. crinita* and *G. barbata* dominated at all studied depths, contributing 73 to 94% of the TMB. The remaining TMB was mainly attributed to species of the genus *Ulva* (Fig. 2). Notably, at a depth of 0.5 m, the TMB values and the proportions of dominant species were comparable to those in 2017, while at 1 m, TMB in 2024 was twice as high as in 2017, although the proportion of dominant species remained similar (Table 2). Epiphytic algae were minimally represented (0–4% of the TMB). The species diversity index ranged from 0.68 to 1.48, indicative of an algal community dominated by a few key species.

Over the past seven years (from 2017 to 2024), the depth distribution of macrophytobenthos in the eastern part of Sevastopol Bay underwent changes, while the species composition of dominant macrophytes remained relatively stable. Notably, in 2024, at all profiles except profile *4*, the TMB at a depth of 0.5 m was lower, while at depths of 1 and 3 m, it was approximately twice as high as in 2017. The significant decrease in TMB at 0.5 m can probably be explained by the destructive impact of an extreme storm in autumn 2023 [27]. Specifically, at profile *2* in 2024, TMB was nearly ten times lower than in 2017 (Table 2). At this depth, only seedlings of *G. barbata* and *E. crinita* were observed, with their proportion decreasing from 55 to 9% of TMB over the study period (Fig. 2). At profile *3*, at a depth of 0.5 m, TMB decreased threefold compared to 2017 values (Table 2). Here, isolated thalli of *G. barbata* were recorded, with its proportion decreasing from 97 to 22% of TMB during this period (Fig. 2). At profile *5*, over the seven-year period, the decrease in TMB at 0.5 m was minimal, while the proportion of *G. barbata* ranged from 73 to 76% of TMB (Table 2). Notably, in 2024, at all studied profiles at a depth of 0.5 m, the benthic vegetation was dominated by annual algae (*Cladophora albida, Carradoriella denudata, Callithamnion corymbosum, Vertebrata subulifera, Brongniartella byssoides, Chondria dasyphylla, Ceramium virgatum*), further indicating the influence of the autumn storm.

A comparative analysis of the composition and quantitative indicators of macrophytobenthos for 2017–2024 at depths of 1 and 3 m revealed several differences. At profile *2* in 2017, *C. laetevirens* dominated the 1–3 m depth range, contributing from 66 to 78% of the TMB, while *G. barbata* and *E. crinita* were absent. In contrast, in 2024, *G. barbata* contributed 41–82% of TMB at these depths (Fig. 2). At profile *3*, at a depth of 1 m, the proportion of *G. barbata* was consistently high, ranging from 85 to 100% of TMB (Fig. 2). At profile *4*, the contribution of *G. barbata* increased from 46–60 to 82–87%, while the proportion of seagrasses decreased from 12–30 to 7–9% of TMB during this period (Fig. 2). Notably, at profile *5* in 2024, benthic vegetation was recorded up to a depth of 3 m, whereas in 2017, macrophytobenthos was observed only up to 1 m (Table 2). During the study period, the combined proportion of *G. barbata* and *E. crinita* at a depth of 1 m remained high, varying slightly from 92 to 94% of TMB (Fig. 2).

Analysis of spatio-temporal changes in macrophytobenthos over nearly half a century revealed significant transformations. According to the hydrobotanical survey of Sevastopol Bay conducted in 1977 by A. A. Kalugina-Gutnik, species of the genus *Ulva* dominated on hard substrates at depths of 0.5–5 m in the eastern part of the bay, while *G. barbata* and *E. crinita* were present in the macrophytobenthos at greater depths [26]. Notably, at the beginning of the 20th century, S.A. Zernov (1913) reported "pure" thickets of *G. barbata* and *E. crinita* in this region [5]. According to a number of authors, for over a century, clusters of eelgrass (*Zostera marina* and *Z. noltei)* have been observed on soft substrates at the apex of the bay (its top) [5, 6]. In 1977, species of the genus *Ulva* were also recorded as part of the higher aquatic vegetation in this area [26].

According to A. A. Kalugina-Gutnik's 1977 survey, along the coastline at profiles *1–3* at a depth of 0.5 m, species of the genus *Ulva* dominated, contributing 85–100% of the TMB (Fig. 2) [26]. Subsequently, I. K. Evstigneeva and I. N. Tankovskaya reported that in 2003–2005 *G. barbata* and *E. crinita* began to appear at this depth in the waters of profile *2* [21]. Studies conducted in 2017 at profiles *1–3* at a depth of 0.5 m confirmed the dominance of *G. barbata* and *E. crinita,* with biomasses of 1412.4 ± 543.9, 1818.9 ± 476.2, and 3921.9 ± 776.2 $g \cdot m^{-2}$, respectively (79, 55, and 97% of the TMB).

At profile *1* in 1977, benthic vegetation extended to a depth of 3 m, with macrophytobenthos consisting almost entirely of species of the genus *Ulva* (95–100% of the TMB). By 2017, the vertical distribution of macrophytes had expanded to a depth of 5 m, with *G. barbata* dominating at 1 m (47%) and species of the genus *Cladophora* predominating at depths of 3–5 m (60% of the TMB) (Fig. 2).

At profile *3* in 1977, *Zostera noltei* was noted at a depth of 1 m, in addition to species of the genus *Ulva*. It is notable that, with an increase in depth from 0.5 to 1 m, the proportion of *Ulva* species decreased from 85 to 56 %, while the proportion *of Z. noltei* increased from 15 to 40% of the TBM (Fig. 2) [26]. In 2017, the TBM index significantly exceeded the 1977 values, which is associated with the formation of nearly monodominant stands *of G. barbata* (97–100% of the TBM) (Fig. 2).

Thus, an analysis of literary sources and our own data on the distribution of macrophytobenthos in the eastern part of Sevastopol Bay over nearly half a century shows that its distribution and composition have changed significantly. The most significant transformation of the plant component occured in the corner of the bay, where higher aquatic vegetation (*Zostera marina, Z. noltei, Stuckenia pectinata, Zannichellia* sp., *Ruppia* sp.) previously grew, but was replaced by thickets of perennial algae (*G. barbata* and *E. crinita)*. These changes can probably be explained by an increase in water salinity in the estuary zone of the Chernaya River [23].

---

5) Zernov, S.A., 1913. [On Studying Life of the Black Sea]. In: IAS, 1913. *Zapiski Imperatorskoy Akademii Nauk*. Saint Petersburg: Imperatorskaya Akademiya Nauk. Vol. 32, iss. 1, 304 p. (in Russian).

6) Kalugina-Gutnik, A.A., 1974. [Bottom Vegetation of Sevastopol Bay]. In: AS USSR, 1974. *Biologiya Morya*. Kiev: Naukova Dumka. Iss. 32, pp. 133–164 (in Russian).

It was concluded in [23] that there has been a steady trend toward increased water salinity in both the surface and bottom waters in the eastern part of the bay in recent decades. At a distance of about 1000 m from the river mouth, the salinity of the water was 17 ‰, during the low-water period, this figure reached 17.6–17.9 ‰ throughout the entire corner of the bay [23]. Second, the construction of the northern and southern parts of the pier, piers and berths, as well as intensive dredging, caused changes in coastal sediment flows and decreased the degree of abrasion throughout the bay [28]. This may have led to a change in the composition of bottom sediments. In the corner part of the bay, at profiles *3* and *4*, where seagrasses previously grew on soft substrates, bedrock has become exposed, providing a substrate for algae attachment.

The transformation of the macrophytobenthos in the eastern part of the bay is characterized by a change in dominant species. The *Ulva* genus, which was previously predominant, is being replaced by *G. barbata* and *E. crinita*, whose population continues to grow.

Over the past two centuries, Sevastopol Bay has experienced intense anthropogenic impact, evidenced by increased concentrations of nutrients in the water, reaching levels 1–2 orders of magnitude higher than in the open waters of the Black Sea [4–6, 10, 23]. The elevated concentrations of pollutants in the bay, including its eastern sector, have significantly impacted biotic components, particularly the structure of benthic phytocenoses. At all profiles of the eastern part of the bay, green algae were abundant, particularly *C. laetevirens*, *Ulva intestinalis L*., and *U. rigida*. These algae are indicators of eutrophication in the water. These algae, as well as *Callithamnion corymbosum* and *Ceramium virgatum*, grow in polluted water from domestic and industrial wastewater.

In recent years, considerable attention has been given to environmental protection measures aimed at reducing the inflow of pollutants into Sevastopol Bay. These measures undoubtedly impact the ecological situation in the bay. For example, L. V. Malakhova with colleagues demonstrated that under current conditions, lower concentrations of polychlorinated biphenyls (PCB 5) were found in the top layer of bottom sediments than at depths of 5 to 20 cm, indicating a decrease in anthropogenic pollution of the bay [12]. Perhaps the improvement in environmental quality has manifested itself in a change in the dominant macrophyte species. Thus, in 2024, *G. barbata* and *E. crinita* experienced mass growth in the studied part of the bay alongside *Dictyota fasciola, Laurencia obtusa, Palisada perforata* (Bory) K.W. Nam., and *Vertebrata subulifera*. These species usually inhabit areas with a relatively low degree of eutrophication [2)].

Conclusions

1. Hydrobotanical studies conducted in the eastern sector of Sevastopol Bay in 2017 and 2024 revealed significant changes in the vertical distribution of microphytobenthos, alongside relative stability in the species composition of the dominant macrophytes. Currently, *Gongolaria barbata* and *Ericaria crinita* dominate the benthic vegetation, and green algae (*Cladophora laetevirens, Ulva intestinalis,*

U. rigida) are also abundant. Notably, during this period, an increase in the contribution of *G. barbata* (from 46–60 to 82–87%) was recorded, while the proportion of seagrasses decreased (from 12–30 to 7–9% of the TBM).

2. Notably, in 2024, there was a decrease in TBM and the proportion of *G. barbata* and *E. crinita* in almost all profiles at a depth of 0.5 m due to the destructive impact of an extreme storm that occurred in the autumn 2023. Meanwhile, at depths of 1 and 3 m, the quantitative indicators of macrophytobenthos biomass were approximately twice as high as in 2017.

3. A comparative analysis of the spatial distribution of macrophytobenthos for 1977–2024 revealed a significant changes in the plant composition, particularly in the corner of the bay, where the communities of higher aquatic vegetation (*Zostera marina, Z. noltei, Stuckenia pectinata, Zannichellia* sp., *Ruppia* sp.) completely changed to perennial macrophytes (*G. barbata* and *E. crinita)*. These changes can probably be explained by an increase in water salinity in the estuary zone of the Chyornaya River, as well as changes in coastal sediment flow dynamics. In the eastern part of the bay*, Ulva* species were replaced by *G. barbata* and *E. crinita* during this period*,* which may indicate a trend toward improvement in environmental conditions.

REFERENCES

1. Costanza, R., d'Arge, R., de Groot, R., Farber, S., Grasso, M., Hannon, B., Limburg, K., Naeem, S., O'Neill, R.V. [et al.], 1997. The Value of the World's Ecosystem Services and Natural Capital. *Nature*, 387, pp. 150–156. https://doi.org/10.1038/387253a0
2. Phillips, R.C. and Milchakova, N.A., 2003. Seagrass Ecosystems. *Morskoi Ecologichesky Zhurnal,* 2(2), pp. 29–39.
3. Short, F.T., Polidoro, B., Livingstone, S.R., Carpenter, K.E., Bandeira, S., Bujang, J.S., Calumpong, H.P., Carruthers, T.J.B., Coles, R.G. [et al.], 2011. Extinction Risk Assessment of the World's Seagrass Species. *Biological Conservation*, 144(7), pp. 1961–1971. https://doi.org/10.1016/j.biocon.2011.04.010
4. Sovga, E.E., Mezentseva, I.V., Khmara, T.V. and Slepchuk, K.A., 2014. [On the Prospects and Possibilities of Assessing the Self-Cleaning Capacity of the Sevastopol Bay Water Area]. *Ekologicheskaya Bezopasnost' Pribrezhnoy i Shel'fovoy Zon i Kompleksnoe Ispol'zovanie Resursov Shel'fa* [Ecological Safety of Coastal and Shelf Zones and Comprehensive Use of Shelf Resources], 28, pp. 153–164 (in Russian).
5. Minkovskaya, R.Ya. and Verzhevskaya, L.V., 2016. Assessment of Water Quality in the Rivers of Sevastopol Region to Determine the Anthropogenic Load on the Black Sea Coast. *Ekologicheskaya Bezopasnost' Pribrezhnoy i Shel'fovoy Zon i Kompleksnoe Ispol'zovanie Resursov Shel'fa* [Ecological Safety of Coastal and Shelf Zones and Comprehensive Use of Shelf Resources], (2), pp. 93–101 (in Russian).
6. Sovga, E.E., Mezentseva, I.V. and Khmara, T.V., 2021. Natural-Climatic and Anthropogenic Factors Determining the Self-Purification Capacity of Shallow-Water Marine Ecosystems in Relation to Reduced Nitrogen Forms. *Ecological Safety of Coastal and Shelf Zones of Sea*, (3), pp. 23–36. https://doi.org/10.22449/2413-5577-2021-3-23-36 (in Russian).
7. Slepchuk, K.A. and Sovga, E.E., 2018. Eutrophication Level of the Eastern Part of the Sevastopol Bay on the Basis of Numerical Modeling of E-Trix Index. *Ecological Safety of Coastal and Shelf Zones of Sea*, (2), pp. 53–59. https://doi.org/10.22449/2413-5577-2018-2-53-59 (in Russian).

8. Bagaev, A.V., Nikishin, V.V., Rauen, T.V., Verzhevskaya, L.V. and Scherbachenko, S.V., 2022. Local Changes of Physical and Biological Parameters of the Sevastopol Bay Surface Waters under the Influence of Rain Drainage. *Physical Oceanography*, 29(2), pp. 152–171. https://doi.org/10.22449/1573-160X-2022-2-152-171
9. Orekhova, N.A., Konovalov, S.K. and Ovsyaniy, E.I., 2013. [Variation of Geochemical Characteristics in the Bottom Sediments of Crimean Coast]. *Ekologicheskaya Bezopasnost' Pribrezhnykh i Shel'fovykh Zon i Kompleksnoe Ispol'zovanie Resursov Shel'fa* [Ecological Safety of Coastal and Shelf Zones and Comprehensive Use of Shelf Resources], 27, pp. 284–288 (in Russian).
10. Orekhova, N.A., Medvedev, E.V. and Ovsyany, E.I., 2018. Influence of the River Chernaya Water on Hydrochemical Regime of the Sevastopol Bay (the Black Sea). *Ecological Safety of Coastal and Shelf Zones of Sea*, (3), pp. 84–91. https://doi.org/10.22449/2413-5577-2018-3-84-91 (in Russian).
11. Mironov, O.G., Kirjukhina, L.N. and Alyomov, S.V., 2003. *Sanitary-Biological Aspects of the Sevastopol Bays Ecology in XX Century*. Sevastopol: ECOSI-Gidrofizika, 185 p. (in Russian).
12. Malakhova, L.V., Malakhova, T.V. and Egorov, V.N., 2019. [Bottom Sediments of Marine and Fresh Water Bodies of the Crimea as a Depot of Persistent Organic Pollutants]. In: O. A. Shpyrko, V. V. Khapaev, S. I. Rubtsova [et al.], eds., 2019. [*Lomonosov Readings 2019: Annual Scientific Conference of Moscow State University. Sevastopol, 3–4 April 2019*]. Sevastopol: MSU Branch in Sevastopol, pp. 209–210 (in Russian).
13. Soloveva, O.V., Tikhonova, E.A., Mironov, O.A. and Barabashin, T.O., 2021. Polycyclic Aromatic Hydrocarbons in the Bottom Sediments of the River – Sea Mixing Zone on the Example of the River Chernaya and the Sevastopol Bay (the Black Sea). *Physical Oceanography*, 28(3), pp. 338–347. https://doi.org/10.22449/1573-160X-2021-3-338-347
14. Chekalov, V.P., 2023. Relationship of the Processes of Aerobic Oxidation and Anaerobic Destruction of Organic Matter in the Bottom Sediments of Coastal Waters of Crimea (Black Sea). *Marine Biological Journal*, 8(3), pp. 87–96.
15. Osadchaya, T.S., Alyomov, S.V., Tikhonova, E.V., Konsulova, T., Todorova, V. and Shtereva, G., 2010. [Features of the Spatial Distribution of Petroleum Hydrocarbons and the Structure of the Macrozoobenthos in Sevastopol and Varna Bays]. *Monitoring Systems of Environment*, 13, pp. 247–255 (in Russian).
16. Viter, T.V., 2013. [Bottom Communities in the Area of the Gollandia Bay Piers and near Regional Power Station (Sevastopol Bay)]. *Ekologicheskaya Bezopasnost' Pribrezhnykh i Shel'fovykh Zon i Kompleksnoe Ispol'zovanie Resursov Shel'fa* [Ecological Safety of Coastal and Shelf Zones and Comprehensive Use of Shelf Resources], 27, pp. 431–438 (in Russian).
17. Makarov, M.V. and Viter, T.V., 2021. Spatial-Time Changes in the Macrozoobentos of the Chernaya River Mouth and the Top of Sevastopol'skaya Bay (South-West Crimea). *Scientific Notes of V.I. Vernadsky Crimean Federal University. Biology. Chemistry*, 7(4), pp. 92–107 (in Russian).
18. Guseva, E.V. and Alyomov, S.V., 2022. Meiobenthos of Sevastopol Bay (Black Sea): Current State and Long-Term Changes. *Ecological Safety of Coastal and Shelf Zones of Sea*, (1), pp. 104–112. https://doi.org/10.22449/2413-5577-2022-1-104-112
19. Alexandrov, V.V., 2000. The Evaluation of Zostera marina L. Coenopopulations State in the Sevastopol Region (the Black Sea). *Ecology of the Sea*, 52, pp. 26–30 (in Russian).
20. Alexandrov, V.V., 2005. Morphostructure of Potamogeton pectinatus L. near Sevastopol (the Black Sea). *Ecology of the Sea*, 68, pp. 13–18 (in Russian).

21. Evstigneeva, I.K. and Tankovskaya, I.N., 2008. [Current State and Variability of Macrophytobenthos of the Ushakova Balka Botanical Nature Monument (Black Sea, Sevastopol Region)]. In: B. N. Panov, 2008. *Current Problems of the Azov-Black Sea Region Ecology: Materials of IV International Conference, 8–9 October 2008, Kerch, YugNIRO*. Kerch: YugNIRO Publishers', pp. 92–98 (in Russian).
22. Evstigneeva, I.K. and Tankovskaya, I.N., 2017. Species' Composition, Ecological Structure and Quantitative Characteristics of the Gollandiya Bay Macroalgae (Black Sea). *Issues of Modern Algology*, (1), 7 (in Russian).
23. Sovga, E.E. and Khmara, T.V., 2020. Influence of the Chernaya River Runoff during High and Low Water on the Ecological State of the Apex of the Sevastopol Bay Water Area. *Physical Oceanography*, 27(1), pp. 28–36. https://doi.org/10.22449/1573-160X-2020-1-28-36
24. Goryachkin, Yu.N. and Dolotov, V.V., 2019. *Sea Coasts of Crimea*. Sevastopol: Colorit, 256 p. (in Russian).
25. Pavlova, E.V. and Shadrin, N.V., eds., 1999. *Sevastopol Aquatory and Coast: Ecosystem Processes and Services for Human Society*. Sevastopol: Akvavita Publ., 290 p. (in Russian).
26. Dulov, V.A., Yurovskaya, M.V., Fomin, V.V., Shokurov, M.V., Yurovsky, Yu.Yu., Barabanov, V.S. and Garmashov, A.V., 2024. Extreme Black Sea Storm in November, 2023. *Physical Oceanography*, 31(2), pp. 295–316.
27. Kalugina-Gutnik, A.A., 1982. Changes in Benthic Vegetation in the Sevastopol Bay from 1967 to 1977. *Ecology of the Sea*, (9), pp. 48–62 (in Russian).
28. Efremova, T.V. and Goryachkin, Yu.N., 2023. Morphodynamics of the Sevastopol Bays under Anthropogenic Impact. *Ecological Safety of Coastal and Shelf Zones of Sea*, (1), pp. 31–47. https://10.29039/2413-5577-2023-1-31-47

Submitted 19.01.2025; accepted after review 13.02.2025;
revised 24.06.2025; published 30.09.2025

About the authors:

Nataliya V. Mironova, Senior Research Associate, A.O. Kovalevsky Institute of Biology of the Southern Seas of RAS (2 Nakhimov Av., Sevastopol, 299011, Russian Federation), PhD (Biol.), **ORCID ID: 0000-0001-7110-7081**, **ResearcherID: Y-1780-2018,** *dr.nataliya.mironova@yandex.ru*

Tatyana V. Pankeeva, Senior Research Associate, A.O. Kovalevsky Institute of Biology of the Southern Seas of RAS (2 Nakhimov Av., Sevastopol, 299011, Russian Federation), DSc (Geogr.), **ORCID ID: 0000-0002-8933-6103**, **ResearcherID: 4920-0290,** *tatyanapankeeva@yandex.ru*

Contribution of the authors:

Nataliya V. Mironova – processing of macrophytobenthos samples (1977, 2017, 2024), analysis and description of the study results, preparation of the article text, selection, systematisation and analysis of literature sources

Tatyana V. Pankeeva – selection, systematisation and analysis of literature sources, preparation of the article text, cartographic materials and the reference list

All the authors have read and approved the final manuscript

ISSN 2413-5577, Ecological Safety of Coastal and Shelf Zones of Sea, 2025, No. 3, pp. 81–95.

Original paper

Effects of Drilling and Cementing Fluids on Indicator Species in Marine Coastal Benthic Systems

I. I. Rudneva [1] *, V. G. Shaida [2], M. V. Medyankina [3], O. V. Shaida [1]

[1] *Marine Hydrophysical Institute of RAS, Sevastopol, Russia*

[2] *Company "EcoService-A", Moscow, Russia*

[3] *Moscow State University of Technology and Management K. G. Razumovsky (First Cossack University), Moscow, Russia*

* *e-mail: svg-41@mail.ru*

Abstract

The paper studies toxicity of drilling and cementing fluids, used in offshore oil and gas operations, at concentrations of 10, 50, 100, 500 and 1000 mg/L for the mass species of benthic marine communities in the coastal part of the Black Sea: the eelgrass *Nanozostera noltii* and the amphipod *Chaetogammarus olivii*. The paper analyses effect of these toxic mixtures on the increase in biomass, leaves and roots of the eelgrass and on the survival of amphipods after 10, 20 and 30 days of exposure. Drilling fluid was shown to be more toxic than cementing fluid for the test organisms. Exposure to 10 mg/L of drilling fluid reduced the plant biomass growth by 49% after 10 days and by 62 and 78% after 20 and 30 days, respectively. With increase in the drilling fluid concentration to 50–100 mg/L, this indicator continued to decline rapidly to 60–80% relative to the control, and at a concentration of 500–1000 mg/L, the plants died. The roots of eelgrass were more sensitive to the toxicant than the leaves: the root growth showed a marked tendency to decrease by 48% relative to the control at toxicant concentrations of 50–100 mg/L after only 10 days. The harmful effect of the cementing fluid on the eelgrass was less pronounced than that of the drilling fluid. Exposed to the cementing fluid, the plants died at the highest concentration of the toxicant (1000 mg/L) after 30 days. No significant differences were found between the leaf growth in the test and control variants, but the root growth decreased significantly by 64 and 90% at 10 and 20 days at cementing fluid concentrations of 500 and 1000 mg/L, respectively. Throughout the experiment, the survival rate of the crustaceans exposed to over 10 mg/L drilling fluid was significantly lower than the control (30–85%). During exposure to the cementing fluid, however, significant differences were observed only at the highest concentration of 1000 mg/L. An ecotoxicological assessment of substances used in oil well drilling is necessary to determine their hazard when used in oil and gas production, as well as to select optimal components in their composition that contribute to reducing environmental damage to benthic marine communities.

Keywords*:* Black Sea, oil and gas complex, pollution, amphipods, *Zostera*, bioassay

© Rudneva I. I., Shaida V. G., Medyankina M. V., Shaida O. V., 2025

This work is licensed under a Creative Commons Attribution-Non Commercial 4.0 International (CC BY-NC 4.0) License

For citation: Rudneva, I.I., Shaida, V.G., Medyankina, M.V. and Shaida, O.V., 2025. Effects of Drilling and Cementing Fluids on Indicator Species in Marine Coastal Benthic Systems. *Ecological Safety of Coastal and Shelf Zones of Sea*, (3), pp. 81–95.

Влияние бурового раствора и тампонажной жидкости на виды-индикаторы морских прибрежных бентосных экосистем

И. И. Руднева [1] *, В. Г. Шайда [2], М. В. Медянкина [3], О. В. Шайда [1]

[1] *Морской гидрофизический институт РАН, Севастополь, Россия*

[2] *ООО «ЭкоСервис-А», Москва, Россия*

[3] *Московский государственный университет технологий и управления им. К.Г. Разумовского (Первый казачий университет), Москва, Россия*

* *e-mail: svg-41@mail.ru*

Аннотация

Исследовали токсичность используемых в морских нефтегазовых операциях бурового раствора и тампонажной жидкости в концентрации 10, 50, 100, 500 и 1000 мг/л для массовых видов бентосных морских сообществ прибрежной части Черного моря – зостеру *Nanozostera noltii* и амфипод *Chaetogammarus olivii*. Анализировали влияние этих токсичных смесей на прирост биомассы, листьев и корней зостеры и на выживаемость амфипод через 10, 20 и 30 сут. Показана бóльшая токсичность бурового раствора по сравнению с тампонажной жидкостью для исследуемых организмов. Под воздействием бурового раствора в концентрации 10 мг/л прирост биомассы растения снизился на 49 % через 10 сут после начала эксперимента, а через 20 и 30 сут – на 62 и 78 % соответственно. При повышении концентрации бурового раствора до 50 и 100 мг/л этот показатель продолжал интенсивно снижаться до 60 и 80 % соответственно по отношению к контролю, а при концентрации 500 и 1000 мг/л растения погибли. Корни зостеры оказались более чувствительны к действию токсиканта, чем листья: прирост корней имел выраженную тенденцию к снижению на 48 % по отношению к контролю при концентрациях токсиканта 50 и 100 мг/л уже через 10 сут. Вредное влияние тампонажной жидкости на зостеру было выражено в меньшей степени, чем влияние бурового раствора. Под воздействием тампонажной жидкости в самой высокой концентрации (1000 мг/л) растения погибли через 30 сут инкубации. Достоверных различий между приростом листьев в опытных и контрольных вариантах не установлено, но прирост корней уже на 10 и 20 сутки достоверно уменьшился на 64 и 90 % при концентрациях тампонажной жидкости 500 и 1000 мг/л соответственно. На протяжении всего эксперимента выживаемость ракообразных, экспонированных в растворах с концентрацией бурового раствора более 10 мг/л, была достоверно ниже контроля на 30–85 %, тогда как при инкубации в растворах с тампонажной жидкостью достоверные различия отмечены только при самой высокой концентрации 1000 мг/л. Экотоксикологическая оценка токсичности веществ, применяемых при бурении нефтяных скважин, необходима для определения их опасности при нефте- и газодобыче, а также для выбора оптимальных компонентов в их составе, способствующих снижению экологического вреда для донных морских сообществ.

Ключевые слова: Черное море, нефтегазовый комплекс, амфиподы, зостера, биотестирование

Для цитирования: Влияние бурового раствора и тампонажной жидкости на виды-индикаторы морских прибрежных бентосных экосистем / И. И. Руднева [и др.] // Экологическая безопасность прибрежной и шельфовой зон моря. 2025. № 3. С. 81–95. EDN TUWYZA.

Introduction

The operation of offshore oil and gas facilities inevitably releases byproducts into the environment, and the rapid expansion of these activities significantly amplifies this impact. Coastal areas, characterized by high biological productivity, are extensively utilized for fishing, aquaculture, recreation, sports, shipping, and mineral extraction. These regions experience maximal and multifaceted anthropogenic stress, which adversely affects natural ecosystems, leading to their transformation and degradation, often resulting in the complete loss of resources or the impossibility of their use due to pollution and the mortality of aquatic organisms. To analyze such harmful processes and identify ways to prevent them, ecotoxicological methods are used. These methods, applied in both natural and laboratory settings, enable the assessment of the consequences of anthropogenic compounds entering the marine environment, evaluating their effects on natural systems, determining pollutant behavior, establishing permissible levels, and assessing their impact on marine biota.

Offshore oil and gas development releases not only oil and its derivatives but also drilling fluids (DFs) and other components used in well construction into the marine environment. DFs are complex mixtures comprising water, suspensions, emulsifiers, aerated liquids, organic solvents, heavy metals, and clay, used to flush wells during drilling [1, 2]. After use, DFs are classified as industrial waste and require proper disposal due to their toxicity, mutagenic and carcinogenic properties. In addition, cementing fluids (CFs) are used during drilling to cement wells. They also have a complex composition and contain hazardous and toxic substances [3, 4]. The volume of these components entering the marine environment is expected to increase, as the number of wells drilled rose from 39,000 in 2020 to 49,600 in 2022, with projections estimating up to 60,000 wells by 2026 [5].

Oil spills primarily affect surface waters and their inhabitants, whereas DF emissions impact benthic communities. Information on the pollution of the marine environment and aquatic organisms by DFs and other substances used in drilling operations is limited and inconsistent [6, 7]. The effects may vary significantly among representatives of different taxonomic groups [8, 9].

Macrophytes and higher aquatic vegetation, mainly represented by eelgrass in coastal benthic biocenoses, are highly vulnerable to drilling operations [10]. These

plants form a unique group, widely distributed in seas and oceans. Their communities play a critical role in the structure and functioning of coastal ecosystems, serving as food and habitat for numerous marine organisms, including commercially important species. Eelgrass exhibits high productivity [11, 12] and, alongside other marine macrophytes, contributes to the utilization of biogenic elements, such as carbon, which is essential for biosphere exchange and biogeochemical cycles. Seaweed and seagrass ecosystems support grazing, detrital, and food webs, stabilize sedimentary deposits, and play an important role in global carbon and nutrient cycles. These ecosystems host diverse flora and fauna, forming complex food chains [12]. The annual ecological value of one acre of seabed covered with algae and seagrasses is estimated to range from $9,000 to $28,000. Aquatic vegetation biocenoses perform many ecosystem functions, including storm protection, provision of food for commercial fish and invertebrates, and nutrient and carbon cycling, which are crucial for understanding the current state of nutrient cycles in the biosphere [13, 14]. However, eelgrass communities face intense anthropogenic impacts, particularly from the oil and gas industry, due to pollution from oil, dispersants, DFs, and heavy metals [15–18]. These plants absorb and accumulate components of these substances, making eelgrass an effective phytoremediator and indicator of polluted waters. Eelgrass is widely used in ecotoxicological studies to assess the accumulation and toxicity of various pollutants, necessitating comprehensive data on its responses to develop criteria for maximum permissible doses [16].

Intense anthropogenic activity has an extremely negative effect on eelgrass [19]. The plant's capacity to actively accumulate pollutants enables its use as a bioindicator for assessing the ecological state of coastal marine zones and in developing test systems for analyzing the toxicity of harmful substances. However, the concentrations of toxicants must be considered, as they can produce variable effects, as demonstrated in the case of oil pollution [20].

Amphipods are widely distributed in coastal zones and dominate benthic communities, including eelgrass beds. They are used in ecotoxicological studies due to their adaptability to laboratory conditions and sensitivity pollutants. As they lack larval stages, both juvenile and sexually mature adult crustaceans serve as test organisms [21, 22].

The study aims to investigate the toxicity of water-based DFs and CFs used in well cementing on dominant benthic species in the coastal Black Sea, specifically the seagrass *Nanozostera noltii* (Hornemann) and amphipods inhabiting its beds, *Chaetogammarus olivii* (H. Milne Edwards, 1830). The research evaluates the effects of stress induced by DFs and CFs from oil and gas production on the survival, growth, and development of these aquatic organisms, comparing the toxicity of

these substances based on the responses of test organisms from the seagrass and crustacean communities.

Material and methodology

DF is a viscous, light brown liquid with an ammonia-like odor, a pH of 10–11, a boiling point above 100°C, and a relative density at 20°C of 1.1–2.0. It is miscible with water and contains sodium chloride, silica and other additives. The substance is stable under normal conditions. CF, used for well cementing, primary consists of a dry cement mixture, defoamers, propylene glycol, calcium compounds, and other additives.

Eelgrass and amphipods were collected from the coastal area of Kazachya Bay (Sevastopol region) and immediately transported to the laboratory. The plants were washed to remove dirt and epiphytic flora and acclimated to experimental conditions in seawater for 3 days at (22 ± 2)°C. Toxicological experiments were conducted in accordance with established recommendations [1)].

One-year-old vegetative eelgrass shoots, with an average weight of 328.5 ± 56 mg, were placed in 1.5 L glass containers (1 L working volume), with three plants per container, maintained at (22 ± 2)°C under constant artificial lighting of 1500 lux. Sexually mature adult amphipods were placed in 500 mL aquariums, with 10 individuals per aquarium, and acclimated to experimental conditions for one week under natural light (12-hour daylight duration) at (22 ± 2)°C. Experiments were carried out in triplicate over 30 days.

Solutions of the test substances at concentrations of 10, 50, 100, 500 and 1000 mg/L were added directly to the water. Natural seawater with a salinity of 18‰, without added substances, served as the control. The water was replaced every 5–7 days. Plant biomass, including leaves and roots, was measured every 10 days. The effect of toxicants on crustaceans was assessed by mortality every 10 days over 30 days. During the experiment, amphipods were fed crushed brown algae and dried daphnia.

The results were statistically processed, and the mean value M and standard error of the mean m were calculated. Comparisons were performed using Student's t-test at a significance level of $p < 0.05$. The correlation between toxicant concentrations and amphipod survival rates was assessed using the CURVEFIT software (version 2.10–L).

[1)] Federal Agency for Fishery, 2009. *On the Approval of Methodological Guidelines for the Development of Water Quality Standards for Water Bodies of Fishery Significance, Including Standards for Maximum Permissible Concentrations of Harmful Substances in Waters of Water Bodies of Fishery Significance:* Order of the Federal Agency for Fishery of the Russian Federation dated August 04, 2009, No. 695. Moscow: Federal Agency for Fishery.

Results

The results revealed patterns and characteristics of the effects of toxicants on the indicator species of benthic systems. Variable effects of DFs and CFs on eelgrass growth and development were observed at different concentrations (Figs. 1–3). As shown in Fig. 1, 10 days after the experiment began, a significant ($p < 0.05$) reduction in plant biomass growth was observed at DF concentrations of 50 mg/L and higher compared to the control. A similar effect was noted after 20 days at a lower DF concentration of 10 mg/L, while at concentrations of 500 and 1000 mg/L, the plants died. After 30 days, the trend of reduced plant biomass growth relative to the control persisted, but the differences were not statistically significant. No correlation was found between DF concentrations and eelgrass biomass growth.

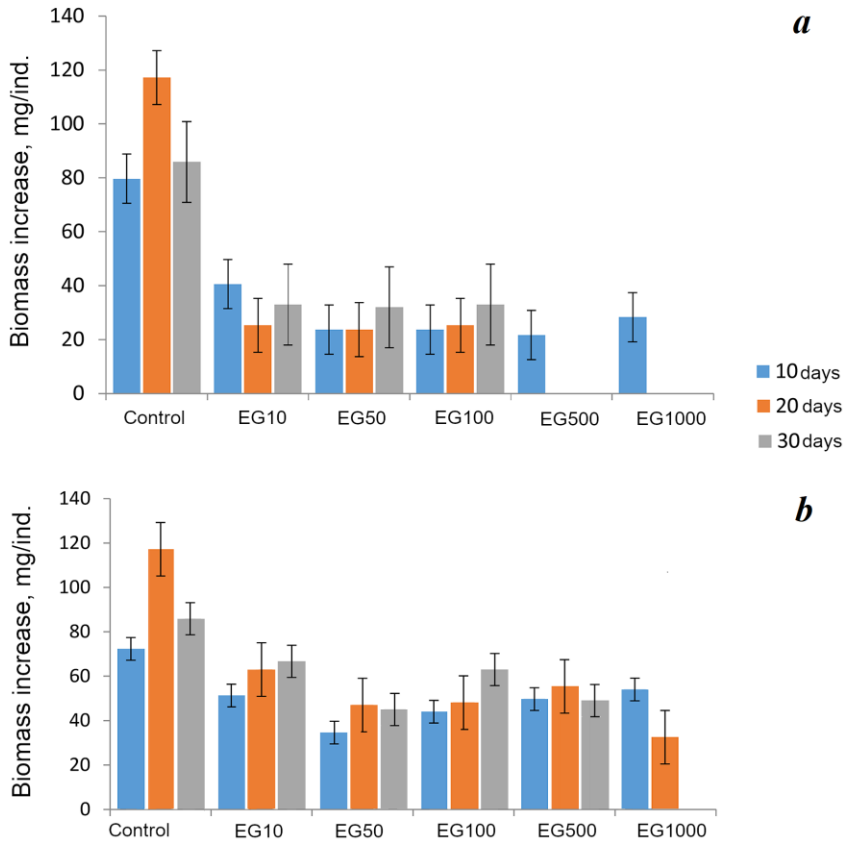

Fig. 1. Increase in seagrass *N. noltii* biomass (mg/specimen, Mean ± SEM) exposed to drilling fluid (*a*) and cementing fluid (*b*) in concentrations of 10 (EG10), 50 (EG50), 100 (EG100), 500 (EG500) and 1000 (EG1000) mg/L

When incubating eelgrass in solutions of toxicants at the studied concentrations for 10 days, no differences were observed compared to the control, although a trend toward reduced biomass growth was noted. After 20 days, a significant ($p < 0.05$) reduction in plant growth was observed at all tested concentrations. After 30 days, plants exposed to 1000 mg/L died, while no significant differences were found in the remaining experimental groups compared to the control. No correlation was found between toxicant concentrations and eelgrass biomass growth.

Changes in eelgrass leaf growth of under the influence of toxicants are shown in Fig. 2. DFs at the studied concentrations did not significantly affect leaf growth throughout the experiment, although a trend toward reduced growth was observed at high concentrations (500 and 1000 mg/L). When incubating eelgrass in a medium

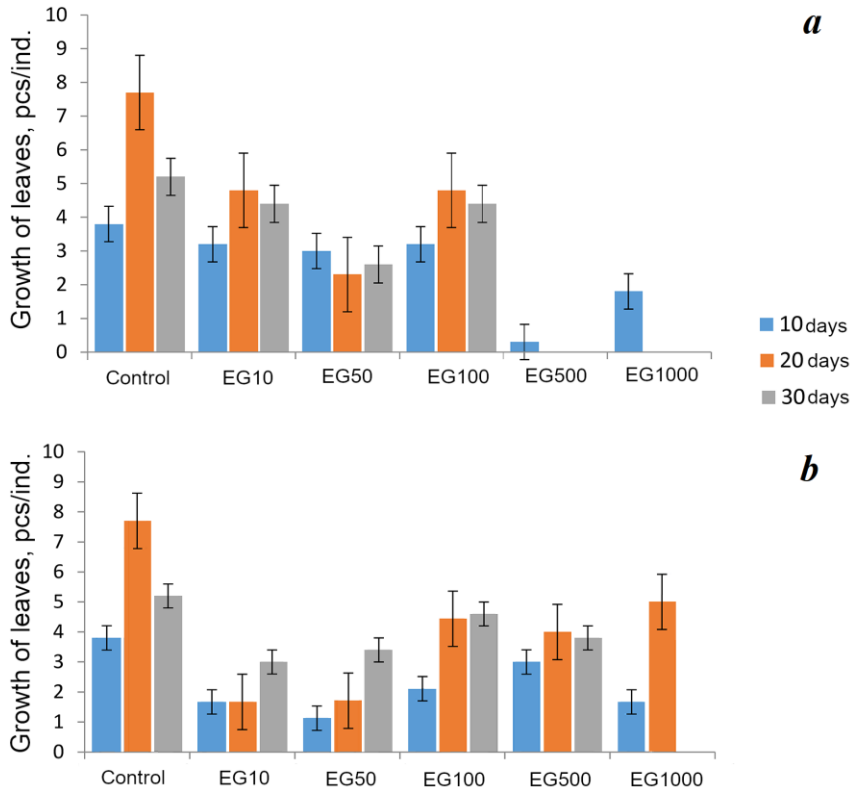

Fig. 2. Growth of seagrass *N. noltii* leaves (pcs./specimen, Mean ± SEM) exposed to drilling fluid (*a*) and cementing fluid (*b*) in concentrations of 10–1000 mg/L. Notation: See Fig. 1

with CFs, no significant differences from the control were observed after 10 days. After 20 days, a significant ($p < 0.05$) reduction in leaf growth was detected at low concentrations (10 and 50 mg/L), but not at higher concentrations. After 30 days, no differences were found between the control and experimental groups at any concentration, except at 1000 mg/L, where the plants died. No correlation was found between leaf growth and the concentrations of either toxicant.

Fig. 3 shows data on the effects of the tested toxicants on eelgrass root growth. A significant ($p < 0.01$) reduction in root growth was observed for plants incubated in DFs at a concentration of 500–1000 mg/L after 10 days. After 20–30 days,

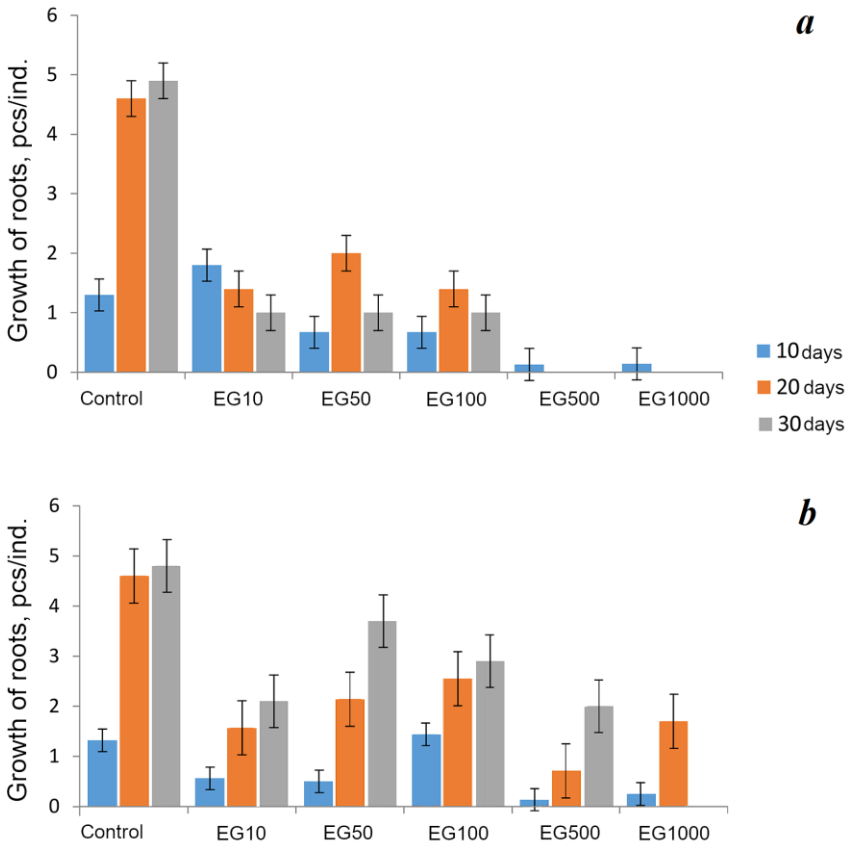

Fig. 3. Growth of seagrass *N. noltii* roots (pcs./specimen, Mean ± SEM) exposed to drilling fluid (*a*) and cementing fluid (*b*) in concentrations of 10–1000 mg/L. Notation: See Fig. 1

the same effect was observed at lower DF concentrations of 10 and 50 mg/L. After 10 days, a moderate correlation was identified between root growth and toxicant concentration ($Y = 610 - 420.9X$, $r = 0.490$, $R^2 = 0.37$).

When incubating eelgrass in media with varying toxicant concentrations, a significant ($p < 0.01$) reduction in root growth was observed after 10 days at concentrations of 500 and 1000 mg/L. This effect persisted after 20 and 30 days, but at 1000 mg/L after 30 days, the plant died. A moderate correlation was identified between root growth and toxicant concentration after 10 days ($Y = 0.94 - X$, $r = 0.39$, $R^2 = 0.23$).

Fig. 4 presents data on the survival of amphipods exposed to DFs and CFs. A significant ($p < 0.05$) reduction in amphipod survival was observed after 10 days at a DF concentration of 50 mg/L. After 20 days of exposure to media with DFs, a significant ($p < 0.05$) reduction in amphipod survival was detected at concentrations of 100 mg/L and higher. A strong correlation was identified between amphipod survival and DF concentration ($Y = 54.4 - 0.05X$, $r = 0.87$, $R^2 = 0.89$).

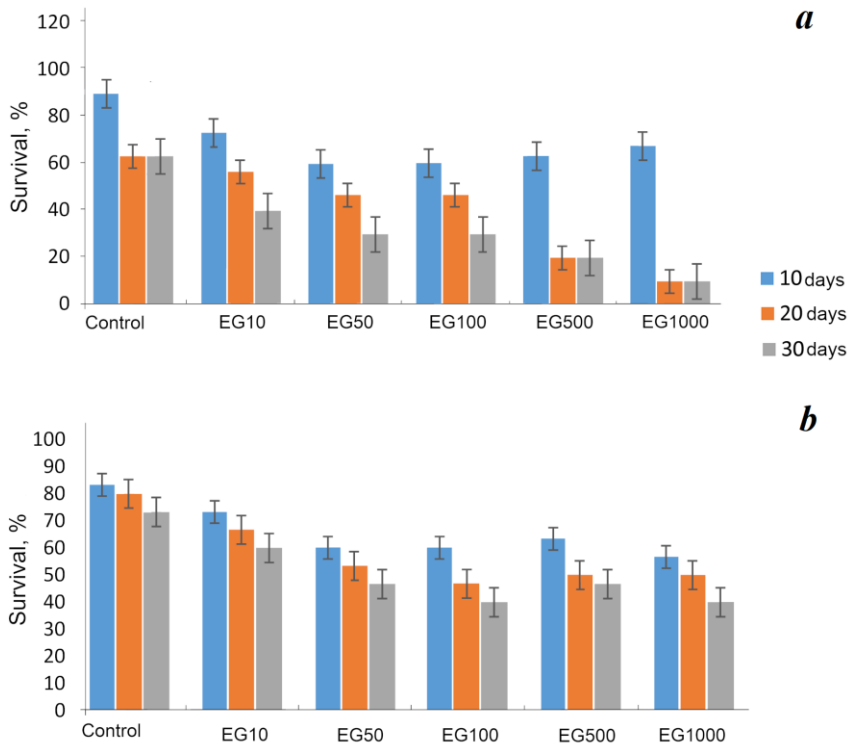

Fig. 4. Survival of amphipods (%, Mean ± SEM) exposed to drilling fluid (*a*) and cementing fluid (*b*) in concentrations of 10–1000 mg/L. Notation: See Fig. 1

After 30 days, in the experimental groups with DFs, the trend persisted, but the correlation was weaker ($Y = 41.9 - 0.04X$, $r = 0.48$, $R^2 = 0.59$). When amphipods were maintained in solutions with varying concentrations of toxic substances, a significant reduction in survival was observed at a concentration of 1000 mg/L across all study periods, but no correlation was found between survival and toxicant concentration.

Discussion of research results

The results demonstrated the toxic effects of the tested substances on representative species of the benthic community, including eelgrass and amphipods. The observed effects varied with toxicant concentration and exposure duration, enabling assumptions about the mechanisms of toxicity and potential consequences for the studied benthic organisms.

Our studies demonstrate that eelgrass biomass growth decreased by 49% after 10 days of incubation in media containing DFs at a concentration of 10 mg/L. With continued exposure, the reduction in biomass growth at this DF concentration was 62–78%. At higher concentrations (50–100 mg/L), biomass growth continued to decline significantly (by 60–80% compared to the control), and at concentrations of 500–1000 mg/L, the plants died. Other researchers have also reported reduced productivity (in terms of carbon absorption and growth rate) in seagrass of the genus *Thalassia* after 10 days of exposure to DF concentrations of 200 and 1000 μL/L [17]. However, our studies found no differences in leaf growth between eelgrass exposed to DFs and the control, whereas root growth showed a marked reduction (by 48%) compared to the control at toxicant concentrations of 50–100 mg/L after just 10 days. In subsequent periods, this trend was observed across all tested concentrations. Notably, eelgrass root growth is influenced by many factors, including soil substrate, oxygen availability, biogenic elements, water mixing, and the presence of toxicants, as confirmed by our findings. Thus, different plant parts responded differently to the effects of DFs, with roots being more sensitive to adverse effects than leaves, consistent with findings from other researchers [23].

The toxic effect of CFs on eelgrass was less pronounced than that of DFs. At the highest CF concentration (1000 mg/L), plants died after 30 days of incubation. After 10 days, no differences in biomass or leaf growth were observed between the control and experimental samples across all tested concentrations, but root growth was significantly reduced at CF concentrations of 500–1000 mg/L. In subsequent experimental periods, leaf growth remained comparable to the control, whereas biomass growth was significantly reduced after 20 days at CF concentration of 50 mg/L and higher. Root growth inhibition persisted at these concentrations from 20 to 30 days, but biomass growth after 30 days showed no significant difference from the control. Thus, it is possible to note different effects of the toxicant

on different parts of the plant, which was established when studying the effect of DFs on eelgrass. Notably, roots were more sensitive to the effects of CFs than leaves, as similarly observed with DFs.

It has been demonstrated that various toxins, including nutrients and sulfides at high concentrations, can severely impair the growth and survival of the eelgrass population [19]. Different plant parts can react differently to toxicants, including biogenic elements, associated with a higher affinity of leaves to ammonium compared to roots. A negative effect on *Zostera noltii* biomass growth was observed at sulfide concentration below 200 μmol/L. Under natural conditions, eelgrass habitat expansion did not occur at sulfide concentrations exceeding 1000 μmol/L, which is associated with reduced root viability upon contact with sulfides. However, researchers have noted that the productivity of *T. testudinum* in laboratory and field conditions unaffected by DFs after 6- and 12-week exposure periods [24], confirming the need to investigate different effects of DFs on benthic flora species.

The impact of DFs on eelgrass can be both direct and indirect. Indirect effects of drilling and DFs arise from habitat degradation. During well drilling, numerous suspended particles are generated, significantly reducing water transparency and impeding sunlight penetration. This inhibits photosynthetic processes in plants and suppresses their growth, including that of epiphytic microflora [25]. When suspended particles settle, they form a layer that restricts nutrient supply to eelgrass roots, an effect particularly pronounced with CFs, as demonstrated in our studies. Consequently, nutrient exchange between the environment and the plant is disrupted. Additionally, the introduction of xenobiotics into water alters its physicochemical properties, further negatively affecting the survival and growth of aquatic organisms.

The direct impact of DFs has a toxic effect due to the presence of heavy metals and organic compounds, which accumulate in plants and impair their physiological functions. This results in the inhibition of overall plant growth and that of specific parts (leaves and roots), as demonstrated in our study, as well as the suppression of dispersal and reproduction. Furthermore, eelgrass beds may become unsuitable habitats for other marine organisms, such as amphipods, fish, and mollusks, that rely on them.

For example, under natural and experimental conditions, researchers have observed changes in the abundance of benthic invertebrates. Macrofauna exposed to DFs or clay used in well cementing exhibited significantly reduced abundance compared to the control group [26]. Our studies demonstrated that CFs were less toxic to amphipods than DFs. Throughout the experiment, the survival rate of amphipods exposed to DF solutions at concentrations above 10 mg/L was significantly lower (by 30–85%) than the control, whereas during incubation in CF solutions, significant differences were observed only at the highest concentration of 1000 mg/L,

when this indicator was 46% lower compared to the control group. Thus, the toxic effects on amphipods were specific to CFs and DFs.

Researchers have observed that, under natural conditions, some seagrasses were less sensitive to oil, dispersed oils and DFs than intertidal communities, including corals, sponges, echinoderms, mangroves, invertebrates and mollusks [27]. Notably, the number of benthic invertebrates was significantly reduced by DFs in laboratory settings, but these effects were not observed in natural environments. In field conditions, invertebrate density was comparable between control and DF-treated areas but significantly lower than in laboratory controls, while species diversity remained consistent between field and laboratory conditions [23].

The global trend of increasing oil and gas production in coastal marine areas poses a significant threat to benthic ecosystems and their inhabitants. Changes in the physicochemical properties of water, increased turbidity, and reduced light availability for aquatic organisms can trigger cascading effects across the marine ecosystem. Given the critical role of seagrasses and their associated invertebrates in coastal ecosystems, this study highlights the vulnerability of benthic communities to the introduction of DFs and their components, particularly under changing environmental conditions [28, 29].

Conclusion

Long-term exposure to DFs and their components disrupts eelgrass metabolic processes, causes leaf mortality, and induces tissue degradation, threatening the overall health and viability of seagrass. Our studies demonstrated that, at a DF concentration of 10 mg/L, plant biomass growth decreased by 49% after 10 days. After 20–30 days, the reduction in biomass growth at this concentration was 62–78%. At higher concentrations (50–100 mg/L), biomass growth declined significantly (by 60–80% relative to the control), and at 500–1000 mg/L, the plants died. Eelgrass roots were more sensitive to DFs than leaves: no differences in leaf growth were observed between DF-exposed eelgrass and the control, whereas root growth was significantly reduced by 48% relative to the control at toxicant concentrations of 50–100 mg/L after just 10 days. The toxic effect of CFs on eelgrass was less pronounced than that of DFs. At the highest toxicant concentration (1000 mg/L), plants died after 30 days of incubation. No significant differences in leaf growth were found between experimental and control groups, but root growth was significantly reduced by 64–90% at CF concentrations of 500–1000 mg/L after 10–20 days. Changes in the growth rate of seagrasses (eelgrass) and reductions in the number of benthic invertebrates, resulting from environmental disturbances and alterations in physicochemical properties, can lead to irreversible modifications of coastal benthic communities. CFs were less toxic to amphipods than DFs, as evidenced by a significant reduction (by 30–85%) in amphipod survival in DF solutions at concentrations above 10 mg/L compared to the control, whereas significant differences in CF solutions were observed only at the highest concentration of 1000 mg/L. Consequently, measures to preserve ecosystems and mitigate the impacts of offshore drilling are essential. Toxicity tests enable the evaluation of biological responses and determination of concentrations at which DF emissions and

drill cuttings discharges affect indicator species and test organisms. These impacts include changes in autotrophic and heterotrophic individuals/populations, community structure, and energy flow processes within seagrass ecosystems and their associated invertebrates. Ecotoxicological methods facilitate the assessment of environmental impacts throughout the drilling cycle. This integrated approach provides valuable insights into the consequences of drilling operations, supporting informed decision-making aligned with environmental safety principles and aiding in the development of environmental profiles and impact assessments for various waste management strategies.

REFERENCES

1. Antia, M., Ezejiofor, A.N., Obasi, C.N. and Orisakwe, O.E., 2022. Environmental and Public Health Effects of Spent Drilling Fluid: An Updated Systematic Review. *Journal of Hazardous Materials Advances*, 7, pp. 100–120. https://doi.org/10.1016/j.hazadv.2022.100120
2. Costa, L.C., Carvalho, C.F., Soares, A.S.F., Souza, A.C.P., Bastos, E.F.T., Guimarães, E.C.B.T., Santos, J.C., Carvalho, T., Calderari, V.H. [et al.], 2023. Physical and Chemical Characterization of Drill Cuttings: A Review. *Marine Pollution Bulletin*, 194, Part A, 115342. https://doi.org/10.1016/j.marpolbul.2023.115342
3. Aslan, J.F., Weber, L.I., Iannacone, J., Lugon Junior, J., Saraiva, V.B. and Oliveira, M.M., 2019. Toxicity of Drilling Fluids in Aquatic Organisms: A Review. *Ecotoxicology Environmental Contamination*, 14(1), pp. 35–47. https://doi.org/10.5132/eec.2019.01.04
4. Marinho, L.S., Pereira, B.C., Guandalim, F.P. and Cavalcante, L.M., 2024. Monitoring of Drilling Fluids and Cuttings as an Environmental Management Tool for Offshore Fluid Operations. In: OTC, 2024. *Proceedings of Offshore Technology Conference, Houston, Texas, USA, May 6–9, 2024*. OTC-35185-MS.
5. Mahmoud, H., Mohammed, A.A.A., Nasser, M., Hussein, I.A. and El-Naas, L.H., 2024. Green Drilling Fluid Additives for a Sustainable Hole-Cleaning Performance: A Comprehensive Review. *Emergent Materials*, 7, pp. 387–402. https://doi.org/10.1007/s42247-023-00524-w
6. Stark, J.S., 2022. Effects of Lubricant Oil and Diesel on Macrofaunal Communities in Marine Sediments: A Five Year Field Experiment in Antarctica. *Environmental Pollution*, 311, 119885. https://doi.org/10.1016/j.envpol.2022.119885
7. Yalman, E., Federer-Kovacs, G., Depci, T., Al Khalaf, H., Aylikci, V. and Aydin, M.G., 2022. Development of Novel Inhibitive Water-Based Drilling Muds for Oil and Gas Field Applications. *Journal of Petroleum Science and Engineering*, 210, 109907. https://doi.org/10.1016/j.petrol.2021.109907
8. Temilola, O., Omoregie, I.P., Michael, K. and Bamidele, A., 2020. Acute Toxicity of Produced Water on Selected Organisms in the Aquatic Environment of the Niger Delta. *Scientific African*, 8, e00460. https://doi.org/10.1016/j.sciaf.2020.e00460
9. Martin, C., Nourian, A., Babaie, M. and Nasr, G.G., 2023. Environmental, Health and Safety Assessment of Nanoparticle Application in Drilling Mud – Review. *Geoenergy Science and Engineering*. 2023. Vol. 226. 211767. https://doi.org/10.1016/j.geoen.2023.211767
10. Olsen J.L., Rouzé, P., Verhelst, B., Lin, Y., Bayer, T., Collén, J., Dattolo, E., Paoli, E.D., Dittami, S.M. [et al.], 2016. The Genome of the Seagrass Zostera marina Reveals Angiosperm Adaptation to the Sea. *Nature*, 530, pp. 331–335. https://doi.org/10.1038/nature16548

11. York, P.H., Carter, A.B., Chartrand, K., Sankey, T., Wells, L. and Rasheed, M.A., 2015. Dynamics of a Deep-Water Seagrass Population on the Great Barrier Reef: Annual Occurrence and Response to a Major Dredging Program. *Scientific Reports*, 5, 13167. https://doi.org/10.1038/srep13167

12. Zhang, Y., Yu, X., Chen, Z., Wang, Q., Zuo, J., Yu, S. and Guo, R., 2023. Review of Seagrass Bed Pollution. *Water*, 15, 3754. https://doi.org/10.3390/w15213754

13. Lewis, M.A. and Devereux, R., 2009. Nonnutrient Anthropogenic Chemicals in Seagrass Ecosystems: Fate and Effects. *Environmental Toxicology and Chemistry*, 28(3), pp. 644–661. https://doi.org/10.1897/08-201.1

14. Vasechkina, E.F., Rudneva, I.I., Filippova, T.A., Naumenko, I.P., Parkhomenko, A.V. and Shaida, V.G., 2023. Photosynthetic Parameters of the Seaweeds Widely Spread near the Crimean Coast. *Regional Studies in Marine Science*, 66, 103170. https://doi.org/10.1016/j.rsma.2023.103170

15. Short, F.T., Kosten, S., Morgan, P.A., Malone, S. and Moore, G.E., 2016. Impacts of Climate Change on Submerged and Emergent Wetland Plants. *Aquatic Botany*, 135, pp. 3–17. https://doi.org/10.1016/J.AQUABOT.2016.06.006

16. Bejarano, A.C., Adams, J.E., McDowell, J., Parkerton, T.F. and Hanson, M.L., 2023. Recommendations for Improving the Reporting and Communication of Aquatic Toxicity Studies for Oil Spill Planning, Response, and Environmental Assessment. *Aquatic Toxicology*, 255, 106391. https://doi.org/10.1016/j.aquatox.2022.106391

17. Price, W.A., Macauley, J.M. and Clark, J.R., 1986. Effects of Drilling Fluids on *Thalassia testudinum* and its Epiphytic Algae. *Environmental Experimental Botany*, 26(4), pp. 321–330. https://doi.org/10.1016/0098-8472(86)90019-5

18. De los Santos, C.B., Arenas, F., Neuparth, T. and Santos, M.M., 2019. Interaction of Short-Term Copper Pollution and Ocean Acidification in Seagrass Ecosystems: Toxicity, Bioconcentration and Dietary Transfer. *Marine Pollution Bulletin*, 142, pp. 155–163. https://doi.org/10.1016/j.marpolbul.2019.03.034

19. Govers, L.L., de Brouwer, J.H.F., Suykerbuyk, W., Bouma, T.J., Lamers, L.P.M., Smolders, A.J.P. and van Katwijk, M.M., 2014. Toxic Effects of Increased Sediment Nutrient and Organic Matter Loading on the Seagrass *Zostera noltii. Aquatic Toxicology*, 155, pp. 253–260. https://doi.org/10.1016/j.aquatox.2014.07.005

20. Hu, C., Yang, X., Gao, L., Zhang, P., Li, W., Dong, J., Li, C. and Zhang, X., 2019. Comparative Analysis of Heavy Metal Accumulation and Bioindication in Three Seagrasses: Which Species is More Suitable as a Bioindicator? *Science of The Total Environment*, 669, pp. 41–48. https://doi.org/10.1016/j.scitotenv.2019.02.425

21. Rudneva, I.I., Medaynkina, M.V. and Shaida, V.G., 2023. Toxic Evaluation of Drilling Fluids on Marine Amphipoda. *Ekosistemy*, 34, pp. 140–144 (in Russian).

22. Duke, B.M., Emery, K.A., Dugan, J.E., Hubbard, D.M. and Joab, B.M., 2023. Uptake of Polycyclic Aromatic Hydrocarbons via High-Energy Water Accommodated Fraction (Hewaf) by Beach Hoppers (Amphipoda, Talitridae) Using Different Sandy Beach Exposure Pathways. *Marine Pollution Bulletin*, 190, 114835. https://doi.org/10.1016/j.marpolbul.2023.114835

23. Girones, L., Oliva, A.L., Negrin, V.L., Marcovecchio, J.E. and Arias, A.H., 2021. Persistent Organic Pollutants (POPs) in Coastal Wetlands: A Review of Their Occurrences, Toxic Effects, and Biogeochemical Cycling. *Marine Pollution Bulletin*, 172, 112864. https://doi.org/10.1016/j.marpolbul.2021.112864

24. Qiao, Y., Zhang, Y., Xu, S., Yue, S., Zhang, X., Liu, M., Sun, L., Jia, X. and Zhou, Y., 2022. Multi-Leveled Insights into the Response of the Eelgrass *Zostera marina* L to Cu than Cd Exposure. *Science of the Total Environment*, 845, 157057. https://doi.org/10.1016/j.scitotenv.2022.157057

25. Mochida, K., Hano, T., Onduka, T., Ito, K. and Yoshida, G., 2019. Physiological Responses of Eelgrass (*Zostera marina*) to Ambient Stresses such as Herbicide, Insufficient Light, and High Water Temperature. *Aquatic Toxicology*, 208, pp. 20–28. https://doi.org/10.1016/j.aquatox.2018.12.018

26. Kelly, J.R., Duke, T.W., Harwell, M.A. and Harwell, C.C., 1987. An Ecosystem Perspective on Potential Impacts of Drilling Fluid Discharges on Seagrasses. *Environmental Management*, 11, pp. 537–562. https://doi.org/10.1007/BF01867661

27. Weber, D.E., Flemer, D.A. and Bundrick, C.M., 1992. Comparison of the Effects of Drilling Fluid on Macrobenthic Invertebrates Associated with the Seagrass, *Thalassia testudinum*, in the Laboratory and Field. *Estuarine, Coastal and Shelf Science*, 35(3), pp. 315–330. https://doi.org/10.1016/S0272-7714(05)80051-4

28. Hasler-Sheetal, H., 2023. Detrimental Impact of Sulfide on the Seagrass *Zostera marina* in Dark Hypoxia. *PLoS ONE*, 18(12), e0295450. https://doi.org/10.1371/journal.pone.0295450

29. Zhang, Y., Yue, S., Gao, Y., Zhao, P., Liu, M., Qiao, Y., Xu, S., Gu, R., Zhang, X. [et al.], 2024. Insights into Response of Seagrass (Zostera marina) to Sulfide Exposure at Morphological, Physiochemical and Molecular Levels in Context of Coastal Eutrophication and Warming. *Plant, Cell and Environment*, 47(12), pp. 4768–4785. https://doi.org/10.1111/pce.15048

Submitted 02.10.2024; accepted after review 06.11.2024;
revised 24.06.2025; published 30.09.2025

About the authors:

Irina I. Rudneva, Leading Research Associate, Marine Hydrophysical Institute of RAS (2 Kapitanskaya St., Sevastopol, 299011, Russian Federation), DSc (Biol.), Professor, **ORCID ID: 0000-0002-9623-9467, Scopus Author ID: 9266541700, ResearcherID: L-3758-2016,** *svg-41@mail.ru*

Valentin G. Shaida, Researcher Engineer, Company "EcoService-A" (17A Verkhnyaya Krasnoselskaya Str., Bldg. 1Б, Of. 8, Moscow, 107140, Russian Federation)

Maria V. Medyankina, Associate Professor, Ecology and nature Use Chair of Department of Biotechnologies and Fisheries, Moscow State University of Technology and Management K. G. Razumovsky (First Cossack University) (14 Shabolovskaya Str., Bldg. 9, Moscow, 119049, Russian Federation), PhD (Biol.), **ORCID ID: 0000-0002-9195-0399,** *mediankina@mail.ru*

Oleg V. Shaida, Leading Engineer, Marine Hydrophysical Institute of RAS (2 Kapitanskaya St., Sevastopol, 299011, Russian Federation), *ovasha@mail.ru*

Contribution of the authors:

Irina I. Rudneva – concept development, task statement

Maria V. Medyankina – processing and description of the study results

Valentin G. Shaida and Oleg V. Shaida – development of methods and carrying out the experimental studies

All the authors have read and approved the final manuscript.

ISSN 2413-5577, Ecological Safety of Coastal and Shelf Zones of Sea, 2025, No. 3, pp. 96–114.

Original paper

Ecoenergy Potential of a Solar-Wind Station in the Khazar Nature Reserve in the Caspian Sea

A. M. Penjiyev *, B. M. Mamedov

Turkmen State Institute of Architecture and Civil Engineering, Ashgabat, Turkmenistan

* *e-mail: ampenjiyev@gmail.com*

Abstract

The article considers solar and wind energy resources and their ecological potential in the Khazar Reserve on Ogurchinsky Island in the Caspian Sea. The methodological basis is formed by the empirical calculations for the preparation of a feasibility study and the creation, development and implementation of energy-efficient technologies based on solar-wind energy equipment in the Reserve. The paper provides an energy, economic and ecological assessment of a solar power station with a capacity of 10 kW·h/day based on theoretical and methodological calculations and taking into account natural and climatic conditions. The station generates electricity (3658.34 kW·h/year), saves organic fuel (1463.336 kg of equivalent fuel) and reduces harmful emissions into the biosphere: SO_2 (30.41 kg), NO_x (16.38 kg), CO (2.13 kg), CH_4 (4.47 kg), CO_2 (2339.64 kg), solids (3.19 kg). One 400 W wind turbine can generate 19.45 kW·h/m^2·year, or an average of 1.62 kW·h/m^2·month, with an equivalent reduction in fuel consumption of 7.78 equivalent fuel. The obtained scientifically substantiated results will contribute to the improvement of social, living, economic and environmental conditions of the island's inhabitants, the conservation of bioresources, and strengthening energy and environmental security. The results of the feasibility study will help implement various solar-wind technological complexes in the region.

Key words: solar-wind energy resources, environmental potentials, mathematical statistics, Khazar Reserve, Ogurchinsky Island, Caspian Sea

For citation: Penjiyev, A.M. and Mamedov, B.M., 2025. Ecoenergy Potential of a Solar-Wind Station in the Khazar Nature Reserve in the Caspian Sea. *Ecological Safety of Coastal and Shelf Zones of Sea*, (3), pp. 96–114.

© Penjiyev A. M., Mamedov B. M., 2025

This work is licensed under a Creative Commons Attribution-Non Commercial 4.0 International (CC BY-NC 4.0) License

Экоэнергетический потенциал солнечно-ветровой станции в Хазарском заповеднике в Каспийском море

А. М. Пенджиев *, Б. М. Мамедов

Туркменский государственный архитектурно-строительный институт, Ашгабат, Туркменистан

* *e-mail: ampenjiyev@gmail.com*

Аннотация

Рассмотрены солнечно-ветровые энергоресурсы и их экологический потенциал в Хазарском заповеднике на острове Огурчинском в Каспийском море. Методологической основой послужили эмпирические расчеты для составления технико-экономического обоснования и создания, разработки и внедрения энергоэффективных технологий на основе солнечно-ветрового энергооборудования в заповеднике. На основе теоретических и методических расчетов и с учетом природно-климатических условий дана энергетическая, экономическая и экологическая оценка солнечной энергетической станции мощностью 10 кВт·ч/сут. Станция вырабатывает электроэнергию – 3658.34 кВт·ч/год, экономит органическое топливо – 1463.336 кг у. т. и сокращает вредные выбросы в биосферу: SO_2 – 30.41 кг, NO_x –16.38 кг, CO – 2.13 кг, CH_4 – 4.47 кг, CO_2 – 2339.64 кг, твердых веществ – 3.19 кг. С помощью одной ветроустановки мощностью 400 Вт можно получить 19.45 кВт·ч/м^2·год электроэнергии (в среднем 1.62 кВт·ч/м^2·мес.), при этом эквивалент сокращения расхода топлива составит 7.78 кг у. т. Полученные научно обоснованные результаты можно использовать для улучшения социально-бытовых, экономических и экологических условий обитателей острова, сохранения биоресурсов и укрепления энергетической и экологической безопасности. Результаты технико-экономического обоснования помогут внедрению различных солнечно-ветровых технологических комплексов в регионе.

Ключевые слова: солнечно-ветровые энергоресурсы, экологический потенциал, математическая статистика, Хазарский заповедник, остров Огурчинский, Каспийское море

Для цитирования: *Пенджиев А. М., Мамедов Б. М.* Экоэнергетический потенциал солнечно-ветровой станции в Хазарском заповеднике в Каспийском море // Экологическая безопасность прибрежной и шельфовой зон моря. 2025. № 3. С. 96–114. EDN XKZNOE.

Introduction

Addressing the challenge of providing energy to protected areas and pastoral farms in the Karakum Desert, which are distant from centralized power grids, necessitates evaluating the potential of renewable energy sources (RES). This effort is also motivated by global climate change concerns and the need to enhance social, economic, and environmental conditions in remote regions of Turkmenistan. Transitioning to RES will reduce reliance on fossil fuels, thereby promoting ecological sustainability and preserving biodiversity [1].

Turkmenistan is undertaking all necessary measures to address this critical issue and is implementing comprehensive mechanisms in collaboration with international organizations to ensure environmental and technological sustainability. This was emphasized by the President of Turkmenistan during speeches at the 78th session of the United Nations General Assembly and the 28th Conference of the Parties to the United Nations Framework Convention on Climate Change.

Turkmenistan has eight state nature reserves (Repetek, Badkhyz, Kopetdag, Syunt-Khasardag, Kaplankyr, Amudarya, Koitendag, and Khazar) and 14 wildlife sanctuaries, covering a total area of 2.0 million ha, or 4% of the country's territory.

The Khazar Nature Reserve spans 270,000 ha, primarily located in the Caspian Sea. It supports over 600 plant species and hosts 466 bird species and 55 marine fish species, five of which are listed in the Red Book. Over 5 million birds migrate to the reserve annually for wintering. The reserve's fauna includes rare and protected species, such as the Caspian seal, long-eared hedgehog, and goitered gazelle, alongside other species like the tolai hare, reed cat, sand cat, and foxes, characteristic of the desert ecosystem [1–4].

The Khazar Nature Reserve includes Ogurchinsky Island (Fig. 1), located in the southeastern Caspian Sea in Turkmenistan (39° 6' N; 53° 6' E). As the largest sandy island in the Caspian Sea, it lies 45 km offshore and forms a narrow spit, 1–1.5 km wide and approximately 42 km long, extending from north to south. Electricity on the island is provided by diesel generators, with organic fuels (diesel, gasoline, kerosene, and liquefied gas) imported by sea, incurring substantial financial costs [1)] [5–7]. The use of diesel fuel results in the emission of pollutants into the environment.

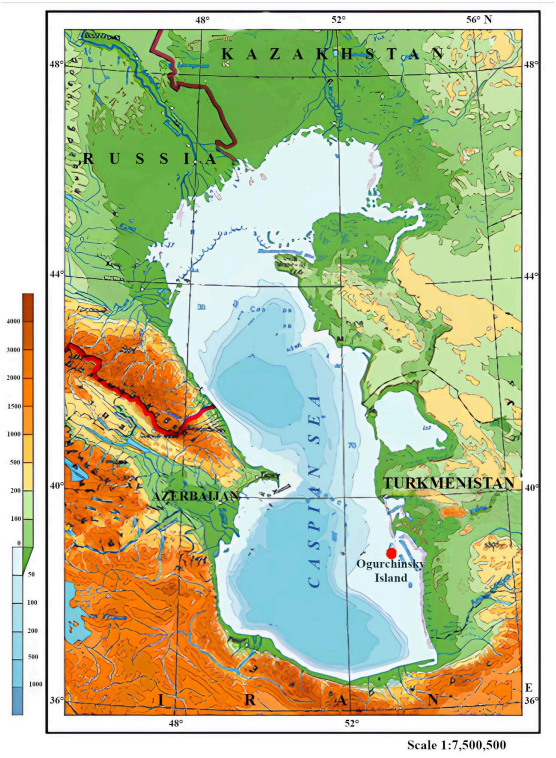

Fig. 1. Location of Ogurchinsky Island (red dot) of the Khazar Nature Reserve in the Caspian Sea [6, 7]

[1)] Gidrometeoizdat, 1989. [*Scientific and Applied Reference Book on the Climate of the USSR*]. Leningrad: Gidrometeoizdat. Series 3. Long-Term Data. Parts 1–6, 502 p. (in Russian).

Systematic measures to ensure the island's energy supply and enhance its economic, food, water, and environmental security can be achieved using renewable energy sources, specifically solar and wind power plants integrated with modern "green" technologies. These measures will also support the conservation of the region's biodiversity. Currently, energy provision in protected areas is limited: electricity is generated by low-capacity gasoline generators, and heating relies on liquefied gas.

A primary drawback of using gasoline-powered generators in protected areas is the significant noise they generate, audible from a distance of 5–10 km, which disturbs the wildlife inhabiting these regions. Additionally, the combustion of fuel emits pollutants into the environment.

The technical limitations of gasoline and diesel generators include a short engine lifespan (600–1,500 h) and high fuel consumption (350–500 g/kW·h). These generators are unable to handle heavy electrical loads and are unsuitable for round-the-clock operation to power household, laboratory, and other electrical appliances [2, 3, 8]. Consequently, a key requirement for modern autonomous power sources is the ability to provide consistent, 24-hour power supply to consumers. Currently, the condition of existing power stations, which rely on gasoline and diesel generators, is considered unsatisfactory due to severe equipment wear and tear.

These limitations can be addressed by deploying solar and wind power stations, tailored to local energy resources, thereby reducing the environmental impact of diesel and gasoline power stations. All of the above makes solving this problem undoubtedly *relevant*.

The most energy-efficient option is to use the solar and wind energy potential of the Khazar Nature Reserve on Ogurchinsky (Ogurjaly) Island in the Caspian Sea. However, implementing solar and wind energy technologies requires developing detailed design and cost estimation documentation, along with a feasibility study (FS) to assess their applicability [1–3].

Degree of development of the topic. The field of solar and wind energy has been advanced by the contributions of prominent scientists, including V.A. Baum, P.P. Bezrukikh, V.I. Vissarionov [2)], V.M. Evdokimov, D.S. Strebkov, R.B. Bayramov, V.P. Kharitonov, U.A. Bekman, D.A. Duffy, J. Twidell, A. Angstrom, M. Jin, H.L. Wigley, and others [3)] [3, 9–15].

[2)] Vissarionov, V.I., ed., 2008. [*Solar Power*]. Moscow: Izdatelskiy Dom MEI, 276 p. (in Russian).

[3)] Vasilev, Yu.S., Bezrukikh, P.P., Elistratov, V.V. and Sidorenko, G.I., 2008. *Estimates of Renewable Energy Resources in Russia.* Saint Petersburg: Izd-vo Politekhn. Un-ta, 250 p. (in Russian).

Turkmen scientists have made significant contributions to the field of solar energy use, achieving notable scientific and practical results. However, the main limitation of this research is its failure to account for the influence of natural and climatic factors, as well as the lack of systematic assessments of solar and wind energy resources, including their technical, economic, and ecological potential.

An analysis of literature sources indicates that the Caspian Sea region and the islands of Turkmenistan possess significant RES. However, existing scientific studies lack assessments of energy efficiency, fail to evaluate economic feasibility, and overlook environmental priorities [2), 3)] [3–5, 9–15].

Based on the analytical studies of solar and wind energy technologies, the goals and objectives for researching the energy resource potential of solar and wind energy in the Khazar Nature Reserve have been established.

The purpose of this study is to systematically evaluate the solar and wind energy potential through innovative computational methods and to assess the energy, economic, and environmental viability of developing and implementing renewable energy technologies in the region under study.

The objective of this study is to summarize and evaluate the technical, economic, and ecological potential of solar and wind power plants on Ogurchinsky Island in the Khazar Nature Reserve, focusing on energy efficiency, fuel savings, and environmental impact. It aims to apply innovative computational methods to systematically assess the energy productivity of converting solar radiation into electrical and thermal energy, determine the basic wind energy potential, and develop regression equations to forecast energy resources for the preparation of a FS.

The subject of the study is the energy efficiency and environmental sustainability of solar and wind power installations on Ogurchinsky Island.

The scientific novelty of the research lies in the development of a systematic methodology for calculating energy efficiency, incorporating natural and climatic conditions and the application of solar and wind energy technologies. Additionally, it involves evaluating the economic and environmental potential of the Khazar Nature Reserve for implementing these technologies on Ogurchinsky Island and preparing a FS.

Research methodology and methods

The methodology and research methods employ a systematic approach, integrating theoretical and practical assessments of solar and wind energy technologies to support the conservation of the island's rich biodiversity and biological resources. The methodological framework includes empirical calculations for the preparation of a FS and the development and implementation of energy-efficient technologies based on solar and wind energy systems for farms in the region under study [2), 3)] [3–5, 14].

Meteorological characteristics of the island

The energy resources of direct solar radiation reaching a horizontal surface under clear skies in Turkmenistan throughout the year range from 1,699.4 to 1,793.0 kW·h/(m²·year) (146–154 kcal/cm²), while diffuse solar radiation under clear skies ranges from 372.3 to 453.0 kW·h/(m²·year) (32–39 kcal/cm²). On cloudy and overcast days, direct solar radiation decreases from 35 to 27%, with the diffuse component increasing to 25–40%. Across Turkmenistan, total solar energy varies from 1,687.7 to 1,897.2 kW·h/(m²·year) (145–163 kcal/cm²). The monthly distribution of the gross energy, technical, and economic potential of solar energy per square meter of surface area [1)] is presented in Fig. 2 [3–7].

As shown in Fig. 2, the island's solar energy resource potential ranges from 44 to 50 kW·h/(m²·month), with total solar radiation on a horizontal surface amounting to 1,685.4 kW·h/(m²·year) and an average monthly radiation of 140.45 kW·h/(m²·month). The annual sunshine duration on the island is 2,668 h, with an average monthly sunshine duration of 222.3 h. In July, the sun rises at 4:44 and sets at 19:16, and in January, it rises at 7:05 and sets at 16:55 [1)] [3, 4, 8].

The temperature regime on the island varies seasonally. The average annual temperature ranges from 4.0 to 27.9°C. From May to October, the average temperature remains around 20.0°C, gradually decreasing to 17.5°C. In January, it reaches

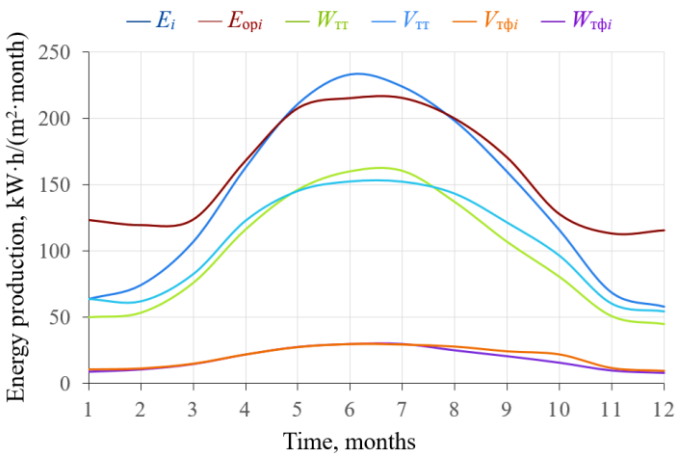

Fig. 2. Distribution of solar energy resource potentials: gross E_{opi} and technical E_i, converted into thermal $W_{тт}$ and electrical energy $W_{тфi}$ specific production into thermal $V_{тт}$ and electrical $V_{тф}$ energy on the territory of the island by month during the year

a minimum of 4.0°C. Climatic data indicate that the maximum average air temperature in January is 11.0°C, rising to 31.1°C in July. The minimum temperature drops to −0.4°C in January and rises to 23°C in July, with an average annual temperature of 11.0°C [1)] [3–7].

Wind resources. The extensive meridional extent of the Caspian Sea and the variety of atmospheric phenomena and circulation patterns result in a complex wind regime and uneven water temperature distribution on the island. These characteristics are influenced by variations in natural and climatic conditions, synoptic situations, atmospheric phenomena, air temperature, and current direction, leading to fluctuations in wind speed [1)] [3–5, 8, 9].

Scientific research indicates that storm wind formation is influenced by terrain characteristics and atmospheric circulation patterns. The average wind speed on the island ranges from 2.4 to 4.6 m/s, with an annual average of 3.3 m/s. Storm winds exceeding 25 m/s have been recorded. The wind rose [1)] in the bay varies seasonally, driven by changes in atmospheric air circulation [3, 4, 16, 17].

Fig. 3 presents the average daily distribution of wind and solar energy potential by month of the year for Ogurchinsky Island.

Wind directions in the Khazar Nature Reserve are influenced by atmospheric circulation and water temperature, ranging from 3% south to 26% west, with prevailing winds from the west (26%), northwest (16%), northeast (15%), and southwest (14%) [1)].

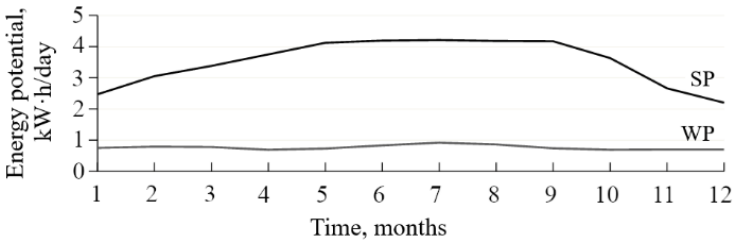

Fig. 3. Average daily distribution of wind (WP) and solar (SP) energy potentials on Ogurchinsky Island by month of the year

Methodology for researching ecoenergy resources

The calculation of solar energy potential was based on the methods [2)] described in [3–5, 12–16], adapted to the conditions of the Caspian region. As previously noted, no studies to date have utilized new methods that incorporate natural and climatic conditions, hydrometeorological factors, and assessments of technical, economic, and environmental indicators for regions in Turkmenistan [8–11].

To assess the solar energy potential on the island, long-term meteorological data were considered, including sunshine duration; angles of incidence on inclined and perpendicular surfaces; hourly solar angles; solar movement parameters (declination relative to inclined surfaces and the horizon, sunrise and sunset times);

characteristics of diffuse radiation and albedo; and average monthly and annual outdoor air and surface temperatures for an operational solar power plant. Additionally, specific energy parameters of the solar power plant and local climatic factors were incorporated.

To develop physical and mathematical models, certain assumptions were adopted: Ogurchinsky Island is regarded as an area with intense solar radiation reaching the surface, geographical and climatic conditions are assumed to be uniform across the island, and average annual meteorological data for the entire island were used [3–5, 9].

Optimal tilt angle of solar converters on the island. To maximize the efficiency of solar energy technologies and installations year-round, the optimal tilt angle of solar converters must be determined, accounting for the geographical characteristics of the installation site. The calculated optimal tilt angles for a solar receiver with an east-west orientation are 54° (−0.82930 rad) in winter, 24° (0.42418 rad) in summer, and an annual average of 39° (0.26664 rad). The energy productivity of photovoltaic modules as a function of tilt angle for Ogurchinsky Island is presented in Fig. 4 [2–4, 7, 19].

Gross solar energy potential – the average annual total solar radiation reaching Ogurchinsky Island, serving as a key energy resource.

To calculate the gross solar energy potential, long-term meteorological data on solar radiation incident on horizontal and optimally inclined surfaces were considered. These data were systematized by month (E_i, where i = 1, 2, ..., 12) [1)] [3–5, 10, 17–20].

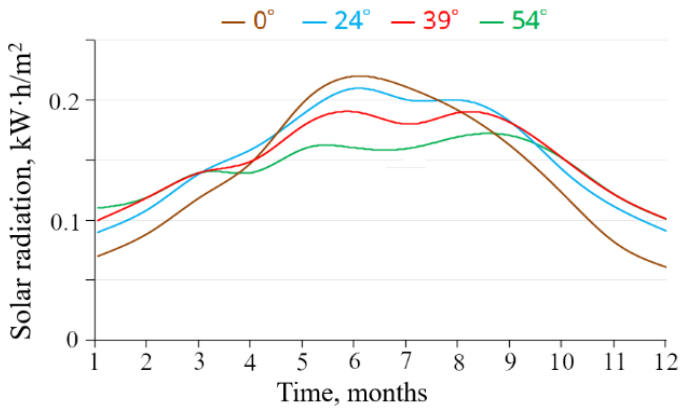

Fig. 4. Receipt of solar radiation at different angles of inclination of the photomodule, the angles equaling 0°; 24°; 54°; 39° (the optimal angle for Ogurchinsky Island)

The calculations were performed taking into account the average cosine of the angle θ of direct solar radiation relative to the normal during a 10-hour interval – from 7:00 to 17:00 – for a photovoltaic module with an area of 0.24 m^2. The average annual solar radiation per unit of horizontal surface area by month under clear skies E_{opi}, accounting for the module area, is calculated using the formula:

$$E_{opi} = \frac{E_{\Pi i}}{\langle \cos\theta \rangle} = \frac{(1-\varepsilon)E_i}{\langle \cos\theta \rangle} = 456.2 \text{ kW·h/(m}^2\text{·month)},$$

where $E_{\Pi i}$ is the average annual direct solar radiation per unit of horizontal surface area by month, kW·h/(m^2·month); E_i is the average annual total solar energy per unit of horizontal surface area by month, kW·h/(m^2·month); cos θ is the average cosine of the angle of incidence of solar rays on a perpendicular surface, varying from 24° in summer to 54° in winter; ε is the radiation coefficient, ranging from 0.14 to 0.28 (with an annual average of 0.221667) [1), 2)] [3–5, 10, 14, 15]. The optimal tilt angle for the island over the year is 39°.

The total solar radiation E for a 10-hour daily interval from 07:00 to 17:00 per unit of horizontal surface area of a photovoltaic module per year is calculated as:

$$E = \sum_i E_i = 404.5 \text{ kW·h/(m}^2\text{·year)}.$$

Consequently, the gross solar radiation potential W_B per 0.24 m² of the island's area is:

$$W_B = E \cdot S_{сэс} = 404.5 \cdot 0.24 = 97.08 \text{ kW·h/year},$$

where $S_{сэс}$ is the area of the solar power plant, m^2.

The technical potential of total annual solar radiation is defined as the amount of energy that can be converted into usable energy in compliance with environmental standards over the course of a year. In this study, it is calculated as the sum of thermal energy obtained from solar radiation conversion for water heating using a solar collector [1), 2)] with an area of 1.58 m^2 and electrical energy generated by a photovoltaic module with an area of 0.24 m^2 [3–5, 10, 14, 15].

Technical potential for converting solar energy to heat water using a water heater. The calculations utilized the parameters of the SCH-12 vacuum solar collector, which is thermally insulated with polyurethane foam and comprises 12 vacuum tubes with 14 mm diameter copper heat pipes. The collector has an area of 1.58 m², a weight of 41 kg, and dimensions of 2000 × 950 × 1420 × 1400 mm. It is designed for year-round operation and can withstand temperatures as low as −40 °C.

The calculations also used thermal parameters, including water temperature T (60 °C); absorption intensity $F(\tau\alpha)$ (0.9); heat transfer coefficient FU_L = 0.005 kW/(m^2·°C); average monthly ambient temperature T_{oi}, °C; latitude φ; declination angle δ; sunshine varying during the i-th month t_{Ci}, h/month; the number of clear and partly cloudy hours, along with operational time t_{Pi}, h/month [2), 3)] [3, 4, 12–15].

The technical potential of the solar collector W_{TTi} per unit of collector area S_T during the operational period from 7:00 to 17:00 is calculated as:

$$\frac{W_{\text{тті}}}{S_{\text{т}}} = E_i F[(\tau\alpha) - U_{\text{L}}\left(T - T_{\text{o}i}\right)\cos(-\delta)\frac{t_{\text{P}i}}{E_i}] = \sum_i W_{\text{тті}} = 102.65 \text{ kW·h/(m}^2\text{·year)},$$

where $S_{\text{т}}$ is the area allocated for the heat collector, m^2; $F(\tau\alpha)$ is the absorption intensity, $F(\tau\alpha) = 0.9$; FU_{L} is the heat transfer coefficient, 0.005; $T_{\text{o}i}$ is the average monthly temperature, °C; δ is the declination angle, degrees; $t_{\text{P}i}$ is the operational duration of solar collector, h/month.

The total of solar thermal energy potential $W_{\text{тт}}$ for a 10-hour daily interval is calculated by summing the monthly contributions:

$$W_{\text{тт}} = 102.65 \cdot S_{\text{т}},$$

where $S_{\text{т}}$ is the area allocated for solar thermal installations, m^2.

The technical potential of electricity generated from the conversion of solar radiation. The calculations are based on the technical specifications of the SIM-30-12-5BB silicon monocrystalline photovoltaic module, with the following characteristics: area 0.24 m^2; length 541 mm; width 439 mm; height 25 mm; power – 30 W; cell size 156 × 55.72 mm; operating voltage 18.67 V; and operating temperature range from −40 to 85 °C.

The following photovoltaic module parameters were incorporated into the calculation formulas: temperature gradient $\chi = 0.004$ K^{-1}; temperature $T_1 = 298$ K; efficiency $\eta_1 = 0.15$; heat transfer coefficient $\lambda = 40$ W/m^2·K; and absorption coefficient $\alpha = 0.97$ [3)] [3–5, 14, 15].

The average monthly operating temperature T_i of the photovoltaic module is calculated using the formula:

$$T_i = \frac{\frac{E_i}{t_{\text{P}i}}\left[\alpha - \eta_1\left(1 + \chi T_1\right)\right] + \langle\lambda\rangle T_{\text{o}i}}{\langle\lambda\rangle - \frac{E_i}{t_{Pi}}\eta_1\chi},$$

where χ – temperature gradient, 0.004 K^{-1}; $T_{1,i}$ – temperature, 298 K; η_1 – efficiency, 0.15; λ – heat transfer coefficient, 40 W/m^2·K; α – absorption coefficient, 0.97.

The technical potential $W_{\text{тф}i}$ for each month at the optimal tilt angle of the photovoltaic module (39°) is calculated based on the area of one photovoltaic module $S_{\text{ф}}$, equal to 0.24 m^2, using the formula:

$$\frac{W_{\text{тф}i}}{S_{\text{ф}}} = E_i\eta_1\left[1 - \chi\left(T_i - T_1\right)\right] = \sum_i W_{\text{тф}i} = 42.7 \cdot S_{\text{ф}},$$

where $S_{\text{ф}}$ is the area of one photovoltaic module, m^2; T_i is the average monthly operating temperature of the photovoltaic module, K.

The total annual technical potential, $W_{\text{тф}}$, W·h/year, is calculated by summing the values across the entire area of the photovoltaic module:

$$W_{\text{тф}} = 42.7 \cdot S_{\text{ф}}.$$

The economic potential of solar energy represents the possible volume of solar radiation converted into thermal and electrical energy on Ogurchinsky Island over the course of a year, considering economic viability. The results are economically

justified for this region based on current prices for energy derived from conventional sources and are expressed in tons of fuel equivalent, in compliance with environmental standards.

To calculate the economic potential of solar energy for water heating, the following parameters were used: hot water temperature $T_H = 60$ °C and cold water temperature $T_C = 15$ °C; technical characteristics of solar collectors: $F(\tau\alpha) = 0.9$; $F \cdot U_L = 0.005$ kW/(m^2·°C); water consumption rate m = 100 kg/(person·day); collector cost $C = 400$ \$/m^2; $T_{SL} = 15$ years; water heat capacity $c_p = 4.17$ kJ/(kg·°C) [3–5, 18–20].

The economic potential of solar thermal collectors installed at an optimal angle to the horizon is calculated using the formula:

$$W_{ЭТi} = V_{Ti} \cdot S_{ЭТ},$$

where $W_{ЭТi}$ is the monthly economic potential (i = 1, 2, …, 12) (summed over all months of the year); $S_{ЭТ}$ is the economically viable area of installed thermal collectors.

The thermal energy generated from solar radiation, V_{Ti}, is calculated as:

$$V_{Ti} = E_{Hi} \cdot F[(\tau\alpha) - U_L\left(T - T_{oi}\right)\frac{t_{Ci}}{E_{Hi}}] = \sum_i V_{Ti} = 8.5 \text{ kW·h/(m}^2\text{·month)},$$

where E_{Hi} is the monthly solar radiation, kW·h/(m^2·year).

The specific volume of solar energy generated determines the economic viability and payback period of solar installations.

The calculated volumetric heat output of a solar water heater, heating water to a temperature of up to 44 °C (m^3/month), is presented in Fig. 5.

The economic potential of solar radiation in the region increases with the amount of energy generated per unit of surface area of the solar collector, considering three key factors: the critical value of specific heat energy output, the economic parameters of energy consumption, and the cost parameters of industrial energy production, accounting for fuel costs and regional environmental factors.

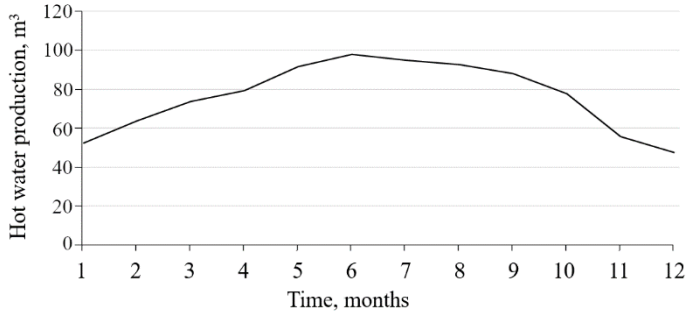

Fig. 5. Volumetric heating output of a solar water heater when heating 1 m^3 water to a temperature of 44°C by months

The calculation of the economic resource potential for obtaining electricity from the conversion of solar radiation is similarly determined by the expression:

$$W_{ЭФi} = V_{фi} \cdot S_{ЭФ},$$

$$V = E_{фi}\eta_1\left[1 - \chi\left(T_i - T_1\right)\right] = \sum_i V = 3.6 \text{ kW·h/(m}^2\text{·month)},$$

where $V_{фi}$ is the amount of energy generated per unit area of the solar battery in the *i*-th month, kW·h/(m²·month); $S_{ЭФ}$ is the economically viable area of installed solar photovoltaic modules, m²; $E_{фi}$ is the average annual solar energy yield per unit area of the solar battery in the *i*-th month of the year, kW·h/(m²·month) [2), 3)] [3, 13–15].

Expected economic indicators of the solar power plant (SPP): the expected electricity output of a single SPP, comprising a single photovoltaic module with an area of 5.2 m² and a capacity of 100 W, oriented south at an optimal tilt angle of 39°, is 5.01 kW·h/day or 60.4 kW·h/year. The total electricity generation for the SPP is 1829.17 kW·h/year. The estimated cost of the SPP is $6,336.96, with a profitability of 6.76%. At an electricity cost of $0.055 per kW·h, the payback period for the photovoltaic SPP is 2.8 years.

The ecological potential of solar radiation on the island contributes to the technical resource potential, which is converted into thermal, electrical, and other energy forms using technological equipment to reduce anthropogenic environmental impacts from fossil fuel use [3–5, 17].

The energy, economic, and environmental potential of a single photovoltaic module on the island yields 42.77 kW·h/year, equivalent to an average of 3.6 kW·h/month of electricity, resulting in a reduction of 17.1 kg of equivalent standard fuel consumption annually. The environmental benefits include reductions in harmful emissions as follows: SO_2 – 0.3555 kg/year; NO_x – 0.1915 kg/year; CO – 0.0248 kg/year; CH_4 – 0.0522 kg/year; CO_2 – 27.35 kg/year; and solid particles – 0.0373 kg/year.

Solar radiation is used to convert energy to heat water to 44 °C. The energy, economic, and environmental potential of this process yields 102.65 kW·h/year, equivalent to an average electricity saving of 8.5 kW·h/month, with a corresponding reduction in fuel consumption of 41.1 kg of fuel oil annually. The environmental benefits include reductions in harmful emissions as follows: SO_2 – 0.853427 kg/year, NO_x – 0.459538 kg/year, CO – 0.05968 kg/year, CH_4 – 0.125328 kg/year; CO_2 – 65.64826 kg/year, and solid particles – 0.08952 kg/year.

Wind energy potential

The HY-400L low-power wind turbine is designed for power generation. Its technical specifications are as follows: rated power of 400 W; maximum power of 500 W; rated voltage of 24 V; start-up wind speed of 2 m/s; cut-in wind speed of 2.5 m/s; rated wind speed of 12 m/s; operating temperature range of −40 to 60 °C; maximum wind speed of 50 m/s; number of blades – 5; rotor diameter – 1.55 m; swept area – 1.89 m; overall dimensions – 118 × 47 × 27 cm.

A single 5 m high wind turbine on the island can generate 19.45 kW·h/m²/year of electricity, equivalent to an average of 1.62 kW·h/m²/month, with a corresponding

reduction in fuel consumption of 7.78 kg. The environmental benefits include reductions in harmful emissions as follows: SO_2 – 0.161706 kg/year; NO_x – 0.087073 kg/year; CO – 0.011308 kg/year; CH_4 – 0.023747 kg/year; CO_2 – 12.43895 kg/year; and solid particles – 0.016962 kg/year [3)] [3, 14–16].

According to the results of the calculations, the use of solar radiation to conserve fuel can reduce the costs of various products and their energy-intensive production processes, enhance the ecological conditions, and improve social and living standards in the Caspian region of Turkmenistan.

Statistical analysis of conditions

Regression equations can be applied when developing a FS and calculating the power requirements of heating devices, as well as determining heat losses under various climatic conditions for the construction of power stations or structures [3–5, 10–12].

When preparing design and cost estimation documentation, including FS, for the construction of solar and wind energy facilities, hydrometeorological data from the Khazar Nature Reserve, along with quantitative estimates of their distribution, are essential to support the work of engineers, cost estimators, and designers.

Hydrometeorological data were processed using mathematical statistics methods. The resulting data were approximated as a simplified scatter plot, represented by a linear regression equation in the form of a correlation ellipse. In a rectangular coordinate system, the linear regression equation is expressed as $y = a + bx$, where a represents the intercept and b denotes the regression coefficient. To analyze the impact of incident solar radiation on the energy output of a photovoltaic module, a regression equation was developed, incorporating the angle of inclination: 0° (horizontal position); 24° (summer period); 54° (winter period); 39° (optimal for the region). Additional factors considered include average, maximum, and minimum temperature regimes, sunshine duration, wind speed, cloudy day duration, precipitation, and soil temperature to forecast energy potential and calculate the coefficient of determination, which quantifies the strength and closeness of the relationship between variables. The resulting equations are presented below.

An important stage in regression analysis is establishing the mathematical relationship between the dependent variable y and the independent variable x. Consequently, the dependent variable y – representing the angle of inclination of the photovoltaic module – was determined on a horizontal surface as follows: 24° for the summer period, 54° for the winter period, and an optimal annual angle of 39°. The independent variable x corresponds to the intensity of solar radiation incident on the surface.

The following regression equations for the tilt angles of photovoltaic modules were obtained:

$$\text{for } 24°: \quad y = 0.0004x + 0.1489; \ R = 0.0012; \tag{1}$$

$$39°: \quad y = 0.0008x + 0.1445; \ R = 0.0079; \tag{2}$$

$$54°: \quad y = 0.0005x + 0.1385; \ R = 0.0054; \tag{3}$$

$$0°: \quad \text{in a horizontal position}$$

$$y = -0.0007x + 0.1435; \ R = 0.0017. \tag{4}$$

Electricity generation by a solar installation with one photovoltaic module:

$$y = -0.0098x + 3.628;\ R = 0.0018. \quad (5)$$

Regression equation for heat energy production by a single solar collector when heating water:

$$y = -0.0239x + 8.7094;\ R = 0.0018. \quad (6)$$

Hot water output, m^3:

$$y = -0.1885x + 77.435;\ R = 0.0015. \quad (7)$$

Electricity generation by a solar power plant with 10 photovoltaic modules with a capacity of 10 kW:

$$y = 0.0164x + 4.9286;\ R = 0.0026. \quad (8)$$

Regression equation and average wind speed dispersion coefficient:

$$y = -0.0038x + 3.4333;\ R = 0.0004. \quad (9)$$

Electricity generation by a single wind turbine:

$$y = 0.0034x + 1.5988;\ R = 0.0074. \quad (10)$$

Using data from scientific climate reference materials and observations from the State Meteorological Service, regression equations were derived as follows:

sunshine hours:

$$y = 0.0573x + 7.46, \quad (11)$$

duration of sunshine:

$$y = 3.3776x + 200.88, \quad (12)$$

average wind speed:

$$y = -0.007x + 5.7788, \quad (13)$$

number of cloudy days:

$$y = -0.1262x + 3.4621, \quad (14)$$

precipitation amount:

$$y = -0.4336x + 11.485, \quad (15)$$

monthly soil temperature:

$$y = 0.6538x + 12.0. \quad (16)$$

To assess the relationship between two variables, x and y, for the island over the course of a year, the following correlation coefficients R were calculated for the conversion of solar energy into electrical energy: 0.0018 for a single photovoltaic module, 0.0018 for a thermal collector, and 0.0015 for hot water production volume. These values indicate a very weak correlation [3–5, 17, 20].

Using the regression equations (1)–(16), it is possible to forecast the range of annual variations for the following parameters: electricity generation by solar and wind power plants, average wind speed, number of cloudy days, precipitation amount, average air temperature, sunshine duration, and monthly soil temperature.

Productivity of wind and solar energy converters in terms of heat and electrical energy production and reduction of harmful emissions into the environment per year on the island

Energy converter	Technical potential, kW·h per year	Fuel consumption equivalent, kg fuel equivalent per year	Substances emission, kg per year					
			SO_2	NO_x	CO	CH_4	CO_2	Solid particles
Solar power plant	42.77	17.110	0.3556	0.1915	0.0248	0.0522	27.3529	0.0373
Wind power plant	19.45	7.780	0.1617	0.0870	0.0113	0.0237	12.4395	0.0169
Water heater	102.65	41.060	0.8534	0.4595	0.0596	0.1253	65.6483	0.0895
Total	164.87	65.948	1.3707	0.7381	0.0958	0.2012	105.440	0.1437

Discussion of results

Based on research utilizing reference data and systematic theoretical and practical calculations, estimates were derived for the solar energy resource potential per square meter on Ogurchinsky Island over the course of a year, encompassing gross, technical, and economic potential converted into thermal and electrical energy. The average monthly direct solar radiation at an optimal inclination angle of 39° is 1900.5 kW·h/(m²·month), while the average annual amount of solar radiation incident on a horizontal surface over a 10-hour daily interval is 1685.4 kW·h/m².

The energy efficiency, economic, and environmental potential of a Sila solar power plant (SPP) with a capacity of 30 W and an area of 0.24 m^2, a SCH-12 water heater (WH) with a heat output reaching 44 °C and an area of 1.58 m^2, and a 400 W wind power plant (WPP) are presented in the table. The table indicates that the technical potential of ten photovoltaic modules, each with an area of 0.24 m^2 and a capacity of 60 W, totals 42.77 kW·h/year. The ecological resource potential of solar energy for conversion into electricity corresponds to a fuel consumption reduction of 17.1 kg

of fuel equivalent per year. Additionally, the technical potential of a single SCH-12 water heater with an absorption area of 1.58 m², capable of heating water to 44 °C, is 102.65 kW·h/year.

The calculated expected values for the total energy productivity of WPP and SPP, when converting solar energy into heat and electricity, amount to 164.87 kW·h/(m^2·year), with associated reductions in harmful environmental emissions per year as follows: fuel savings – 65.948 L/year, emission reductions of SO_2 – 1.3707 kg/year, NO_x – 0.7381 kg/year, CO – 0.09585 kg/year, CH_4 – 0.20129 kg/year, CO_2 – 105.4401 kg/year, and solid particles – 0.14378 kg/year [3] [9, 15, 16].

Fig. 6 illustrates the overall dynamics of the average daily energy productivity of WPP and SPP for electricity generation and thermal energy production, presented by month of the year.

The installation of 10 photovoltaic modules, each with an area of 5.2 m², on the island for laboratory research would yield the following results: an annual electricity generation of 1,829.2 kW·h, an average monthly generation of 60.4 kW·h, and an average daily generation of 5.0 kW·h/day. Monthly fuel savings would amount to 24.16 kg, with corresponding reductions in harmful emissions as follows: SO_2 – 0.502163 kg/month, NO_x – 0.270395 kg/month, CO – 0.035116 kg/month, CH_4 – 0.073744 kg/month, CO_2 – 38.62791 kg/month, and solid particles – 0.052674 kg/month.

The energy efficiency of the VSF-1 water heating system, when heating water to 44 °C, yields an annual output of 914.52 m^3/year, with an average monthly output of 76.21 m^3.

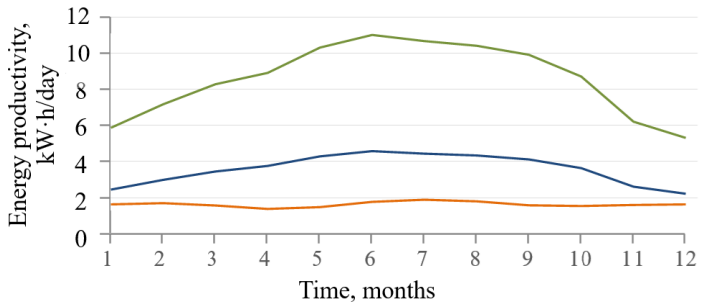

Fig. 6. Dynamics of average daily energy productivity of renewable energy sources, solar power plants, electricity and warm water production on Ogurchinsky Island by months: orange line – wind energy production, blue line – solar energy production, green line – conversion of solar energy to heat. The numerals stand for months

To optimize the use of solar energy stations and installations throughout the year, it is essential to determine the optimal inclination angle of the solar converter based on the geographical location of the site. The calculated optimal inclination angles for a solar receiver with an east-west orientation on Ogurchinsky Island, by month, are as follows: 54° (−0.82930 rad) for winter; 24° (0.42418 rad) for summer, and an annual optimal angle of 39° (0.26664 rad).

When designing a SPP with automated solar radiation tracking based on the inclination angle for Ogurchinsky Island, the graphs in Fig. 5 [2–4, 7] can be used.

The expected environmental reduction potential for harmful emissions when using solar and wind energy technologies throughout the year on Ogurchinsky Island has been calculated as follows:

– SPP: with an annual electricity generation of 164.87 kW·h/(m²·year), fuel savings amount to 65.948 kg of fuel equivalent/year, with emission reductions of SO_2 – 1.3707 kg/year, NO_x – 0.7381 kg/year, CO – 0.09585 kg/year, CH_4 – 0.20129 kg/year, CO_2 – 105.4401 kg/year, and solid particles – 0.14378 kg/year [3, 4, 9, 16].

– WH: with an annual output of 102.65 kW·h/(m^2·year), fuel savings amount to 41.06 kg of fuel equivalent per year, with emission reductions of SO_2 – 0.8534 kg/year, NO_x – 0.45953 kg/year, CO – 0.0596 kg/year, CH_4 – 0.1253 kg/year, CO_2 – 65.64826 kg/year, and solid particles – 0.08952 kg/year.

– WPP: with an annual electricity generation of 19.45 kW·h/(m^2·year), fuel savings amount to 7.78 kg of fuel equivalent per year, with emission reductions of SO_2 – 0.161706 kg/year, NO_x – 0.087073 kg/year, CO – 0.011308 kg/year, CH_4 – 0.023747 kg/year, CO_2 – 12.43895 kg/year, and solid particles – 0.016962 kg/year.

The results, obtained using mathematical statistics methods for regression equations (1)–(16), are essential for implementing solar-wind energy complexes and power plants in the southern sector of the Caspian Sea.

Conclusion

The energy resources of solar radiation, along with their technical, economic, and environmental potential, have been evaluated based on the hydrometeorological and natural climatic conditions of the Khazar Nature Reserve in the Caspian Sea. These conditions include sunshine duration, the inclination angle of the optimally oriented receiver surface, the hour angle of solar declination, direct and diffuse radiation, albedo, and average monthly and annual outdoor air temperatures. The energy parameters and operating time of a SPP with an area of 10.4 m^2, oriented at an average annual optimal inclination angle of 39°, were analyzed. Calculations indicate an average annual electricity generation of 10.03 kW·h/day, a total annual electricity generation of 3658.34 kW·h, organic fuel savings of 1463.336 kg per year, and reductions in harmful emissions as follows: SO_2 – 30.41 kg/year; NO_x – 16.38 kg/year; CO – 2.13 kg/year; CH_4 – 4.47 kg/year; CO_2 – 2339.64 kg/year; solid substances – 3.19 kg/year.

The cost of an SPP with an energy output of 10 kW·h/day is $12,673.9. The average daily energy consumption of the laboratory premises, when operating essential electrical appliances, is 10.03 kW·h/day, with a cost of $0.055 per kW·h, excluding transportation costs via the Caspian Sea. Preliminary calculations indicate that the payback period for the photovoltaic SPP is 5 years and 6 months, with a profitability of 6.76% and a net profit of $2,234.01 over 10 years.

The findings confirm that utilizing solar and wind energy resources is a prioritized, promising, environmentally sustainable, and economically viable solution for electricity supply, energy security, and other applications along the Caspian Sea.

The results obtained from regression equations (1)–(16) will be valuable for preparing design and cost estimation documentation, as well as FS, to support the implementation of solar and wind energy technologies in the region.

The implementation of these technologies will address various energy supply challenges at the Khazar Nature Reserve on Ogurchinsky Island. The adoption of modern electronic technologies will enhance the reliability of data obtained from flora and fauna observations, support the conservation of biological resources and biodiversity, improve social and living conditions for workers and residents, and reduce the anthropogenic impact on the ecosystem. These efforts will contribute to Turkmenistan's National and State Energy, Socio-Economic and Environmental Sustainable Development Programs, as well as the Paris Agreement on Climate Change, the outcomes of the 28th session of the Conference of the Parties to the UN Framework Convention on Climate Change (COP28), and other national and international initiatives.

REFERENCES

1. Berdymuhamedov, G.M., 2018. [*Turkmenistan on the Way to Achieving the Sustainable Development Goals*]. Ashgabat: Turkmen State Publishing Service, 465 p.
2. Penjiyev, A.M., Astanov, N.G. and Penjiyev, M.A., 2011. Use of Solar Power Stations in Reserve Zones of Turkmenistan to Improve Arid Ecosystems. *Alternativnaya Energetika i Ekologiya (ISJAEE)*, (12), pp. 38–45 (in Russian).
3. Penjiyev, A.M., 2023. [*Eco-Energy Resources of Renewable Energy Sources*]. Moscow: RUSCIENCE, 400 p. (in Russian).
4. Strebkov, D.S., Penjiyev, A.M. and Mamedsachatov, B.D., 2012. *Development of Solar Energy in Turkmenistan*. Moscow: GNU VIESKh, 498 p. [in Russian].
5. Penjiyev, A.M., 2022. Wave Energy Resources of the Caspian Sea on the Coast of Turkmenistan. *Applied Solar Energy*, 58(2), pp. 306–310. https://doi.org/10.3103/s0003701x22020141
6. Kostianoy, A.G., Lebedev, S.A., Zonn, I.S., Lavrova, O.Yu. and Solovyov, D.M., 2011. *Satellite Monitoring of Turkmenistan*. Moscow: Signal, 16 p. (in Russian).
7. Lebedev, S.A., 2012. Mean Sea Surface Model of the Caspian Sea. *Sovremennye Problemy Distantsionnogo Zondirovaniya Zemli iz Kosmosa*, (3), pp. 224–234 (in Russian).
8. Nefedova, L.V. and Teterina, N.V., 2010. [Assessment of the Environmental Impact When Organising Energy Supply for Nature Reserves Using Renewable Energy Sources]. *Ecological Studies. Hazards. Soltions*, 16, pp. 48–52 (in Russian).
9. Penjiyev, A.M., 2012. [*Climate Change and Possibilities to Reduce the Anthropogenic Load*]. LAP LAMBERT Academic Publishing, 164 p. (in Russian).

10. Penjiyev, A.M. and Astanov, N.G., 2014. Theoretical and Methodical Calculations of Potential of Solar Power Resources on Southeast Karakum. *Alternativnaya Energetika i Ekologiya (ISJAEE)*, (7), pp. 65–86 (in Russian).
11. Penjiyev, A.M., 2017. Economic Examination of Efficiency of Innovative Technology. *Research Result: Economic Research*, (4), pp. 3–14. https://doi.org/10.18413/2409-1634-2017-3-1-3-15 (in Russian).
12. Penjiyev, A.M., 2017. [*GIS Basics in the Development of Renewable Energy*]. LAP LAMBERT Academic Publishing, 308 p. (in Russian).
13. Strebkov, D.S., 2019. [*Basics of Solar Energetics*]. Moscow: Sam Poligrafist, 326 p. (in Russian).
14. Bezrukikh, P.P., Arbuziv, Yu.D., Borisov, G.A., Vissarionov, V.I., Evdokimov, V.M., Malinin, N.K., Ogorodov, N.V., Puzakov, V.N., Sidorenko, G.I. and Shpak, A.A., 2002. [*Resources and Efficiency of Renewable Energy Use in Russia*]. Saint Petersburg: Nauka, 314 p. (in Russian).
15. Arbuzov, Yu.D. and Evdokimov, V.M., 2012. [*Basics of Photoelectricity*]. Moscow: GNU VIESKh, 292 p. (in Russian).
16. Kharitonov, V.P., 2010. [*Basics of Wind Energetics*]. Moscow: GNU VIESKh, 340 p. (in Russian).
17. Penjiyev, A.M., 2019. Use of Wind-Energetic Installations for Providing Water to Karakum. *Problems of Desert Development*, (3–4), pp. 85–87 (in Russian).
18. Vasiliev, Yu.S. and Khrisanov, N.I., 1991. [*Ecology of Use of Renewable Energy Sources*]. Leningrad: Izd-vo LGU, 343 p. (in Russian).
19. Strebkov, D.S. and Penjiyev, A.M., 2019. Solar Power Plants with Parabolic Trough Concentrators in the Desert Area of Karakum. *Applied Solar Energy*, 55(3), pp. 195–206. https://doi.org/10.3103/S0003701X19030083
20. Penjiyev, A.M., 2018. Thermal Regime in Combined Cultivation Constructions. *Applied Solar Energy*, 54(3), pp. 196–204. https://doi.org/10.3103/S0003701X18030118

Submitted 16.09.2024; accepted after review 27.01.2025;
revised 24.06.2025; publlished 30.09.2025

About the authors:

Ahmet M. Penjiyev, Associate Professor, Turkmen State Institute of Architecture and Civil Engineering (1 B. Annanova Str., Ashgabat, 744001, Turkmenistan), DSc (Tech.), DSc (Agric.), *ampenjiyev@gmail.com*

Batyr M. Mamedov, Rector, Turkmen State Institute of Architecture and Civil Engineering (1 B. Annanova Str., Ashgabat, 744001, Turkmenistan), DSc (Tech.), DSc (Agric.), *tdbgi@online.tm*

Contribution of the authors:

Ahmet M. Penjiyev – basic concept statement, scientific supervision, statement of study goals and objectives, calculations, text preparation, revision of literary analysis, text editing

Batyr M. Mamedov – analysis and discussion of the study results, formulation and editing of conclusions

All the authors have read and approved the final manuscript.

Original paper

Wave Buoy Logger for Coastal Studies

Yu. Yu. Yurovsky *, O. B. Kudinov

Marine Hydrophysical Institute of RAS, Sevastopol, Russia
** e-mail: y.yurovsky@mhi-ras.ru*

Abstract

The paper presents prototype wave buoy loggers designed to collect raw data from a built-in inertial motion unit without transmitting the data to the user. These buoys require maintenance but have a significantly simpler design and much lower cost compared to unattended analogs, making them particularly useful for various coastal studies. The study aims to demonstrate that measuring wave parameters in field conditions with acceptable accuracy is achievable without loss of data quality. The buoys were tested in a field experiment at the Black Sea Hydrophysical Sub-Satellite Polygon of Marine Hydrophysical Institute, Russian Academy of Sciences. Reference measurements were obtained using wire wave gauges installed on the Stationary Oceanographic Platform (44.393047°N, 33.984596°E). Three identical buoys were deployed near the platform using different mooring configurations: a heavy anchor with an elastic insert (rubber cord), a heavy anchor without an elastic insert, and a buoy suspended directly from the platform without an anchor. Continuous measurements were conducted over seven days, during which significant wave height varied from 0.2 to 1 m, and wind speeds ranged from 0 to 15 m/s, coming from east-erly, westerly, and northerly directions. Under these conditions, the root-mean-square error in estimating significant wave height was no more than 5–6 cm (both with and without the rubber cord), with the linear regression coefficient deviating from 1 by less than 5%. The root-mean-square errors for the spectral peak wave period and direction were 0.37–0.62 s and 50–65°, respectively. These errors are comparable to the resolution of the applied methods and the natural statistical variability of wave parameter estimates.

Keywords: buoy, wave gauge, inertial measurements, wind waves, wave parameters, oceanographic platform, field experiment

Acknowledgements: The work was funded by the Russian Scientific Foundation grant 24-27-00153 “Measuring waves with small buoys: methods, validation, prospects of miniaturization”.

For citation: Yurovsky, Yu.Yu. and Kudinov, O.B., 2025. Wave Buoy-Logger for Coastal Studies. *Ecological Safety of Coastal and Shelf Zones of Sea*, (3), pp. 115–127.

© Yurovsky Yu. Yu., Kudinov O. B., 2025

This work is licensed under a Creative Commons Attribution-Non Commercial 4.0 International (CC BY-NC 4.0) License

Волноизмерительный буй-логгер для прибрежных исследований

Ю. Ю. Юровский *, О. Б. Кудинов

Морской гидрофизический институт РАН, Севастополь, Россия
** e-mail: y.yurovsky@mhi-ras.ru*

Аннотация
Представлены прототипы волноизмерительных буев-логгеров, предназначенных для сбора исходных данных со встроенных в них инерциальных датчиков, без передачи их на берег. Буи такого типа нуждаются в обслуживании, но имеют существенно более простую конструкцию и низкую стоимость по сравнению с необслуживаемыми аналогами, что может быть востребовано в различных прибрежных исследованиях. Цель работы – продемонстрировать в натурных условиях, что предлагаемый тип буев может эффективно использоваться для измерения характеристик волнения без потери качества данных. Испытания буев проведены в натурном эксперименте на Черноморском гидрофизическом подспутниковом полигоне Морского гидрофизического института РАН. В качестве референтной информации о волнах использованы данные измерений струнными волнографами, установленными на стационарной океанографической платформе (44.393047° с. ш., 33.984596° в. д.). Три одинаковых буя были установлены вблизи платформы с использованием разных вариантов удерживающего устройства: на массивном якоре с эластичной вставкой (амортизатором) и без нее, а также без якоря на подвесе с платформы. Непрерывные измерения велись в течение 7 сут, в течение которых высота значительных волн менялась от 0.2 до 1 м, скорость ветра от 0 до 15 м/с при его восточном, западном, северном направлениях. В этих условиях среднеквадратичная ошибка оценки высоты значительных волн составила не более 5–6 см (с амортизатором и без него) при отклонении коэффициента линейной регрессии от единицы не более чем на 5 %. Среднеквадратичные ошибки периода и направления волн спектрального пика составили 0.37–0.62 с и 50–65° соответственно при измерении буем с амортизатором и без него. Такие ошибки измерений сопоставимы с разрешающей способностью используемых методов и естественным статистическим разбросом средних оценок параметров волн.

Ключевые слова: буй, волнограф, инерциальные измерения, ветровые волны, параметры волн, океанографическая платформа, натурный эксперимент

Благодарности: работа выполнена при финансовой поддержке гранта Российского научного фонда № 24-27-00153 «Волнографические измерения с помощью малогабаритных буев: методология, валидация, перспективы миниатюризации».

Для цитирования: *Юровский Ю. Ю., Кудинов О. Б.* Волноизмерительный буй-логгер для прибрежных исследований // Экологическая безопасность прибрежной и шельфовой зон моря. 2025. № 3. С. 115–127. EDN UVGARW.

Introduction

In marine research, episodic short-term observations of surface waves are often required for targeted experiments. This is particularly true in coastal research, such as when studying wave nonlinearity in the coastal zone [1, 2], wave interaction with currents [3], the formation of bottom sediments [4–6], beach and coastline dynamics [7, 8], and other phenomena [9–12]. In such conditions, traditional wave buoys,

designed for continuous monitoring of waves at any point in the ocean, are not always feasible due to their relatively high cost. For short-term coastal studies, many of their features are redundant, including autonomous power supplies, large memory capacity, multi-channel communication systems, and massive high-strength hulls. Additionally, specialized experiments often require up to several dozen such buoys to enable simultaneous measurements across a section or grid.

In this context, it is practical to develop a simple wave measuring device that records only the measurements from a sensor sensitive to wave motion, such as a buoy logger. The increasing use of small, low-cost microelectromechanical inertial motion units (IMUs) in wave-measuring devices also supports this solution [11, 13–16].

The paper presents the results of field trials of a prototype device developed at Marine Hydrophysical Institute (MHI). The experiment involved three identical buoy samples configured differently. It is known that the retaining device can influence wave measurements by buoy sensors [1), 2)] [2]. Thus, to extend the service life of the system and mitigate jolts when the hull interacts with steep waves, an elastic element, typically a section of rubber cord several meters long with maximum elasticity, is included in the anchoring device [17]. To demonstrate the effect of the retaining line clearly, three mooring options were tested: a standard anchor cable without an elastic insert, a cable with a highly elastic insert (within limits ensuring retention during the experiment), and a methodological option – a bifilar suspension without an anchor from the oceanographic platform.

The aim of this study is to demonstrate in real-life conditions that buoy loggers built using readily available components can perform short-term measurements of wave characteristics with acceptable quality.

Materials and methods

Equipment

The buoy is based on the MPU9250 inertial motion unit (IMU), which integrates a microelectromechanical accelerometer, gyroscope, and magnetometer. As previously demonstrated [14, 18], such IMUs, despite their relatively low cost, are suitable for measuring sea wave characteristics. The buoy records initial measurements of three-axis acceleration, angular velocities, magnetic field, and IMU temperature at a sampling frequency of 25 Hz. These data are stored on a memory card with a capacity of up to 32 GB using an Atmega328p microcontroller synchronized with universal time via a DS3231-based real-time clock.

---

1) Earle, M.D., 1996. *Nondirectional and Directional Wave Data Analysis Procedures*. NDBC technical document 96-01. Stennis Space Center, 43 p.

2) Gryazin, D.G., 2000. [*Calculation and Design of Buoys for Measuring Sea Waves*]. Saint Petersburg: SpbGITMO (TU), 134 p. (in Russian).

The circuit is housed in a sealed plastic cylindrical hull, mounted on a printed circuit board rigidly fixed in the hull's axial plane. The IMU is positioned within 1.5 mm of the hull's axis (the board's thickness) and is vertically offset to align its center as closely as possible with the point of the hull's resonant oscillations. The hull is equipped with a lenticular float, a 40 cm diameter disc with chamfers, made of 100 mm thick expanded polystyrene. A stainless-steel eyelet is attached to the hull's base, connecting to a ballast (for adjusting the hull's draft) and a retaining cable via a swivel.

Power is supplied by six 18650 lithium-ion batteries with a total capacity of approximately 48 W·h, positioned at the base of the hull on both sides of the board.

For additional verification of measurement quality, a second IMU (a BNO055) was mounted on the back of the board. The axes of both motion units were aligned as closely as possible (within 180° rotation accuracy), and the distance between their centers was no more than 4 mm.

Experiment

The experiment was conducted in October 2024 at the Black Sea Hydrophysical Sub-Satellite Polygon near the Stationary Oceanographic Platform (Fig. 1). Bathymetry data were sourced from https://www.ncei.noaa.gov/products/etopo-global-relief-model.

Buoy *1* was deployed approximately 200 m from the platform at a location with a sea depth of about 27 m. A massive stone weight with a dry mass of approximately 70 kg served as an anchor. The buoy was connected to the weight using an eight-strand nylon cord with a core diameter of 8 mm.

Buoy *2* was deployed at the same depth, but approximately 50 m closer to the platform. Unlike the first buoy, it was connected to the anchor cable via a 7 m long, 6 mm diameter nylon-braided rubber cord (hereinafter referred to as the rubber cord). The parameters of this rubber cord were chosen to prevent breakage during the experiment while ensuring maximum elasticity of the connection.

Buoy *3* was positioned between two platform supports on a bifilar suspension made of nylon cord, approximately 8 m from the pile foundation. This setup was designed to evaluate the feasibility of conducting methodological work from the platform without the need for more costly anchor-based deployments.

Buoys *1* and *2* were deployed for approximately 7 days, while Buoy *3* was deployed only on the final day of measurements.

Parallel measurements of wave parameters were conducted from the platform using wire-resistive wave gauges, which recorded sea surface levels with an accuracy of ±1 cm at frequencies up to 5 Hz [19, 20]. These measurement data serve as reference data in this study. Additionally, auxiliary meteorological observations were conducted using standard hydrometeorological instruments. Specifically, wind speed and direction at a height of 21 m were measured using a cup anemometer and wind vane.

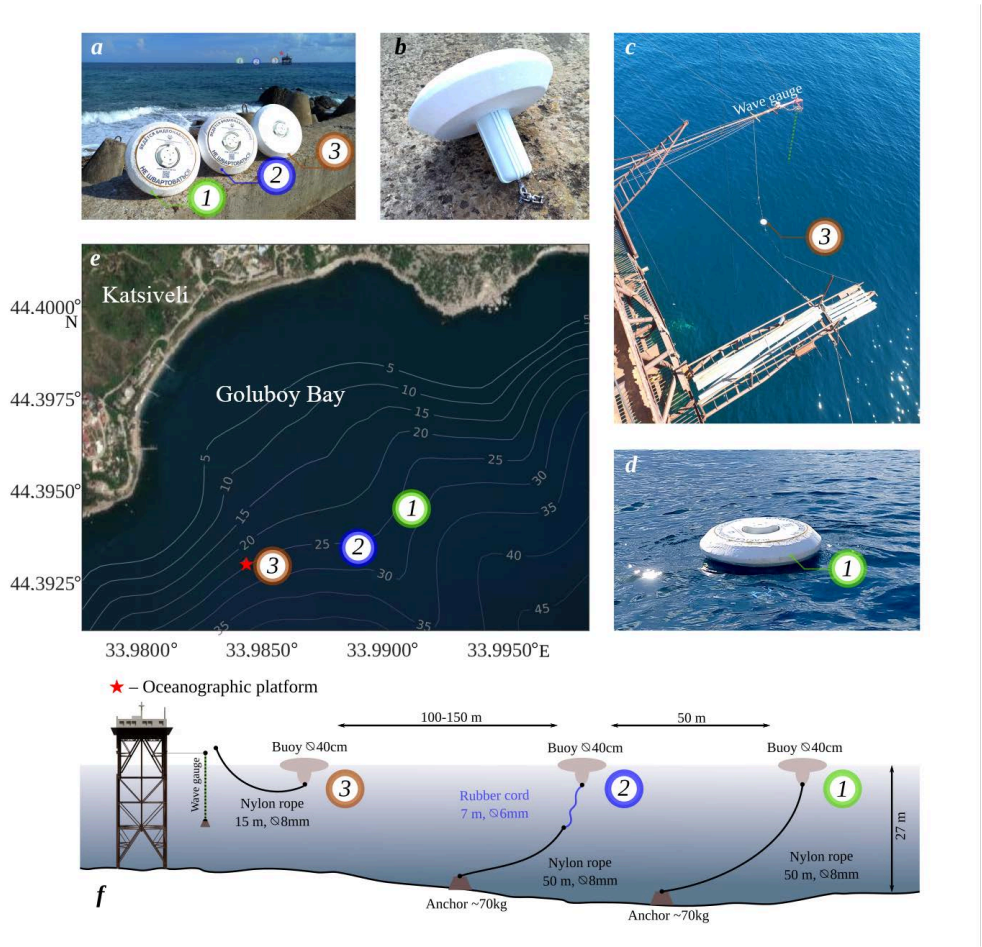

F i g . 1 . Field experiment setup: *a*, *b* – buoy exterior design; *c* – deployment of Buoy *3* from the platform; *d* – deployment of Buoy *1* with anchor; *e* – satellite image of the study site with bathymetry overlay (URL: https://www.arcgis.com/apps/View/index.html?appid=504e3ff67457481e839bb941a709350f); *f* – schematic depth profile illustrating buoy deployment configurations

Data processing methodology

In this study, the raw data from the buoys consist of time series of three-axis acceleration, angular velocity, and magnetic field, while wire-resistive wave gauges provide synchronous measurements of sea surface elevations at six points (the center and vertices of a pentagon with a 25 cm radius). To estimate wave characteristics, we applied a well-established method described in [21], which derives the frequency-angle spectrum as a truncated Fourier series based on measurements of vertical displacements and inclinations in two orthogonal planes:

$$S(f, \theta) = a_0 + \Sigma\, a_n \cos(n\theta) + b_n \sin(n\theta), \quad (1)$$

where f is the frequency and θ is the wave direction (defined as the direction from which the waves propagate relative to the north).

For measurements with wire-resistive wave gauges, instantaneous slopes ζ and elevations z were estimated by fitting a plane (using the least squares method) based on six elevation measurements at points with known horizontal coordinates. The coefficients for formula (1) in this case are as follows:

$$a_0 = C_{11}/\pi, \quad a_1 = Q_{12}/k\pi, \quad b_1 = Q_{13}/k\pi,$$
$$a_2 = (C_{11} - C_{22})/k^2\pi, \quad b_2 = 2C_{23}/k^2\pi, \quad (2)$$

where C_{mn} and Q_{mn} are the real and imaginary parts of the spectrum estimate $S_{mn} = C_{mn} + iQ_{mn}$. The subscripts denote the parameters for which the spectrum is calculated: 1 for elevations; 2 for slopes ζ_x in the east-west direction; 3 for slopes ζ_y in the north-south direction. The wave number is calculated using the dispersion relation $k = (2\pi f)^2/g$, where g is the acceleration due to gravity.

For buoy measurements, vertical accelerations were used in place of elevations, assuming the buoy closely follows the wave slopes. In this case, equations (2) take the form:

$$a_0 = C_{11}/\pi\,(2\pi f)^4, \quad a_1 = Q_{12}/k\pi\,(2\pi f)^2, \quad b_1 = Q_{13}/k\pi\,(2\pi f)^2,$$
$$a_2 = (C_{22} - C_{33})/k^2\pi, \quad b_2 = 2C_{23}/k^2\pi,$$

where subscript 1 denotes vertical acceleration. The slopes were calculated similarly to [14] from the measured angular velocities η taking into account the current orientation of the buoy relative to true north:

$$\eta_x = -\left(\eta_{0x}\sin(\phi) + \eta_{0y}\cos(\phi)\right), \quad \eta_y = -\left(\eta_{0x}\cos(\phi) - \eta_{0y}\sin(\phi)\right),$$

where η_{0x}, η_{0y} are the angular velocities measured by the gyroscope, and the azimuth angle ϕ, corrected for the local magnetic declination (7.3°) at the experiment site, was determined from the horizontal components of the measured magnetic field: $\phi = \mathrm{Arg}(m_x + i m_y)$. Unknown offsets in the magnetic field measurements, arising from the magnetization of buoy components, were determined using the condition that the absolute value of the geomagnetic field intensity vector M is constant:

$$(m_{ix} - m_{0x})^2 + (m_{iy} - m_{0y})^2 + (m_{iz} - m_{0z})^2 = M^2,$$

where m_{ix}, m_{iy}, m_{iz} are the magnetometer measurements at time i.

Based on the calculated one-dimensional elevation spectrum $S(f) = \pi a_0$, the significant wave height was estimated as:

$$H_s = 4\sqrt{\int S(f)df},$$

where the lower integration limit f_1 was determined by the first local minimum in the elevation spectrum to avoid low-frequency noise inherent in measurements

with buoy IMUs [22] (this issue does not apply to measurements with wire-resistive wave gauges).

The spectral peak frequency f_p and its corresponding period T_p were determined based on the maximum of the elevation spectrum, provided that $f > f_1$.

The mean wave direction θ_p at the spectral peak, according to [21], is given by: $\theta_p = \mathrm{Arg}(a_1 + i b_1)$.

The recordings were divided into one-minute sequential fragments, from which the squared Fourier transforms were calculated and then averaged over 30-minute intervals to obtain the spectrum estimate (equation (1)).

Results

The frequency spectra of elevations, derived from wave gauge and Buoy *1* and Buoy *2* measurements, are shown in Fig. 2 as a function of time for the entire measurement period (results for Buoy *3*, deployed for a significantly shorter period, are omitted for brevity). Wind speed during this period (Fig. 2, *a*) varied from 0 to 15 m/s, with directions from the east, west, and north. Thus, during the week-long experiment, measurements were conducted under the most typical conditions for this water area.

As shown in Fig. 2, *b*, which presents the reference spectra, various conditions were observed: fading waves and swells (October 3), developing wind waves (October 7 and 9), and several spectral peaks (October 4, 8, and 9). These features are also evident in the spectra derived from Buoy *1* and Buoy *2* measurements. However, these spectra differ from the reference spectra, with an underestimated high-frequency component $f > 1.5$ Hz and an overestimated low-frequency component $f < f_p$. The first effect arises due to the weak response of the hull to waves shorter than its characteristic size [23]. This effect has minimal impact on significant wave height estimates because the elevation spectrum decays rapidly with frequency f^{-4}. The second effect can introduce significant errors in wave height estimates, as demonstrated in [22]. To address this, the estimate H_s in this study is calculated starting from the frequency f_1, defined as the first local minimum in the elevation spectrum. This approach is equivalent to high-frequency filtering, commonly applied to raw measurement data from buoys [1)]. However, for measurements with wire-resistive wave gauges, such filtering is unnecessary, as the spectral density at low frequencies (below the peak) is several orders of magnitude lower than in the spectral maximum region.

The time series of significant wave heights calculated using this method are shown in Fig. 3, *b*. Notably, despite the absence of additional calibration, the results demonstrate strong agreement between the wave gauge measurements and all three buoy configurations across all setup types.

The differences between the measurement data from the BNO055 motion unit and MPU9250 in this figure are within the thickness of the graph line and are therefore not shown. Thus, the consistency of results across six samples of two different motion unit models indicates that the factory calibration of these IMUs provides the specified accuracy (typically within a few percent).

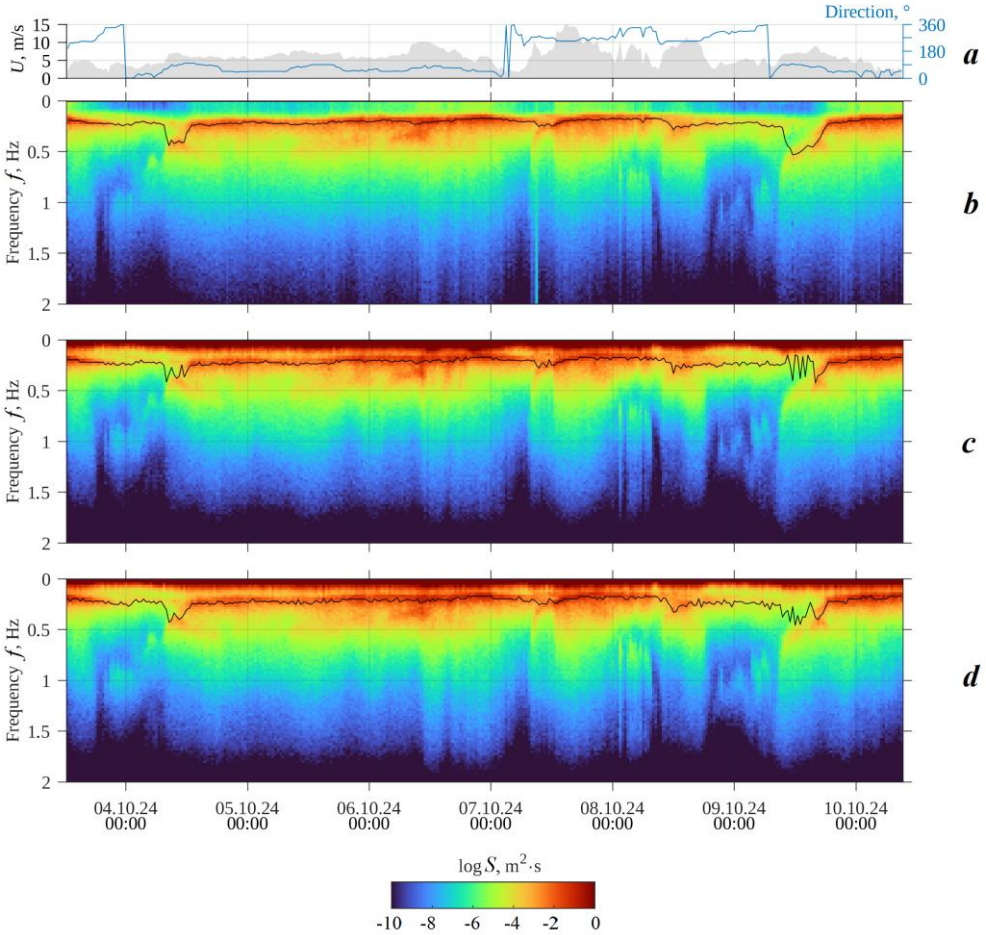

F i g . 2 . Wind speed and direction (*a*) during the experiment, frequency spectrum evolution from measurements of (*b*) wave gauge, (*c*) Buoy *1* without rubber cord, (*d*) Buoy *2* with rubber cord

Notably, more significant differences arise from the presence of an elastic rubber cord in the retaining device, as evident for October 6 and 7. The differences between the measured and reference wave heights in these two cases have opposite signs. This is likely due to the complex current patterns observed during the experiment, with strong currents often opposing the wind and waves. However, the influence of currents requires separate study and is beyond the scope of this work.

Analysis of the calculated spectral peak wave periods (Fig. 3, *c*) shows strong agreement between observations and reference values. However, in cases of young waves superimposed on swell (October 4 and 9), discrepancies were observed when spectral peaks of similar amplitude at different frequencies produced an effect resembling chattering. Notably, when a rubber cord was used (Buoy *2*, orange line), this effect was significantly reduced.

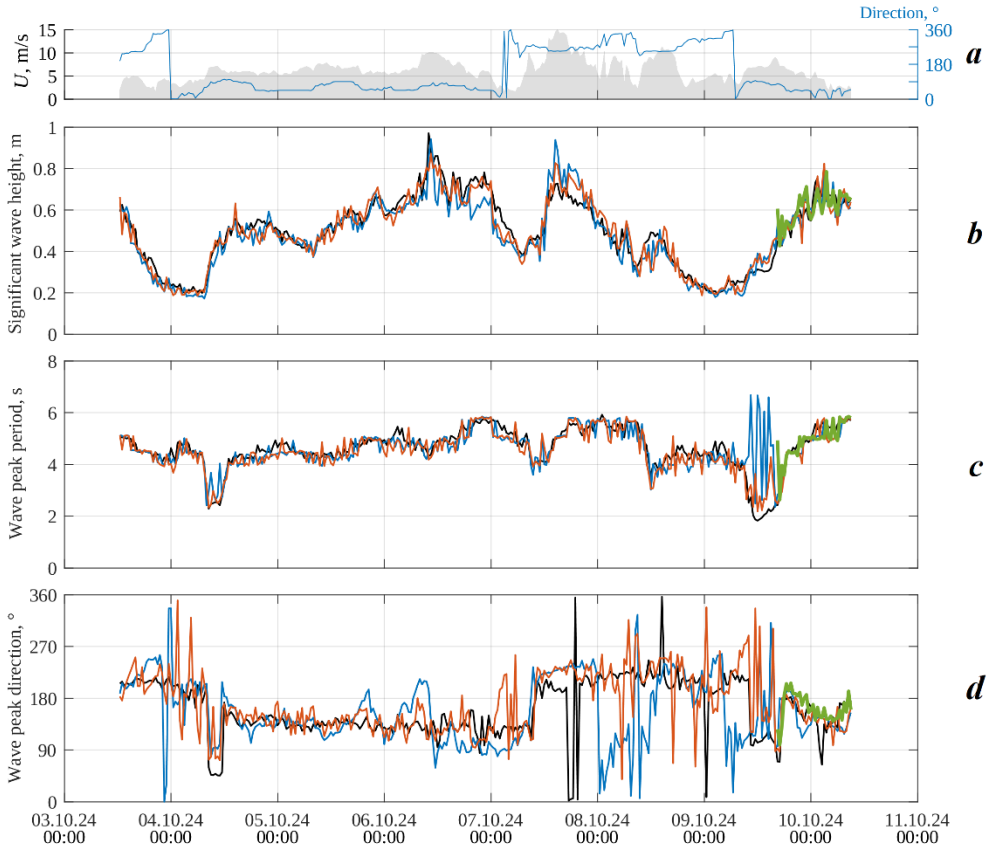

F i g . 3 . Wind speed and direction (*a*) during the experiment, time series of wave parameters estimated from measurements of wave gauge (black) and Buoys *1* (blue), *2* (orange), *3* (green): *b* – significant wave height; *c* – spectral peak wave period; *d* – spectral peak wave direction

The greatest discrepancies with reference measurements are observed in the estimates of spectral peak wave directions (Fig. 3, *d*). Although mean values are determined with high accuracy, short-term spikes occur, primarily during weak winds (between October 3 and 4, and after October 8). Notably, similar features, though less pronounced, are also present in reference measurements from wire wave gauges, due to the specifics of the directional spectrum calculation algorithm, which is restricted to the first five terms of the Fourier series (equation (1)). The use of a rubber cord improves the accuracy of direction estimates (e.g., see Fig. 3, *d*, blue curve after October 8). The non-standard bifilar suspension from the platform exhibited unexpectedly small deviations from the reference values.

Scatterplots for the three wave parameters discussed, H_s, T_p and θ_p, are shown in Fig. 4, along with statistical metrics. For Buoys *1* and *2*, which provide the most

data, high correlation coefficients for significant wave heights are observed, exceeding 0.93, with a linear regression coefficient deviation from unity of no more than 5%. The root-mean-square error of measurements was ~ 6 cm for setups with a rubber cord and 5 cm for those without. Notably, measurements were taken at spatially separated points, so a significant portion of this error is attributed to the statistical variability of H_s, which is typically 10–15% [1)].

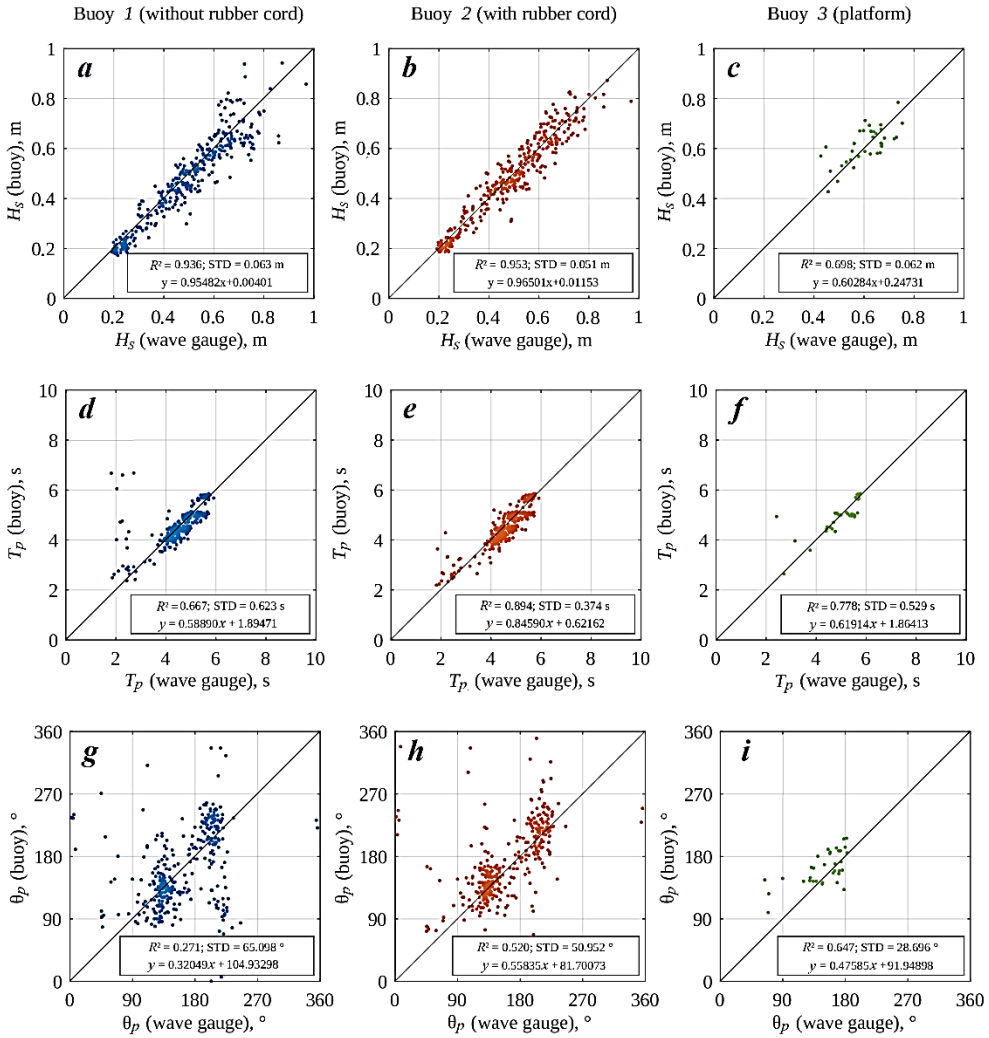

F i g . 4 . Wave parameters: significant wave height (*a*, *b*, *c*), spectral peak wave period (*d*, *e*, *f*) , spectral peak wave direction (*g*, *h*, *i*) obtained by Buoy *1* (without rubber cord) (*a*, *d*, *g*), Buoy *2* (with rubber cord) (*b*, *e*, *h*), Buoy *3* (platform deployment) (*c*, *f*, *i*) compared with reference wave gauge measurements

The consistency between the estimated and reference values of the spectral peak wave period T_p is lower, as discussed previously, due to the chattering effect described above. Meanwhile, when obvious outliers are excluded, the correlation coefficient reaches values comparable to those for significant wave height estimates.

The largest discrepancies with reference measurements are observed for wave directions of 50–65° (Fig. 4, *g*, *h*, *i*), consistent with the analysis of the time series (Fig. 3, *d*). However, this deviation is comparable to the resolution of the method used (approximately 90°) [1)] [21].

The use of an elastic rubber cord improves the accuracy of estimates in all cases compared to reference values, though the improvement is modest, despite deliberately selecting the most elastic (but least reliable) rubber cord.

Conclusion

This study presents the results of field tests of wave-measuring buoy loggers developed at Marine Hydrophysical Institute, designed with maximal simplicity to record initial measurement data on a memory card.

The experiment was conducted near the MHI Stationary Oceanographic Platform. Three buoys with identical IMUs were tested in three different configurations: without an elastic rubber cord, with an elastic rubber cord, and with a bifilar suspension from the platform. Comparison with reference measurements from wire-resistive wave gauges showed strong agreement across all estimates for the three setups. For example, in the observed range of significant wave heights (0.2–1 m), the root-mean-square error of height measurements was no more than 5 cm for the setup with an elastic rubber cord and no more than 6 cm without it. Corresponding values for spectral peak wave periods were 0.37 s and 0.62 s, and for spectral peak wave directions were 50° and 65°. Therefore, when there is a high risk of buoy loss, the elastic rubber cord can be omitted from the retaining device at the cost of a slight reduction in data accuracy.

A key limitation of the measuring devices presented in this study is the need for maintenance, including data retrieval and battery replacement. However, this measurement approach may be suitable for various coastal tasks or specialized experiments that do not require long-term deployments.

The advantages of this approach include its extremely low cost, which is 2 to 3 orders of magnitude lower than that of traditional unattended models. This enables extensive field studies of waves across sections or grids, where multiple identical devices are needed. Additionally, a significant advantage, in our view, is that researchers have access to raw data directly from the IMU without preprocessing. This enhances the transparency and flexibility of further analysis and allows the processing algorithm to be adapted based on specific research objectives.

REFERENCES

1. Kuznetsov, S. and Saprykina, Y., 2021. Nonlinear Wave Transformation in Coastal Zone: Free and Bound Waves. *Fluids*, 6(10), 347. https://doi.org/10.3390/fluids6100347
2. Brown, A.C. and Paasch, R.K., 2021. The Accelerations of a Wave Measurement Buoy Impacted by Breaking Waves in the Surf Zone. *Journal of Marine Science and Engineering*, 9(2), 214. https://doi.org/10.3390/jmse9020214
3. Masson, D., 1996. A Case Study of Wave-Current Interaction in a Strong Tidal Current. *Journal of Physical Oceanography*, 26(3), pp. 359–372. https://doi.org/10.1175/1520-0485(1996)026<0359:ACSOWI>2.0.CO;2
4. Goryachkin, Y.N., Udovik, V.F. and Kharitonova, L.V., 2010. Estimations of the Parameters of the Flux of Sediments near the West Coast of the Bakal'skaya Spit Under the Conditions of Heavy Storms in 2007. *Physical Oceanography*, 20(5), pp. 356–365. https://doi.org/10.1007/s11110-011-9091-9
5. Saprykina, Y.V., Samiksha, S.V. and Kuznetsov, S.Yu., 2021. Wave Climate Variability and Occurrence of Mudbanks Along the Southwest Coast of India. *Frontiers in Marine Science*, 8, 671379. https://doi.org/10.3389/fmars.2021.671379
6. Andreeva, N., Saprykina, Y., Valchev, N., Eftimova, P. and Kuznetsov, S., 2021. Influence of Wave Climate on Intra and Inter-Annual Nearshore Bar Dynamics for a Sandy Beach. *Geosciences*, 11(5), 206. https://doi.org/10.3390/geosciences11050206
7. Goryachkin, Y.N. and Kosyan, R.D., 2020. Formation of a New Island of the Coast of Crimea. *Oceanology*, 60(2), pp. 286–292. https://doi.org/10.1134/S0001437020020034
8. Zhou, Y., Feng, X., Liu, M. and Wang, W., 2023. Influence of Beach Erosion during Wave Action in Designed Artificial Sandy Beach Using XBeach Model: Profiles and Shoreline. *Journal of Marine Science and Engineering*, 11(5), 984. https://doi.org/10.3390/jmse11050984
9. Shimura, T., Mori, N., Baba, Y. and Miyashita, T. Ocean Surface Wind Estimation from Waves Based on Small GPS Buoy Observations in a Bay and the Open Ocean. *Journal of Geophysical Research: Oceans*, 127(9), e2022JC018786. https://doi.org/10.1029/2022jc018786
10. Divinsky, B.V. and Kuklev, S.B., 2022. Experiment of Wind Wave Parameter Research on the Black Sea Shelf. *Oceanology*, 62(1), pp. 14–19. https://doi.org/10.31857/S003015742201004X
11. Rainville, E., Thomson, J., Moulton, M. and Derakhti, M., 2023. Measurements of Nearshore Ocean-Surface Kinematics Through Coherent Arrays of Free-Drifting Buoys. *Earth System Science Data*, 15(11), pp. 5135–5151. https://doi.org/10.5194/essd-15-5135-2023
12. Kinsela, M.A., Bradley, D.M., Ingleton, T.C., Doyle, T.B., Sutherland, M.D., Doszpot, N.E., Miller, J.J., Holtznagel, S.F. [et al.], 2024. Nearshore Wave Buoy Data from Southeastern Australia for Coastal Research and Management. *Scientific Data*, 11(1), 190. https://doi.org/10.1038/s41597-023-02865-x
13. Veras Guimarães, P., Ardhuin, F., Sutherland, P., Accensi, M., Hamon, M., Pérignon, Y., Thomson, J., Benetazzo, A. and Ferrant, P., 2018. A Surface Kinematics Buoy (SKIB) for Wave-Current Interaction Studies. *Ocean Science*, 14(6), pp. 1449–1460. https://doi.org/10.5194/os-14-1449-2018
14. Yurovsky, Y.Yu. and Dulov, V.A., 2020. MEMS-Based Wave Buoy: Towards Short Wind-Wave Sensing. *Ocean Engineering*, 217, 108043. https://doi.org/10.1016/j.oceaneng.2020.108043

15. Rabault, J., Nose, T., Hope, G., Müller, M., Breivik, Ø., Voermans, J., Hole, L. R., Bohlinger, P., Waseda [et al.], 2022. OpenMetBuoy-v2021: An Easy-to-Build, Affordable, Customizable, Open-Source Instrument for Oceanographic Measurements of Drift and Waves in Sea Ice and the Open Ocean. *Geosciences*, 12(3), 110. https://doi.org/10.3390/geosciences12030110
16. Feddersen, F., Amador, A., Pick, K., Vizuet, A., Quinn, K., Wolfinger, E., MacMahan, J.H. and Fincham, A., 2024. The Wavedrifter: A Low-Cost IMU-Based Lagrangian Drifter to Observe Steepening and Overturning of Surface Gravity Waves and the Transition to Turbulence. *Coastal Engineering Journal*, 66(1), pp. 44–57. https://doi.org/10.1080/21664250.2023.2238949
17. Joosten, H., 2006. Directional Wave Buoys and their Elastic Mooring. *International Ocean Systems*, 10(4), pp. 18–21.
18. Yurovsky, Yu.Yu. and Dulov, V.A., 2017. Compact Low-Cost Arduino-Based Buoy for Sea Surface Wave Measurements. In: IEEE, 2017. *Proceedings of Progress in Electromagnetic Research Symposium – Fall (PIERS – FALL), 19–22 November 2017*. Singapore: IEEE, pp. 2315–2322. https://doi.org/10.1109/PIERS-FALL.2017.8293523
19. Bondur, V.G., Dulov, V.A., Murynin, A.B. and Yurivsky, Yu.Yu., 2016. Studying Marine Wave Spectra in a Wide Range of Wavelengths Using Satellite and In Situ Data. *Issledovanie Zemli iz Kosmosa*, (1–2), pp. 7–24. https://doi.org/10.7868/S0205961416010048
20. Smolov, V.E. and Rozvadovskiy, A.F., 2020. Application of the Arduino Platform for Recording Wind Waves. *Physical Oceanography*, 27(4), pp. 430–441. doi:10.22449/1573-160X-2020-4-430-441
21. Longuet-Higgins, M.S., Cartwright, D.E. and Smith, N.D., 1961. Observations of the Directional Spectrum of Sea Waves Using the Motions of a Floating Buoy. In: NAS, 1961. *Ocean Wave Spectra: Proceedings of a Conference, Easton, Maryland, May 1–4, 1961*. Englewood Cliffs: Prentice-Hall, pp. 111–132.
22. Ashton, I.G.C. and Johanning, L., 2015. On Errors in Low Frequency Wave Measurements from Wave Buoys. *Ocean Engineering*, 95, pp. 11–22. https://doi.org/10.1016/j.oceaneng.2014.11.033
23. Stewart, R.H., 1977. A Discus-Hulled Wave Measuring Buoy. *Ocean Engineering*, 4(2), pp. 101–107. https://doi.org/10.1016/0029-8018(77)90013-0

Submitted 09.12.2024; accepted after review 21.01.2025;
revised 24.06.2025; published 30.09.2025

About the authors:

Yury Yu. Yurovsky, Leading Research Associate, Marine Hydrophysical Institute of RAS (2 Kapitanskaya St., Sevastopol, 299011, Russian Federation), Ph.D. (Phys.-Math.), **Scopus Author ID: 24377122700, ORCID ID: 0000-0002-9995-3965,** *yyyurovsky@gmail.com*

Oleg B. Kudinov, Research Associate, Head of Laboratory, Marine Hydrophysical Institute of RAS (2 Kapitanskaya St., Sevastopol, 299011, Russian Federation), Ph.D. (Tech.), **IstinaResearcherID (IRID): 19314165**, *obk91@mail.ru*

Contribution of the authors:

Yury Yu. Yurovsky – development of methodologies and conducting field trials, processing, analysis and description of the study results, preparation of the article text

Oleg B. Kudinov – development and production of the measuring devices, conducting field trials

All the authors have read and approved the final manuscript.

Original paper

Spectral Features of Hydroacoustic Signals

A. V. Nerush *, N. A. Tuzov, I. N. Kartsan

FSAEI HPE «Sevastopol State University», Sevastopol, Russia

* *e-mail: nerush03@mail.ru*

Abstract

The paper analyses spectral and time-frequency characteristics of hydroacoustic signals of animal and anthropogenic origin, as well as background signals. The study aims to classify and identify these signals to address ecological monitoring tasks in the marine environment and to develop effective criteria for signal differentiation for automated assessment of the acoustic situation in coastal and shelf zones. We used methods of spectral and time-frequency analysis along with comparative analysis based on a review of current scientific literature. Characteristic features of spectra and spectrograms for various groups of signal sources were identified. Signals were classified according to their acoustic origin, and key parameters for signal identification under high noise conditions were determined, including spectral shapes, presence of harmonics, pulse durations, and specific temporal patterns. A feature set in the form of numerical vectors was created for subsequent application in machine learning algorithms and automatic recognition systems. The developed approach can be integrated into ecological monitoring systems for coastal waters and advanced navigation solutions.

Keywords: spike, harmonic, sound localization, hydroecholocation, identification, natural noise, technogenic noise, pulse, broadband

Acknowledgements: This study was carried out with the support of the Russian Science Foundation grant № 24-21-20070, https://rscf.ru/project/24-21-20070/

For citation: Nerush, A.V., Tuzov, N.A. and Kartsan, I.N., 2025. Spectral Features of Hydroacoustic Signals. *Ecological Safety of Coastal and Shelf Zones of Sea*, (3), pp. 128–140.

© Nerush A. V., Tuzov N. A., Kartsan I. N., 2025

This work is licensed under a Creative Commons Attribution-Non Commercial 4.0 International (CC BY-NC 4.0) License

Спектральные особенности гидроакустических сигналов

А. В. Неруш *, Н. А. Тузов, И. Н. Карцан

ФГАОУ ВО «Севастопольский государственный университет», Севастополь, Россия

* *e-mail: nerush03@mail.ru*

Аннотация

Анализируются спектральные и временно-частотные характеристики гидроакустических сигналов животного и антропогенного происхождения, также фоновые сигналы, с целью их классификации и идентификации для решения задач экологического мониторинга морской среды, а также формирования эффективных критериев дифференциации сигналов для автоматизированной оценки акустической обстановки в прибрежных и шельфовых зонах. Использованы методы спектрального и временно-частотного анализа, а также сравнительного анализа на основе обзора современной научной литературы. Выделены характерные особенности спектров и спектрограмм для различных групп источников сигналов. Проведена классификация сигналов по типу акустического происхождения, определены ключевые параметры идентификации сигнала в условиях высокой шумовой нагрузки – форма спектров, наличие гармоник, длительность импульсов и специфические временны́е паттерны. Сформирован набор признаков в виде числовых векторов для последующего применения в алгоритмах машинного обучения и системах автоматического распознавания. Разработанный подход может быть интегрирован в системы экологического мониторинга прибрежных акваторий и перспективные навигационные решения.

Ключевые слова: всплеск, гармоника, идентификация сигналов, естественный шум, техногенный шум, импульс, широкополосность, акустический сигнал, спектр

Благодарности: исследование выполнено за счет гранта Российского научного фонда № 24-21-20070, https://rscf.ru/project/24-21-20070/

Для цитирования: *Неруш А. В., Тузов Н. А., Карцан И. Н.* Спектральные особенности гидроакустических сигналов // Экологическая безопасность прибрежной и шельфовой зон моря. 2025. № 3. С. 128–140. EDN KDFFTZ.

Introduction

Hydroacoustic underwater monitoring systems play a key role in modern marine science and technology, enabling effective research and monitoring of the ocean environment. The development of these systems is driven by the need to obtain accurate and timely information about the underwater environment, which is crucial for both scientific research and ensuring the safety of maritime operations [1)]. Modern hydroacoustic technologies, based on digital signal processing and spectral analysis methods, allow various underwater sound sources to be identified and classified with high accuracy, which is critical for underwater navigation, communication, and environmental monitoring tasks [1, 2].

[1)] Zakharov, I.S., 2004. [*Development of National Hydroacoustic Means: The Early 1920s–The Late 1950s*. Doctoral Thesis]. Saint Petersburg, 390 p. (in Russian).

The development of domestic hydroacoustic equipment began in the mid-20th century, when the fundamental principles of acoustic signal research in aquatic environments were established. The subsequent decades, particularly the late 20th and early 21st centuries, saw significant progress in spectral and time-frequency analysis of hydroacoustic data, greatly improving the efficiency of signal processing and interpretation [3]. Modern research focuses on optimizing processing algorithms, including the use of discrete and fast Fourier transforms, vector-phase methods and trajectory-space filtering, aimed at enhancing the extraction of informative features from noise sources and improving the accuracy of determining their coordinates and directionality [4, 5].

Despite the availability of a wide range of specialized methods for analyzing hydroacoustic signals, many are tailored to highly specific tasks and limited in their application to particular classes of sound sources. Existing methods often fail to adequately provide a unified description of the spectral characteristics of signals varying in nature and origin, including both anthropogenic and bioacoustic sources. This creates a gap in digital processing technologies, hindering the broader application of hydroacoustic systems in areas such as automated eco-monitoring of marine ecosystems and comprehensive classification of underwater objects [2, 4–6].

The increasing anthropogenic impact on the underwater environment and the growing volume of information from underwater sources necessitate the development of precise methods for analyzing and identifying acoustic signals to enhance the reliability of underwater navigation and communication systems [1, 3, 7]. Environmental monitoring tasks are becoming increasingly critical, as they require simultaneous recording and analysis of both bioacoustic signals and anthropogenic noise, complicating the interpretation of the acoustic environment.

Although effective algorithms for processing hydroacoustic signals have been developed in recent years, including optimized Fourier analysis methods [4] and vector-phase approaches [8, 9], they typically focus on highly specialized tasks and do not provide a comprehensive description of both spectral and time-frequency characteristics of heterogeneous signals. Specifically, there are no universal methods that enable a uniform description of both bioacoustic and anthropogenic signals, limiting data integration in environmental monitoring and navigation systems [9–12].

The study aims to systematically analyze the spectral and time-frequency characteristics of various hydroacoustic signals, focusing on identifying unique features that enable reliable source identification and classification. The proposed approach facilitates a unified description of the spectral properties of both anthropogenic and bioacoustic signals, expanding the applicability of standard digital processing methods and enhancing the accuracy and versatility of hydroacoustic monitoring systems.

Materials and methods

The first stage of the study involved data collection and filtering. The analyzed signals were sourced from the AXDS Portals open database of hydroacoustic recordings, containing data from bottom stations, hydrophones, and other sensors deployed in coastal and oceanic areas [2)]. The recordings were in WAV format with sampling rates ranging from 4 to 64 kHz, depending on the source type and equipment. For analysis, sound fragments of 5 to 60 s were selected, representing typical samples of each signal class – biological, anthropogenic, and natural background noise. The total number of independent recordings for each signal type was 20–30, enabling the derivation of averaged spectra with acceptable statistical stability.

The recorded signals underwent preliminary processing to remove external interference and artifacts caused by equipment limitations. Digital filtering methods were applied to isolate significant frequency ranges and reduce the impact of background noise [3].

The fast Fourier transform was used to identify the primary frequency components of each signal. This method enabled the derivation of power spectra, characterizing the distribution of signal energy across frequencies. The signal spectrum is defined as the set of amplitudes and initial phases of harmonic oscillations at various frequencies, which collectively reconstruct the original signal. The spectra were analyzed to identify dominant frequencies, harmonics, and patterns characteristic of specific signal groups. The basis of spectral analysis was the discrete Fourier transform, defined for a discrete signal $x[n]$ with N samples by the formula:

$$X[k] = \sum_{n=0}^{N-1} x[n] \, e^{\frac{-j 2\pi k n}{N}},$$

where $k = 0, 1, ..., N–1$ is the frequency index.

To investigate changes in the spectral structure over time, time-frequency analysis methods, including spectrogram construction, were employed. This enabled the identification of unique temporal structures, such as burst periodicity, pulse duration, and signal attenuation dynamics.

A comparative analysis of different signal types was conducted to identify unique features distinguishing animal, anthropogenic, and natural background noise signals. Key parameters included spectral shape, presence of harmonics, pulse duration, and specific temporal patterns. The spectra presented reflect typical characteristics of each signal class but do not account for variability due to species differences, seasonal and hydrometeorological conditions, or technical device characteristics.

---

2) Axiom Data Science. *Data Portal Documentation*. 2025. Available at: https://help.axds.co/portals/overview.html#data-views-overview [Accessed: 22 August 2025].

The algorithm for analyzing spectra and spectrograms involved performing a Fourier transform, constructing spectrograms, analyzing peak frequencies, estimating signal bandwidth, calculating the spectral centroid to detect periodicities, and evaluating the signal autocorrelation function [4].

For use in machine learning algorithms, formalized spectral and temporal features (dominant frequency, bandwidth, harmonic amplitude parameters) were extracted and represented as numerical vectors, serving as input features for machine learning models [5]. These features are designed for classifying hydroacoustic signals by source type, including bioacoustic and anthropogenic noise. Such signals exhibit consistent structure and reproducibility in their spectral patterns, enabling their use in training datasets for developing recognition models without requiring manual labeling of the original signals.

To implement all stages of the analysis, general-purpose software tools were used, including digital signal processing libraries in MATLAB and Python, as well as data visualization tools. The reliability of the results was evaluated using cross-validation techniques, which involve repeatedly partitioning the dataset into training and test subsets to minimize the impact of random factors in the analysis.

The effectiveness of the developed methods was evaluated using independent datasets from the publicly available AXDS Portals database, which contains verified examples of the investigated noise types, confirming their applicability to a wide range of hydroacoustic signal identification tasks [2].

Results and discussion

The signals *sea lion barking* and *killer whale singing* are examples of animal sounds with relatively complex frequency structures [6, 7]. The spectrum of the *sea lion barking signal* (Fig. 1, *a*) exhibits a prominent peak at approximately 400 Hz, reaching a spectral power density value of 1.93. Attenuated bursts at frequencies of 60 and 330 Hz indicate the presence of harmonics, contributing to the characteristic low timbre, resembling a hoarse bark.

The signal spectrogram (Fig. 1, *b*) clearly illustrates the concentration of primary sound energy in the low-frequency range.

The spectrum of the *killer whale singing* signal (Fig. 2, *a*) exhibits the clearest signal structure among the signals analyzed in the study. It spans a broad frequency range, reflecting a complex harmonic structure and diverse acoustic elements in killer whale vocalizations. Multiple peaks occur between 0 and 11 kHz, with the most prominent at frequencies of 1.3, 2, and 2.1 kHz. These frequency components of the signal are associated with communication and environmental orientation [6].

The signal spectrogram (Fig. 2, *b*) is characterized by a number of bright bands located within the 0 to 11 kHz range. High-frequency components manifest as additional vertical bands, highlighting the broadband nature of the signal.

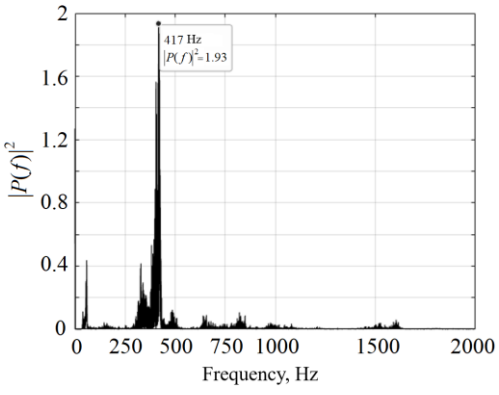

a

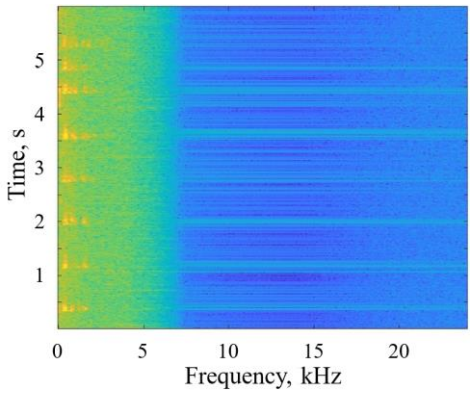

b

Fig. 1. Spectral analysis of the *sea lion barking* signal: *a* – spectrum; *b* – spectrogram

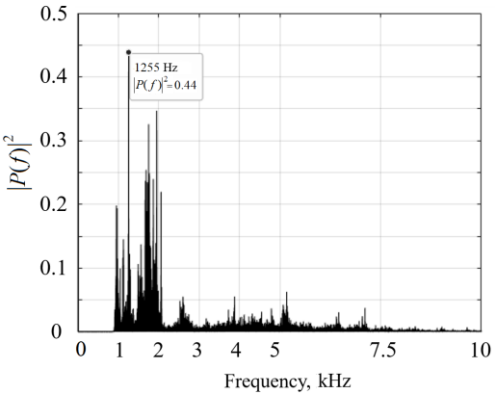

a

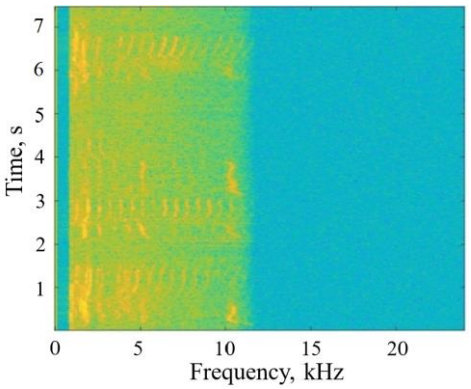

b

Fig. 2. Spectral analysis of the *killer whale singing* signal: *a* – spectrum; *b* – spectrogram

The *explosion* and *sonar* signals are characterized by distinct narrowband peak frequencies. The *explosion* signal exhibits a different frequency power distribution compared to the *sonar* signal, as evidenced in both the obtained spectrum (Fig. 3, *a*) and the spectrogram (Fig. 3, *b*). The maximum spectral power density (0.88) was observed in the 140–180 Hz range [8, 9].

The spectrum of the *sonar* signal (Fig. 4, *a*) exhibits a series of narrowband peaks within the 2.3 to 3.3 kHz range. In the spectrogram (Fig. 4, *b*), these appear as recurring bright horizontal bands. Their periodicity, consistent width, and intensity highlight the stability and predictability of the signal. This frequency composition is characteristic of signals employed by sonar devices [9].

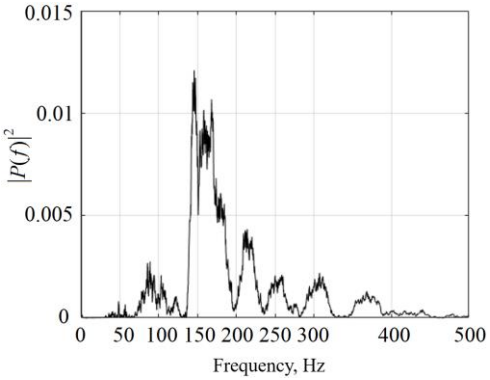

a

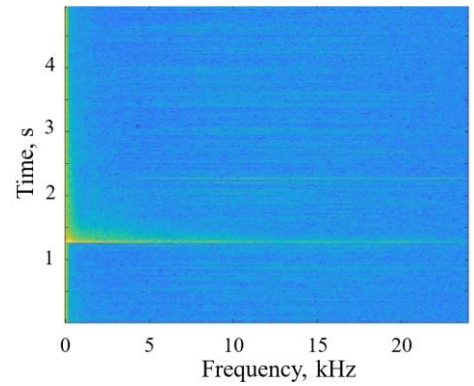

b

F i g . 3 . Spectral analysis of the *explosion* signal: *a* – spectrum; *b* – spectrogram

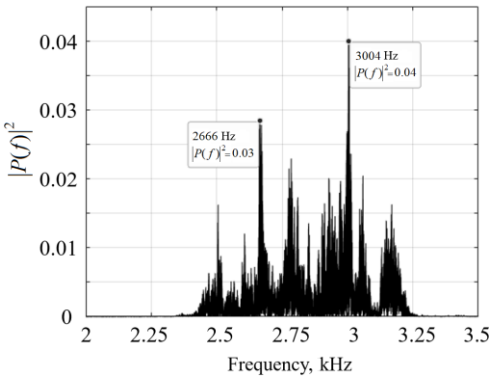

a

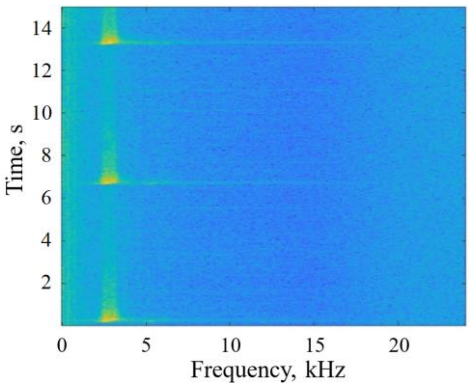

b

F i g . 4 . Spectral analysis of the *sonar* signal: *a* – spectrum; *b* – spectrogram

The described structure enables identification of this signal type. Specifically, stable frequency peaks facilitate accurate determination of the signal source. For instance, the power peak at a frequency of 3 kHz serves as a key indicator of sonar activity, as this frequency range is not typical of natural sound sources. Unlike the short-term explosion signal, sonar produces consistent radiation, allowing for reliable identification and precise measurement in noisy conditions [10].

The signals *scuba diver's breathing* and *cruise ship noise* exhibit a significant constant component. The *scuba diver's breathing* signal is characterized by a dominant peak at near-zero frequency with a spectral power density of 18 (Fig. 5, *a*),

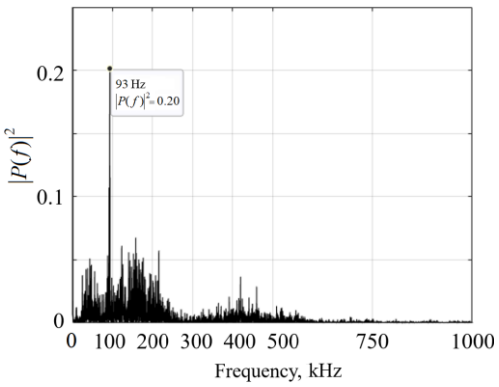

a

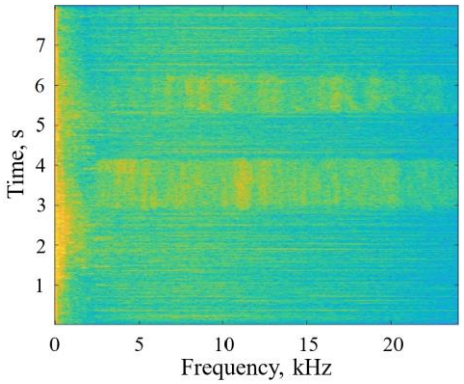

b

Fig. 5. Spectral analysis of the *scuba divers breathing* signal: *a* – spectrum; *b* – spectrogram

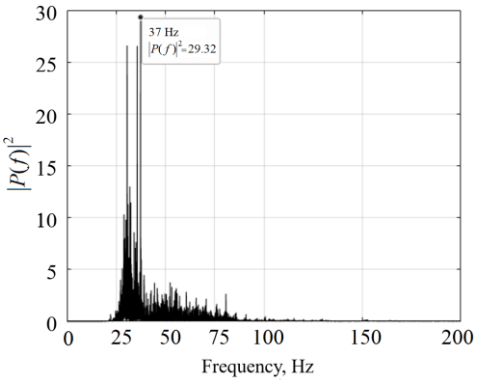

a

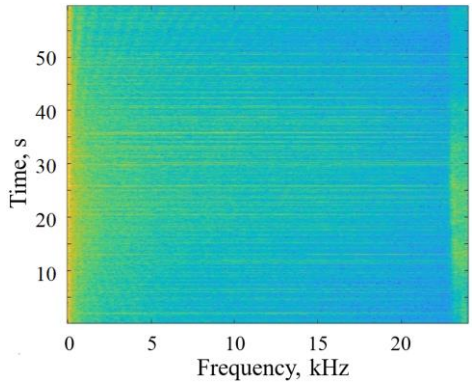

b

Fig. 6. Spectral analysis of *cruise ship noise* signal: *a* – spectrum; *b* – spectrogram

appearing as a bright vertical band with an irregular right edge in the spectrogram (Fig. 5, *b*). This indicates a zero-frequency component, likely due to the continuous exhalation of air bubbles. A minor peak at a frequency of about 100 Hz may reflect the periodicity of breathing cycles or turbulence from exhaled air flow. The constant component results from the continuous breathing process, ensuring spectral stability.

The spectrum of the *cruise ship noise* signal (Fig. 6, *a*) exhibits a prominent peak at a frequency of about 40 Hz with a spectral power density of 29.3, indicating a significant constant component, likely due to the operation of the ship's engines. A peak at a frequency of 37 Hz results from low-frequency hull vibrations, while a peak at a frequency of 80 Hz may correspond to auxiliary mechanisms or cavitation processes. The spectrogram (Fig. 6, *b*) displays a persistent bright band at near-zero

frequency throughout the recording. Analysis of phase shifts between signal components enables identification of time delays and relationships, facilitating determination of the location and nature of noise sources [11].

The *water noise* and *bottlenose dolphin's whistle* signals exhibit characteristic stability and harmonic components. The spectrum of the *water noise* signal (Fig. 7, *a*) and its spectrogram (Fig. 7, *b*) reveal a broad frequency range, with dominant power concentrated in the low-frequency band (up to 8 kHz), beyond which intensity rapidly decreases with increasing frequency. The signal's homogeneous nature is evidenced by its spectral power density.

The *bottlenose dolphin's whistle* shows two distinct peaks in its spectrum (Fig. 8, *a*), appearing as two well-defined structures in the spectrogram (Fig. 8, *b*). The first peak (1.26 kHz) corresponds to the fundamental frequency of background noise. The second peak (7.5 kHz) represents the average frequency of the "whistle" band (6–10 kHz), with variations in intonation depending on the message transmitted by the bottlenose dolphin through the hydroacoustic channel [6]. This peak also reflects the fundamental tone of the whistle and its first harmonic. The first harmonic, visible in the spectrogram (Fig. 8, *b*), displays uniform intensity and clear boundaries. These acoustic features serve as identifiers that can be classified as anomalies in the signal [12].

The spectral analysis demonstrates that each studied signal possesses a distinct spectral profile. Biological signals exhibit complex frequency structures with prominent harmonics, anthropogenic signals display distinct peaks at specific frequencies, and natural noise shows a uniform energy distribution in the low-frequency range [10, 12].

Signals of animal origin demonstrate significant variability in their spectral characteristics. The *sea lion barking* signal is characterized by energy concentration in the low-frequency range with prominent, stable harmonics. The *killer whale singing* signal displays a complex structure, reflecting a broad frequency range of vocalizations and diverse echolocation clicks. These features facilitate the study of marine mammal communicative behavior. The *bottlenose dolphin's whistle* signal, distinguished by two pronounced peaks, possesses a unique temporal structure that is readily distinguishable in the aquatic environment [6, 9].

Anthropogenic signals exhibit more predictable spectral characteristics. The *explosion* signal manifests as a short-term pulse with a sharp peak at near-zero frequency and rapid attenuation, enabling precise event timing. The *cruise ship noise* signal features a zero-frequency component at near-zero frequency and periodic peaks at higher frequencies. This structure helps to identify such signals when assessing the environmental impact of anthropogenic noise and developing methods to enhance signal clarity. The *sonar* signal exhibits a series of narrowband peaks,

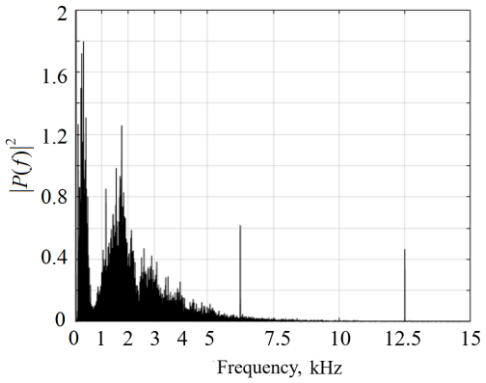

a

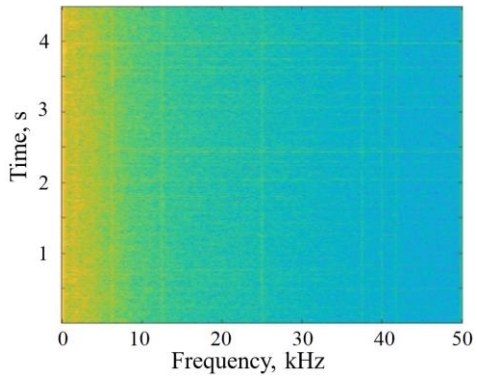

b

Fig. 7. Spectral analysis of *water noise* signal: *a* – spectrum; *b* – spectrogram

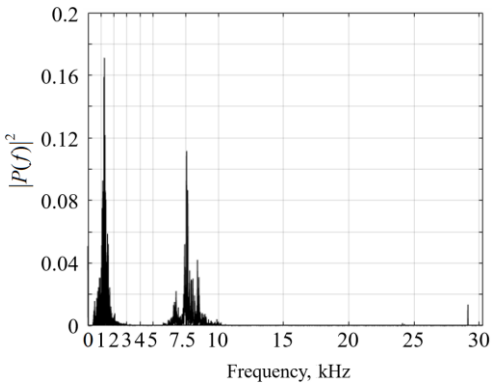

a

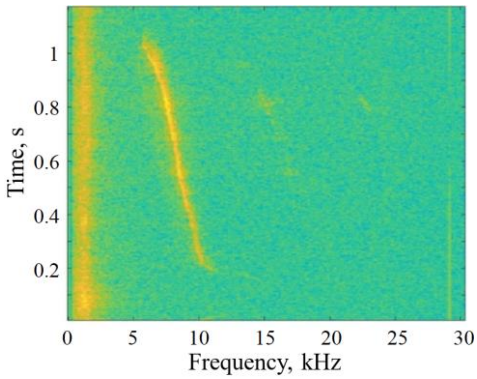

b

Fig. 8. Spectral analysis of *bottlenose dolphin's whistle*: *a* – spectrum; *b* – spectrogram

ensuring high accuracy in sounding and resistance against external interference, which is critical for underwater navigation and communication systems [9, 10].

Natural background noises exhibit distinct characteristics. The *water noise* signal displays a uniform spectrum in the low-frequency range and remains stationary over time, making it a reference signal for calibrating hydroacoustic devices and systems. The spectrum of the *scuba diver's breathing* signal is concentrated in the lowest frequency range, reflecting the slow variation of breathing sounds synchronized with inhalation and exhalation. Frequencies associated with turbulence and the consistency of breathing, influenced by immersion depth, are valuable for analyzing human physiological processes in underwater environments and designing diver life support systems.

The distinct spectral-temporal profiles of animal-derived signals enable the study of marine mammal behavior and communication. The characteristics of anthropogenic signals are used to evaluate their impact on marine fauna and develop measures to reduce it. The stability and predictability of natural background noise spectral characteristics provide a foundation for calibrating hydroacoustic instruments and systems, ensuring measurement accuracy [12, 13].

The analysis of spectrograms enables the development of algorithms for automatic recognition of sound sources, which is essential for the operation of passive acoustic surveillance and ecological monitoring systems. These data play a critical role in studying the acoustic ecology of marine ecosystems, developing underwater navigation and communication systems, and monitoring anthropogenic impacts on the marine environment and its inhabitants [14, 15].

Conclusion

Analysis of hydroacoustic signals revealed distinct spectral and time-frequency characteristics, enabling accurate identification of animal, anthropogenic, and natural background noise sources. A comparative evaluation of the signals highlighted their unique features, which can enhance the effectiveness of ecological monitoring and navigation systems.

Formalized features are represented as numerical vectors, suitable for machine learning tasks, particularly for classifying signals by source type. This approach enhances the detection of acoustic sources and broadens the application of hydroacoustic technologies in underwater environmental monitoring and anthropogenic impact assessment.

The research findings are highly relevant, providing a foundation for advancing underwater navigation technologies and developing new approaches to acoustic data analysis.

References

1. Dikarev, A.V., Dmitriev, S.M., Kubkin, V.A., Vasilenko, A.V. and Abelentsev, A.P., 2024. Determining the Accuracy of Range Measurements between Underwater Objects Using Underwater Acoustic Modems. *Marine intellectual technologies*, (2-1), pp. 145–154 (in Russian).
2. Martynov, V.L., Bozhuk, N.M., Ilyin, G.V., Krechetova, E.V., Shimanskaya, M.S. and Shimanskaya, G.S., 2023. Optimization of Hydroacoustic Information Systems of Underwater Vehicles to Improve the Efficiency of Underwater Search. *Marine Intellectual Technologies*, (1-1), pp. 149–157 (in Russian).
3. Pavlikov, S.N., Kopaeva, E.Yu., Kolesov, Yu.Yu., Petrov, P.N. and Kryuchkov, A.N., 2022. Hydroacoustic Method. *Marine Intellectual Technologies*, 1(1), pp. 208–214 (in Russian).
4. Ponomarev, A.A., Solovjev, D.S., Rodionov, D.D., Dolotcev, A.A. and Nuzhnyj, D.A., 2024. Optimization of Audio Signal Processing Algorithms Based on Discrete and Fast Fourier Transform Methods. In: V. V. Kuzina, ed., 2024. *Proceedings of the XXVIII International Scientific and Technical Conference "Information and Computing Technologies and their Applications". Penza, 26–27 August 2024*. Penza: PSAU, pp. 208–211 (in Russian).

5. Butyrsky, Ye., Vasilyev, V. and Rahuba, V., 2021. System of Views on Improving the Processing of Hydroacoustic Signals. *Morskoy Sbornik*, (8), pp. 37–45 (in Russian).
6. Myatiyeva, N.A., 2015. Whales' "Songs" as a Reflection of Scientific and Technical Progress in the Music of the Second Half of the XXth Century. *Actual Problems of Higher Musical Education*, (4), pp. 73–77 (in Russian).
7. Tugbaeva, A.S., Itskov, A.G., Milich, V.N. and Shirokov, V.A., 2022. Distinguishing Underwater Objects Based on Periodogram Analysis of Reflected Sonar Signals. *Chemical Physics and Mesoscopy*, 24(3), pp. 388–399 (in Russian).
8. Zharikov, D.S. and Ivanova, E.M., 2019. The Influence of the Shape of Underwater Shock Waves on Hydrodynamic Parameters. In: BMSTU, 2019. *Proceedings of the Twelfth All-Russian Conference of Young Scientists and Specialists (with International Participation) "The Future of Mechanical Engineering in Russia". Moscow, 24–27 September 2019*. Moscow: BMSTU, pp. 699–704 (in Russian).
9. Losev, G.I., 2022. Development of a Trajectory-Space Filtering Algorithm for Noise Emission from Moving Objects. *Al'manac of Modern Metrology*, (3), pp. 83–93 (in Russian).
10. Losev, G.I., 2023. Vector-Phase Algorithm for Determining the Directionality of Hydroacoustic Noise Sources. In: Russian Acoustical Society, 2023. *Proceedings of the XXXV Session of Russian Acoustical Society, Moscow, February 13–17, 2023*. Moscow: GEOS, pp. 372–378 (in Russian).
11. Konson, A.D. and Volkova, A.A., 2022. Noise Signal Modulation at the Ship Rolling and Pitching due to Fluctuating Interference of Beams. *Fundamental and Applied Hydrophysics*, 15(4), pp. 74–81 (in Russian).
12. Grinenkov, A.V. and Mashoshin, A.I., 2024. Algorithm for Determining the Coordinates and Motion Parameters of an Underwater Noise Source without Special Maneuvering of Observer Vessel. *Gyroscopy and Navigation*, 32(2), pp. 98–122 (in Russian).
13. Anyukhin, S.G., Proshutinsky, D.A. and Permyakov, M.P., 2022. Criteria for Selection of Means for Detecting Underwater Intruder Depending on the Features of Protected Objects Water Area. *Akademicheskiy Vestnik Voysk Natsionalnoy Gvardii Rossiyskoy Federatsii*, (2), pp. 37–42 (in Russian).
14. Kartsan, I., Lutsyshen, V., Nerush, A. and Tuzov, N., 2024. Method for Estimating the Informativity Contained in a Hydroacoustic Signal. *Modern Innovations, Systems and Technologies*, 4(3), pp. 501–514 (in Russian).
15. Kartsan, I.N., Neruch, A.V. and Tuzov, N.A., 2024. Evaluation of Transcribing Abilities in Hydroacoustic Communication Channel. *Zašita Informacii. Inside*, (5), pp. 62–65 (in Russian).

Submitted 12.02.2025; accepted after review 21.03.2025;
revised 24.06.2025; published 30.09.2025

About the authors:

Alena V. Nerush, Laboratory Research Assistant, Sevastopol State University (33 Universitetskaya St., Sevastopol, 299053, Russian Federation), **ORCID ID: 0009-0008-7547-9227,** *nerush03@mail.ru*

Nikolai A. Tuzov, Laboratory Research Assistant, Sevastopol State University (33 Universitetskaya St., Sevastopol, 299053, Russian Federation), **ORCID ID: 0009-0004-6131-2355,** *tuzov.nikol@gmail.com*

Igor N. Kartsan, Professor of IT Security Chair, Sevastopol State University (33 Universitetskaya St., Sevastopol, 299053, Russian Federation), DSc (Tech.), Associate Professor, **Scopus Author ID: 56825941300**, **ORCID ID: 0000-0003-1833-4036,** *kartsan2003@mail.ru*

Contribution of the authors:

Alena V. Nerush – critical analysis of materials, processing and describing the study results, preparing the text, drawing conclusions

Nikolai A. Tuzov – experiment conduction, literature analysis on the study topic, analysis and discussion of the results, preparing graphic materials for the article

Igor N. Kartsan – problem statement, analytical research on the content, preparation of the article text and graphic materials

All the authors have read and approved the final manuscript.

ISSN 2413-5577, Ecological Safety of Coastal and Shelf Zones of Sea, 2025, No. 3, pp. 141–162.

Original paper

Optical Characteristics of Atmospheric Aerosol over the Black Sea and Reservoirs of the Middle and Lower Volga for 2022–2024

D. V. Kalinskaya [1, 2] *, **A. A. Molkov** [1, 3]

[1] *Lobachevsky Nizhny Novgorod State University, Nizhny Novgorod, Russia*
[2] *Marine Hydrophysical Institute of RAS, Sevastopol, Russia*
[3] *A.V. Gaponov-Grekhov Institute of Applied Physics of RAS, Nizhny Novgorod, Russia*
* *e-mail: kalinskaya_d_v@mail.ru*

Abstract
The paper presents the results of a comprehensive analysis of atmospheric aerosol based on *in situ* photometer SPM measurements data, MODIS (Aqua/Terra) and VIIRS satellite data, and HYSPLIT air flow modeling data. The study was conducted by comparing the optical characteristics obtained during the same periods over the Black Sea region and tracking the movement of aerosol towards reservoirs located in different parts of the Volga River: the Middle Volga (Gorky and Cheboksary Reservoirs) and the Lower Volga (Kuybyshev and Volgograd Reservoirs). The analysis revealed the days of dust aerosol presence in the atmosphere. We compared the periods when high values of the aerosol optical depth (AOD) and low values of the Angstrom exponent were obtained for the Black Sea and for the Volga River. The periods when high values of AOD and low values of the Angstrom exponent were obtained simultaneously for the Black Sea and for the Volga River region were identified. A key finding of this study is the stability of the aerosol optical characteristics over the Black Sea and the Kuybyshev Reservoir, which persisted even during intensive dust transport from the Sahara Desert. This proves that regional algorithms for the Black Sea can be used to restore the brightness coefficients from satellite data when there is dust aerosol in the atmosphere over the Volga River reservoirs. The presented results provide a preliminary description of the atmosphere optical characteristics in the study regions and may be useful for testing the accuracy of standard atmospheric correction algorithms for satellite data.

Keywords: SPM, MODIS, VIIRS, SILAM, backward trajectories of HYSPLIT, Angstrom exponent, dust aerosol, smoke aerosol, aerosol optical depth, AOD, Volga, Black Sea, atmospheric aerosol

Acknowledgements: The work was carried out at the expense of the RNF grant No. 23-17-00071 (“Volga bio-optical algorithms”), https://rscf.ru/project/23-17-00071. The authors express their gratitude to S. M. Sakerin and D. M. Kabanov for providing the SPM photometer and its software and for the possibility of using high-quality photometric measurement data. The authors also thank Air Resources Laboratory (ARL) and the developers of HYSPLIT for providing high-quality simulation data in a timely manner. The authors express their gratitude to Kapustin I.A. and Leshchev G.V. for their participation in performing *in situ* measurements. For the Black Sea the researches were performed

© Kalinskaya D. V., Molkov A. A., 2025

This work is licensed under a Creative Commons Attribution-Non Commercial 4.0 International (CC BY-NC 4.0) License

under state assignment of the Marine Hydrophysical Institute of the Russian Academy of Sciences FNNN-2024-0012 “Analysis, diagnosis and operational forecast of the state of hydrophysical and hydrochemical fields of marine waters based on mathematical modeling using data from remote and contact measurement methods” (“Operational Oceanology”).

For citation: Kalinskaya, D.V. and Molkov, A.A., 2025. Optical Characteristics of Atmospheric Aerosol over Reservoirs of the Middle and Lower Volga in Comparison with the Black Sea for the Period 2022–2024. *Ecological Safety of Coastal and Shelf Zones of Sea*, (3), pp. 141–162.

Оптические характеристики атмосферного аэрозоля над Черным морем и водохранилищами Средней и Нижней Волги за 2022−2024 годы

Д. В. Калинская [1, 2] *, **А. А. Мольков** [1, 3]

[1] *Нижегородский государственный университет им. Н. И. Лобачевского, Нижний Новгород, Россия*
[2] *Морской гидрофизический институт РАН, Севастополь, Россия*
[3] *Институт прикладной физики им. А. В. Гапонова-Грехова РАН, Нижний Новгород, Россия*
* *e-mail: kalinskaya_d_v@mail.ru*

Аннотация

Представлены результаты комплексного анализа атмосферного аэрозоля с использованием натурных фотометрических измерений *SPM*, спутниковых данных *MODIS* (*Aqua*/*Terra*), *VIIRS*, а также моделирования траекторий перемещения воздушных потоков *HYSPLIT*, проведенного в рамках сопоставления оптических характеристик атмосферного аэрозоля над регионом Черного моря и водохранилищами бассейна р. Волги (Горьковским, Чебоксарским, Куйбышевским и Волгоградским). Анализ основан на данных, полученных в одни и те же периоды, с последующим отслеживанием перемещения аэрозоля в направлении волжских водохранилищ. В ходе работы выявлены дни с присутствием в атмосфере пылевого аэрозоля. Проведено сравнение периодов, в которые были получены высокие значения аэрозольной оптической толщины и низкие − параметра Ангстрема над Черным морем и Волгой. Выявлены периоды, когда данные аномалии наблюдались синхронно в обоих регионах. Ключевой результат данного исследования состоит в том, что оптические характеристики аэрозоля над Черным морем и Куйбышевским водохранилищем в период интенсивного пылевого переноса со стороны пустыни Сахары не претерпели значимых изменений. Это свидетельствует о возможности применения региональных алгоритмов, разработанных для Черного моря, при восстановлении коэффициентов яркости по спутниковым данным над водоемами р. Волги в условиях присутствия в атмосфере пылевого аэрозоля. Представленные результаты формируют предварительное описание оптических характеристик атмосферы в исследуемых регионах и могут быть использованы для оценки точности стандартных алгоритмов атмосферной коррекции спутниковых данных.

Ключевые слова: *SPM, MODIS, VIIRS, SILAM*, обратные траектории *HYSPLIT*, параметр Ангстрема, пылевой аэрозоль, дымовой аэрозоль, аэрозольная оптическая толщина, AOT, Волга, Черное море, атмосферный аэрозоль

Благодарности: работа выполнена за счет гранта РНФ № 23-17-00071 («Волжские биооптические алгоритмы»), https://rscf.ru/project/23-17-00071. Авторы выражают признательность С. М. Сакерину и Д. М. Кабанову за предоставление фотометра *SPM* и программное обеспечение к нему и за возможность использования качественных данных фотометрических измерений. Также авторы благодарят *Air Resources Laboratory's* (*ARL*) и разработчиков *HYSPLIT* за своевременное предоставление качественных данных моделирования. Авторы выражают благодарность И. А. Капустину и Г. В. Лещеву за участие в выполнении натурных измерений. Исследования над Черным морем выполнены в рамках темы государственного задания Морского гидрофизического института РАН FNNN-2024-0012 «Анализ, диагноз и оперативный прогноз состояния гидрофизических и гидрохимических полей морских акваторий на основе математического моделирования с использованием данных дистанционных и контактных методов измерений («Оперативная океанология»)».

Для цитирования: *Калинская Д. В., Мольков А. А.* Оптические характеристики атмосферного аэрозоля над Черным морем и водохранилищами Средней и Нижней Волги за 2022−2024 годы // Экологическая безопасность прибрежной и шельфовой зон моря. 2025. № 3. С. 141–162. EDN AIMHIF.

Introduction

The primary objective of satellite oceanography is to obtain reliable information about the state of various water bodies and to study trends in changes in their water quality as well as to assess the impact of anthropogenic and biogenic factors on water areas. A variety of natural phenomena, including forest fires, dust storms and volcanic eruptions, as well as a range of technological processes, result in an increase in the amount of harmful substances entering the atmosphere and hydrosphere [1–3]. When solid fuels are burned, toxic chemicals are released into the environment as part of the exhaust gases. The most prevalent of these are carbon monoxide, sulfur dioxide, nitrogen oxides, hydrocarbons and dust [4–6].

The growing pollution of air basins in several cities demonstrates the substantial impact of modern industrial production on the natural environment, disrupting the existing balance and cycle of substances and energy. Therefore, long-term programs to maintain the normal functioning of natural ecological systems are becoming increasingly important [2−6].

The objects of study are the Black Sea (western and Crimean coasts, where the AERONET (AErosol RObotic NETwork) Galata_Platform (43.0° N, 28.2° E) and Sevastopol (44.58° N, 33.43° E)) and the Volga River reservoirs. The first measurements of atmospheric characteristics over the Black Sea were made as early as 1910, and systematic photometric observations within the framework of the international AERONET program have been conducted since 2006. In 2015, the second stage of photometric measurements was initiated using the domestic SPM (Sun Photometer Mobile) photometer analogous to the AERONET instruments.

Unlike the Black Sea, comprehensive studies of the Volga as a single ecological system have not yet been conducted. Effective river monitoring requires analysis of the entire water system, including three interrelated components: the atmosphere,

the aquatic environment and the aquatic organisms. The water body ecological and toxicological state is determined by interdependent processes such as water exchange with the atmosphere, transport of toxic substances through the air and entry of pollutants into the water [7]. Therefore, a comparison of data from these two regions enables the identification of both general patterns of aerosol transport and transformation, and processes that are specific to each region.

In 1995–2003, a large amount of data on gas emissions into the atmosphere was obtained in the Volga River basin. Analysis of this data revealed a trend toward improvement in atmospheric conditions: total gas emissions into the atmosphere over the Volga basin decreased by 2.0 million tons, from 9.1 million tons in 1995 to 7.1 million tons in 2003. In 2017–2019, as part of the federal project "Revitalization of the Volga," a concept was developed to reduce diffuse pollution of the Volga [8], based on an analysis of hydrological data on pollutants and atmospheric parameters.

Nevertheless, the current data are insufficient to solve a significant applied problem, namely the use of optical satellite information to assess the quality of the Volga River waters. Furthermore, the role of long-range intensive aerosol transport, particularly the influence of intensive air flow from the Black Sea region on atmospheric characteristics over the Volga basin, remains under-researched. In order to resolve these issues, a thorough investigation is necessary that incorporates data regarding the state of the atmosphere and the aquatic environment.

In this regard, the present study focuses on comparing the optical characteristics of atmospheric aerosols over the Black Sea and the Volga reservoirs, which allows for the identification of general patterns of aerosol particle transport and transformation in both regions.

The analysis employed *in situ* data, MODIS (Aqua/Terra) satellite data, Visible Infrared Imaging Radiometer Suite (VIIRS) data and the results of air flow modeling using the HYSPLIT model for four reservoirs located in different parts of the Volga River: the Middle Volga (Gorky and Cheboksary Reservoirs) and the Lower Volga (Kuybyshev and Volgograd Reservoirs) (Fig. 1), in comparison with similar data obtained over the Black Sea.

For each of the regions studied, background characteristics of atmospheric aerosols were determined, serving as a reference point for assessing the consequences of aerosol impact. Background characteristics in this work refer to the average values of optical parameters calculated with the exclusion of emissions. The background aerosol in the regions under study consists primarily of submicron fractions of mineral dust and other aerosols (predominantly sulphate) of continental origin. These particles have penetrated through the cloud filter into the upper troposphere at an altitude of 2–3 km over the oceans and 5 km over the continents and have been distributed there relatively evenly, with a particle number concentration of ~ 300 cm^{-3} at standard temperature and pressure [9].

To compare, Table 1 demonstrates such background characteristics of atmospheric aerosol as aerosol optical depth (AOD) at a wavelength of 500 nm (AOD(500)) and Angstrom exponent (α) in different regions. For instance, in the Northern Tian Shan region, which is affected by dust aerosols, the AOD(500) value during the period of aerosol transport to the region was found to be 0.74 ± 0.14, which exceeds the background values (Table 1) by more than three times [10]. In the Baikal region, which is mainly affected by seasonal fires, the AOD values exceed background levels by six to eight times across most of the spectrum when smoke is present in the atmosphere [11]. The background values for the region of Middle Urals, which is subject to dust emissions and smoke transport from fires, are presented based on the results of optical characteristic measurements conducted at the Kourovka Astronomical Observatory (Sverdlovsk Oblast) and in Ekaterinburg [12]. The estimation of background values of atmospheric aerosol for central Russia can be made based on the variability of optical characteristics obtained in Moscow and the Moscow region. Thus, background values for this region, according to data from the Zvenigorod Scientific Station of A. M. Obukhov Institute of Atmospheric Physics RAS, are given in [13]. For the Siberian region, background values for atmospheric aerosols were obtained from photometric measurements at the Fonovaya station, Tomsk Oblast. During periods of intense fire in this region, the AOD(500) index has been recorded at 0.95 ± 0.86, which is approximately six times higher than background values and 2.5 times higher than the typical values for smoke aerosols [14]. The establishment of background levels is a prerequisite for the subsequent identification of anomalies caused by long-range transport of aerosols.

Table 1. Background optical characteristics of atmospheric aerosol obtained over various regions

Region/city	Background AOD(500)	Angstrom exponent α
Northern Tian Shan	0.24 ± 0.09	–
Baikal region	< 0.1	–
Sverdlovsk Oblast	0.135 ± 0.128	–
Ekaterinburg	0.168 ± 0.126	1.239 ± 0.3
Zvenigorod	0.17 ± 0.06	1.46 ± 0.4
Tomsk Oblast	0.16 ± 0.08	1.4 ± 0.4

In particular, periods were selected for analysis when the values of AOD and the Angstrom exponent deviated significantly from background levels. This facilitated the identification of episodes of intensive air flow from the Black Sea region towards the Volga basin, and the subsequent quantitative assessment of their impact on the optical properties of the atmosphere over reservoirs.

Ground-based photometric measurements were used to verify satellite data and modeling results. Ground-based solar photometry is one of the main remote sensing methods for determining the composition of atmospheric gases and aerosols, along with satellite remote sensing. The primary benefit of satellite systems is their extensive coverage capacity, which facilitates the description of the spatial distribution of the optical characteristics of the atmosphere (e.g., MODIS radiometers on the Terra and Aqua satellites). However, the underlying surface reflectivity is unpredictable enough, which significantly limits the AOD determination accuracy, allowing reliable data to be obtained only in a narrow spectral range. This creates serious difficulties in determining the composition of aerosol particles. The advent of remote sensing methods has contributed to the emergence of innovative ship- and satellite-based technologies and systems, facilitating the operational monitoring of water quality in such eutrophic water bodies as the Gorky, Kuybyshev and Volgograd Reservoirs. In light of the constraints imposed by remote methods, *in situ* studies of aerosols employing photometers continue to be a pertinent undertaking. The factors influencing the composition of aerosols, including meteorological conditions, are not yet fully elucidated.

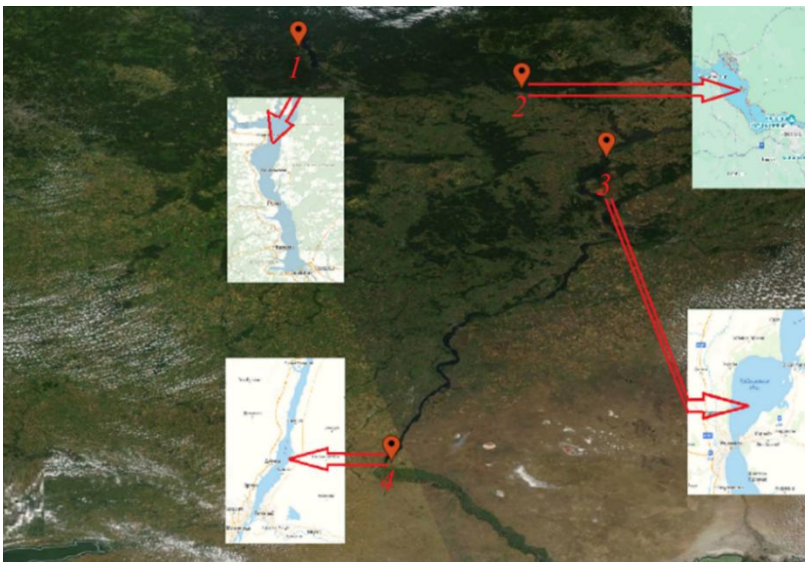

Fig. 1. Location of the study geographical objects on the Volga River. The numbers denote reservoirs: *1* – Gorky Reservoir; *2* – Cheboksary Reservoir; *3* – Kuybyshev Reservoir; *4* – Volgograd Reservoir (Satellite VIIRS)

This study aims at a comprehensive analysis of the optical characteristics of atmospheric aerosols over the Black Sea and four reservoirs in the Volga River basin (Gorky and Cheboksary in the Middle Volga, Kuybyshev and Volgograd in the Lower Volga) in 2022–2024 based on *in situ* measurements, satellite observations (MODIS/Aqua-Terra, VIIRS) and HYSPLIT air flow trajectory modeling data. The research objectives include comparing the spatio-temporal variability of aerosol parameters over the specified regions, tracking the transport of aerosol masses from the Black Sea towards the Volga reservoirs, and analyzing the characteristics of their distribution over these water areas.

Instruments and materials

The AOD was determined using *in situ* measurements obtained from two types of solar photometer: the AERONET reference instrument Cimel [15] and its domestic counterpart SPM (Sun Photometer Mobile) [16]. Both instruments operate in the wavelength range of 340–2134 nm. When operating and calibration conditions are met, the error in determining AOD is 0.01–0.02 and in determining the atmosphere moisture content is approximately 0.1 g/cm². A detailed description of the calibration and calculation methods for the desired characteristics is provided in [16–18].

Satellite data on AOD and Angstrom exponent were obtained using the MAIAC (Multi-Angle Implementation of Atmospheric Correction) algorithm based on MODIS/Terra and MODIS/Aqua data [19, 20]. The spatial resolution of the algorithm is 1 km, which facilitates the tracking of small-scale urban pollution, smoke from fires (including small local outbreaks), and dust storms. The selection of this product was determined by its accessibility, high resolution, and capacity to monitor aerosol dynamics in near real time.

In order to analyze the sources of aerosol transport in the Black Sea region as well as the Gorky, Kuybyshev and Volgograd Reservoirs, the results of modeling the backward trajectories of air flow movements were used. This modeling was carried out using the HYSPLIT (Hybrid Single-Particle Lagrangian Integrated Trajectory model developed by Air Resources Laboratory (ARL)) software package [1)]. The simulation results demonstrate the predominance of western air mass transport in the region under study [1)]. This study presents the first analysis of not only backward but also forward trajectories of air currents over the Black Sea. This made it possible to compare optical characteristics with the time shift of aerosol movement over the Black Sea and, several days later, over the reservoirs.

The VIIRS radiometer set provides users with Deep Blue NASA Standard Level-2 (L2) aerosol products from the Joint Polar Satellite System (JPSS). Since 17 February 2018, the VIIRS Deep Blue Aerosol (DBA) algorithm has been used

[1)] Available at: http://ready.arl.noaa.gov/HYSPLIT.php [Accessed: 25.08.2025].

to obtain AOD values [21, 22]. The Deep Blue algorithm is used to analyze data obtained over land, while the Satellite Ocean Aerosol Retrieval (SOAR) algorithm is used over water areas. Data obtained in certain VIIRS operating ranges and processed using two algorithms described above provide ultimately reference AOD L2 Deep Blue values at a wavelength of 550 nm for the region under study [22, 23].

The Dark Target/Bright Target Algorithm (DBA) was applied to VIIRS data to create a long-term climate data series on atmospheric aerosols. The DBA algorithm was originally developed to detect aerosols over bright surfaces. To achieve this objective, a global database of surface reflectivity coefficients with a resolution of 0.1° in the visible spectrum was created using the method described in [24]. The aerosol type and AOD are determined simultaneously using look-up tables based on satellite observations. The MODIS Collection 6 (C6) data are reprocessed using an algorithm that employs three different approaches to determine surface reflectivity coefficients in different terrain types (arid/semi-arid regions, vegetated, urban/built-up and transitional areas). To identify smoke aerosols, the spectral curvature method is used, based on the ratio of surface reflectivity coefficients at wavelengths of 412/488 and 488/670 nm. In addition to VIIRS data, new models of non-spherical dust particles are also used to improve the accuracy of AOD determination. In 2020, the latest V011 DB L2 aerosol products were integrated into the data processing system. The methodology permits the extension of the range of detectable surfaces from the brightest to the very darkest [24, 25], improving aerosol monitoring capabilities significantly.

One of the tasks of the DBA and SOAR algorithms is to determine the types of atmospheric aerosols during the daytime in the absence of clouds and snow. Over land, the aerosol type is classified based on the AOD values, Angstrom exponent (α), Lambert-equivalent reflectivity (LER) and brightness temperature. The combined aerosol type over land and ocean is determined based on pixels that have passed quality control [21, 22, 24].

CALIPSO satellite data were analyzed to determine the predominant aerosol type. The main objective of CALIPSO is to measure the characteristics of aerosols and clouds on a global scale. The CALIPSO algorithm classifies aerosols by type based on the measured depolarization coefficient (δv): pure marine aerosol ($\delta v \in [0.025–0.05]$), particles of polluted dust or smog ($\delta v \in [0.05–0.15]$), most likely dust aerosol ($\delta v \in [0.15–0.5]$). The spatial resolution for most types of aerosols is 80 km, with the exception of clean marine and polluted continental aerosols. About 80% of smog and 60% of polluted dust aerosols are found over the water surface. Clean dust is distributed approximately evenly over both land and water surfaces [25, 26].

Measurements of the optical characteristics of the atmosphere over the Black Sea and the Volga River were carried out from small vessels or from the shore. The periods of atmospheric aerosol measurements over the reservoirs of the Volga River are shown in Table 2. Measurements over the Black Sea were carried out simultaneously.

Table 2. Qualitative and quantitative data on measurements of main atmosphere optical characteristics over reservoirs of the Volga River

Reservoir	Period	Number of measurements
Gorky Reservoir	Spring–summer 2022–2024	292
Cheboksary Reservoir	09.09.2023–10.09.2023; 16.09.2023–17.09.2023	18
Kuybyshev Reservoir	17.07.2023–28.07.2023; 09.09.2023–16.09.2023	58
Volgograd Reservoir	28.05.2024–07.06.2024	13

As Table 2 shows, in the case of the Gorky Reservoir, the focus is on seasonal trends rather than specific periods. This discrepancy can be attributed to the fact that while expeditions in the region of the reservoir were ongoing, the measurements were taken over the course of a single day, a week or more.

During expeditions to study the optical properties of the atmosphere over the Middle and Lower Volga region, data were obtained on the AOD variability across the entire operating range of the SPM photometer, namely at 11 wavelengths: 340, 379, 441, 501, 548, 675, 872, 940, 1244, 1020 and 1556 nm. The most interesting channels for research are those close to satellite channels: comparative analysis of remote and *in situ* data makes it possible to solve many problems in both optics and hydrophysics in general. For central Russia, the AOD values above 0.3 at a wavelength of 500 nm are considered to be high. The present study determines the type of aerosol and the region that was the source of aerosol activity for dates with such values.

Results

As previously mentioned, 2015 marked the start of a period in which the optical properties of atmospheric aerosols over the Black Sea were monitored using an SPM photometer. This enabled a new stage of comparative studies of different regions equipped with similar instruments to begin. The nearest water body where photometric measurements are carried out is the Volga River basin. This paper presents a comparative analysis of the optical characteristics of atmospheric aerosols obtained over the Black Sea (in the western and Crimean coastal zones), alongside data from regular measurements taken over the Gorky, Cheboksary, Kuybyshev and Volgograd Reservoirs, as well as in the Nizhny Novgorod Oblast, between April 2022 and July 2024. The activity of dust and smoke aerosol transport from forest fires was also studied during this period.

Analysis of seasonal AOD trends in many regions of central and southern Russia revealed a primary maximum in spring and a secondary maximum in summer, the latter of which is more pronounced during intense forest fires. As is well known,

a large number of forest fires are recorded in both the Black Sea region and the Nizhny Novgorod Oblast during the summer period. These fires can cause cloudiness in the atmosphere and, accordingly, lead to an increase in the values of the main optical characteristics of atmospheric aerosols during this period [25]. It is known that dust and smoke aerosols are characterised by AOD values that are more than twice the monthly average [1−3]. Fig. 2 shows average daily values of AOD(500) for the period of synchronous atmospheric studies over the Black Sea (Crimean coast (Fig. 2, *a*) and western coast of the Black Sea (Fig. 2, *b*)) and the Volga River basin (Fig. 2, *c*). As can be seen, high AOD(500) values were recorded over the Volga River in April, July and August 2022 as well as in April 2023. To determine the main source of aerosol input that has the greatest impact on the properties of the underlying surface as determined by remote sensing methods, it is necessary to analyze the seasonal and daily variability of aerosol optical characteristics.

Fig. 2, *b* shows that the maximum AOD values were observed on 13 April, 6, 7, 24–27 July, 5–8, 24–27 August in 2022; on 12, 24–28 April, 25–27 May, 18, 26–28 July in 2023; and on 4 June 2024. In general, increases in AOD values are not short-term events occurring over the course of a single day, but rather periodic in nature. This can be the result of intense dust transport and large-scale forest fires, the latter of which are a source of burning biomass aerosols (smoke aerosols). The only exception is a slight increase in AOD in the summer of 2024. However, it should be noted that measurements only began at the end of May in 2024.

Gorky Reservoir

Since 2022, the SPM photometer has been continuously monitoring optical characteristics in the study area, providing background characteristics of atmospheric aerosols over the Gorky Reservoir and Nizhny Novgorod. In the 2016–2017 studies, the background values were considered to be AOD(500) ≈ 0.18 and $\alpha \approx 1.45$, but later regular measurements covering not only the summer period showed that the background values in the study region were lower: AOD(500) = 0.12 and $\alpha = 1.22$ [26]. Analysis of particle size distribution revealed no predominance of particles of a certain size, whether large or small, for background aerosols.

To identify sources of aerosol activity, satellite data were analyzed for all days on which elevated values of atmospheric aerosol optical properties were recorded during *in situ* measurements.

As Fig. 2 shows, the average daily AOD(500) value of 0.28 recorded on 13 April 2022 is the highest one for the entire spring period of 2022. The results of modeling the backward trajectories of air flows for that day using the HYSPLIT model showed the movement of dust aerosol at an altitude of 3 km from the Karakum side. This means that the increase in AOD on 13.04.2022 is due to the presence of dust aerosol in the atmosphere over the region under study.

During the summer of 2022, a significant number of days were observed to have elevated AOD values, with levels exceeding more than twice the annual average

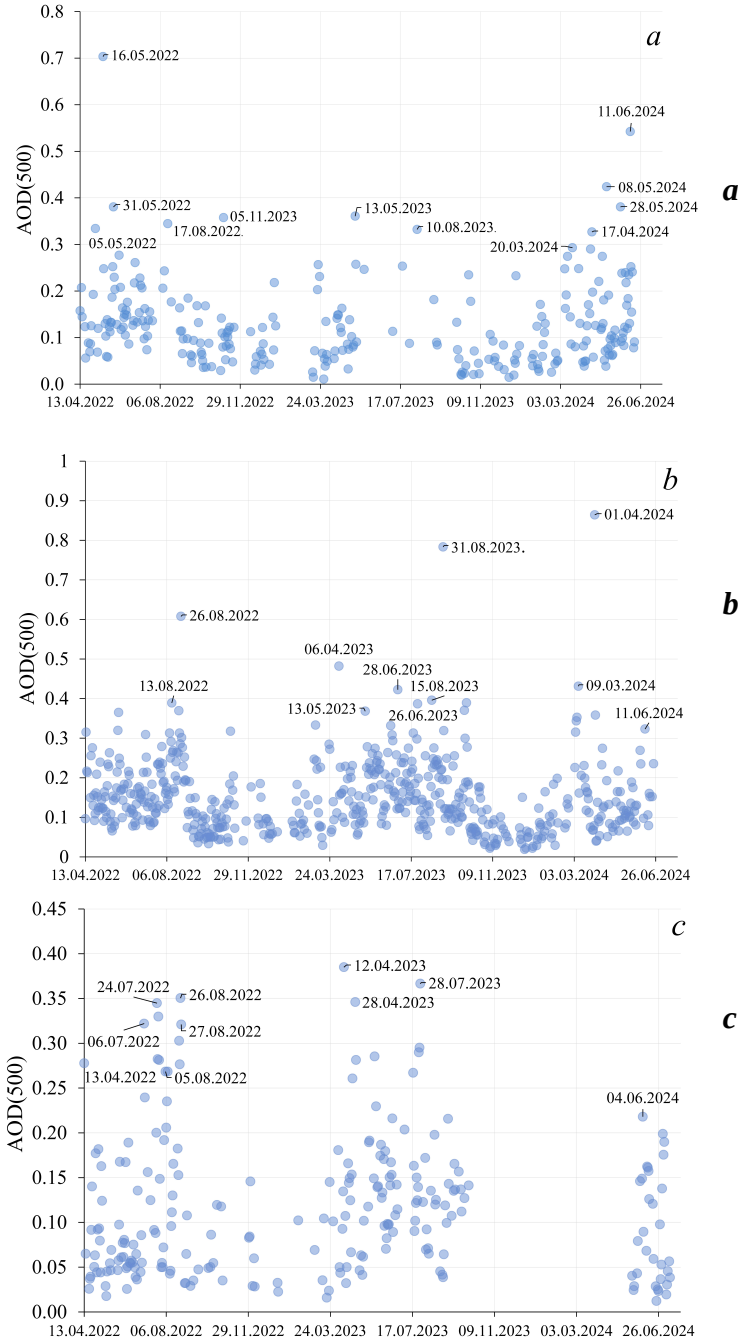

Fig. 2. Average variability of aerosol optical depth (AOD) at a wavelength of 500 nm: over the Black Sea, the Southern Coast of Crimea zone and the Kerch Strait, from *AERONET* station data (288 days) (*a*); over the Black Sea, from Section_7 station (Romania) (568 days) (*b*); over the Volga River, from stations data (224 days) (*c*)

across the entire spectral range. A thorough analysis of satellite data, complemented by the findings from backward trajectory modeling, revealed that the observed increase in AOD values was predominantly attributable to the presence of smoke aerosols from forest fires, which were localized east of the Gorky Reservoir. The average daily AOD(500) value of 0.39 on 12 April 2023 represents the maximum for the entire measurement period under study. The maximum AOD value (AOD(500) = 0.45) on that day was recorded at 14:00. Satellite data indicates that MAIAC AOD values over the Gorky Reservoir were within the range of (0.4 ± 0.01). The backward trajectories of air flows were simulated using the HYSPLIT software package, with the start time of the simulation set at 14:00 UTC, the time when the maximum AOD values were recorded. The transport area coincided with the area in which the AIRS MODIS/Aqua algorithms determined an increased concentration of dust aerosols. A thorough examination of the contribution of coarse and fine aerosol particles to the total AOD(500) revealed that elevated AOD values were predominantly attributable to the presence of fine particles, which constituted up to 80% of the total. MAIAC satellite data confirm that AOD values exceed background levels, which is consistent with the results of *in situ* measurements.

The VIIRS Deep Blue algorithm for 24 April 2023 identified the presence of dust particles, as well as mixed and background aerosols (Fig. 3). High Angstrom exponent values for 24–28 April 2023 ($\alpha > 2$) confirm that the elevated AOD values are attributable to the presence of finely dispersed absorbing aerosols in high concentrations.

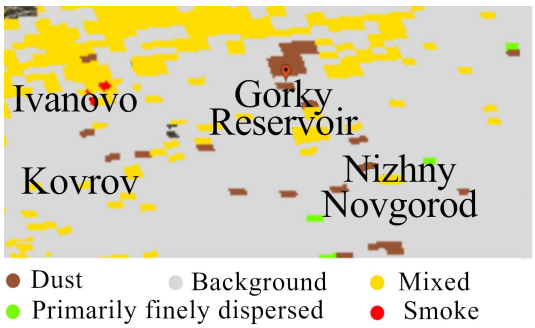

Fig. 3. Satellite images obtained using the VIIRS spectroradiometer (flight time 10:33 UTC) using the VIIRS Deep Blue algorithm for 24 April 2023 (Archive AERDB_L2_VIIRS_NOAA20_NRT doi:10.5067/VIIRS/AERDB_L2_VIIRS_NOAA20_NRT.002; AERDB_L2_VIIRS_NOAA20 doi:10.5067/VIIRS/AERDB_L2_VIIRS_NOAA20.002 (date of access: 20 January 2024)

High AOD values were also recorded at the end of April and the end of July 2023. Analysis of model and satellite data to determine the source of aerosol activity that influenced the variability of AOD values at the end of April 2023 revealed no signs of dust transport or intense fires, when the smoke could have moved into the atmosphere of the region under study.

The values of AOD(500) were determined to be 0.29 on 25 May 2023, at $\alpha = 0.7$. When determining the predominant aerosol type using the VIIRS Deep Blue algorithm, the presence of mixed and fine aerosols was detected on that day.

Statistical analysis revealed that AOD values exceeding the monthly average were observed on 26 of the 226 days of observation. Elevated AOD values were mainly observed on days when smoke and dust aerosols were present in the atmosphere over the study region, but they were also recorded on days when anthropogenic aerosols were detected. In some cases, the origin of aerosol activity could not be ascertained.

Given the absence of documented transport from Africa via the Black Sea during the study period, a direct comparison between the optical characteristics obtained for this reservoir and those of the Black Sea stations was not feasible.

Cheboksary Reservoir

The expedition to the Cheboksary Reservoir was the shortest, with a duration of four days. During this period, AOD(500) values approximating the background values for the Nizhny Novgorod region were obtained (average AOD(500) = 0.11).

Average Angstrom exponent $\alpha = 1.7$ demonstrates the predominance of fine particles during the study period. This is confirmed by data on particle size distribution: the contribution of the coarse mode is only 21% of the total AOD(500) value.

Analysis of optical characteristic data for the periods 9–10 and 16–17 September 2023 for the Black Sea stations confirmed the presence of fine and background aerosols over the entire Black Sea water area (average AOD(500) values for both stations did not exceed 0.12).

Kuybyshev Reservoir

In this area, high AOD(500) values (twice as high as background levels) were recorded on 26–28 July 2023. During the entire expedition period, the maximum AOD values over the Kuybyshev Reservoir were recorded on 28 July 2023 (average daily AOD(500) value = 0.38, with AOD(500) = 0.43 at 10:00, which is twice the background values for central Russia). On the same day, the Angstrom exponent values were below 1.0 (Fig. 4). An analysis of the particle size distribution revealed that large particles constituted 45% of the total. Such a set of optical characteristics is typically obtained when recording arid aerosol over the region under study.

A comparative analysis of optical characteristics over the same period at the Kuybyshev Reservoir and the Black Sea revealed that two days before the maximum values were recorded over the Volga, high AOD values and low Angstrom exponent values were obtained at the Black Sea AERONET Galata_Platform (AOD(510) = 0.4 and $\alpha = 0.7$) and Sevastopol (AOD(510) = 0.39 and $\alpha = 0.8$) stations. The transport of dust aerosols from Africa towards Crimea and central Russia can last from one day to more than a week. This means that the aerosol recorded on 28 July 2023 over the Kuybyshev Reservoir could have been present in the atmosphere of the Black Sea on 26 July. This assumption can be confirmed by the results of HYSPLIT modeling of backward and forward air flow trajectories. Over the Black Sea, the maximum daily values of the AOD and the minimum values of the Angstrom exponent were recorded at 14:00 UTC at the Galata_Platform station (AOD(510) = 0.48; $\alpha = 0.48$) and at 16:00 at the Sevastopol station (AOD(500) = 0.4; $\alpha = 0.66$). Over the Black Sea, the maximum daily values of the AOD and the minimum values of the Angstrom exponent were recorded at 14:00 UTC at the Galata_Platform station (AOD(510) = 0.48; $\alpha = 0.48$) and at 16:00 at the Sevastopol station ((AOD(500) = 0.4; $\alpha = 0.66$). A thorough analysis

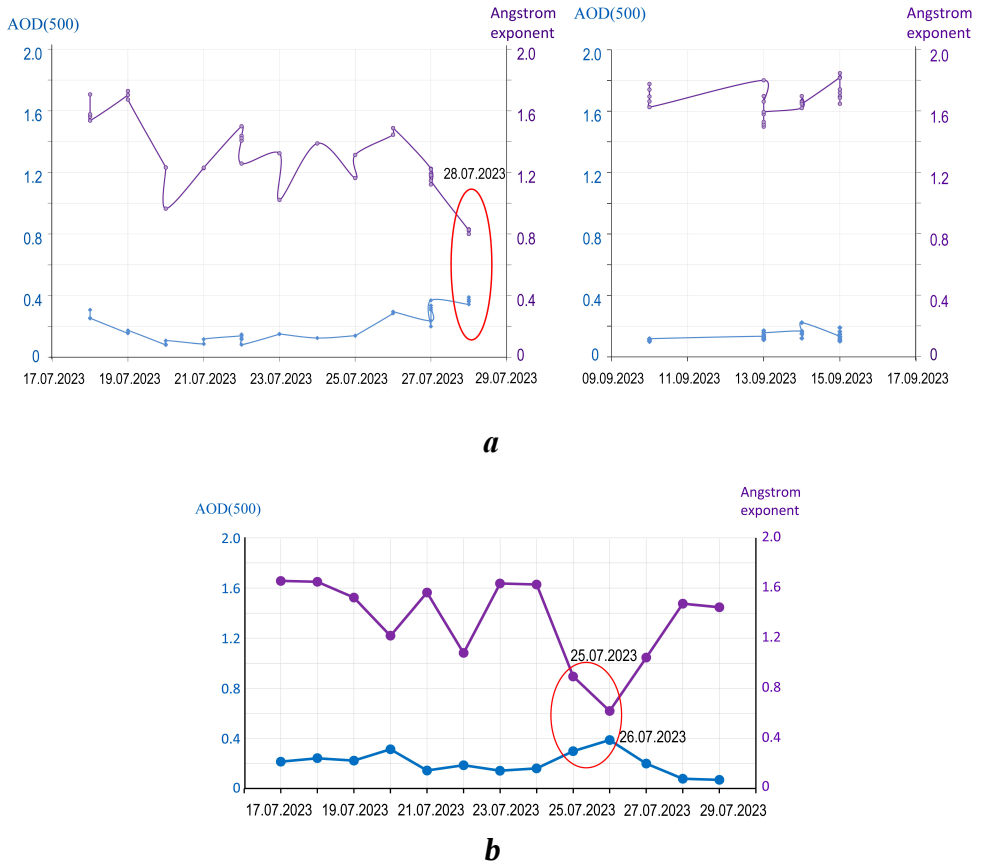

Fig. 4. Variability of the AOD and the Angstrom exponent during the expeditions over the Kuybyshev Reservoir (*a*) and over the Black Sea (*b*). The red ellipses denote cases of high AOD values and low Angstrom exponent values

of the variability of optical characteristics during the movement of dust aerosol over the Black Sea stations and over the Kuybyshev Reservoir indicates that the aerosol has not undergone any changes in composition or properties. The optical characteristics obtained on 26 July 2023 over Sevastopol and on 28 July over the Kuybyshev Reservoir differ minimally. Taking into account the distance from the Black Sea Galata_Platform and Sevastopol stations to the Kuybyshev Reservoir (~ 2000 km), the speed of dust aerosol movement was determined (~ 50 km/h).

Given the highest AOD(500) values over the Kuybyshev Reservoir were obtained on 28 July 2023 in the morning hours, the backward trajectories of air flows were calculated using the HYSPLIT model for 10:00 UTC. Analysis of modeling data revealed that at an altitude of 3 km, air mass transfer from the Sahara Desert is recorded (Fig. 5, *b*). As can be seen, based on the backward trajectories of air masses, the transfer from Africa was recorded both over the Black Sea AERONET stations (Fig. 5, *a*, *c*) and over the Kuybyshev Reservoir (Fig. 5, *e*).

The results of forward transport modeling confirm the presence of an air mass that was located over the Black Sea at an altitude of 3 km on 26 July 2023 and appeared over the Volga region on 28 July (Fig. 5, *b*, *d*).

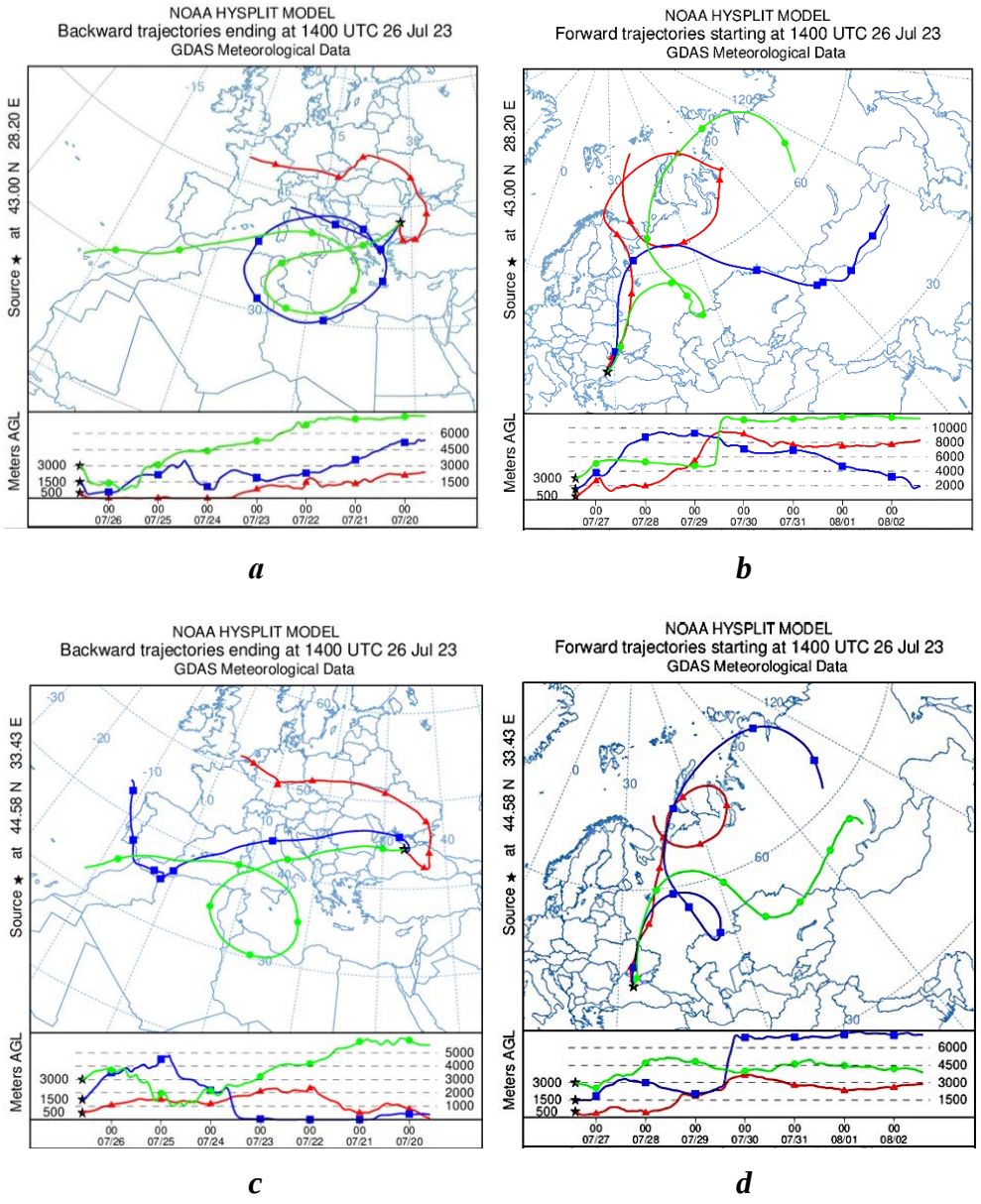

a ***b*** ***c*** ***d***

Fig. 5. HYSPLIT air flow simulation data: backward (*a*) and forward (*b*) trajectories for Galata_Platform station; backward (*c*) and forward (*d*) trajectories for Sevastopol station for 26 July 2023; backward trajectories for Kuybyshev Reservoir for 28 July 2023 (*e*)

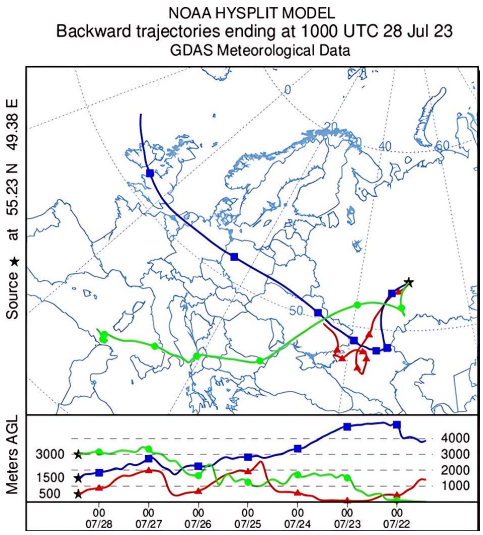

e

Continued Fig. 5

A satellite image of the Black Sea central part also shows a trail of haze, which can be dust aerosol transported from Africa. Satellite AOD measurements are not available for the Volga River. However, AOD values in the coastal region exceed background levels and exhibit minimal variation from the *in situ* SPM data for that particular day (according to MODIS data, AOD(500) values range from 0.35 to 0.36). To confirm the presence of a dust aerosol source, the CALIPSO satellite data were analyzed (Fig. 6).

1A thorough analysis of aerosol type data employing the CALIPSO satellite algorithm over the specified water body revealed the presence of substantial amounts of both polluted and clean dust aerosol. In conclusion, the results of both modeling and remote sensing confirm that the elevated AOD values, low Angstrom exponent values and high concentration of large aerosol particles are due to the presence of arid-origin particles in the atmosphere. A comprehensive analysis of the spatio-temporal variability of the optical properties of aerosols over the Kuybyshev Reservoir and the Black Sea it indicated that during intense dust transport from the Sahara Desert, the characteristics of aerosols remained constant, despite the difference in the time of their detection over the regions.

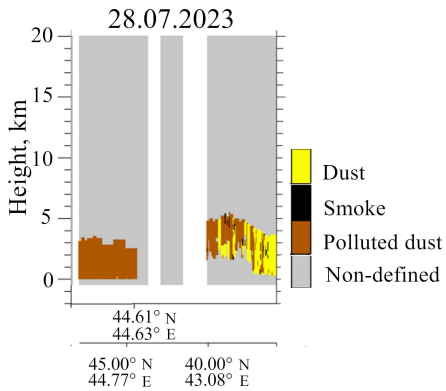

Fig. 6. CALIPSO satellite data for 28 July 2023

Consequently, upon detection of dust aerosols over the Volga River reservoirs, regional algorithms can be implemented to restore water brightness coefficients for the Black Sea.

Expedition data on this reservoir were obtained during the period from 31 May 2024 to 5 June 2024. The average values of the main optical characteristics for the study period were: AOD(500) = 0.16; $\alpha = 1$. On 31 May 2024, $\alpha = 0.4$, and the AOD values across the entire spectral range were at an average level.

Satellite (MODIS and VIIRS) measurements of the AOD for 31 May 2023 confirmed the presence of an area with elevated values southwest of the Volgograd Reservoir (Republic of Kalmykia) (Fig. 7). Analysis of backward trajectories based on HYSPLIT modeling results showed the transport of dust aerosols from the Karakum Desert on 30–31 May 2024.

Analysis of VIIRS and Aqua/MODIS satellite images (True Color channel) for 31 May 2024 over the Volgograd Reservoir revealed variable cloud cover during the flyovers of satellites at 10:02 and 10:28 UTC, respectively. The clearest image with minimal cloud cover was obtained using Terra/MODIS (True Color) at 7:24 UTC. It is well established that dust particles facilitate the process of moisture coagulation, leading to the formation of clouds comprising both fine and coarse dust aerosol fractions subsequent to the dust aerosol passage [27, 28]. The results of wind speed modeling using the ICON software package [29] at all altitudes up to 1500 m demonstrated transport from the Karakum Desert. The maximum wind transport intensity was documented at an altitude of 500 m (Fig. 8), which corresponded to the results of the HYSPLIT backward trajectory modeling.

The expedition measurements for the study period from 31 May 2024 to 7 June 2024, obtained over the Volgograd Reservoir, were compared with data from simultaneous observations over the Black Sea. Since the elevated AOD values over the Volgograd Reservoir recorded on 31 May 2024 were caused by the advection of dust aerosols from the Karakum Desert, air currents over the Black Sea prior to this event were not considered. However, it is noteworthy that on 4 and 5 July 2024, abnormally high AOD values were recorded over the Black Sea, with maximum values of AOD(500) = 0.3 and AOD(500) = 0.29, respectively. These values are more than one and a half times higher than the standard background levels. On these dates, measurements were obtained using an SPM photometer aboard R/V *Professor Vodyanitsky* (during its 131st voyage). A comprehensive analysis of *in situ* photometric measurements, VIIRS satellite data and HYSPLIT air flow modeling results confirmed the transport of dust aerosols to the study region (Fig. 9). Despite the fact that dust aerosol transport from Africa is frequently observed over the Black Sea during the spring and summer months, it is challenging to make an unequivocal quantitative evaluation of their contribution to the sea surface brightness coefficient in May and June for this region due to the coinciding intense phytoplankton bloom, which also results in a substantial increase in this parameter [30].

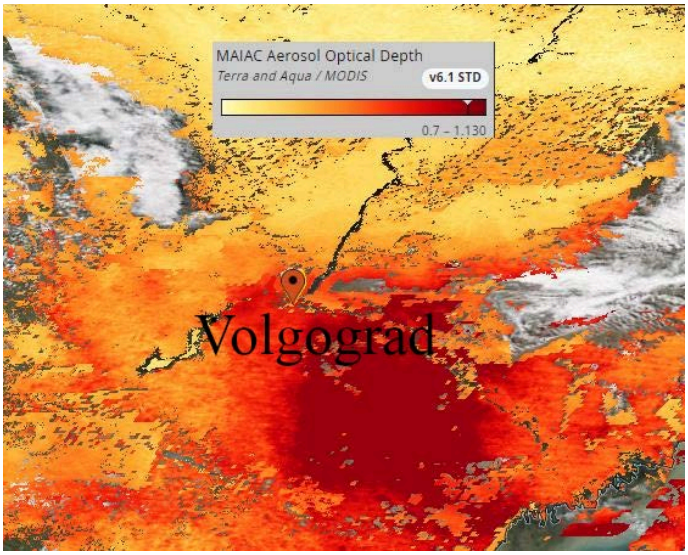

a

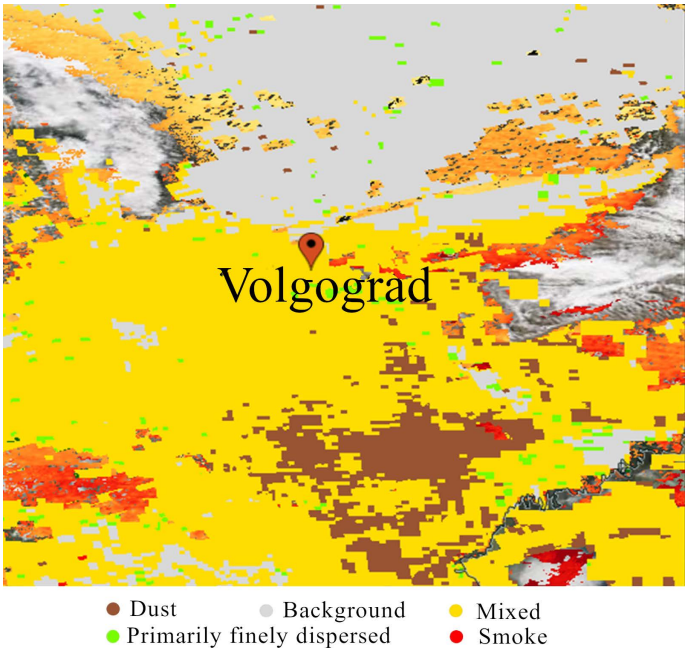

b

Fig. 7. Satellite data of MODIS (flight time 10:28 UTC) and VIIRS (flight time 10:02 UTC) for 30 May 2024: AOD distribution from the MAIAC algorithm (*a*), aerosol type determination from the VIIRS Deep Blue algorithm (*b*)

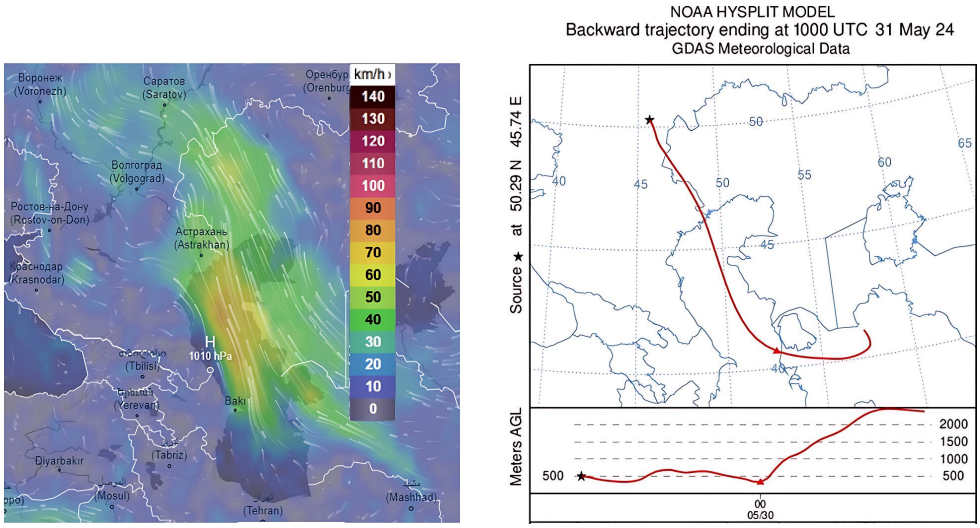

a ***b***

Fig. 8. The results of modeling wind speeds according to the ICON model (*a*); backward trajectories of air flow movement according to the HYSPLIT model (*b*) at an altitude of 500 m

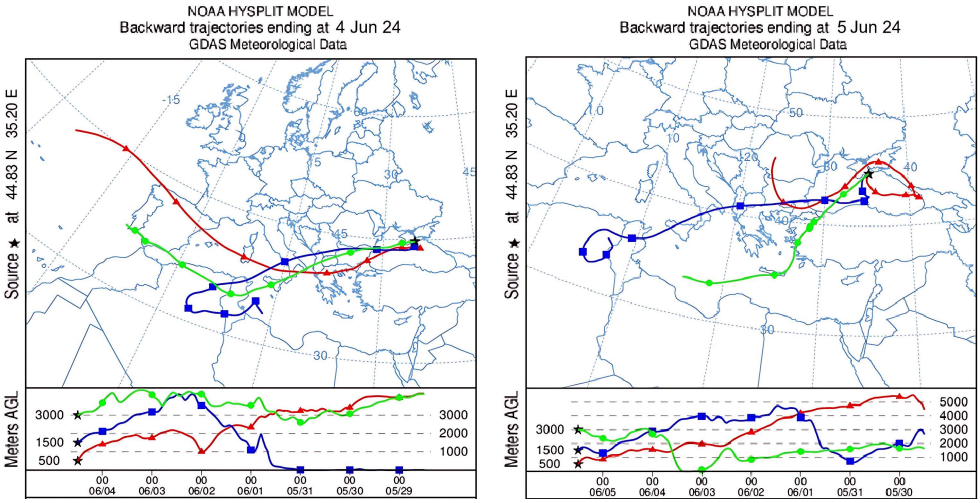

a ***b***

Fig. 9. The results of backward trajectories of air flow movement modeling according to the HYSPLIT model for 4 June 2024 (*a*) and 5 June 2024 (*b*)

Conclusion

A comparative analysis of the primary optical characteristics of the atmosphere above the Black Sea and four reservoirs on the Volga River was conducted, resulting in the identification of periods with background values and episodes with abnormally high AOD values. For these periods, a detailed analysis of satellite data and the results of air flow modeling was performed. In the majority of cases, the increase in AOD values in the studied regions was explained by dust aerosol advection. A comprehensive study of the transport of dust from the African continent has led to the identification of the temporal patterns of dust aerosol movement across the Black Sea towards the Kuybyshev Reservoir. Taking into account the distance between the Black Sea Galata_Platform and Sevastopol stations, and the Kuybyshev Reservoir, the average speed of dust aerosol movement was calculated (~ 50 km/h). The spring and summer periods have been identified as those of high AOD values and low Angstrom exponent over the Black Sea and the Volga River region. An important result of this study is the invariability of the optical characteristics of aerosols over the Black Sea and the Kuybyshev Reservoir during episodes of intense dust transport from the Sahara Desert. This indicates the possibility of using regional algorithms developed for the Black Sea to restore brightness coefficients based on satellite data over the Volga River reservoirs, considering the presence of dust aerosol.

REFERENCES

1. Rozenberg, G.V., Gorchakov, G.I., Georgievskiy, Yu.S. and Lyubovtseva, Yu.S., 1980. [Optical Parameters of Atmospheric Aerosol]. In: G. S. Golitsyn and A. M. Yaglom, eds., 1980. [*Atmospheric Physics and Climate Problems*]. Moscow: Nauka, pp. 216–257 (in Russian).
2. Ginzburg, A.S., Gubanova, D.P. and Minashkin, V.M. Influence of Natural and Anthropogenic Aerosols on Global and Regional Climate. *Russian Journal of General Chemistry*, 79, pp. 2062–2070. https://doi.org/10.1134/S1070363209090382
3. Kondratyev, K.Ya., 2004. Atmospheric Aerosol as a Climate Forming Component of the Atmosphere. 1. Properties of Various Types of Aerosols. *Optika Atmosfery i Okeana*, 17(1), pp. 5–24 (in Russian).
4. Lisitzin, A.P., 2011. Arid Sedimentation in the Oceans and Atmospheric Particulate Matter. *Russian Geology and Geophysics*, 52(10), pp. 1100–1133. https://doi.org/10.1016/j.rgg.2011.09.006
5. Bukharina, I.L., Zhuravleva, A.N. and Bolshova, O.G., 2012. [*Urban Planting: Ecological Aspect*]. Izhevsk: Udmurtskiy Gos. Un-t, 204 p. (in Russian).
6. Tsalikov, R.H., Akimov, V.A. and Kozlov, K.A., 2009. [*Assessment of Natural, Technogenic and Ecological Security of Russia*]. Moscow: BNII GOChS, 464 p. (in Russian).
7. Tomilina, I.I., Gapeeva, M.V. and Lozhkina, R.A., 2018. Assessment of Water Quality and Bottom Sediments of the Volga River Reservoirs Based on Toxicity and Chemical Composition. *Transactions of Papanin Institute for Biology of Inland Waters RAS*, (82), pp. 107–131 (in Russian).
8. Koposov, E.V., Paleev, A.V., Sobol, S,V., Vinogradova, T.P., Kaschenko, O.V., Katraeva, I.V., Ivanov, A.V., Panyutin, A.A., Ryzhova, T.S. and Vinogradov, M.A., 2008. [*Environmentally Safe, Sustainable Development of the Volga Basin: Aspects of International Scientific Cooperation*]. Nizhniy Novgorod: NNGASU, 178 p. (in Russian).

9. Monin, A.S. and Shishkov, Yu.A., 2000. Climate as a Problem in Physics. *Physics-Uspekhi*, 170(4), pp. 444–445. https://doi.org/0.1070/PU2000v043n04ABEH000678
10. Sverdlik, L.G., 2014. Peculiarities of Absorbing Aerosol Radiative Properties. *Science and New Technologies*, (4), pp. 26–31 (in Russian).
11. Yakovleva, I.P. and Tashchilin, M.A., 2022. Aerosol Optical Depth Spectral Characteristics Under Exposure to Forest Fire Smoke in the Baikal Region. In: I. P. Yakovleva, ed., 2022. *Proceedings of the XVII Young Scientists' Conference "Interaction of Fields and Radiation with Matter"*. Irkutsk: ISTP SB RAS, pp. 343–344 (in Russian).
12. Luzhetskaya, A.P. and Poddubny, V.A., 2019. Features of Temporal Variability of Aerosol Optical Depth in the Middle Urals According to Long-Term Observations at the Urban and Background Sites. *Optika Atmosfery i Okeana*, 32(11), pp. 889–895. https://doi.org/10.15372/AOO20191102 (in Russian).
13. Gorchakova, I.A., Tarasova, T.A., Sviridenkov, M.A., Anikin, P.P. and Romashova, E.V., 2009. Modeling Radiative Forcing by Background Aerosol on the Basis of Measurement Data. *Izvestiya, Atmospheric and Oceanic Physics*, 45(4), pp. 467–477. https://doi.org/10.1134/S0001433809040070
14. Zhuravleva, T.B., Kabanov, D.M., Nasrtdinov, I.M., Russkova, T.V., Sakerin, S.M., Smirnov, A. and Holben, B.N., 2017. Radiative Characteristics of Aerosol During Extreme Fire Event over Siberia in Summer 2012. *Atmospheric Measurement Techniques*, 10(1), pp. 179–198. https://doi.org/10.5194/amt-10-179-2017
15. Holben, B.N., Eck, T.F., Slutsker, I., Tanré, D., Buis, J.P., Setzer, A., Vermote, E., Reagan, J.A., Kaufman, Y.J. [et al.] 1998. AERONET – A Federated Instrument Network and Data Archive for Aerosol Characterization. *Remote Sensing of Environment*, 66(1), pp. 1–16. https://doi.org/10.1016/S0034-4257(98)00031-5
16. Sakerin, S.M., Kabanov, D.M., Rostov, A.P., Turchinovich, S.A. and Turchinovich, Yu.S., 2004. System for Network Monitoring of Radiatively Active Atmospheric Constituents. Part I. Sun Photometers. *Optika Atmosfery i Okeana*, 17(4), pp. 354–360 (in Russian).
17. Kabanov, D.M. and Sakerin, S.M., 1995. Results of Investigation of Total Moisture Content in the Atmosphere by Optical Hygrometry Method. Part 1. Analysis of the Method and Calibration Results. *Optika Atmosfery i Okeana*, (6), pp. 852–860 (in Russian).
18. Kabanov, D.M., Veretennikov, V.V., Voronina, Y.V., Sakerin, S.M. and Turchinovich, Y.S., 2009. Information System for Network Solar Photometers. *Atmospheric and Oceanic Optics*, 22(1), pp. 121–127. https://doi.org/10.1134/S1024856009010187
19. Lyapustin, A. and Wang, Y., 2007. *MAIAC-Multi-Angle Implementation of Atmospheric Correction for MODIS*. NASA, 77 p.
20. Wang, W., Mao, F., Pan, Z., Du, L. and Gong, W., 2017. Validation of VIIRS AOD Through a Comparison with a Sun Photometer and MODIS AODs over Wuhan. *Remote Sensing*, 9(5), 403. https://doi.org/10.3390/rs9050403
21. Cao, C., Xiong, J., B;onski, S., Liu, Q., Uprety, S., Shao, X., Bai, Y. and Weng, F., 2013. Suomi NPP VIIRS Sensor Data Record Verification, Validation, and Long-Term Performance Monitoring. *Journal of Geophysical Research: Atmospheres*, 118(20), pp. 11664–11678. https://doi.org/10.1002/2013JD020418
22. Lee, J., Hsu, N.C., Kim, W.V., Sayer, A.M. and Tsay, S.-C., 2024. VIIRS Version 2 Deep Blue Aerosol Products. *Journal of Geophysical Research: Atmospheres*, 129(6), e2023JD040082. https://doi.org/10.1029/2023JD040082
23. Hsu, N.C., Tsay, S.-C., King, M.D. and Herman, J.R., 2004. Aerosol Properties over Bright-Reflecting Source Regions. *IEEE Transactions on Geoscience and Remote Sensing*, 42(3), pp. 557–569. https://doi.org/10.1109/TGRS.2004.824067

24. Hsu, N.C., Jeong, M.-J., Bettenhausen, C., Sayer, A.M., Hansell, R., Seftor, C.S., Huang, J. and Tsay, S.-C., 2013. Enhanced Deep Blue Aerosol Retrieval Algorithm: The Second Generation. *Journal of Geophysical Research: Atmospheres*, 118(16), pp. 9296–9315. https://doi.org/10.1002/jgrd.50712

25. Kalinskaya, D.V. and Papkova, A.S., 2019. Correlation of the Atmospheric Aerosol Optical Characteristics Data by CALIPSO and MODIS Satellites Measurements and SPM Photometer. In: IO RAS, 2019. *Proceedings of X Anniversary All-Russia Conference «Current problems in optics of natural waters» (ONW'2019)*. Saint-Petersburg: KHIMIZDAT. Vol. 10, pp. 283–287 (in Russian).

26. Kalinskaya, D.V. and Molkov, A.A., 2023. Spatio-Temporal Variability of the Aerosol Optical Depth over the Gorky and Cheboksary Reservoirs in 2022–2023. *Remote Sensing*, 15(23), 5455. https://doi.org/10.3390/rs15235455

27. Izmailova, A.V., 2016. Water Resources of the Lakes of Russia. *Geography and Natural Resources*, 37(4), pp. 281–289. https://doi.org/10.1134/S1875372816040016

28. Varenik, A.V., Kalinskaya, D.V., Myslina, M.A. and Khoruzhy, D.S., 2019. [Changes in the Nutrients Content in the Seawater Surface Layer after Atmospheric Precipitation]. In: MHI, 2019. [*Proceedings of the All-Russia Scientific Conference: Seas of Russia: Fundamental and Applied Research*. *Sevastopol, 23–28 September 2019*]. Sevastopol: MHI, pp. 51–52 (in Russian).

29. Sofiev, M., Vira, J., Kouznetsov, R., Prank, M., Soares, J. and Genikhovich, E., 2015. Construction of the SILAM Eulerian Atmospheric Dispersion Model Based on the Advection Algorithm of Michael Galperin. *Geoscientific Model Development*, 8(11), pp. 3497–3522. https://doi.org/10.5194/gmd-8-3497-2015

30. Churilova, T.Ya. and Suslin, V.V., 2012. On Causes of *Emiliania huxleyi* Domination in Phytoplankton of Deep Waters Part of the Black Sea in Early Summer. In: MHI, 2012. *Ekologicheskaya Bezopasnost' Pribrezhnoy i Shel'fovoy Zon i Kompleksnoe Ispol'zovanie Resursov Shel'fa* [Ecological Safety of Coastal and Shelf Zones and Comprehensive Use of Shelf Resources]. Sevastopol: MHI. Iss. 26(2), pp. 195–203 (in Russian).

Submitted 21.01.2025; accepted after review 11.03.2025;
revised 24.06.2025; published 30.09.2025

About the authors:

Daria V. Kalinskaya, Junior Research Associate, Marine Hydrophysical Institute of RAS (2 Kapitanskaya Str., Sevastopol, 299011, Russian Federation), **Scopus Author ID: 56380591500**, *kalinskaya@mhi-ras.ru*

Aleksandr A. Molkov, Senior Research Associate, A.V. Gaponov-Grekhov Institute of Applied Physics of RAS (46 Ulianova Str., Nizhny Novgorod, 603950, Russian Federation), PhD (Phys.-Math.), **Scopus Author ID: 55377777800**, **ResearcherID: A-3623-2014**, *a.molkov@inbox.ru*

Contribution of the authors:

Daria V. Kalinskaya – photometric measurements over the Black Sea, data processing, article text writing, text editing

Aleksandr A. Molkov – photometric measurements over the Volga River reservoirs

All the authors have read and approved the final manuscript.